Compositional Model for Predicting Multilayer Reflectances and Transmittances in Color Reproduction

THÈSE Nº 3576 (2006)

PRÉSENTÉE LE 14 JUIN 2006

À LA FACULTÉ INFORMATIQUE ET COMMUNICATIONS

Laboratoire de systèmes périphériques

SECTION D'INFORMATIQUE

ÉCOLE POLYTECHNIQUE FÉDÉRALE DE LAUSANNE

POUR L'OBTENTION DU GRADE DE DOCTEUR ÈS SCIENCES

PAR

Mathieu Hébert

DEA image, Université Jean Monnet, Saint-Etienne, France

de nationalité française

acceptée sur proposition du jury :

Prof. S. Süsstrunk, présidente du jury
Prof. R. Hersch, directeur de thèse
Prof. M. Elias, rapporteur
Prof. J. Lafait, rapporteur
Prof. L. Zuppiroli, rapporteur

Lausanne, EPFL
2006

Quoi qu'on fasse, on reconstruit toujours le monument à sa manière. Mais c'est déjà beaucoup de n'employer que des pierres authentiques.

Marguerite Yourcenar,
Carnets de notes de "Mémoires d'Hadrien"

Acknowledgements

First of all, I would like to express my gratitude to Prof. Roger D. Hersch, director of my research program. Despite the distance between Lausanne and Lyon, he continuously sustained and supervised my work. I thank him for trusting in my capacities and for the pertinence of his advice. It is also a pleasure to thank Prof. Jean-Marie Becker, who taught me so much about mathematics and pedagogy. Meeting him was a determining point in my life, and perhaps the reason for pursuing my carrier on a scientific track. I thank Prof. Jourlin for the opportunity of discovering the field of image and color processing and for the impetus he gave me for my career.

Many persons have contributed to the development of my research. I specially thank Lionel Simonot of the University of Poitiers and Patrick Emmel from Clariant for their interesting discussions. I am grateful to Eric Charron from the Laboratoire d'Optique des Solides in Paris, to Prof. Hartmut Schmidt from the University of Technology of Darmstadt, to Prof. Plummer from the École Polytechnique Fédérale de Lausanne, and to Mr. Luc Choulet, for having generously accepted to give me some time and letting me benefit from their experience. Many thanks to my colleagues Matthieu, Isaac and Laurent, for their precious help and for spending together enjoyable time during these four years. I also thank Mrs. Moira Lanthelme for her help, and my friends, especially Jo, Mathias, Siegfried, Nico and Broqui, for their interest in my work and their nonscientific or artistic point of view.

I would like to finish by expressing my gratitude to my family: my parents and my brother for their constant encouragement, and of course my wife, Valou, who has brought me poetry at times when it is lacking in technical science, and revealed me, day in, day out, a colorful world which I would not know without her.

Abstract

The color of materials such as paints, prints and glass may be characterized by a reflectance or a transmittance spectrum. Modeling their reflectance and their transmittance requires describing the interaction of light, from the light source to the observer, across the different layers and interfaces. Each layer and interface behaves as a light reflector and transmitter, and is given the generic name of "biface". Multilayer specimens, called "multifaces", result from the superposition of various bifaces between which light is subject to multiple reflections and transmissions.

We establish a multiple reflection-transmission model which describes the transfers of fluxes between the different bifaces using the basic laws of geometrical optics. This approach is valid for multilayer specimen composed of strongly scattering and/or nonscattering layers and flat interfaces. Weakly scattering layers and rough interfaces are allowed if they are surrounded by strongly scattering layers.

We first develop the multiple reflection-transmission model in a general manner, i.e. regardless to the specific optical properties of the bifaces. The light multiple reflection-transmission process is represented by a Markov chain. The well established mathematical tools provided by the Markov theory enable deriving the formulae for the reflectance and transmittance of superposed bifaces. Then, we show how the multiple reflection-transmission formulae are applied for a specific multiface and for a specific measuring geometry. We retrieve as special cases of our general model the Kubelka model for stacked intensely scattering layers, the Williams-Clapper model for a diffusing background coated with a non-scattering layer, the Saunderson correction, and the Clapper-Yule model for high quality halftone prints. We finally explore new possibilities offered by the multiple reflection-transmission model, both for developing new reflectance or transmittance models and for checking the relevance of parameters deduced from measured data. We develop a method for characterizing papers independently of the measuring geometry by modeling two superposed sheets of paper and draw the bases of a reflectance and transmittance prediction model for recto-verso halftone prints.

Keywords : Multilayer reflectance and transmittance, multiple reflections and transmissions, compositional spectral prediction model, Kubelka-Munk theory, Williams-Clapper model, Clapper-Yule model, Markov chains.

Résumé

La couleur de matériaux multicouches que l'on rencontre dans les peintures ou les imprimés peut être caractérisée par un spectre de réflectance ou de transmittance. Pour prédire de tels spectres, il est nécessaire de décrire l'interaction de la lumière avec les différents constituants du multicouche (couches et interfaces), de la source lumineuse à l'observateur. Chacun de ces constituants se comporte comme un réflecteur et un transmetteur lumineux, auquel on donne le nom générique de "biface". Dans les multicouches, "appelés multifaces", la lumière est sujette à un phénomène de réflexion-transmission multiple entre les différents bifaces superposés.

Nous proposons un modèle de réflexion-transmission multiple où les transferts de flux entre bifaces sont établis d'après les lois de l'optique géométrique. Cette approche est valable pour des multicouches composés de couches fortement diffusantes, de couches non diffusantes, et d'interfaces planes. Elle reste valable avec des interfaces rugueuses et des couches faiblement diffusantes lorsque celles-ci sont directement bordées par des couches fortement diffusantes.

Nous développons d'abord le modèle général de réflexion-transmission multiple, sans spécifier la nature diffusante ou non des bifaces. Le processus de transfert lumineux est représenté par une chaîne de Markov. La théorie de Markov nous offre les outils mathématiques permettant d'obtenir efficacement les formules de réflectance et de transmittance du multicouche. Nous montrons ensuite comment la réflectance et la transmittance des faces doivent être spécifiées pour un multicouche et une géométrie de mesure donnés. Nous obtenons ainsi un modèle compositionnel valable pour tout type de multicouche correspondant à un multiface régulier. Le modèle de Kubelka, spécifique aux empilements de couches fortement diffusantes ayant toutes le même indice de réfraction, le modèle de Williams-Clapper, spécifique aux fonds diffusants couverts d'une couche transparente colorée, la correction de Saunderson, ainsi que le modèle de Clapper-Yule valable pour les imprimés en demi-ton à linéature élevée deviennent des cas particuliers de notre modèle compositionnel. Enfin, nous explorons quelques nouvelles possibilités offertes par notre modèle, tant pour prédire des réflectance et des transmittances de multicouches (papiers, imprimés), que pour vérifier des valeurs de spectre déduites de mesures (spectre de transmittance d'une encre, paramètres intrinsèques d'un papier). Nous établissons également les bases d'un modèle de prédiction spectral pour des échantillons imprimés en demi-tons à la fois sur le recto et sur le verso.

Mots-clés : Réflectance et transmittance multicouches, réflexions et transmissions multiples, modèle compositionnel de prédiction de spectres, théorie de Kubelka-Munk, modèle Williams-Clapper, modèle Clapper-Yule, chaînes de Markov.

Contents

Introduction

For thousands of years, the visual aspect of man-made objects has undergone multiple modifications due to the ingeniosity of craftmen and artists, creating new styles and satisfying new clients. The increasing complexity of the crafmanship (and later on the industry) of potteries, ceramics, glasses, paintings and printing processes, etc. has been developed on a basis of trial-and-error. In a very late stage, with geometrical optics in the 17th century and wave nature of light in the 19th century, a thorough understanding of these complex processes has taken place. It has appeared that the concept of "color" is very complex because it mixes three agents : light itself, matter and the human vision system [ZB03].

This practical complexity of the domain of color and the growing needs of industry in terms of quality and reproducibility explains that more or less ad hoc models have been proposed in a sporadic manner, for different classes of material. On the one side, physical models describe the changes of propagation and of spectrum that light undergoes when interacting induced with material objects. On the other side, psychophysical models study how the spectral image of objects carried by light is analyzed and interpreted by the human visual system in terms of color, contrast [HV04], transparency [SIM02], gloss [OKV04], etc.

The present work focuses on the physical aspect of color, i.e. on the relationship between light spectra considered respectively before and after reflection or transmission by an object, given by a reflectance or a transmittance spectrum. For predicting such spectra for a given multilayer object, it is necessary to describe the behavior of light in each layer and at each interface between the layers, which may extremely complex due to coexistence of multiple phenomena of reflection, refraction, scattering [Cha60, BS63], diffraction, extinction or interference [BW99], generally dependent on the directionality and the polarization of light.

In order to simplify the multilayer reflectance and transmittance model, we consider only natural incident light, which is incoherent and unpolarized [BW99]. We also consider multilayers as being superpositions of layers and interfaces between these layers, each one being responsible of light reflection, transmission and possibly absorption. We assume that the reflectance and the transmittance of the different layers and interfaces can be determined independently, using for each one a specific model relying on geometrical optics: non-scattering layers may be characterized thanks to Beer's law [Per95]; intensely scattering layers thanks to the Kubelka-Munk two-flux theory [KM31]; categories of weakly scattering layers thanks to a particular solution of the radiative transfer equation [Cha60]; flat interfaces thanks to Fresnel's formulae [BW99] and rough interfaces with large roughness thanks to a microfacet model [TS67]. Thanks to the principle of conservation of energy, absorption is considered as the complementary of reflection and transmission. Multilayers containing layers or interfaces for which the wave nature of light should be explicitly taken into account are excluded from the present study. Non-scattering layers are assumed to be thick enough for avoiding interference phenomena.

For predicting the reflectance and the transmittance of the multilayer specimens speci-

fied above, we introduce a new modelization methodology which has been primarily developed for paper and prints but may also be suitable for other multilayer objects, such as glass slices or photographs. In our approach, light interacting with colored objects consists of a collection of directed photons that are subject to reflection or transmission. Various models using this reflection/transmission basis have appeared in the 1950s. They concern complex materials, such as paper or pigmented coating, but use a reduced number of parameters and a relatively simple mathematical development: Kubelka's model [Kub54] expresses the reflectance and the transmittance of superposed intensely scattering layers as functions of the reflectance and the transmittance of each layer; Williams and Clapper [WC53] modeled the reflectance of a diffusing background coated with a non-scattering absorbing layer, as a function of the reflectance of the background and the transmittance of the non-scattering layer; Clapper and Yule [CY53] developed a model for halftone prints similar to the Williams-Clapper model, with some simplifications in the equations [HH04]. The accuracy of these models has been experimentally stated for the type of specimens that they concern. However, as a major drawback, they are not general enough for being simply extended to new types of colored supports. For instance, the Williams-Clapper model, initially developed for photographs, cannot be used anymore if one likes to protect a photograph with a tinted glaze. None of the models mentioned above enables considering such a multilayer comprising a paper sheet, a colored coating and a glass layer with an eventual air layer between them, all layers having reflecting and transmitting interfaces. One would have to develop a specific model for that special case [SHH06]. Furthermore, if one places behind the glaze a halftone print instead of a photograph, another specific model should be again developed. We thus see the practical interest that would provide a more general model where the optical phenomena of reflection and transmission would be described independently of the material.

Radiometry defines functions permitting to characterize illuminations, reflections and transmissions regardless of specified objects. We follow the same idea for multilayers, by describing light reflections and transmissions inside an abstract specimen composed of unspecified superposed elements. Every element able to reflect or/and transmit light, i.e. every layer and interface between layers, is represented by a single concept named "biface". The adjacency of two bifaces and the mutual exchange of light between them due to multiple reflection-transmission are represented by the fundamental concept of "composition" of bifaces. In a first step, the reflectance and the transmittance of the bifaces are characterized for its both sides (named "faces"). In a second step, a multiple reflection-transmission model describes the transfers of fluxes between the faces contained in the multilayer specimen (named "multiface"). The obtained general expressions for reflectance and transmittance of multifaces are, in the most general case, irreducible infinite sums, but they can often be reduced to exact closed-form formulae. These formulae characterize the composition of bifaces and are by consequent called "composition formulae".

Our compositional model aims at embodying all types of interfaces (flat, rough) and layers (transparent, weakly or intensely scattering). It should be capable of considering as well polished glass slices as matte paper sheets, in which light behaves in an extremely different manner. For the purpose of generality, we have created an appropriate formalism comprising: 1) a classification of the bifaces according to their light scattering properties, 2) different well-defined types of reflectances and transmittances, 3) a graphical

framework permitting to visualize the multiple reflection-transmission of light within multifaces, 4) a notational framework including a matrix-like formulation for the composition of bifaces.

The notion of composition and the compositional formulae, as well as the conditions for their validity and the way for using them in special applications, are the main contribution of this thesis. The present dissertation is structured according to four parts, each one being composed of two chapters:

Part I (Chap. 1 and 2) **— Basic definitions**

Chapter 1 gives the definitions of reflectance and transmittance and presents briefly commonly used measuring devices. Chapter 2 gives the definitions of face, biface and multiface, on which our formalism relies. Bifaces and multifaces are classified according to their scattering properties.

Part II (Chap. 3 and 4) **— Optical properties of interfaces and layers**

This second part presents the characteristics of bifaces, i.e. of interfaces and of layers. The different types of interfaces and of layers are presented in two chapters according to their scattering properties. Chapter 3 concerns flat interfaces and transparent layers (grouped into the concept of "transparent bifaces"), which have in common the property of being nonscattering. Chapter 4 deals with rough interfaces and scattering layers ("scattering bifaces"). Intensely scattering layers ("Lambertian bifaces") are considered separately.

Part III (Chap. 5 and 6) **— The compositional model**

The compositional model is presented in two parts: in the first part (Chapter 5), the reflectance and transmittance formulae for multifaces (the "compositional formulae") are established regardless to the nature of the bifaces. Then, in Chapter 6, we show how the reflectance and transmittance of each biface are specified, first in general, then in the special cases of multifaces considered in the existing models of Kubelka [Kub54], of Saunderson [Sau42], of Williams and Clapper [WC53], of Shore and Spoonhower [SS00] and of Simonot, Hébert and Hersch [SHH06].

Part IV (Chap. 7 and 8) **— Application of the compositional model to papers and prints**

We apply our compositional model to papers, in Chapter 7, and to prints, in Chapter 8. We develop a method for characterizing papers independently of the measuring geometry by modeling two superposed sheets of paper. We also compare the coherence between ink transmittances deduced from the measure of the reflectance and of the transmittance of monocolorant prints. Finally, we draw the bases of a reflectance and transmittance model for recto-verso halftone prints.

Crown-shaped glossy coating deposited on a matte magenta flat tint. The surface reflection on top of the glossy area as well as the multiple reflections taking place beneath the air-coating interface are responsible of remarkable changes of color compared to the matte area (Front page of [Hel02], photograph by Siegfried Marque).

Chapter 1.

Reflectance and transmittance

Radiometry aims at characterizing rigorously the intuitive concepts of light quantity and spatial location, without having to consider specifically any type of material. In the present chapter, we first recall the four fundamental radiometric quantities: flux, irradiance, intensity and radiance (Sect. 1.1). They permit to characterize the two main phenomena of interest in our study, i.e. reflection and transmission. The fractions of incident light that are reflected and transmitted by the material are thus represented by the reflectance and the transmittance (Sect. 1.2) whose definition necessitates specifying explicitly the conditions of illumination and the conditions of observation. We define special types of reflectance and transmittance for the needs of the next chapters, called "directional" when the incident light comes from a single direction, "diffuse" when it comes from the whole hemisphere with a nonhomogenous angular distribution, and "Lambertian" when it comes from the hemisphere with a homogenous angular distribution. Finally, we propose a survey of common devices used for measuring reflectances and transmittances (Sect. 1.3).

1.1 Basic concepts of radiometry

Radiometry defines four fundamental quantities relative to radiations: radiant flux, irradiance, radiant intensity and radiance [McC94]. These quantities can be applied to light and can be measured in practice with instruments in laboratories.

We consider that incident light is natural, i.e. incoherent and unpolarized. Natural unpolarized light may be modeled by two independent and equal linearly polarized components [BW99]. The radiometric quantities may therefore be decoupled into these two components. There is no time-dependent behavior in the system, which excludes phosphorescence[1]. The energy of different wavelengths is decoupled, i.e. the energy associated with a certain region of space or surface at wavelength λ_1 is independent of the energy at wavelength λ_2, which excludes phenomena of fluorescence[2]. Every radiometric quantity may therefore be a wavelength-dependent function.

1.1.1 The four fundamental radiometric quantities

Radiant flux Φ (or simply *flux*) is the energy flowing through a surface per unit time. Flux is expressed in watts.

---

[1] *Phosphorescence*: Persistent emission of light following exposure to and removal of incident radiation.

[2] *Fluorescence*: The emission of electromagnetic radiation stimulated in a substance by the absorption of incident radiation and persisting only as long as the stimulating radiation is continued.

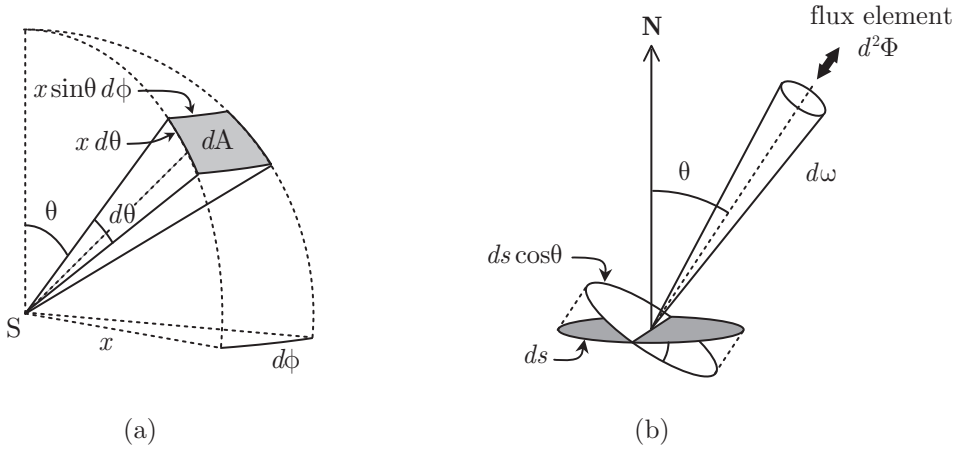

Fig. 1.1: Geometry for the definitions of (a) solid angle and (b) radiance.

The *solid angle* $d\omega$ *subtended by area* dA *at point* S is the ratio of the area dA of a portion of sphere of center S to the squared radius x of this sphere

$$d\omega = dA/x^2 \tag{1.1}$$

A solid angle subtended by an infinitesimally small area on a sphere, whose location is specified by the zenithal angle θ and the azimuthal angle ϕ, is called a *differential solid angle* (Fig. 1.1a). Its relation with angles θ and ϕ is given by

$$d\omega = \sin\theta d\theta d\phi \tag{1.2}$$

In order to clarify some angle-dependent expressions, we will often designate directions using a differential solid angle instead of a pair of zenithal and azimuthal angles.

The *irradiance* E (also called *brightness*) is the radiant flux per unit area that is incident on, passing through or emerging from a specified point in a specified surface (expressed in watts/m^2). Considering a flux $d\Phi$ flowing through a given set of directions (e.g. the hemisphere) relatively to an element ds of area, the irradiance is

$$E = \frac{d\Phi}{ds} \tag{1.3}$$

A flux element $d^2\Phi(d\omega)$ flowing within a differential solid angle $d\omega$ defines an *element of irradiance* $dE(d\omega)$

$$dE(d\omega) = \frac{d^2\Phi(d\omega)}{ds} \tag{1.4}$$

The *radiant intensity* I is the radiant flux per unit solid angle that is incident on, passing through or emerging from a point in space and propagating in a specified direction $d\omega$ (expressed in watts/steradian). For a flux element $d\Phi(\mathrm{d}\omega)$ flowing through a differential solid angle $d\omega$

$$I(d\omega) = \frac{d\Phi(d\omega)}{d\omega} \tag{1.5}$$

The *radiance* L is the flux per unit projected area and per solid angle that is incident on, passing through or emerging from a specified point in a specified surface in a specified direction [expressed in watts/(steradian.m^2)]. The defining equation of radiance is

$$L(d\omega) = \frac{d^2\Phi(d\omega)}{ds^P d\omega} = \frac{d^2\Phi(d\omega)}{ds\cos\theta\sin\theta d\theta d\phi} \tag{1.6}$$

where $d^2\Phi(d\omega)$ is the element of flux, $d\omega = \sin\theta d\theta d\phi$ is the differential solid angle in a specified direction (θ,ϕ), and $ds^P = ds\cos\theta$, called *projected area*, is the area of the projection of elemental area ds onto a plane perpendicular to direction (θ,ϕ) (Fig. 1.1b).

1.1.2 Relation between irradiance and radiance

Combining (1.4) and (1.6) yields the following relation

$$dE(d\omega) = L(d\omega)\cos\theta d\omega \tag{1.7}$$

where the solid angle $d\omega = \sin\theta d\theta d\phi$ denotes the direction of radiance L and element of irradiance dE. An equivalent angular notation would give

$$dE(\theta,\phi) = L(\theta,\phi)\cos\theta\sin\theta d\theta d\phi$$

Summing up the elements of irradiance over the hemisphere Ω yields an irradiance E. By integrating (1.7), one obtains the relationship between irradiance and radiance

$$E = \int_{d\omega\in\Omega} dE(d\omega) = \int_{d\omega\in\Omega} L(d\omega)\cos\theta d\omega = \int_{\phi=0}^{2\pi}\int_{\theta=0}^{\pi/2} L(\theta,\phi)\cos\theta\sin\theta d\theta d\phi \tag{1.8}$$

1.1.3 Radiance invariance

The radiance emitted by a surface element ds_1 towards a second surface element ds_2 is equal to the radiance received by ds_2 from ds_1. This property is called the *radiance invariance principle* [McC94, p. 111]. It allows saying, for example, that the radiance captured by a detector observing a piece of paper is equal to the radiance emitted by the paper towards the detector.

Let us call $\mathbf{N}_1$ and $\mathbf{N_2}$ the normal vectors of ds_1 and of ds_2 and take a point P_1 on surface element ds_1 and a point P_2 on surface element ds_2 (Fig. 1.2). The segment $[P_1P_2]$ of length x forms an angle θ_1 with $\mathbf{N_1}$ and an angle θ_2 with $\mathbf{N_2}$. Differential solid angle $d\omega_1$, subtended at point P_1 by ds_2, and solid angle $d\omega_2$, subtended at point P_2 by ds_1, are [see Eq. (1.1)]

$$d\omega_1 = ds_2^P/x^2 \quad \text{and} \quad d\omega_2 = ds_1^P/x^2 \tag{1.9}$$

where $ds_2^P = ds_2\cos\theta_2$ and $ds_1^P = ds_1\cos\theta_1$ are the projected areas of ds_2 and of ds_1 respectively. It follows from (1.9) that

$$\frac{ds_1^P}{d\omega_2} = \frac{ds_2^P}{d\omega_1} \tag{1.10}$$

which may be written in the form

$$ds_1 \cos\theta_1 d\omega_1 = ds_2 \cos\theta_2 d\omega_2 \tag{1.11}$$

Eqs. (1.11) is called the *principle of reciprocity of transfer volume* [Gla95, p. 655].

A flux element $d^2\Phi$ flows along $[P_1P_2]$. By inserting relation (1.9) into the defining expression for radiance [Eq. (1.6)], one obtains

$$L_1 = \frac{d^2\Phi}{ds_1 \cos\theta_1 d\omega_1} = \frac{d^2\Phi}{ds_2 \cos\theta_2 d\omega_2} = L_2 \tag{1.12}$$

Hence, the radiance L_1 emitted by ds_1 is equal to radiance L_2 received by ds_2.

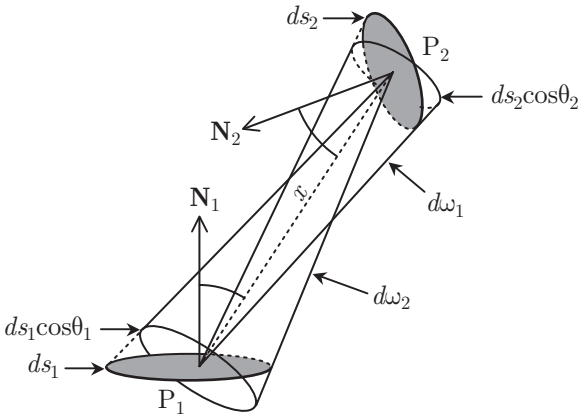

Fig. 1.2: The radiance emitted by ds_1 towards ds_2 is equal to the radiance received by ds_2 from ds_1.

1.1.4 Lambert's law

The radiance L emitted by a perfectly diffuse emitter is independent of the direction of emission, i.e. it is constant. Such emitters are called *Lambertian emitters* since the element of irradiance they reflect in each direction of the space verify Lambert's cosine law (this property is a consequence of Eq. (1.7) with a constant radiance). According to Eq. (1.8), the irradiance emitted by a Lambertian emitter is [McC94, p.18]

$$E = L \int_{\phi=0}^{2\pi} \int_{\theta=0}^{\pi/2} \cos\theta \sin\theta \, d\theta \, d\phi = \pi L \tag{1.13}$$

Conversely, when an irradiance E is emitted by a Lambertian emitter, a radiance equal to E/π flows in every direction of the hemisphere.

1.2 Definitions of reflectance and transmittance

The fractions of light that are reflected and transmitted by a given material are commonly called "reflectance" and "transmittance". However, since materials generally have a directional dependence in their response to the incident light, there exist various types of reflectance and transmittance. One should consider the directions from which the incident flux incomes as well as the directions at which the reflected and transmitted fluxes are observed. We present here successively the three mains sorts of functions: bidirectional reflectance and transmittance functions, (Sect. 1.2.1), reflectance and transmittance (Sect. 1.2.2), and reflectance and transmittance factor (Sect. 1.2.3).

1.2.1 BRDF and BTDF

According to Nicomedus [Nic77], the reflection process of light is embodied in the fundamental equation relating an element of irradiance $dE(d\omega_i)$, coming from direction $d\omega_i$, and the radiance $L_r(d\omega_r)$ reflected in direction $d\omega_r$

$$L_r(d\omega_r) = f_R(d\omega_i, d\omega_r) dE(d\omega_i) \tag{1.14}$$

Function f_R, depending on the incidence and reflection directions, is the *bidirectional reflectance distribution function* (BRDF). It is a ratio of reflected radiance to incident monodirectional irradiance

$$f_R(d\omega_i, d\omega_r) = \frac{L_r(d\omega_r)}{dE(d\omega_i)} \tag{1.15}$$

The *bidirectional transmittance distribution function* (BTDF) f_T is similarly defined, for a transmitting specimen

$$f_T(d\omega_i, d\omega_t) = \frac{L_t(d\omega_t)}{dE(d\omega_i)} \tag{1.16}$$

Lambertian reflectors and transmitters: A reflector is said to be *Lambertian* when its BRDF is a constant, i.e., is independent of the incidence and the reflection directions. Likewise, a Lambertian transmitter has a constant BTDF.

1.2.2 Reflectance and transmittance

The *reflectance* R is the dimensionless ratio of a reflected element of flux $d\Phi_r$ to an incident element of flux $d\Phi_i$, both fluxes being respectively contained within specified solid angles Γ_r and Γ_i. The *transmittance* T is the ratio of a transmitted element of flux $d\Phi_t$ to an incident element of flux $d\Phi_i$, respectively contained within solid angles Γ_t and Γ_i

$$R_{\Gamma_i \to \Gamma_r} = \frac{d\Phi_r(\Gamma_r)}{d\Phi_i(\Gamma_i)} \quad \text{and} \quad T_{\Gamma_i \to \Gamma_r} = \frac{d\Phi_t(\Gamma_t)}{d\Phi_i(\Gamma_i)} \tag{1.17}$$

Assuming that the incident, the reflected and the transmitted fluxes are relative to the same element of surface, reflectance and transmittance are also ratios of irradiances

$$R_{\Gamma_i \to \Gamma_r} = \frac{E_r(\Gamma_r)}{E_i(\Gamma_i)} \quad \text{and} \quad T_{\Gamma_i \to \Gamma_r} = \frac{E_t(\Gamma_t)}{E_i(\Gamma_i)} \tag{1.18}$$

Γ_i is called *incidence solid angle*, and Γ_r and Γ_t are called *observation solid angles*. The observation solid angles may be different from the sets of directions over which the incident light is reflected and transmitted. Every reflectance is related to the BRDF by the following equation

$$R_{\Gamma_i \to \Gamma_r} = \frac{\int_{d\omega_i \in \Gamma_i} \int_{d\omega_r \in \Gamma_r} f_R(d\omega_i, d\omega_r) L_i(d\omega_i) \cos\theta_i d\omega_i \cos\theta_r d\omega_r}{\int_{d\omega_i \in \Gamma_i} L_i(d\omega_i) \cos\theta_i d\omega_i} \tag{1.19}$$

where f_R is the BRDF of the reflector, $d\omega_i = \sin\theta_i d\theta_i d\phi_i$ and $d\omega_r = \sin\theta_r d\theta_r d\phi_r$ are differential solid angles according to which the integrations are performed, and L_i is a radiance function specifying the angular distribution of the incident flux within the incidence solid angle. The detailed calculation leading to relation (1.19) is given in Appendix A.1. An analog relation exists between the BTDF $f_T(d\omega_i, d\omega_t)$ and the transmittance $T_{\Gamma_i \to \Gamma_r}$

$$T_{\Gamma_i \to \Gamma_t} = \frac{\int_{d\omega_i \in \Gamma_i} \int_{d\omega_t \in \Gamma_t} f_R(d\omega_i, d\omega_t) L_i(d\omega_i) \cos\theta_i d\omega_i \cos\theta_t d\omega_t}{\int_{d\omega_i \in \Gamma_i} L_i(d\omega_i) \cos\psi_i d\omega_i} \tag{1.20}$$

However, definitions (1.19) and (1.20) are two general for the needs of our study. We will encounter only three configurations of incidence solid angle, reflection solid angle and incidence angular distribution. We consequently define three types of reflectance, named "directional", "diffuse" and "Lambertian" (Fig. 1.3). Every reflector is assumed to be isotropic, i.e. to have a reflectance independent of the azimuth angle of incidence. Equivalent definitions could be formulated for transmittance.

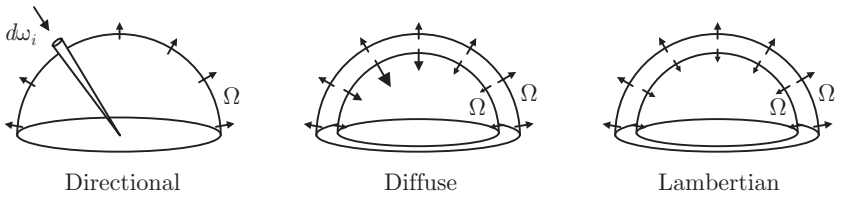

Fig. 1.3: Directional, diffuse and Lambertian reflectances.

– **Directional reflectance**, $R(\theta_i)$, is defined for a directional incident light, i.e. for an element of irradiance $dE(d\omega_i)$ coming from a single direction $d\omega_i = \sin\theta_i d\theta_i d\phi_i$. The whole flux reflected over the hemisphere is observed. The radiance reflected in a particular direction $d\omega_r$ is given by Eq. (1.14). The corresponding element of irradiance is

$$dE_r(d\omega_r) = L_r(d\omega_r) \cos\theta_r d\omega_r = f_R(d\omega_i, d\omega_r) dE(\theta_i) \cos\theta_r d\omega_r$$

By summing up all the reflected elements of irradiance over the hemisphere, one obtains

the total reflected irradiance. The ratio of this total reflected irradiance to the incident irradiance $dE(d\omega_i)$ gives the directional reflectance $R(\theta_i)$, whose expression as a function of the BRDF f_R is

$$R(\theta_i) = \int_{d\omega_r \in \Omega} f_R(d\omega_i, d\omega_r) \cos\theta_r d\omega_r \tag{1.21}$$

Directional reflectances will be used as directional functions characterizing the optical properties of certain optical elements.

– **Diffuse reflectance**, R_{dif}, is defined for a nonuniformly distributed incident light coming from all directions of the hemisphere (hemispherical incidence solid angle Ω). The angular distribution of the incident flux is characterized by a radiance function $L_i(d\omega_i)$. All the flux reflected over the hemisphere is observed (hemispherical observation solid angle Ω). The diffuse reflectance is related to the BRDF by

$$R_{dif} = \frac{\int_{d\omega_i \in \Omega} \int_{d\omega_r \in \Omega} f_R(d\omega_i, d\omega_r) L_i(d\omega_i) \cos\theta_i d\omega_i \cos\theta_r d\omega_r}{\int_{d\omega_i \in \Omega} L_i(d\omega_i) \cos\theta_i d\omega_i} \tag{1.22}$$

It is also related to the directional reflectance $R(\theta_i)$ by

$$R_{dif} = \frac{\int_{d\omega_i \in \Omega} R(\theta_i) L_i(d\omega_i) \cos\theta_i d\omega_i}{\int_{d\omega_i \in \Omega} L_i(d\omega_i) \cos\theta_i d\omega_i} \tag{1.23}$$

which derives from a combination of Eqs. (1.21) and (1.22). The angle distribution of the reflected light may be represented by a radiance function L_r related to the incident radiance function L_i and to the BRDF by

$$L_r(d\omega_r) = \int_{d\omega_i \in \Omega} f_R(d\omega_i, d\omega_r) L_i(d\omega_i) \cos\theta_i d\omega_i \tag{1.24}$$

– **Lambertian reflectance**, R_L, is defined for a uniformly distributed incident light coming from all directions of the hemisphere (Lambertian illumination). The angular distribution of the incident flux is characterized by a constant radiance L_i (Sect. 1.1.4). The whole flux reflected over the hemisphere is observed (hemispherical observation solid angle Ω). Lambertian reflectance is expressed as a function of the BRDF as in Eq. (1.22), but since here L_i is a constant, it may be taken out of the integrals

$$R_L = \frac{L_i \int_{d\omega_i \in \Omega} \int_{d\omega_r \in \Omega} f_R(d\omega_i, d\omega_r) \cos\theta_i d\omega_i \cos\theta_r d\omega_r}{L_i \int_{d\omega_i \in \Omega} \cos\theta_i d\omega_i} \tag{1.25}$$

The term L_i disappears from the expression for R_L, and the integral at the denominator can be simplified as

$$\int_{d\omega_i \in \Omega} \cos\theta_i d\omega_i = \int_{\phi_i=0}^{2\pi} \int_{\theta_i=0}^{\pi/2} \cos\theta_i \sin\theta_i d\theta_i d\phi_i = \pi \tag{1.26}$$

Therefore, the relation between the Lambertian reflectance and the BRDF becomes

$$R_L = \frac{1}{\pi}\int_{d\omega_i\in\Omega}\int_{d\omega_r\in\Omega} f_R(d\omega_i, d\omega_r)\cos\theta_i d\omega_i \cos\theta_r d\omega_r \tag{1.27}$$

The Lambertian reflectance may also be expressed as a function of the directional reflectance, which will be frequently useful in the next chapters. The combination of (1.21) and (1.27) yields

$$R_L = \frac{1}{\pi}\int_{d\omega_i\in\Omega} R(\theta_i)\cos\theta_i d\omega_i = \frac{1}{\pi}\int_{\phi_i}^{2\pi}\int_{\theta_i}^{\pi/2} R(\theta_i)\cos\theta_i \sin\theta_i d\theta_i d\phi_i \tag{1.28}$$

Furthermore, owing to the assumption of anisotropy of reflectors, the integrated terms are independent of the azimuth angle ϕ_i. The integration according to that angle yields a factor 2π. Using some trigonometry, one obtains the following relation between the Lambertian and the directional reflectances

$$R_L = \int_{\theta_i=0}^{\pi/2} R(\theta_i)\sin 2\theta_i d\theta_i \tag{1.29}$$

1.2.3 Reflectance and transmittance factor

The *reflectance factor* $\hat{R}$ is the ratio of the flux $d\Phi$ reflected by a specimen to the flux $d\Phi_{ref}$ reflected by a certain reference support illuminated and observed in the same way. According to that definition, $\hat{R}$ is also a ratio of irradiances, a ratio of radiances and a ratio of reflectances

$$\hat{R} = \frac{d\Phi}{d\Phi_{ref}} = \frac{dE(d\omega)}{dE_{ref}(d\omega)} = \frac{L(d\omega)}{L_{ref}(d\omega)} = \frac{R}{R_{ref}} \tag{1.30}$$

The reference support is generally a perfect white diffuser, such as a barium sulfate ($BaSO_4$) white tile, whose reflectance is almost 1 for the wavelengths in the visible spectrum. In the printing field, the reference support is sometimes chosen to be the unprinted printing support itself.

Remark: When the reference reflectance is 1, the reflectance factor and the reflectance indicate the same dimensionless quantity. This may be one reason why the term "reflectance" is often used in the literature instead of the term "reflectance factor".

The *transmittance factor* is the ratio of the flux transmitted by a specimen to the flux transmitted by a reference transmitter, which may be simply air (transmittance 1).

1.3 Measuring geometries

Measurement setups are composed of a light source and a capturing device. Although there are many different sorts of sources and detectors, standard setups generally use a directional or a Lambertian light source and a radiance detector or an integrating sphere for the capture of light. BRDFs or BTDFs are measured using a goniophotometer, composed of a collimated light source and a radiance detector that can be positioned at any angle.

1.3.1 Setups for reflectance and transmittance measurements

Integrating spheres are spherical cavities internally coated with a nonabsorbing material behaving as a perfect diffuser [PER93], e.g. barium sulfate ($BaSO_4$). In reflectance measurements, integrating spheres play the role of diffuser for the illuminating flux. The light reflected by the specimen is thus captured by a radiance detector, oriented at 0° or 8°. The corresponding geometries are called the "diffuse/0°" geometry or respectively the "diffuse/8°" geometry. Integrating spheres may also be used for the capture of the light reflected by the specimen. The incident light is often directional and oriented at 0° or 8°, yielding the so-called "0°/diffuse" geometry or respectively the "8°/diffuse" geometry (Fig. 1.4).

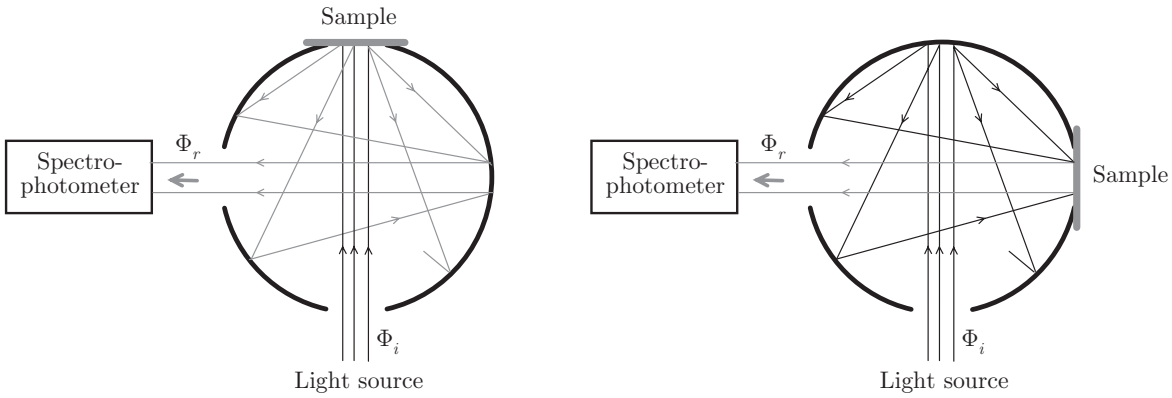

Fig. 1.4: Integrating spheres used in a 0°/diffuse geometry (left) and a diffuse/0° geometry (right).

In contrast with integrating spheres, a radiance detector captures only a fraction of the flux having interacted with the specimen. This fraction depends on the detector area and solid angle, which are generally unknown. With radiance detectors, one often considers the capture of radiance instead of flux. Thus, the optical properties of specimens are characterized by the ratio of the captured radiance L_d to the incident irradiance E_i, which is not precisely a reflectance, but is proportional to a reflectance

$$R_{rad} = \xi \cdot \frac{L_d}{E_i} \tag{1.31}$$

where ξ, called "apparatus constant", is defined by Eq. (A.12) (Appendix A.2). The apparatus constant is characteristic of each detector, and is generally not known. In order to cancel it, measures are performed in reference to a perfect white diffuser. The ratio $(L_d/E_i)_{ref}$ for this reference support is equal to $1/\pi$, yielding a reflectance $R_{ref} = \xi/\pi$. We thus characterize the specimen by a reflectance factor $\hat{R}_{rad}$, given by the ratio R_{rad}/R_{ref}, which is independent on the apparatus constant (see Appendix A.2).

$$\hat{R}_{rad} = \frac{\pi}{\xi} R_{rad} = \pi \frac{L_d}{E_i} \tag{1.32}$$

The so-called *bidirectional geometry* is formed by both a directional light source and a radiance detector. The so-called "45°/0° geometry", widely used for measuring reflectances, is a bidirectional geometry where light is incident at 45° and a radiance detector captures light at 0°. In order to reduce the influence of an unexpected anisotropy in the observed portion of the specimen, photospectrometers built on the 45°/0° geometry generally illuminate the specimen from all the azimuth angles instead of a single one. The light source has therefore the form of an empty cone of angle 45° (Fig. 1.5).

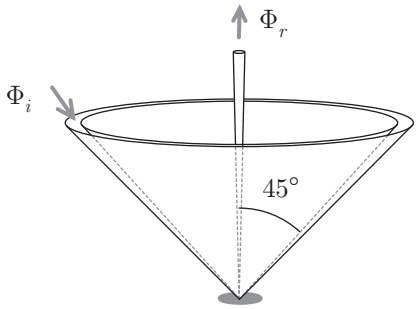

Fig. 1.5: Representation of the 45°/0° geometry for reflectance measurements.

For transmittance measurements, we may place the specimen between a diffusing light table and an integrating sphere or a radiance detector. The light table may be considered as a Lambertian emitter. The specimen is preferably raised from the light table, for ensuring that it has a uniform relative refractive index with air, with a sufficient distance in order to avoid multiple reflections with the surface of the table.

1.3.2 Measuring the BRDF

The measure of BRDF is performed with a goniophotometer. A directional light source and a radiance detector are attached to rotating arms, which permits to measure reflected flux for any couple of directions of incidence and observation.

The flux $d^2\Phi$ captured by the radiance detector is proportional to the BRDF f_R when the portion of the specimen's surface observed by the detector is completely illuminated by the incident light beam

$$d^2\Phi = k f_R(\theta_i, \theta) \tag{1.33}$$

However, it frequently happens that the observed portion of specimen is only partially illuminated, especially when the observation direction reaches grazing angles for which the radiance detector intercepts a very large portion of the specimen's surface. In this case, the flux captured by the detector is proportional to the BRDF multiplied by the cosine of the observation angle

$$d^2\Phi = k\, f_R(\theta_i,\theta)\cos\theta \tag{1.34}$$

The operation of multiplication by cosθ permitting to convert the measured flux into the BRDF is called "the cosine correction". We develop in Appendix A.3 a full explanation of the relationship between the flux captured by the detector and the BRDF, as well as a precise description of the cosine correction.

Summary

The radiometric definitions of flux, irradiance and radiance, recalled at the beginning of this chapter, provide a solid theoretical framework for describing the spatial location of light with respect to materials. Thus, considering a single or a set of direction(s) for the incident and the observed lights, reflections and transmissions can be rigorously characterized.

The most fundamental function describing the reflection property of a specimen is the BRDF, defined as the ratio of the radiance reflected in a given direction to the incident irradiance coming from a single direction. It is therefore a function of the incident and of the reflection directions. It may be interpreted as the "pulse responses" of the material, the "pulse" being the directional incident light.

Reflectance is defined as a ratio of fluxes, i.e. the ratio of a reflected flux to an incident flux. A same material may have several reflectances according to the way it is illuminated (incidence solid angle, angular distribution of the incident flux) and the way it is observed (observation solid angle). Three types of reflectances have been defined: "directional reflectance" for a directional incident light, "diffuse reflectance" for a non-uniformly distributed incident light, and "Lambertian reflectance" for a uniformly distributed incident light. For these three types of reflectance, the observation solid angle is the whole hemisphere.

Since in most applications the incident flux is not directly measurable, another type of reflectance, called "reflectance factor", is defined. It corresponds to the ratio of the flux reflected by material to the flux reflected by a reference white diffuser illuminated and observed in the same circumstances.

In analogy to reflection, transmission of light is characterized by a Bidirectional Transmittance Distribution Function (BTDF), by a directional, a diffuse or a Lambertian transmittance, or by a transmittance factor.

Chapter 2.
Faces, bifaces, multifaces

We introduce a general representation of multilayer materials, according to which they are decomposed into unit optical elements able to reflect or/and transmit light, called "bifaces". Bifaces may be layers, or interfaces between layers. The multilayer is thus considered as a superposition of bifaces. The two sides of a biface are also considered as distinct optical elements, called "faces". The concepts of face, biface and multiface allow a hierarchical representation of multilayer specimen (Sect. 2.1). Faces are characterized by their reflectance and their transmittance. They are classified according to their propensity to scatter light (Sect. 2.2). Bifaces are characterized by the reflectances and the transmittances of their two faces, gathered into a pseudo-matrix called "transfer matrix". This pseudo-matrix has a general form, called the "fundamental transfer matrix" until the conditions of illumination and observation on both sides of the biface are specified. The specification of the illumination and the observation geometries allows obtaining a particular transfer matrix (Sect. 2.3). Multifaces result from a superposition of bifaces. Special definitions are introduced for their most external bifaces because their reflectance and transmittance depend on the type of detector and light source that are used (Sect. 2.4).

2.1 Introduction

The interaction of light with planar multilayer specimens results from a succession of unit events where light may be reflected, refracted, absorbed, scattered, or subject to more complex phenomena such as diffraction, dispersion etc. However, many multilayer specimens may be considered simply as a superposition of homogenous unit optical elements, i.e. layers and interfaces between layers, between which the transfers of light can be described thanks to models relying on geometrical optics. The multilayers concerned by this approach are composed of non-scattering layers or/and intensely scattering layers with flat interfaces, as well as possibly some categories of weakly scattering layers and of rough interfaces specified in Chap. 4.

Layers and interfaces are all able to reflect and transmit light. They are called "bifaces" (Fig. 2.1). The multilayer specimen is thus called a "multiface", corresponding to a superposition of bifaces. Layers or interfaces often have different reflection and transmission properties according to the side on which the incident light incomes. Bifaces are therefore considered as the junction of two "faces", corresponding each one to a different side of the biface.

A paper sheet, for example, is a multiface composed of three bifaces: the paper layer and its two bordering interfaces. A white background coated with a transparent coloring layer having the same refractive index is also a multiface composed of three bifaces: the white background, the transparent layer, and the interface between the layer and air.

More examples will be further encountered in the next chapters. This chapter presents the general definitions, properties and representations of faces, bifaces, and multifaces.

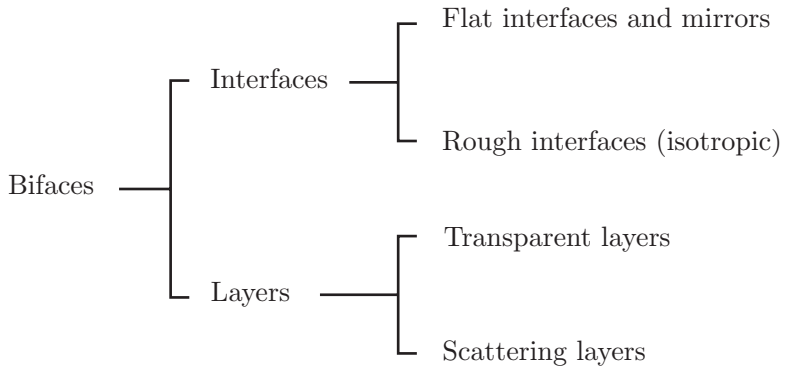

Fig. 2.1: Main categories of bifaces.

2.1.1 Definitions

The term *biface* designates any infinitely large, planar, regular and azimuthally isotropic optical element able to reflect or/and transmit light. It stands for (Fig. 2.1):

– *Layers*, having parallel and plane boundaries; they may absorb or/and scatter light;

– *Interfaces* between layers, or between a layer and a surrounding medium; they may be flat or rough; metallic mirrors are special cases of bifaces having a zero transmittance.

The concept of biface excludes curved optical elements, anisotropic roughness for the interfaces, nonconstant thickness and anisotropic scattering for layers. Bifaces may possibly received light from their *upper side* and their *lower side*, the terms "upper" and "lower" being relative to a previously established convention.

The term *face* designates a single side of biface. It reflects light towards the side of incidence and transmits light at the other side of the biface. Thus, bifaces have an *upper face* and a *lower face*.

The term *multiface* designates any superposition of bifaces.

2.1.2 Hierarchical representation of multilayer specimens

Multiface, biface and face concepts permit a hierarchical description of the interaction of light with the multilayer material (Fig. 2.2). The faces are at the basic level of the hierarchy. The interaction of light with each face may be described according to an appropriate optical model, from which the face's reflectance and transmittance may be derived (Chapter 3 and 4). The bifaces, at the middle level of the hierarchy, are characterized by the reflectance and the transmittance of their two faces. The multiface is at the top in the hierarchy. Its reflectance and transmittance are obtained by combining the reflectances and the transmittances of its bifaces (see Chapter 5).

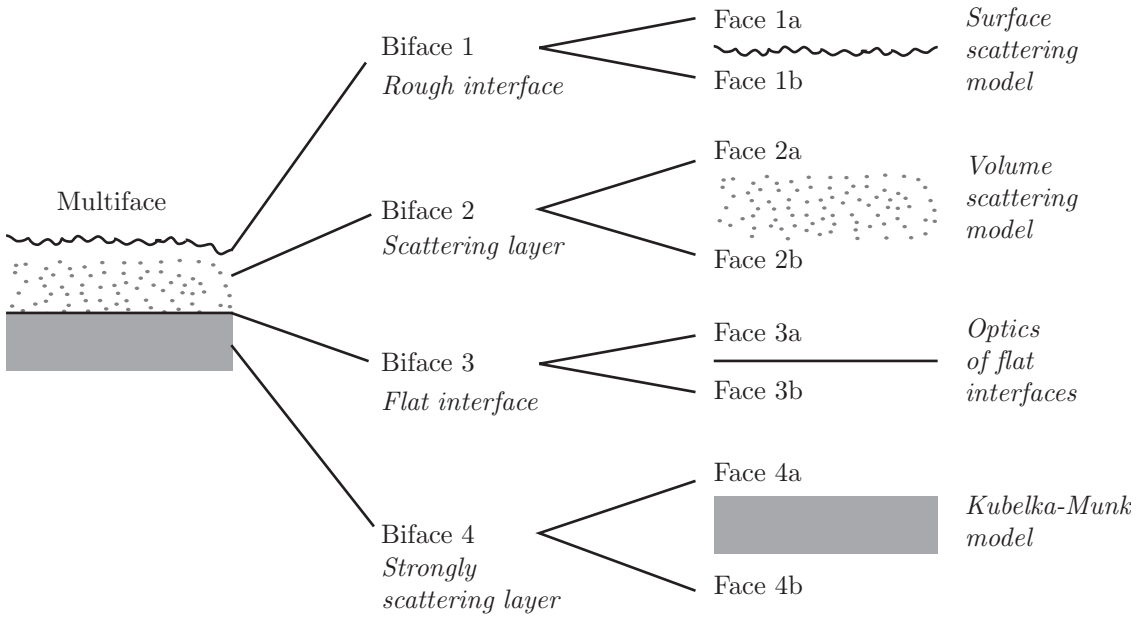

Fig. 2.2: Hierarchical representation of a multilayer specimen (multiface) composed of a rough interface, a scattering layer, a flat interface and a strongly scattering layer (bifaces). On the right-hand side, one finds the type of optical model that may be used for characterizing the reflectance and the transmittance of the corresponding faces. These models will be presented in Chapters 3 and 4.

2.2 Faces

A face represents one side of layer or one side of interface. It is characterized by its directional reflectance $R(\theta)$ and its directional transmittance $T(\theta)$, which may be directly determined by optical laws or may be deduced from the BRDF or BTDF according to Eq. (1.21). Regarding the scattering properties of the different existing types of faces, we define the three following categories:

– **Transparent faces**, which do not scatter light. There exists a bijective relation between the directions of incidence and of reflection, as well as between the directions of incidence and of transmission (Snell's laws, see Sect. 3.1.1). The directions of reflection and of transmission are called the *regular directions*. The directional reflectance can be derived directly from the basic laws of optics, e.g. Fresnel formulae (see Sect. 3.2.1) and Beer's law (see Sect. 3.3.1).

– **Lambertian faces**, which scatter light uniformly. The incident light is assumed to be completely scattered as soon as it penetrates the face, with a subsequent cancellation of its angular distribution. The reflected and transmitted lights are Lambertian. Their reflectance and transmittance are invariant, i.e. independent of the illumination geometry.

– **Scattering faces**, which scatter light nonuniformly. Their BRDF and BTDF are necessary for the modelization of their reflectance and transmittance (see Chapter 4).

Particular faces: a face of transparent layer has a null BRDF, and therefore a null reflectance. Opaque layers and mirrors have a single face since they can be illuminated only on

one side. Their BTDF, and thereby their transmittance, is zero.

2.3 Bifaces

A biface results from the union of its two faces, both characterized by their respective reflectance and transmittance. As long as the conditions of illumination and of observation are not specified, we express their directional reflectances and transmittances as functions of the angular variable θ. According to a certain convention of sense, one face is called the "upper face", the other being called the "lower face". The biface is therefore characterized by an *upper reflectance* $R(\theta)$ and an *upper transmittance* $T(\theta)$ characteristic of its upper face, and a *lower reflectance* $R'(\theta)$ and a *lower transmittance* $T'(\theta)$ characteristic of its lower face.

In order to easy the development of the compositional model, we gather these four terms using a matrix-like notation: the upper transmittance and reflectance are placed on the first row, and the lower reflectance and transmittance on the second row, by respecting the following order

$$\begin{bmatrix} T(\theta) & R(\theta) \\ R'(\theta) & T'(\theta) \end{bmatrix} \tag{2.1}$$

This pseudo-matrix is called the *fundamental transfer matrix* of the biface[1].

Once the conditions of illumination and observation on the faces are specified, we can determine their reflectances and transmittances. Thus, we obtain a *particular transfer matrix*. In order to express the conversion of the fundamental transfer matrix into a particular transfer matrix, we introduce special notations. The illumination geometry is denoted by the symbols *dir*, *diff* and *L*, standing respectively for directional, diffuse and Lambertian. The illumination on the upper face (resp. on the lower face) is specified by a left superscript (resp. a right subscript) associated to the brackets of the fundamental transfer matrix. When the biface is observed by a capturing device, we also specify the type of observation, using symbols *sph* for an integrating sphere or *rad* for a radiance detector.

Let us take an example. Consider a biface illuminated by directional light at angle ψ on its upper face and by Lambertian light on its lower face. The left superscript $dir(\psi)$ and the right subscript L are associated to the fundamental transfer matrix. The biface has the particular transfer matrix composed of the directional upper reflectance $R(\psi)$, the directional upper transmittance $T(\psi)$, the Lambertian lower reflectance r' and the Lambertian lower transmittance t'

$$^{dir(\psi)\rightarrow}\begin{bmatrix} T(\theta) & R(\theta) \\ R'(\theta) & T'(\theta) \end{bmatrix}_{\leftarrow L} = \begin{bmatrix} T(\psi) & R(\psi) \\ r' & t' \end{bmatrix} \tag{2.2}$$

[1] Transfer matrices are not matrices in the classical sense since matrix operations such as sum (+) and product (.) are not defined. The considered transfer matrices will be combined according to a special composition law, noted ○ (see Chap. 5).

Bifaces are classified according to the same categories as faces, i.e. transparent, scattering and Lambertian:

– **Transparent** bifaces have two transparent faces; flat interfaces and transparent layers are examples of transparent bifaces.

– **Lambertian** bifaces have two Lambertian faces; they correspond to strongly scattering layers. Their reflectance and the transmittance are independent of the conditions of illumination. Therefore, they are characterized by an invariant transfer matrix.

– **Scattering** bifaces are bifaces that are neither transparent nor Lambertian. Rough interfaces and scattering layers are examples of scattering bifaces.

2.4 Multifaces

A multiface corresponds to the superposition of at least two bifaces. By definition, since it is able to reflect and transmit light, it is also a biface. As every biface, it has a transfer matrix defined for given angular distributions at the upper and the lower sides. This one is noted **G** and called *global transfer matrix*. Its components are called *upper global reflectance* (R_U), *upper global transmittance* (T_U), *lower global reflectance* (R_V) and *lower global transmittance* (T_V)

$$\mathbf{G} = \begin{bmatrix} T_U & R_U \\ R_V & T_V \end{bmatrix} \tag{2.3}$$

Among the superposed bifaces, the two most external ones are called *external bifaces*, the other ones being called *central bifaces*. External bifaces play a special role since they transfer light between the central bifaces and the surrounding media and are thereby directly concerned by the selected geometries for the light sources and for the capturing devices. The fundamental transfer matrices of the upper and the lower external bifaces will be generically denoted in the following way

$$\begin{bmatrix} P_u(\theta) & S_u(\theta) \\ R_u(\theta) & X_u(\theta) \end{bmatrix} \quad \text{and} \quad \begin{bmatrix} X_v(\theta) & R_v(\theta) \\ S_v(\theta) & P_v(\theta) \end{bmatrix} \tag{2.4}$$

where subscripts u or v are relative to the upper or the lower biface respectively, and where:

– $S(\theta)$ is the directional **external reflectance**, which characterizes the reflection of light from the light source to the capturing device;

– $P(\theta)$ is the directional **penetration transmittance**, which characterizes the transmission of light from the surrounding medium to the central bifaces;

– $R(\theta)$ is the directional **internal reflectance**, which characterizes the reflection of light from the central bifaces to themselves;

– $X(\theta)$ is the directional **exit transmittance**, which characterizes the transmission of light from the central bifaces towards the capturing device.

Central bifaces are simply characterized by their upper and lower reflectance and transmittance, i.e. by a fundamental transfer matrix of the form

$$\begin{bmatrix} T(\theta) & R(\theta) \\ R'(\theta) & T'(\theta) \end{bmatrix} \tag{2.5}$$

Fundamental transfer matrices (2.4) and (2.5) will be converted into particular transfer matrices when the illumination and observation condition will have been specified. Fig. 2.4 shows a multiface composed of three bifaces, called "upper", "central" and "lower". Their respective upper and lower reflectances and transmittances are termed like in Eqs. (2.4) and (2.5).

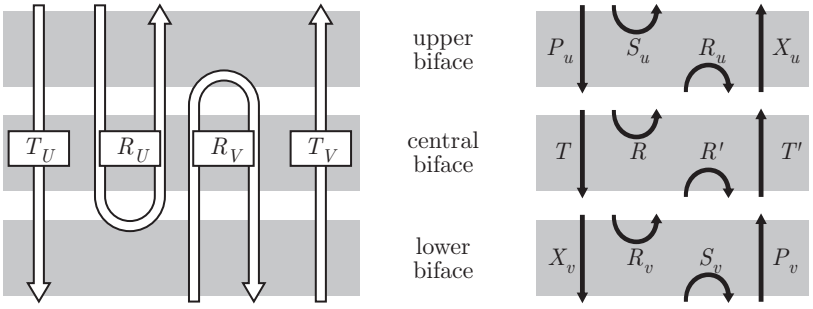

Fig. 2.3: Global reflectances and transmittances of a multiface (left) and reflectances and transmittances of the upper, the central and the lower bifaces (right). The letters S, P, R and X designate respectively external reflectances, penetration transmittances, internal reflectances and exit transmittances.

The classification into transparent, scattering and Lambertian bifaces introduced in Sect. 2.2.2 also applies for multifaces, with the following properties:

– **Transparent multifaces** are composed only of transparent bifaces;

– **Lambertian multifaces** have Lambertian external bifaces, but can have any type of central bifaces[1];

– **Scattering multifaces** are multifaces that are neither transparent nor Lambertian.

Summary

Multilayer specimen are assumed to be composed of planar optical elements called "bifaces" having homogenous and isotropic properties at the macroscopic scale. Three types of bifaces are distinguished: those which do not scatter light are called "transparent bifaces", those which scatter light are called "scattering bifaces", and those which, due to

[1] With Lambertian external bifaces, the incident light is perfectly diffused upon penetration. The light emerging at both sides of the multiface are uniformly distributed (Lambertian). Thus, the multiface as the same properties as a Lambertian biface.

strong scattering, reflect and transmit Lambertian light independently of the geometry of illumination are called “Lambertian bifaces”.

A biface has two “faces” corresponding to its two lightenable sides. Each face is characterized by its directional reflectance and transmittance. Thus, the biface is characterized by a “fundamental transfer matrix” containing the directional reflectances and transmittances of its two faces. Lambertian bifaces are an exception, since their face reflectance and transmittance are invariant. They are characterized by an “invariant transfer matrix”.

When specific geometries of illumination and observation are considered, faces have a particular reflectance and transmittance and bifaces have a “particular transfer matrix”. When the geometry of observation is not specified, it should be considered that the solid angle of observation is the whole hemisphere.

The multifaces result from the superposition of bifaces. The two bifaces in direct contact with the surrounding media are called “external”. They are characterized by an “external reflectance”, a “penetration transmittance”, an “internal reflectance” and an “exit transmittance”.

The two next chapters are dedicated to the characteristics of transparent bifaces (Chapter 3), of scattering and Lambertian bifaces (Chapter 4), and of multifaces (Chapter 5). The specification of the illumination and observation geometries is presented in Chapter 6, where the terminology specific to the external bifaces will be used.

Chapter 3.
Optical properties of transparent bifaces

Transparent bifaces reflect and transmit light without scattering. Directional light is split into a pair of reflection and transmission directions, called the regular directions, which are determined by Snell's laws (Sect. 2.1). When the two surrounding media have different refractive indices, the directions of transmission and of incidence are different. We have three types of transparent bifaces: flat interfaces, characterized by the Fresnel formulae (Sect. 2.2), transparent layers, characterized by Beer's law (Sect. 2.3), and transparent multifaces, resulting from the superposition of flat interfaces and transparent layers. Sect. 2.4 presents one example of transparent multiface, composed of a transparent layer bounded by flat interfaces.

3.1 Generalities on transparent bifaces

Bifaces are transparent when they do not scatter light (Sect. 2.3). The images of an object that they reflect and transmit are perfectly clear. Among the transparent bifaces, we find the flat interfaces between two media of different refractive indices, and the transparent layers, i.e. the absorbing but nonscattering layers of constant thickness. Stacked transparent layers, composed of an alternation of transparent layers and flat interfaces, are also transparent bifaces since none of their components scatter light. Mirrors are special cases, composed of only one face having a zero transmittance.

The two faces of transparent bifaces may have a different reflectance and a different transmittance. However, both faces reflect and transmit a directional incident light into a single pair of directions, the *regular directions*, determined by Snell's laws. They are completely characterized by their directional reflectance and transmittance, from which one may deduce their diffuse and Lambertian reflectances and transmittances.

3.1.1 Snell's laws

The principal characteristic of transparent faces consists of the bijective relations existing between the directions of incidence, of reflection and of transmission.

Let us consider an incident flux coming from direction (θ_i,ϕ_i), also denoted by the differential solid angle $d\omega_i = \sin\theta_i d\theta_i d\phi_i$. The reflected and transmitted fluxes are also directional, flowing respectively into directions (θ_r,ϕ_r) and (θ_t,ϕ_t), denoted by the differential solid angles $d\omega_r = \sin\theta_r d\theta_r d\phi_r$ and $d\omega_t = \sin\theta_t d\theta_t d\phi_t$ (Fig. 3.1). These directions are related by *Snell's laws*, which are generally formulated for flat interfaces, but still remain valid for any transparent biface:

1. The three directions of incidence, of reflection and of transmission belong to a same plane, the *plane of incidence*, also containing the normal of the face. Therefore, zenithal

angles are such that $\phi_r = \phi_t = \phi_i + \pi$.

2. The angles of reflection and of incidence are equal, i.e. $\theta_r = \theta_i$.

3. The angles of transmission and of incidence are related by the "sine formula" involving the refractive indices of the biface's surrounding media, n_i and n_t

$$n_i \sin\theta_i = n_t \sin\theta_t \tag{3.1}$$

Reflection and transmission directions given by Snell's laws are called the *regular directions*. The regular direction of reflection is also called *specular direction*. When the media surrounding the transparent biface have different refractive indices ($n_i \neq n_t$), the direction of transmission differs from the direction of incidence and is called *direction of refraction.*

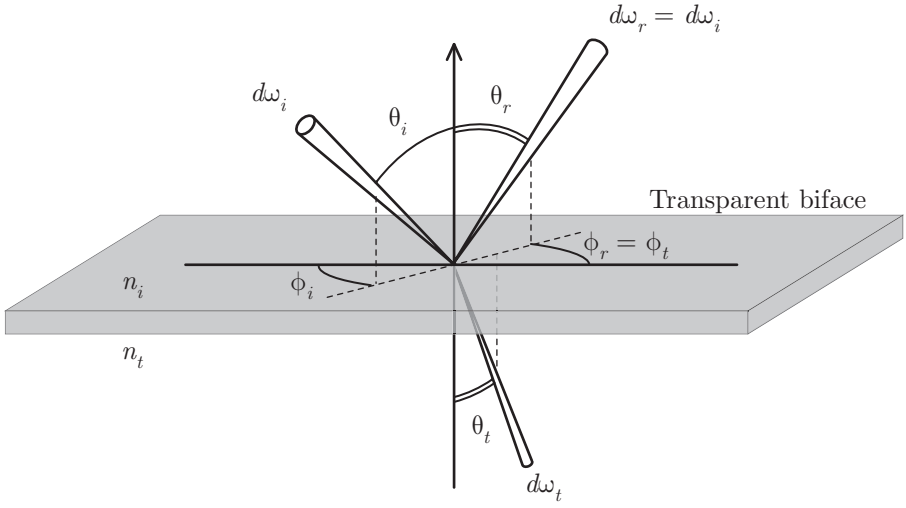

Fig. 3.1: Directional incident flux illuminating a transparent face surrounded by media of respective refractive indices $n_i \neq n_t$. The incidence, the reflection and the transmission solid angles belong to the plane of incidence. The reflection conserves the angle and the solid angle of incidence. The refraction modifies the angle and the solid angle of incidence.

Let us find the relationship between $d\omega_i$, $d\omega_r$ and $d\omega_t$. According to Snell's first law, one has $d\phi_i = d\phi_r = d\phi_t$. It follows from Snell's second law that $\sin\theta_i d\theta_i = \sin\theta_r d\theta_r$ and therefore that the reflection and incidence solid angles are equal ($d\omega_r = d\omega_i$). For the transmission, by differentiating Eq. (3.1), one finds that $n_i \cos\theta_i d\theta_i = n_t \cos\theta_t d\theta_t$. Let us write the member-by-member product of this relation with Eq. (3.1), and multiply both sides with the azimuthal solid angles $d\phi_i = d\phi_t$. One obtains

$$n_i \sin\theta_i \cdot n_i \cos\theta_i d\theta_i \cdot d\phi_i = n_t \sin\theta_t \cdot n_t \cos\theta_t d\theta_t \cdot d\phi_t \tag{3.2}$$

which may be written as

$$n_i^2 \cos\theta_i d\omega_i = n_t^2 \cos\theta_t d\omega_t \tag{3.3}$$

Obviously, when $n_i = n_t$, the incident light exits the transparent biface in the same direction as the direction of incidence, with the same solid angle.

3.1.2 Radiance invariance at a transparent face

We are now interested in the transmission of directional flux across a transparent biface. We would like to find the relationship[1] between the incident radiance L_i and the transmitted radiance L_r.

The solid angles associated to these radiances satisfy Eq. (3.3). By multiplying both members of Eq. (3.3) by an elemental area ds, one obtains the relation

$$n_i^2 ds \cos\theta_i d\omega_i = n_t^2 ds \cos\theta_t d\omega_t \tag{3.4}$$

which generalizes the principle of reciprocity of transfer volume expressed by Eq. (1.11). The incident element of flux $d^2\Phi_i$ is attenuated by a factor $T(\theta_i)$ when crossing the biface, $T(\theta_i)$ being the directional transmittance of the biface. The transmitted flux is $d^2\Phi_t = T(\theta_i)d^2\Phi_i$. The transmitted radiance L_t is

$$L_t = \frac{d^2\Phi_t}{ds\cos\theta_t d\omega_t} = \frac{T(\theta_i)\, d^2\Phi_i}{\left(n_i/n_t\right)^2 ds\cos\theta_i d\omega_i} = \left(\frac{n_t}{n_i}\right)^2 T(\theta_i)\frac{d^2\Phi_i}{ds\cos\theta_i d\omega_i} \tag{3.5}$$

The righter fraction in Eq. (3.5) corresponds to the incident radiance L_i

$$L_t = \left(\frac{n_t}{n_i}\right)^2 T(\theta_i) L_i \tag{3.6}$$

Eq. (3.6) generalizes the radiance invariance principle expressed by Eq. (1.12), embodying the refraction at the interface [Wol98]. The term $\left(n_t/n_i\right)^2$, characterizing the effect of the refraction, becomes one as the two media surrounding the transparent biface are of same refractive index.

Remark: We may develop a similar expression as (3.6) for the reflection of radiance. It can be easily shown that

$$L_r = R(\theta_i) L_i \tag{3.7}$$

with $R(\theta_i)$ the directional reflectance of the transparent biface.

3.1.3 Reflectance and transmittance of transparent bifaces

A transparent face is completely characterized by its directional reflectance $R(\theta)$ and its directional transmittance $T(\theta)$, which may be directly determined by optical laws (e.g. Fresnel formulae for flat interfaces or Beer's law for transparent layers) or should be obtained using a model (e,g., for stacked transparent layers having different refractive indices, by a multiple reflection transmission model).

---

[1] This relation has been established by McCluney in [McCL94, p. 112] in the particular case of a flat interface between two media of different refractive indices.

The polarization of the incident light shall be taken into account. We consider natural light, which is modeled as the sum of two independent linearly polarized components: a component polarized in parallel to the incidence plane, and a component polarized perpendicularly [BW99, p. 47]. We note $E_i^{\perp}$ and $E_i^{\parallel}$ the corresponding irradiances and E_i the total irradiance of natural light

$$E_i = E_i^{\perp} + E_i^{\parallel} \tag{3.8}$$

Since natural light is unpolarized in average, the polarized irradiances are equal

$$E_i^{\perp} = E_i^{\parallel} = \frac{E_i}{2} \tag{3.9}$$

When the irradiance E_i is reflected by a transparent biface, the reflected irradiance E_r is composed of a parallel component $E_r^{\perp} = R^{\perp}(\theta)E_i^{\perp}$ and a perpendicular component $E_r^{\parallel} = R^{\parallel}(\theta)E_i^{\parallel}$. The directional reflectance $R(\theta)$ for incident natural light is

$$R(\theta) = \frac{1}{2}\left[R^{\perp}(\theta) + R^{\parallel}(\theta)\right] \tag{3.10}$$

Likewise, the directional transmittance $T(\theta)$ for incident natural light is

$$T(\theta) = \frac{1}{2}\left[T^{\perp}(\theta) + T^{\parallel}(\theta)\right] \tag{3.11}$$

Every transparent face is characterized by a fundamental transfer matrix whose elements are its upper and lower directional reflectances and transmittances for natural light

$$\begin{bmatrix} T_u(\theta) & R_u(\theta) \\ R_v(\theta) & T_v(\theta) \end{bmatrix} \tag{3.12}$$

3.2 Flat interfaces

Two media of different refractive indices have in common a planar border called *interface*. If one of the media is metallic, its refractive index is a complex number, whose real part ν represents the *simple index of refraction* and whose imaginary part κ represents the *attenuation index* [BW99, p. 737], also called *extinction coefficient*. The interface has a *relative index of refraction* $n = n_1/n_0$ defined as the ratio of the refractive index of the medium of transmission (n_1) to the refractive index of the medium of incidence (n_0).

3.2.1 Fresnel formulae

The fractions of directional incident flux (or element of irradiance) that are reflected and transmitted by the interface are respectively called *reflection coefficient* and *transmission coefficient*. They are given by Fresnel formulae. They depend on the relative refractive index of the interface and the direction and the polarization of the incident light. The notions presented here are stated in detail in [BW99, pp. 40–53].

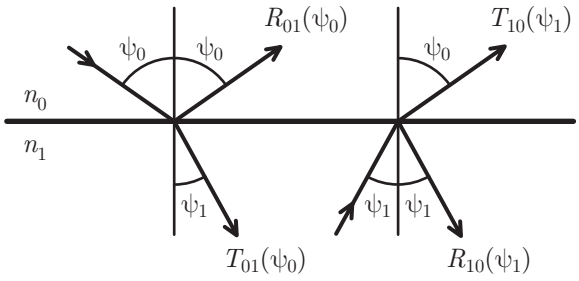

Fig. 3.2: Fresnel reflection and transmission coefficients giving the directional reflectances and transmittances of both faces of a flat interface between two media of refractive indices n_0 and n_1.

Let us consider a directional light coming from medium 0 at angle θ_0. The corresponding angle of refraction is $\theta_1 = \arcsin(\sin\theta_0/n)$ [Eq. (3.1)]. When n is complex (metallic reflection), θ_1 is a complex angle having therefore only an algebraic meaning. For the perpendicular component the reflection coefficient $R_{01}^{\perp}(\theta_0)$ is

$$R_{01}^{\perp}(\theta_0) = \frac{\sin^2(\theta_0 - \theta_1)}{\sin^2(\theta_0 + \theta_1)} \tag{3.13}$$

For the parallel component, the reflection coefficient is

$$R_{01}^{\parallel}(\theta_0) = \frac{\tan^2(\theta_0 - \theta_1)}{\tan^2(\theta_0 + \theta_1)} \tag{3.14}$$

Fresnel formulae (3.13) and (3.14) can also be presented under an expanded form as functions of the angle of incidence θ_0, and the relative index of refraction of the interface $n = \nu + i\kappa$ [Gla95]

$$R_{01}^{\perp}(\theta_0) = \frac{(a - \cos\theta_0)^2 + b^2}{(a + \cos\theta_0)^2 + b^2} \tag{3.15}$$

and

$$R_{01}^{\parallel}(\theta_0) = R_{01}^{\perp}(\theta_0)\frac{(a + \cos\theta_0 - 1/\cos\theta_0)^2 + b^2}{(a - \cos\theta_0 + 1/\cos\theta_0)^2 + b^2} \tag{3.16}$$

with a and b given by

$$\begin{aligned} 2a^2 &= \sqrt{(\nu^2 - \kappa^2 - \sin^2\theta_0)^2 + 4\nu^2\kappa^2} + (\nu^2 - \kappa^2 - \sin^2\theta_0) \\ 2b^2 &= \sqrt{(\nu^2 - \kappa^2 - \sin^2\theta_0)^2 + 4\nu^2\kappa^2} - (\nu^2 - \kappa^2 - \sin^2\theta_0) \end{aligned} \tag{3.17}$$

When both media have a real refractive index, the relative index of refraction of the interface n is also real. The reflection and the transmission are said to be *vitreous*. The Fresnel formulae become

$$R_{01}^{\perp}(\theta_0) = \left(\frac{\cos\theta_0 - \sqrt{n^2 - \sin^2\theta_0}}{\cos\theta_0 + \sqrt{n^2 - \sin^2\theta_0}} \right)^2 \tag{3.18}$$

and

$$R_{01}^{\parallel}(\theta_0) = \left(\frac{n^2\cos\theta_0 - \sqrt{n^2 - \sin^2\theta_0}}{n^2\cos\theta_0 + \sqrt{n^2 - \sin^2\theta_0}} \right)^2 \tag{3.19}$$

For natural incident light, according to Eq. (3.10), the Fresnel reflection coefficient is

$$R_{01}(\theta_0) = \frac{1}{2}\left[R_{01}^{\perp}(\theta_0) + R_{01}^{\parallel}(\theta_0) \right] \tag{3.20}$$

The polarized reflection coefficients $R_{01}^{\perp}(\theta_0)$ and $R_{01}^{\parallel}(\theta_0)$ being different, the two linearly polarized irradiances $E_r^{\perp}$ and $E_r^{\parallel}$ are also different [BW99, p. 46]. It follows that the reflected light is in average partially polarize. If that light reaches again an interface, the reflection on this second interface cannot be characterized by (3.20) since its incident light is not unpolarized. However, the reflected light is still incoherent, which means that irradiances components $E_r^{\perp}$ and $E_r^{\parallel}$ are independent of each other. One can consider separately the reflection of each component by the second interface and sum afterwards their respective contribution.

The Fresnel transmission coefficient is defined by

$$T_{01}(\theta_0) = \frac{1}{2}\left[T_{01}^{\perp}(\theta_0) + T_{01}^{\parallel}(\theta_0) \right] \tag{3.21}$$

It is related to the reflection coefficient by the principle of conservation of the energy at the interface

$$T_{01}(\theta_0) = 1 - R_{01}(\theta_0) \tag{3.22}$$

which is also valid for the parallel and the perpendicular polarizations. Like for the reflection, the light transmitted across the interface is incoherent and partially polarized, i.e. the two transmitted linearly-polarized irradiances are independent but not equal.

For both polarizations, and thereby for natural light, the reflection coefficients satisfy the following properties of reciprocity

$$R_{01}(\theta_0) = R_{10}(\theta_1) \tag{3.23}$$

and

$$T_{01}(\theta_0) = T_{10}(\theta_1) \tag{3.24}$$

with θ_0 and θ_1 related by Snell's third law [Eq. (3.1)].

3.2.2 Reflectance and transmittance of flat interfaces

Since reflection coefficients are defined as ratios of a reflected flux to a directional incident flux, they are directional reflectances. Likewise, transmission coefficients are direc-

tional transmittances. Therefore, flat interfaces between media of refractive indices n_0 and n_1 have the fundamental transfer matrix

$$\begin{bmatrix} T_{01}(\theta) & R_{01}(\theta) \\ R_{10}(\theta) & T_{10}(\theta) \end{bmatrix} \tag{3.25}$$

In Fig. 3.2, the flat interface is illuminated at angle ψ on its upper face and at angle ψ_1 on its lower face. Using the notations introduced in Sect. 2.3 for such an illumination geometry, the interface has the particular transfer matrix

$$^{dir(\psi_0)\rightarrow}\begin{bmatrix} T_{01}(\theta) & R_{01}(\theta) \\ R_{10}(\theta) & T_{10}(\theta) \end{bmatrix}_{\leftarrow dir(\psi_1)} = \begin{bmatrix} T_{01}(\psi_0) & R_{01}(\psi_0) \\ R_{10}(\psi_1) & T_{10}(\psi_1) \end{bmatrix} \tag{3.26}$$

Let us now consider Lambertian illuminations. The Lambertian reflectance and transmittance of the upper face are called r_{01} and t_{01}. Those of the lower face are called r_{01} and t_{01}. They derive from Fresnel reflection and transmission coefficients, which are directional reflectances and transmittances, according to Eq. (1.29)

$$r_{01} = \int_{\theta=0}^{\pi/2} R_{01}(\theta)\sin 2\theta d\theta \,, \tag{3.27}$$

$$t_{01} = \int_{\theta=0}^{\pi/2} T_{01}(\theta)\sin 2\theta d\theta \,, \tag{3.28}$$

$$r_{10} = \int_{\theta=0}^{\pi/2} R_{10}(\theta)\sin 2\theta d\theta \,, \tag{3.29}$$

and

$$t_{10} = \int_{\theta=0}^{\pi/2} T_{10}(\theta)\sin 2\theta d\theta \tag{3.30}$$

Properties (3.22), (3.23) and (3.24) of Fresnel formulae permit to establish the relationship between r_{01}, t_{01}, r_{10} and t_{10}. Eq. (3.22) represents the conservation of energy at the interface for directional illumination. Energy is also conserved for Lambertian illuminations

$$r_{01} + t_{01} = 1 \quad \text{and} \quad r_{10} + t_{10} = 1 \tag{3.31}$$

There also exists a relation between t_{10} and t_{01}. In (3.30), integration is performed according to the angle in the upper medium (now denoted θ_0). Thanks to the bijective relation between θ_0 and the angle θ_1 beneath the interface, one can perform a change of variable and integrate according to θ_1. Relation (3.24) gives $T_{10}(\theta_1) = T_{01}(\theta_0)$. The reciprocity of transfer volume (see Sect. 1.1.3), yields $n_0^2 \sin 2\theta_0 d\theta_0 = n_1^2 \sin 2\theta_1 d\theta_1$. Thus, t_{10} becomes

$$t_{10} = \int_{\theta_0=0}^{\pi/2} T_{10}(\theta_0)\sin 2\theta_0 d\theta_0 = (n_0/n_1)^2 \int_{\theta_0=0}^{\pi/2} T_{01}(\theta_0)\sin 2\theta_0 d\theta_0 \tag{3.32}$$

where the most right integral corresponds to t_{01} [Eq. (3.28)]. The Lambertian transmittances of the upper and the lower faces of a flat interface are therefore related by

$$t_{10} = \left(n_0/n_1\right)^2 t_{01} \tag{3.33}$$

When both its faces receive a Lambertian illumination, using the notation introduced in Sect. 2.3, the flat interface has the particular transfer matrix

$$\overset{L\rightarrow}{\begin{bmatrix} T_{01}(\theta) & R_{01}(\theta) \\ R_{10}(\theta) & T_{10}(\theta) \end{bmatrix}}_{\leftarrow L} = \begin{bmatrix} t_{01} & r_{01} \\ r_{10} & t_{10} \end{bmatrix} = \begin{bmatrix} t_{01} & 1-t_{01} \\ 1-t_{01}/n^2 & t_{01}/n^2 \end{bmatrix} \tag{3.34}$$

Judd [Jud42] tabulated the values of directional (0° and 45°) and Lambertian reflectances and transmittances for real relative refractive indices comprised between 1 and 2. For instance, considering an interface of refractive index 1.5, Eq. (3.34) takes the values

$$\begin{bmatrix} t_{01} & r_{01} \\ r_{10} & t_{10} \end{bmatrix} \simeq \begin{bmatrix} 0.9 & 0.1 \\ 0.6 & 0.4 \end{bmatrix} \tag{3.35}$$

3.3 Transparent layers

Transparent layers are layers made of a homogenous absorbing but nonscattering medium having flat and parallel boundaries. Light crosses them along a straight line without reflection. They have therefore a null BRDF and a null reflectance. Their two faces have the same directional transmittance $T(\theta)$, determined by Beer's law. They are always considered separately from their bounding interfaces, i.e. they are assumed to have the same refractive index as their surrounding media.

3.3.1 Beer's law

A directional flux traversing a path of length x within a nonscattering medium of absorption coefficient α is attenuated by a factor Θ given by Beer's law [Per95]

$$\Theta = e^{-\alpha x} \tag{3.36}$$

3.3.2 Transmittance of a transparent layer

Directional light crossing a transparent layer perpendicularly to its surface is attenuated by a factor t, called *normal transmittance* of the layer. It is assumed to be independent of the polarization of the incident light. According to Beer's law, t is a function of the layer's thickness h and of its absorption coefficient α

$$t = e^{-\alpha h} \tag{3.37}$$

When directional light comes at angle θ, the length of its path across the layer is $h/\cos\theta$ (Fig. 3.3). It is attenuated by a factor $T(\theta)$ that may be expressed as a function of the normal transmittance t

$$T(\theta) = e^{-\alpha h/\cos\theta} = t^{1/\cos\theta} \tag{3.38}$$

$T(\theta)$ is the directional transmittance of the transparent layer. The exponent $1/\cos\theta$ is called the *relative path length* of the oblique light.

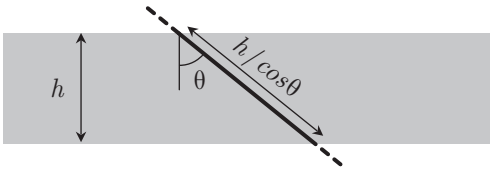

Fig. 3.3: Path length traversed by a light ray crossing at angle θ a transparent layer of thickness h.

The fundamental transfer matrix of a transparent layer is

$$\begin{bmatrix} t^{1/\cos\theta} & 0 \\ 0 & t^{1/\cos\theta} \end{bmatrix} \tag{3.39}$$

Its Lambertian transmittance T is derived from its directional transmittance according to Eq. (1.29)

$$T = \int_{\theta=0}^{\pi/2} T(\theta)\sin 2\theta d\theta = \int_{\theta=0}^{\pi/2} t^{1/\cos\theta}\sin 2\theta d\theta \tag{3.40}$$

3.3.3 Superposed transparent layers

Let us consider k superposed transparent layers having the same refractive index and having respectively the normal transmittances t_1, t_2, …, t_k. They form again a transparent layer, whose normal transmittance t is the product of the normal transmittances t_i ($i = 1, 2, \ldots, k$). The directional transmittance of the multiface is also the product of the respective normal transmittances of the layers

$$T(\theta) = t^{1/\cos\theta} = (t_1 t_2 \ldots t_k)^{1/\cos\theta} = t_1^{1/\cos\theta} t_2^{1/\cos\theta} \ldots t_k^{1/\cos\theta} = T_1(\theta)\, T_2(\theta) \ldots T_k(\theta) \tag{3.41}$$

The Lambertian transmittance T of the multiface is expressed as in Eq. (3.40) with the directional transmittance $T(\theta)$ given by Eq. (3.41). T cannot be obtained by the product of the respective Lambertian transmittances of the transparent layers. This is simply shown by the inequality

$$T = \int T_1(\theta) T_2(\theta) \ldots T_k(\theta)\sin 2\theta d\theta \neq \int T_1(\theta)\sin 2\theta d\theta \int T_2(\theta)\sin 2\theta d\theta \ldots \int T_k(\theta)\sin 2\theta d\theta \tag{3.42}$$

Such an inequality is encountered for every transparent multiface: its Lambertian reflectance (idem for the transmittance) shall be calculated from its directional reflectance but not from the Lambertian reflectances of its faces. We call this the "principle of directionality of multifaces".

3.4 Transparent multifaces

We just saw a special case of transparent multiface, composed only of transparent layers. Let us now consider superpositions of transparent layers and flat interfaces. When they contain two or more interfaces, light is subject to multiple reflections and transmis-

sions. The reflected and transmitted lights, which are directional if the incident light is directional, are composed of a multitude of components, each one having been multiply reflected and transmitted a certain number of times. We shall first calculate the directional reflectance of the multiface for linearly polarized light, i.e. the parallel component and the perpendicular component. Then the contributions of these components are averaged according to Eqs. (3.11).

By way of example, we consider a transparent layer surrounded by two different media of distinct refractive indices. The transparent layer together with its two flat interfaces forms a transparent multiface called "interfaced layer". The refractive indices of the upper medium, the layer and the lower medium are denoted respectively n_0, n_1 and n_2. In order to avoid interference phenomena, the transparent layer, having a normal transmittance t, has a thickness h significantly larger than the wavelengths of light.

We call $R^{\perp}_{012}(\theta_0)$, $R^{\parallel}_{012}(\theta_0)$ and $R_{012}(\theta_0)$ the directional reflectances of the interfaced layer defined respectively for a $\perp$-polarized, a $||$-polarized and an unpolarized incident light coming from medium 0 with an angle θ_0. The corresponding directional transmittances are called respectively $T^{\perp}_{012}(\theta_0)$, $T^{\parallel}_{012}(\theta_0)$ and $T_{012}(\theta_0)$.

3.4.1 Multiple reflection-transmission of polarized directional light

Directional incident irradiance $E_i^{\perp}$, of perpendicular polarization, comes with an angle θ_0 from the upper medium (refractive index n_0). Once having penetrated the layer, it remains directional but is subject to multiple reflections between the interfaces, illustrated by Fig. 3.4. At each interaction with an interface, it is split into a reflected component and a transmitted component. The transmitted components exit definitively the interfaced layer and contribute to the total reflected irradiance or the total transmitted irradiance. The reflected components are alternately reflected by the two interfaces. Our goal is to express the total reflected and transmitted irradiances, called $E_r^{\perp}$ and $E_t^{\perp}$.

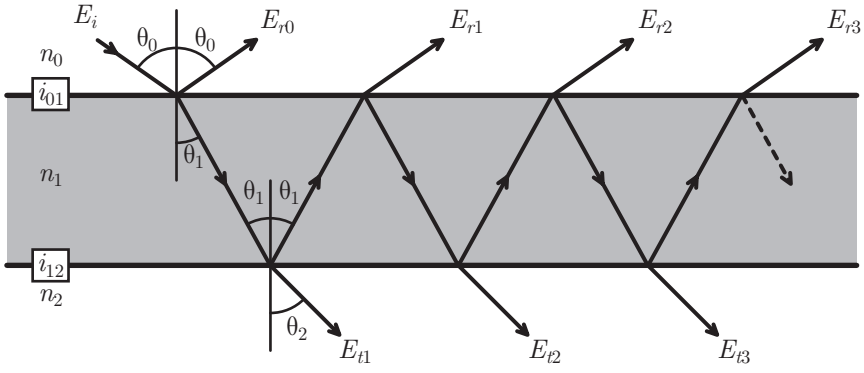

Fig. 3.4: Multiple reflection-transmission of light within a transparent layer interfaced by two flat interfaces.

During the multiple reflection-transmission process, light remains in the plane of incidence and therefore follows a constant azimuthal direction (Snell's first law, Sect. 3.1.1). However, according to the medium in which it propagates, it follows different zenithal angles, noted θ_0 in the upper medium, θ_1 in the transparent layer and θ_2 in the lower medium. According to Snell's third law, angles θ_1 and θ_2 are related to θ_0 by

$$n_0 \sin\theta_0 = n_1 \sin\theta_1 = n_2 \sin\theta_2 \tag{3.43}$$

Let us express the irradiance components emerging successively in the upper and the lower surrounding media. A fraction $R_{01}^{\perp}(\theta_0)$ of the incident irradiance $E_i^{\perp}$ is reflected by the interface i_{01} and follows the specular direction. This reflected component forms an irradiance $E_{r0}^{\perp} = R_{01}^{\perp}(\theta_0) E_i^{\perp}$, which is a first contribution to the total reflected irradiance $E_r^{\perp}$.

A fraction $T_{01}^{\perp}(\theta_0)$ of $E_i^{\perp}$ is refracted into the layer. Along its path of relative length $1/\cos\theta_1$ across the layer, the transmitted light is attenuated by a factor $t^{1/\cos\theta_1}$ due to absorption (Beer's law). Once having reached the interface i_{12}, the irradiance $T_{01}^{\perp}(\theta_0) t^{1/\cos\theta_1} E_i^{\perp}$ is transmitted into the lower medium (fraction $T_{12}^{\perp}(\theta_1)$) and reflected back into the layer (fraction $R_{12}^{\perp}(\theta_1)$). The irradiance transmitted into the lower medium, called $E_{t0}^{\perp}$, is the first contribution to the total transmitted irradiance $E_t^{\perp}$.

$$E_{t0}^{\perp} = T_{01}^{\perp}(\theta_0)\, T_{12}^{\perp}(\theta_1)\, t^{1/\cos\theta_1} E_i^{\perp} \tag{3.44}$$

The irradiance reflected back into the layer, equal to $T_{01}^{\perp}(\theta_0)\, R_{12}^{\perp}(\theta_1)\, t^{1/\cos\theta_1} E_i^{\perp}$, crosses again the layer (attenuation factor $t^{1/\cos\theta_1}$ due to absorption) and is either internally reflected by the interface i_{01} (Fresnel reflection factor $R_{10}^{\perp}(\theta_1)$), or transmitted (Fresnel transmission factor $T_{10}^{\perp}(\theta_1)$) into the upper medium. This irradiance transmitted into the upper medium, $E_{r1}^{\perp}$, is the second contribution to the total reflected irradiance $E_r^{\perp}$

$$E_{r1}^{\perp} = T_{01}^{\perp}(\theta_0)\, R_{12}^{\perp}(\theta_1)\, T_{10}^{\perp}(\theta_1)\, t^{2/\cos\theta_1} E_i^{\perp} \tag{3.45}$$

Then, light continues to be alternately reflected by interfaces i_{01} and i_{12}, with an irradiance component exiting the interfaced layer simultaneously to each reflection. By expressing the successive irradiances $E_{rk}^{\perp}$ exiting in the upper medium and summing them, we obtain the total reflected irradiance, from which we deduce the reflectance of the interfaced layer for the perpendicularly-polarized component. The same is done for the transmittance. The k^{th} irradiance exiting into the upper medium, called $E_{rk}^{\perp}$, crosses $2k$ times the layer and is internally reflected k times by the interface i_{12} and $k-1$ times by the interface i_{10}. The generic expression for $E_{rk}^{\perp}$ is therefore

$$E_{rk}^{\perp} = T_{01}^{\perp}(\theta_0) \left[R_{10}^{\perp}(\theta_1)\right]^{k-1} \left[R_{12}^{\perp}(\theta_1)\right]^{k} t^{2k/\cos\theta_1}(\theta_1)\, T_{10}^{\perp}(\theta_1)\, E_i^{\perp} \quad \left(\text{for } k = 1,\, 2,\, 3...\right) \tag{3.46}$$

The sum of the reflected irradiances $E_{rk}^{\perp}$ ($k = 0,\, 1,\, 2...$) yields the total reflected irradiance $E_r^{\perp}$

$$E_{rk}^{\perp} = R_{01}^{\perp}(\theta_0)\, E_i^{\perp} + \frac{T_{01}^{\perp}(\theta_0)\, T_{10}^{\perp}(\theta_1)}{R_{10}^{\perp}(\theta_1)} E_i^{\perp} \sum_{k=1}^{\infty} \left[R_{10}^{\perp}(\theta_1)\, R_{12}^{\perp}(\theta_1)\, t^{2/\cos\theta_1}\right]^{k} \tag{3.47}$$

The infinite sum is a geometrical series. Since θ_0 and θ_1 are related by Snell's law, we have

$T_{10}^{\perp}(\theta_1) = T_{01}^{\perp}(\theta_0)$. Eq. (3.47) can be simplified as

$$E_r^{\perp} = R_{01}^{\perp}(\theta_0) E_i^{\perp} + \frac{\left[T_{10}^{\perp}(\theta_1)\right]^2 R_{12}^{\perp}(\theta_1) t^{2/\cos\theta_1}}{1 - R_{10}^{\perp}(\theta_1) R_{12}^{\perp}(\theta_1) t^{2/\cos\theta_1}} E_i^{\perp} \tag{3.48}$$

Similarly, the k^{th} irradiance exiting into the lower medium, called $E_{tk}^{\perp}$, crosses $2k+1$ times the layer. It is internally reflected k times by the interface i_{12} and k times by the interface i_{10}. The generic expression for $E_{tk}^{\perp}$ is therefore

$$E_{tk}^{\perp} = T_{01}^{\perp}(\theta_0)\left[R_{10}^{\perp}(\theta_1)\right]^k \left[R_{12}^{\perp}(\theta_1)\right]^k t^{\frac{2k+1}{\cos\theta_1}} T_{12}^{\perp}(\theta_1) E_i^{\perp} \quad (\text{for } k = 0,\ 1,\ 2,\ 3...) \tag{3.49}$$

The sum of the transmitted irradiances $E_{tk}^{\perp}$ yielding a geometric series, gives $E_t^{\perp}$

$$E_t^{\perp} = T_{01}^{\perp}(\theta_0)\, T_{12}^{\perp}(\theta_1)\, t^{1/\cos\theta_1} E_i^{\perp} \sum_{k=0}^{\infty} \left[R_{10}^{\perp}(\theta_1) R_{12}^{\perp}(\theta_1) t^{2/\cos\theta_1}\right]^k = \frac{T_{01}^{\perp}(\theta_0)\, T_{12}^{\perp}(\theta_1)\, t^{1/\cos\theta_1}}{1 - R_{10}^{\perp}(\theta_1) R_{12}^{\perp}(\theta_1) t^{2/\cos\theta_1}} E_i^{\perp} \tag{3.50}$$

3.4.2 Directional reflectance and transmittance for polarized and natural light

The directional reflectance $R_{012}^{\perp}(\theta_0)$ and transmittance $T_{012}^{\perp}(\theta_0)$ for perpendicularly-polarized incident light are given respectively by the ratio $E_r^{\perp}/E_i^{\perp}$ deduced from Eq. (3.48)

$$R_{012}^{\perp}(\theta_0) = R_{01}^{\perp}(\theta_0) + \frac{\left[T_{10}^{\perp}(\theta_1)\right]^2 R_{12}^{\perp}(\theta_1) t^{2/\cos\theta_1}}{1 - R_{10}^{\perp}(\theta_1) R_{12}^{\perp}(\theta_1) t^{2/\cos\theta_1}} \tag{3.51}$$

and by the ratio $E_t^{\perp}/E_i^{\perp}$ deduced from Eq. (3.50)

$$T_{012}^{\perp}(\theta_0) = \frac{T_{01}^{\perp}(\theta_0)\, T_{12}^{\perp}(\theta_1)\, t^{1/\cos\theta_1}}{1 - R_{10}^{\perp}(\theta_1) R_{12}^{\perp}(\theta_1) t^{2/\cos\theta_1}} \tag{3.52}$$

Since the parallel and the perpendicular polarization components follow the same path within the interfaced layer, directional reflectance $R_{012}^{\parallel}(\theta_0)$ and transmittance $T_{012}^{\parallel}(\theta_0)$ are expressed as $R_{012}^{\perp}(\theta_0)$ and $T_{012}^{\perp}(\theta_0)$ with the adequate Fresnel coefficients

$$R_{012}^{\parallel}(\theta_0) = R_{01}^{\parallel}(\theta_0) + \frac{\left[T_{10}^{\parallel}(\theta_1)\right]^2 R_{12}^{\parallel}(\theta_1) t^{2/\cos\theta_1}}{1 - R_{10}^{\parallel}(\theta_1) R_{12}^{\parallel}(\theta_1) t^{2/\cos\theta_1}} \tag{3.53}$$

and

$$T_{012}^{\parallel}(\theta_0) = \frac{T_{01}^{\parallel}(\theta_0) T_{12}^{\parallel}(\theta_1) t^{1/\cos\theta_1}}{1 - R_{10}^{\parallel}(\theta_1) R_{12}^{\parallel}(\theta_1) t^{2/\cos\theta_1}} \tag{3.54}$$

For natural incident light, the expressions obtained for the perpendicular and the parallel polarization components are averaged

$$R_{012}(\theta_0) = \frac{1}{2}\left[R_{012}^{\perp}(\theta_0) + R_{012}^{\parallel}(\theta_0)\right] \quad \text{and} \quad T_{012}(\theta_0) = \frac{1}{2}\left[T_{012}^{\perp}(\theta_0) + T_{012}^{\parallel}(\theta_0)\right] \tag{3.55}$$

Let us now consider that the directional light comes from the lower medium with an incidence angle θ_2. The description of the multiple reflections occurring within the bonded layer is the same as when light comes from the upper medium. We obtain the same reflectance and transmittance expressions as above with exchanged subscripts 0 and 2. The reflectance $R_{210}(\theta_2)$ and the transmittance $T_{210}(\theta_2)$ of the interfaced layer are

$$R_{210}(\theta_2) = \frac{1}{2}\left[R_{210}^{\perp}(\theta_2) + R_{210}^{\parallel}(\theta_2)\right] \quad \text{and} \quad T_{210}(\theta_2) = \frac{1}{2}\left[T_{210}^{\perp}(\theta_2) + T_{210}^{\parallel}(\theta_2)\right] \tag{3.56}$$

with

$$R_{210}^{*}(\theta_2) = R_{21}^{*}(\theta_2) + \frac{\left[T_{12}^{*}(\theta_1)\right]^2 R_{10}^{*}(\theta_1)\, t^{1/\cos\theta_1}}{1 - R_{12}^{*}(\theta_1) R_{10}^{*}(\theta_1)\, t^{2/\cos\theta_1}} \quad \text{and} \quad T_{210}^{*}(\theta_2) = \frac{T_{21}^{*}(\theta_2)\, T_{10}^{*}(\theta_1)\, t^{1/\cos\theta_1}}{1 - R_{12}^{*}(\theta_1) R_{10}^{*}(\theta_1)\, t^{2/\cos\theta_1}} \tag{3.57}$$

where the symbol * represents either $\perp$ or $\parallel$.

Remark: Let us consider the reciprocity of the directional transmittance of the interfaced layer. According to relation (3.43), we can take Fresnel coefficients $T_{10}^{*}(\theta_1)$ and $T_{21}^{*}(\theta_2)$ in place of $T_{01}^{*}(\theta_0)$ and $T_{12}^{*}(\theta_1)$. Thus, the expression (3.57) for $T_{012}^{*}(\theta_0)$ and the expression for $T_{012}^{*}(\theta_0)$ become identical, for the two polarization components and thereby for natural light

$$T_{210}(\theta_2) = T_{012}(\theta_0) \tag{3.58}$$

Summary

The directional reflectance and transmittance are fundamental functions for the transparent bifaces since they permit to derive the other types of reflectance and transmittance (diffuse and Lambertian). In the case of a flat interface, they are given by Fresnel formulae, and in the case of the transparent layers they are derived from Beer's law. In the case of transparent multifaces, resulting from the superposition of transparent layers and flat interfaces, the directional reflectance and transmittance depend on the polarization of the incident light, due to the Fresnel formulae. Their diffuse and Lambertian reflectances and transmittances must be derived from the directional reflectance and transmittance ("principle of directionality").

As an example of transparent multiface with two flat interfaces, we have developed the directional reflectance and transmittance of transparent layers surrounded by media of different refractive indices. The same reasoning line could be followed for transparent multifaces comprising more than two interfaces. One would consider a directional polarized incident light, express the contribution of the irradiance components exiting into the upper and the lower surrounding media, and average them to obtain the total reflected and transmitted irradiances [SHH06].

For the sake of simplicity, we propose in Chapter 5 a new formalism and a mathematical method thanks to which the directional reflectance and transmittance of multifaces can be obtained much more easily.

Chapter 4.

Optical properties of scattering and Lambertian bifaces

Scattering and Lambertian bifaces scatter light. Directional light is reflected and transmitted into all directions. Using the formalism introduced in Chapter 2, we characterize scattering bifaces by their fundamental transfer matrix, whose elements can be derived from BRDFs and BTDFs, themselves obtainable from an appropriate optical model. We draw up a survey of classical scattering models for two main types of scattering bifaces: rough interfaces (Sect. 4.1) and scattering layers (Sect. 4.2). Strongly scattering layers, which correspond to Lambertian bifaces, are presented separately (Sect. 4.3). They are characterized by an invariant transfer matrix, independently of the geometry of illumination. We show how their invariant upper and lower reflectances and transmittances can be obtained using the Kubelka-Munk model. We introduce a new way of solving the Kubelka-Munk differential equation system using the Laplace transform. We obtain general solutions, convertible into reflectance and transmittance expressions as the boundary conditions are specified. When the layer has no border, its reflectance and transmittance are called "intrinsic". More general expressions are also developed considering the presence of a biface at each of its boundaries.

4.1 Rough interfaces

Rough interfaces are scattering bifaces. They reflect and transmit directional incident light into an enlarged set of directions. Their topography may be represented by a random function h depending on the coordinates x and y of the horizontal plane (Fig. 4.1). Function h is determined by a probability distribution, generally parameterized by a characteristic vertical length, the *root-mean-square (r.m.s.) height* σ, and by a characteristic horizontal length, the *correlation length* τ [Sto95]. Another parameter is also commonly used: the *r.m.s. slope* m, corresponding to the ratio σ/τ [TS67].

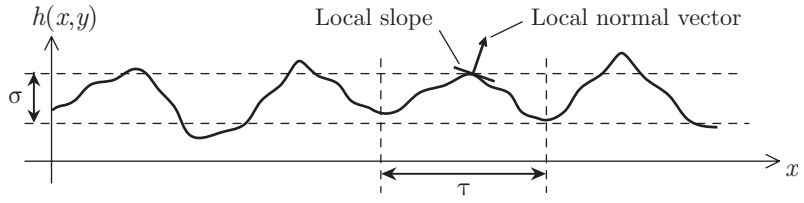

Fig. 4.1: Profile of the elevation function h of a rough interface. The random pattern has a r.m.s. height σ and a correlation length τ. The r.m.s. slope m of the interface is the ratio σ/τ.

Most models assume that the local slope within rough interfaces follows a Gaussian distribution [BS63, Sto95]. In order to ease the application of optical laws, local slopes are converted into local normal vectors [Ger03, HH05], denoted by the differential solid angle $d\omega_h = \sin\theta_h d\theta_h d\phi_h$ (Fig. 5.2). For an isotropic Gaussian distribution of slopes, the probability distribution function D of the normal vector orientations is

$$D(d\omega_h) = \frac{e^{-\tan^2\theta_h/2m^2}}{2\pi m^2 \cos^3(\theta_h)} \tag{3.59}$$

Function D given by Eq. (3.59) is known as the *Beckmann function* [Sto95, CT82, NIK91]. It depends only on the polar angle θ_h due to the assumption of roughness azimuthal isotropy.

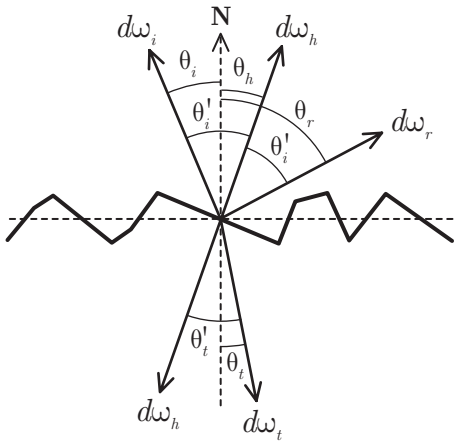

Fig 5.2: 2D representation of a rough interface. The directional incident light (direction denoted by the differential solid angle $d\omega_i$) hits a small protion of interface having the normal vector $d\omega_h$. It is reflected and transmitted into directions $d\omega_r$ and $d\omega_t$ respectively.

4.1.1 Directional and Lambertian reflectances of rough interfaces

In our compositional model, rough interfaces are characterized by their fundamental transfer matrix, whose elements are the upper and lower directional reflectances (resp. R_u and R_v) and transmittances (resp. T_u and T_v)

$$\begin{bmatrix} T_u(\theta) & R_u(\theta) \\ R_v(\theta) & T_v(\theta) \end{bmatrix} \tag{3.60}$$

In a recent work [HH05], we have studied the influence of the surface roughness in the reflectance of printed papers. For this purpose, we have considered a rough paper-air interface illuminated on its upper side by directional incident light (incident angle ψ) and on its lower side by Lambertian light, coming from the paper substrate. For such illumi-

nation geometries, using the notations introduced in Sect. 2.3 [see Eq. (2.2)], the rough interface has the particular transfer matrix

$$\overset{dir(\psi)\rightarrow}{\begin{bmatrix} T_u(\theta) & R_u(\theta) \\ R_v(\theta) & T_v(\theta) \end{bmatrix}_{\leftarrow L}} = \begin{bmatrix} T_u(\psi) & R_u(\psi) \\ r_i & t_i \end{bmatrix} \tag{3.61}$$

where r_i is a Lambertian reflectance, expressed according to Eq. (1.29)

$$r_i = \int_{\theta=0}^{\pi/2} R_v(\theta) \sin 2\theta d\theta \tag{3.62}$$

Parameter r_i represents the fraction of Lambertian light issued from the paper that is internally reflected by the rough interface. It is central in color prediction models since it determines how much light is subject to multiple reflections between the paper and the interface (see Sects. 6.3.1 and 7.1.1 or [HH04]). It can be deduced from reflectance measurements or computed using a model.

We considered a rough air-print interface having a relative refractive index of 1.53. Its slope was assumed to follow a Gaussian distribution function. By modeling the reflection of light on that interface at the print side, we concluded that r_i increases with the r.m.s. slope m but in a very small proportion compared to the reflectance r_{10} [Eq. (3.27)] of a flat interface (Table 4.1). This explains why the Williams-Clapper model (see Sect. 6.3.2) and the Clapper-Yule model (see Sect. 8.3.2), initially restricted to supports having a flat surface (e.g. coated or calendered paper sheets), are also accurate for mate supports [HECC05].

Table 4.1: Evolution with roughness of the Lambertian reflectance r_i of a rough interface, with $n = 1.53$ (variation to the reflectance of a flat interface in percent)

r.m.s slope m	0	0.05	0.1	0.2
$\arctan(m)$	0°	2.9°	5.7°	11.3°
r_i	$r_{10} = 0.614$	0.614 (0.1 %)	0.615 (0.2 %)	0.618 (0.6 %)

Directional reflectances and transmittances of rough interfaces can be deduced from their BRDF and their BTDF using Eq. (1.21). BRDFs and BTDFs may be determined experimentally [EM00, EM01, Sto95] or computed thanks to an optical model.

4.1.2 BRDF and BTDF models

Two main approaches enable the study of reflection and transmission by rough interfaces [NIK91]:

– **Physical optics**, based directly on the electromagnetic wave theory and Maxwell's equations [BW99, p. 1]. Models relying on physical optics shall be used when the wavelength of light is large or comparable to the characteristic lengths of the roughness pat-

terns, specified by the r.m.s. height σ and the correlation length τ [Dur03]. In such case, the diffraction of the incident waves by the corrugations of the interface is dominant. It is assumed that the interface does not have any discontinuity or sharp arc compared to the wavelength of incident light. It may therefore be represented locally by its tangent plane, on which light is reflected according to Snell's law and diffracted because of the small size of the plane. This *tangent plane approximation* is the basis of the Beckmann's model [BS63], also known as *Kirchhoff's approximation* [Ogi91].

– **Geometrical optics**, on the other hand, explains the behavior of light when its wavelength is small compared to the roughness characteristic lengths. Diffraction are assumed to be negligible. *Slope distribution models*, such as the well-known models of Torrance and Sparrow [TS67] and of Cook and Torrance [CT82] consider the rough interface as a set of randomly inclined microfacets reflecting and transmitting light like flat interfaces.

According to slope distributions models [TS67, CT82, NIK91], the BRDF f_R of a rough interface is

$$f_R(d\omega_i,d\omega_r) = \frac{D(\theta_h)\, G(\theta_i,\theta_r)\, R_{01}(\theta'_i)}{4\cos\theta_i \cos\theta_r} \tag{3.63}$$

When the medium of transmission is non-metallic, the BTDF is [Sta01]

$$f_T(d\omega_i,d\omega_t) = \frac{D(\theta_h)\, G(\theta_i,\theta_t)\, T_{01}(\theta'_i)}{\Gamma(\theta'_i)\cos\theta_i \cos\theta_r} \tag{3.64}$$

In Eqs. (3.63) and (3.64), differential solid angles $d\omega_i = \sin\theta_i d\theta_i d\phi_i$, $d\omega_r = \sin\theta_r d\theta_r d\phi_r$ and $d\omega_t = \sin\theta_t d\theta_t d\phi_t$ denote respectively the directions of incidence, of reflection and of transmission (Fig. 4.2); angle θ_h represents the inclination of the interface's local normal vector; it is related to the angles of incidence and reflection by

$$\theta_h = \arccos\left[(\cos\theta_i + \cos\theta_r)/\sqrt{2(1+\cos\theta_i\cos\theta_r + \sin\theta_r\sin\theta_i\cos(\phi_r-\phi_i))}\right]; \tag{3.65}$$

angle θ'_i denotes the local angle of incidence of light and is related to the angles of incidence and reflection by

$$\theta'_i = \frac{1}{2}\arccos\left(\cos\theta_r\cos\theta_i - \sin\theta_r\sin\theta_i\cos(\phi_r-\phi_i)\right); \tag{3.66}$$

function D is the probability distribution function of the local normal vector, given by Eq. (3.59); function G is a shadowing function that is presented below; R_{01} is the Fresnel reflection coefficient of the interface (see Sect. 3.2.1); $\Gamma(\theta'_i)$ expresses the spreading of the transmitted solid angle due to the refraction by the interface

$$\Gamma(\theta'_i) = \frac{\left(\cos\theta'_i - \sqrt{n^2-\sin\theta'_i}\right)^2}{n\sqrt{n^2-\sin\theta'_i}} \tag{3.67}$$

Shadowing: a rough interface may comprise shadow areas, which increase with the roughness and the incidence angle of light. Interface elements belonging to shadow areas do not

contribute to the reflection nor the transmission. This phenomenon is called *shadowing*. Likewise, reflected and transmitted light may be partially blocked by neighboring corrugations. This phenomenon, sometimes called *masking* [TS67], is equivalent to shadowing but depends on the angle of observation instead of the angle of incidence (Fig. 4.3).

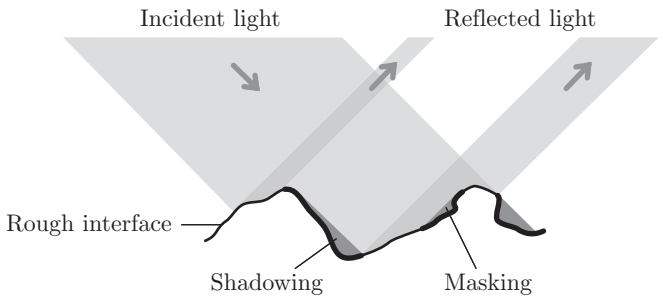

Fig. 4.3: Some areas (bold line) within the rough interface are not illuminated due to shadowing. Some other areas are not observed due to masking.

The fraction of facets that really contributes to the reflection of light from direction $d\omega_i$ to direction $d\omega_r$ is given by function $G(\theta_i,\theta_r)$, product of two similar functions g, one for shadowing, and the other one for masking

$$G(\theta_i,\theta_r) = g(\theta_i)\, g(\theta_r) \tag{3.68}$$

Using a statistical model, Smith computed the following shadowing function g [Smi67]

$$g(\theta,\theta_i') = \begin{cases} \dfrac{1}{\Lambda_m(\theta)+1} & \left(\text{if } \cos\theta_i' > 0\right) \\ 0 & \left(\text{if } \cos\theta_i' < 0\right) \end{cases} \tag{3.69}$$

where θ_i' is the local angle of incidence given by Eq. (3.66) and where function Λ_m, parameterized by the surface's r.m.s. slope m, is defined as

$$\Lambda_m(\theta) = \frac{1}{2}\left[\frac{1}{\sqrt{\pi}} \cdot \frac{\sqrt{2}m}{\cot\theta} \exp\left(-\frac{\cot^2\theta}{2m^2}\right) - \operatorname{erfc}\left(\frac{\cot\theta}{\sqrt{2}m}\right)\right]$$

Note that both functions g in Eq. (3.68) use the same angle θ_i' since, according to Snell's laws, the local angle of incidence is equal to the local angle of reflection (see Fig. 5.2).

Function g is comprised between 0 (facets completely shadowed or masked) and 1 (facets completely illuminated). At small and medium incidence angles, the illuminated fraction of the facet's area is close to 1. The shadowing effect is thus small enough to be neglected. However, ignoring the shadowing at high incidence angles may yield an overestimation of the reflected and transmitted irradiances, and a subsequent violation of the energy conservation principle. According to Bruce [Bru04] and Caron [CLA02], shadowing should be taken into account when the incidence angle is higher than a limit angle θ_{shad}

depending on the r.m.s. slope m of the rough interface

$$\theta_{shad} = \frac{\pi}{2} - \arctan\left(\sqrt{2}m\right) \tag{3.70}$$

The same considerations apply for masking.

4.2 Scattering layers

The optical properties of a medium are generally characterized by its refractive index. If the latter is constant, a light ray crosses the medium along a straight line without any deviation. However, when light encounters small fluctuations of refractive index within the medium, a portion of the incident light is scattered. In the atmosphere, scattering yields the white color of clouds (Mie scattering [Mie08]), the blue color of the sky [ZB03] and the redness of sunsets (Rayleigh scattering [Ray99]). Scattering also occurs in liquids. Milk, for example, is composed of a suspension of almost transparent fat droplets which scatter light and give to milk its white and opaque aspect. In the case of oceans, scattering is coupled to absorption, which produces the characteristic bluish color. Light is also scattered in solid heterogeneous media, such as painting [Sim02], paper, cotton, human tissues [Pra88], etc.

Different types of scattering are encountered according to the composition, shape, size and concentration of the heterogeneities, often considered as particles immerged into a binder. The polarization and the wavelength of the incident light may have a strong influence on scattering. We present here some commonly used parameters and models relative to scattering, mainly borrowed from the works of Durant [Dur03] and of Simonot [Sim02]. We show in particular the distinction between scattering layers and Lambertian layers, the latter being especially studied in Sect. 4.3.

4.2.1 Scattering parameters

A radiance traversing a path of length x into a scattering and absorbing medium undergoes an exponential attenuation T described by the Beer-Lambert law

$$T = e^{-K_{ext}x} \tag{3.71}$$

where K_{ext} is the *extinction coefficient* (in m^{-1}). The inverse of the extinction coefficient is the *extinction free-mean-path length* l_{ext}, characterizing the distance along which a radiance is attenuated by a factor 1/e

$$l_{ext} = 1/K_{ext} \tag{3.72}$$

The extinction coefficient may be decomposed into a component K_{sca} relative to scattering and a component K_{abs} relative to absorption

$$K_{ext} = K_{sca} + K_{abs} \tag{3.73}$$

Free-mean-path lengths are also defined for scattering l_{sca} and for absorption l_{abs}

$$l_{sca} = 1/K_{sca} \quad \text{and} \quad l_{abs} = 1/K_{abs} \tag{3.74}$$

The scattering and absorbing medium is said to be *homogenous* when it has at every point the same coefficients K_{sca} and K_{abs}. Note that Beer's law presented in Sect. 2.3.1 corresponds to the special case where $K_{sca} = 0$.

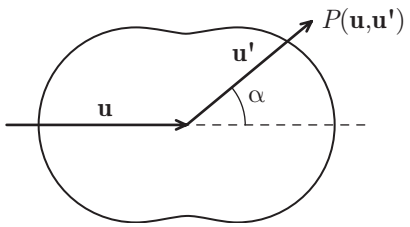

Fig. 4.4: Phase function of a scattering medium.

As an effect of scattering, the path of light is modified. The change of direction is specified by a *phase function*, $P(\mathbf{u},\mathbf{u'})$, giving the density of probability for light to be scattered from an initial direction $\mathbf{u}$ to a direction $\mathbf{u'}$ (Fig. 4.4). $P(\mathbf{u},\mathbf{u'})$ being a probability, it is always positive and is expected to satisfy the condition of normalization

$$\frac{1}{4\pi}\int_{\Sigma} P(\mathbf{u},\mathbf{u}')d\omega' = 1 \tag{3.75}$$

where $d\omega'$ is the differential solid angle associated to the outgoing direction $\mathbf{u'}$ and Σ is the entire sphere. When scattering is isotropic, one has $P(\mathbf{u},\mathbf{u'}) = 1$ for every pair of directions $(\mathbf{u},\mathbf{u'})$. Otherwise, anisotropic scattering may be characterized by a parameter g defined as the average cosine of the scattering angle

$$g = \frac{1}{4\pi}\int_{\Sigma} P(\mathbf{u},\mathbf{u}')\cos(\mathbf{u},\mathbf{u}')d\omega' \tag{3.76}$$

The incident light is mainly scattered backwards when g is close to –1 or forwards when g is close to 1. For isotropic scatterings, $g = 0$. Parameter g is used for defining the *transport free-mean-path length* l_{trans}, corresponding to the distance from which one may consider that light has completely lost the memory of its original direction of incidence

$$l_{trans} = \frac{l_{sca}}{1-|g|} \tag{3.77}$$

The *optical thickness* τ of a scattering or/and absorbing layer having a thickness h and an extinction coefficient K_{ext} is defined as

$$\tau = K_{ext}h \tag{3.78}$$

When $\tau \gg 1$, a directional incident light is almost completely attenuated. When τ is small, the layer is translucid, i.e. we can distinguish an object located beneath the layer. After a certain number of scattering events, light propagates in an isotropic manner, i.e. it becomes Lambertian.

4.2.2 Types of scattering

The notion of optical thickness defined above allows estimating the number of scattering events that a light ray undergoes across a given layer of the considered medium. In the particular case of a weakly absorbing medium ($K_{abs} \ll K_{sca}$), the optical thickness describes the strength of scattering. We may distinguish four scattering modes, according to the value of the optical thickness of the layer:

– ballistic scattering: $\tau \ll 1$ ($h \ll l_{sca}$), in which light is almost not scattered,

– single scattering: $\tau \approx 1$ ($h \approx l_{sca}$) in which light is scattered once in the medium (Rayleigh scattering [Ray99], Mie scattering [Mie08]),

– multiple scattering: $\tau > 1$ ($h > l_{sca}$), in which light is scattered various times [Kor94],

– diffusion: $\tau \gg 1$ ($h \gg l_{sca}$) where scattering events occur so many times that the resulting scattering is isotropic. According to Eq. (3.77), since parameter g defined by Eq. (3.76) is equal to 0, the transport length is given by the scattering length. The incident light has therefore completely lost the memory of its incident direction.

For low concentrations of particles, it is assumed that they do not interact one with each other. Scattering is said to be *independent*. Describing the scattering by one particle is sufficient to determine the scattering by the whole medium. For high concentrations of particles, scattering becomes *dependent*. In the case of independence, geometrical optics may be used when the size of the particles are large compared to the wavelength of the incident light. However, when the particles are small compared to the wavelength, light is diffracted. In this case, scattering may be modeled by the Rayleigh scattering theory [Ray71, Ray99, Des91]. The Mie scattering theory describes the diffraction of light by spherical particles of complex refractive index in a dielectric medium (real refractive index) [Mie08]. Note that, excepted for exceptional phenomena such as the Raman effect, scattering does not modify the wavelength of the incident light.

Coming back to the classification of bifaces introduced in Sect. 2.3, we will consider that a layer is transparent when $h \ll l_{sca}$, Lambertian when $h \gg l_{sca}$. Otherwise, the layer is considered to be a scattering biface.

4.2.3 The radiative transfer equation

In many applications, a simple phenomenological approach, based on the notion of directed light ray and conservation of energy, provides a realistic description of the scattering phenomenon. Considering a sufficiently large portion of the heterogeneous medium, the scattering process is described by a simple equation: the *radiative transfer equation* [Cha60]. A priori, it is valid only when the scattering free-mean-path length l_{sca} is large compared to the wavelength of the incident light and to the dimension of the heterogeneities responsible of the scattering, but specific studies have shown that its domain of validity can be enlarged to other cases [Dur03, Car03].

The radiative transfer equation expresses the conservation of the radiant flux in a given element of volume and a given direction. This energy balance shall be performed everywhere in the medium and in every direction. Let us consider a small cylinder of section dS and of length dl oriented according to the incident direction $\mathbf{u}$. Radiance $L(\mathbf{u})$ decreases along this direction due to absorption and scattering

$$\frac{dL(\mathbf{u})}{dl} = -\big(K_{abs} + K_{sca}\big)L(\mathbf{u}) \tag{3.79}$$

At the same time, the cylinder receives radiances $L(\mathbf{u'})$ from all directions $\mathbf{u'}$ and scatters them partially towards direction $\mathbf{u}$, which increases radiance $L(\mathbf{u})$. The portion of radiance $L(\mathbf{u'})$ that contributes to radiance $L(\mathbf{u})$ is $\frac{K_{sca}}{4\pi}P\big(\mathbf{u'},\mathbf{u}\big)L(\mathbf{u'})d\omega'$, where $P\big(\mathbf{u'},\mathbf{u}\big)$ is the phase function of the considered cylindrical element of volume. By summing up the contributions of all directions $\mathbf{u'}$ and adding the resulting global contribution to Eq. (3.79), one obtains the radiative transfer equation

$$\frac{dL(\mathbf{u})}{dl} = -\big(K_{abs} + K_{sca}\big)L(\mathbf{u}) + \frac{K_{sca}}{4\pi}\int_{\Sigma} P\big(\mathbf{u'},\mathbf{u}\big)L\big(\mathbf{u'}\big)d\omega' \tag{3.80}$$

This equation has no general solution. An exact or approximated solution must be searched for every particular scattering medium. Various solutions have been developed. Let us mention the three principal ones [Sim02]:

– The ***N*-fluxes method**, which allows converting the integrodifferential equation (3.80) into a differential equation system thanks to an angular discretization. Solutions are obtained for azimuthally isotropic media, the discretization being performed only according to the zenithal angle [MR71]; the simplest particular case is the two-flux Kubelka-Munk model [KM31, Kub48]. Four-flux models have also been developed [MLG84, MG86].

– The **discrete ordinate method** [SCWJ88], which is an exact but computationally expansive method. The assumption of azimuthal isotropy is not necessary. Discretization according to the azimuthal angle is avoided thanks to a Fourier series development for the scattered fluxes and a spherical harmonic decomposition of the phase function.

– The **auxiliary function method** [EE02], which avoids angular discretization. An auxiliary function is introduced into the radiative transfer equation and decomposed into spherical harmonics. The radiative transfer equation is thus converted into an integral equation system, which can be solved numerically.

4.3 Lambertian layers

The free-mean-path length l_{sca} of a strongly scattering layer is very small compared to the layer thickness (Sect. 4.2.2). Incident light looses the memory of its initial angular distribution as soon as it penetrates the layer. We can therefore assume that any illumination geometry leads to a same reflectance and a same transmittance, called *intrinsic*. Since light is scattered a large number of times within the layer, it is Lambertian at every point of the layer, especially at the layer's bounding planes. We can also assume that light exiting the layer is unpolarized. Strongly scattering layers satisfy the conditions for being a Lambertian biface (Sect. 2.2) and are thus said to be *Lambertian layers*.

The reflection and transmission by Lambertian layers can be modeled by the Kubelka-Munk two flux model [KM31, Kub48, Kub54], with a satisfying accuracy if the layer is weakly absorbing [Kli71, VN97]. An intent of alternative model relying on Markov chains has been proposed for paper by Simon and Trachsler [ST03]. In the present section, we will present only the Kubelka-Munk model, and propose a new method for solving its famous differential equation system.

4.3.1 Kubelka-Munk two-flux model

The scattering proposed by Kubelka and Munk [KM31] was initially introduced for predicting the reflectance of paints, but it has been also used in a wide range of domains where uniform and infinitely large layers of a scattering medium are encountered. It corresponds to a special case of the radiative transfer theory where the phase function is reduced to a pair of opposite directions or, more precisely, of opposite sets of directions covering respectively the upper and the lower hemispheres [Kub54]. Thus, it is said to be a "two-fluxes scattering model". The model can be equivalently expressed in terms of irradiances instead of fluxes, which corresponds to considering the fluxes relatively to a unit area.

4.3.2 Differential equation system

The interest of the Kubelka-Munk model lies in the simple differential equation system expressing the scattering and absorption phenomena within the layer. The differential equations involve the upward and the downward oriented irradiances, functions of the depth in the layer. Another interest of this model is the fact that the solutions of the differential equation system have an analytical expression.

The layer, having a thickness h, is made of a homogenous absorbing and scattering medium having an absorption coefficient K and a scattering coefficient S, both ones being functions of the wavelength. In the layer, a Lambertian irradiance i_r propagates upwards and a Lambertian irradiance i_t propagates downwards. Both i_r and i_t are functions of the depth x at which they are located in the layer. Depth 0 corresponds to the layer's boundary that receives the incident irradiance I_0. Depth h corresponds to its other boundary (Fig. 4.5).

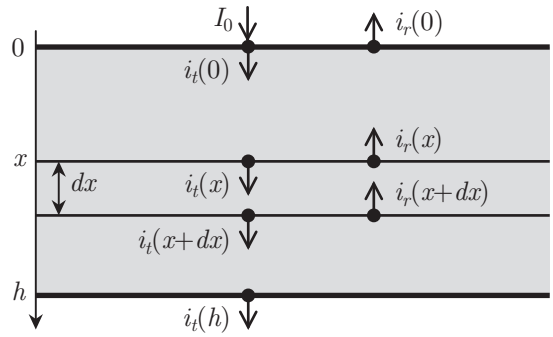

Fig. 4.5: Upward and downward irradiances crossing a sublayer of thickness dx at a depth x in the scattering layer.

Let us consider at a given depth x a sublayer of infinitesimal thickness dx. The sublayer receives the downward irradiance $i_t(x)$ on the one side and the upward irradiance $i_r(x+dx)$ on the other side. In the sublayer, a fraction $S\,dx$ of both irradiances $i_r(x)$ and $i_t(x)$ is backscattered, leading to a mutual exchange of irradiance. A fraction $K\,dx$ is absorbed.

While crossing the sublayer, the upward irradiance $i_r(x+dx)$ loses both the absorbed irradiance $K\,i_r(x)\,dx$ and the backscattered irradiance $S\,i_r(x)\,dx$. It gains the backscattered irradiance $S\,i_t(x)\,dx$. The irradiance $i_t(x)$ leaving the sublayer is therefore

$$i_r(x) = i_r(x+dx) - (K+S)i_r(x)dx + Si_t(x)dx \tag{3.81}$$

The downward irradiance $i_t(x)$ loses the absorbed irradiance $K\,i_t(x)\,dx$ and the backscattered irradiance $S\,i_t(x)\,dx$. It gains the backscattered irradiance $S\,i_r(x)\,dx$. The irradiance $i_t(x+dx)$ leaving the sublayer is

$$i_t(x+dx) = i_t(x) - (K+S)i_t(x)dx + Si_r(x)dx \tag{3.82}$$

According to the definition of the derivative, when $dx \to 0$

$$\frac{d}{dx}i = \frac{i(x+dx) - i(x)}{dx} \tag{3.83}$$

By rearranging Eqs. (3.81) and (3.82), we obtain the Kubelka-Munk differential equation system

$$\begin{cases} \dfrac{d}{dx}i_r(x) = (K+S)i_r(x) - Si_t(x) \\ \dfrac{d}{dx}i_t(x) = Si_r(x) - (K+S)i_t(x) \end{cases} \tag{3.84}$$

4.3.3 Solutions for the differential equation system

There exists a very simple method for solving the differential equation system (3.84), that we have not found anywhere in the literature. Thanks to the Laplace transform [HS98], we can convert the differential equation system into a linear equation system much more easy to solved.

The Laplace transform associates to a causal function $f(x)$ the function $F(p)$ such that

$$F(p) = \int_0^\infty f(t)e^{-pt}dt \tag{3.85}$$

It is linear, i.e. it transforms $af(x) + bg(x)$ into $aF(p) + bG(p)$. The derivative of a function f is transformed into $pF(p) - f(0)$, where the constant $f(0)$ is the value of f at $x = 0$. Calling $I_r(p)$ and $I_t(p)$ the respective transforms of $i_r(x)$ and $i_t(x)$, the differential equation system (3.84) is transformed into the following linear equation system, depending on the two unknown functions $I_r(p)$ and $I_t(p)$

$$\begin{cases} pI_r(p) - i_r(0) = (K+S)I_r(p) - SI_t(p) \\ pI_t(p) - i_t(0) = SI_r(p) - (K+S)I_t(p) \end{cases} \tag{3.86}$$

This system has the two following solutions

$$I_r(p) = \frac{i_r(0)(p+aS) - Si_t(0)}{p^2 - b^2S^2} \tag{3.87}$$

and

$$I_t(p) = \frac{i_t(0)(p - aS) + Si_r(0)}{p^2 - b^2S^2} \tag{3.88}$$

with

$$a = (K + S)/S \quad \text{and} \quad b = \sqrt{a^2 - 1} \tag{3.89}$$

Since $p/\left(p^2 - b^2S^2\right)$ and $bS/\left(p^2 - b^2S^2\right)$ are the respective Laplace transforms of $\cosh(bSx)$ and $\sinh(bSx)$, one concludes[1] that $I_r(p)$ is the Laplace transform of

$$i_r(x) = i_r(0)\cosh(bSx) + \frac{1}{b}\left(a i_r(0) - i_t(0)\right)\sinh(bSx) \tag{3.90}$$

and $I_t(p)$ is the Laplace transform of

$$i_t(x) = i_t(0)\cosh(bSx) + \frac{1}{b}\left(i_r(0) - a i_t(0)\right)\sinh(bSx) \tag{3.91}$$

Expressions (3.90) and (3.91) are the general solutions of the Kubelka-Munk differential equation system [HH06].

4.3.4 Intrinsic reflectance and transmittance of a Lambertian layer

Let us now derive from general solutions (3.90) and (3.91) the intrinsic reflectance and transmittance of a scattering layer considered without interface nor any type of biface at its boundaries. An incident irradiance I_0 illuminates the upper side of the scattering layer. The intrinsic reflectance of the scattering layer is the fraction of the incident irradiance I_0 that exits the layer at the upper side, i.e. the ratio $i_r(0)/I_0$. The intrinsic transmittance is the fraction of the incident irradiance I_0 exiting at the lower side, i.e. the ratio $i_t(h)/I_0$. Let us therefore express $i_r(0)$ and $i_t(h)$.

At $x = 0$, the downward irradiance $i_t(0)$ is the incident irradiance

$$i_t(0) = I_0 \tag{3.92}$$

At $x = h$, the upward irradiance $i_r(h)$ is zero, since the scattering layer is not illuminated from below

$$i_r(h) = 0 \tag{3.93}$$

By setting $x = h$ and inserting relations (3.92) and (3.93) into Eq. (3.90), one obtains

$$i_r(0) = I_0 \frac{\sinh(bSh)}{b\cosh(bSh) + a\sinh(bSh)} \tag{3.94}$$

---

[1] When a function has a Laplace transform, this latter is unique. The converse is also true. The Laplace transform is bijective from the set of functions admitting a Laplace transform to the set of Laplace transforms.

Likewise, one takes $x = h$ and replaces, in Eq. (3.91), $i_t(0)$ and $i_r(0)$ by their respective expressions (3.92) and (3.94). One derives from Eq. (3.89) the relation $b^2 = a^2 - 1$. Finally, using the classical relation of hyperbolic trigonometry $\cosh^2(bSh) - \sinh^2(bSh) = 1$, one obtains

$$i_t(h) = I_0 \frac{b}{b\cosh(bSh) + a\sinh(bSh)} \tag{3.95}$$

The ratio $i_r(0)/I_0$ gives the intrinsic reflectance ρ of the scattering layer

$$\rho = \frac{i_r(0)}{I_0} = \frac{\sinh(bSh)}{b\cosh(bSh) + a\sinh(bSh)} \tag{3.96}$$

and the ratio $i_r(h)/I_0$ gives its intrinsic transmittance τ

$$\tau = \frac{i_t(h)}{I_0} = \frac{b}{b\cosh(bSh) + a\sinh(bSh)} \tag{3.97}$$

As expected, these expressions of intrinsic reflectance and transmittance are identical to those derived by classical solving methods [Kub48].

4.3.5 Lambertian layer bordered by bifaces

Let us now consider that the layer is bounded at $x = 0$ by a biface whose upper face has a reflectance s_u and a transmittance p_u and whose lower face has a reflectance r_u and a transmittance x_u. At $x = h$, the Lambertian layer is bordered by another biface having a reflectance r_v and a transmittance x_v (Fig. 4.6).

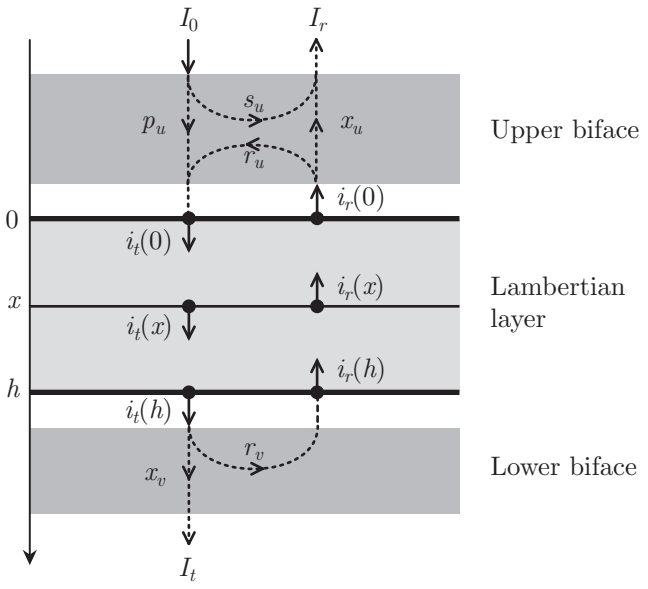

Fig. 4.6: Reflections and transmissions occurring at the boundaries of the Lambertian layer.

This biface receives on its upper face an irradiance I_0 coming from the light source. A fraction s_u of I_0 is directly reflected and a fraction p_u crosses the biface. On its lower face, it receives the upward irradiance $i_r(0)$ from the Lambertian layer. A fraction r_u is internally reflected and a fraction x_u emerges across the biface. Hence, at $x = 0$, the downward irradiance $i_t(0)$ is

$$i_t(0) = p_u I_0 + r_u i_r(0) \tag{3.98}$$

At $x = h$, the lower biface receives the downward irradiance $i_t(h)$ and reflects it in a proportion r_v. There is no light coming from below. Hence, the upward irradiance $i_r(h)$ is

$$i_r(h) = r_v i_t(h) \tag{3.99}$$

Let us insert the boundary equation (3.98) into the general solution (3.90) of $i_r(x)$ for $x = h$, and use the boundary equation (3.99)

$$i_t(h) = \frac{1}{r_v} i_r(0)\cosh(bSh) + \frac{1}{b r_v}\big[a\, i_r(0) - \big[p_u I_0 + r_u i_r(0)\big]\big]\sinh(bSh) \tag{3.100}$$

We also insert the boundary equation (3.98) into the solution (3.91) of $i_t(x)$ for $x = h$

$$i_t(h) = \big[p_u I_0 + r_u i_r(0)\big]\cosh(bSh) + \frac{1}{b}\big(i_r(0) - a\big[p_u I_0 + r_u i_r(0)\big]\big)\sinh(bSh) \tag{3.101}$$

Eqs. (3.100) and (3.101) form a linear equation system depending on the two unknown variables $i_r(0)$ and $i_t(h)$, i.e. on the two irradiances exiting the print. The solutions of this equation system are

$$i_r(0) = p_u I_0 \frac{\big(1 - a r_v\big)\sinh(bSh) + b\, r_v \cosh(bSh)}{\big(a - r_u - r_v + a r_u r_v\big)\sinh(bSh) + b\big(1 - r_u r_v\big)\cosh(bSh)} \tag{3.102}$$

and

$$i_t(h) = p_u I_0 \frac{b}{\big(a - r_u - r_v + a r_u r_v\big)\sinh(bSh) + b\big(1 - r_u r_v\big)\cosh(bSh)} \tag{3.103}$$

A fraction x_u of irradiance $i_r(0)$ emerges across the upper biface. It forms, conjointly with the irradiance $s_u I_0$ reflected by the upper biface, a total irradiance I_r

$$I_r = s_u I_0 + x_u i_r(0) \tag{3.104}$$

The ratio I_r / I_0 corresponds to the global reflectance R_b of the bordered Lambertian layer

$$R_b = s_u + p_u x_u \frac{\big(1 - a r_v\big)\sinh(bSh) + b r_v \cosh(bSh)}{\big(a - r_u - r_v + a r_u r_v\big)\sinh(bSh) + b\big(1 - r_u r_v\big)\cosh(bSh)} \tag{3.105}$$

Likewise, a fraction x_v of irradiance $i_t(h)$ emerges across the lower biface, forming an emerging irradiance $I_t = x_v i_t(h)$. The ratio I_t / I_0 is the global transmittance T_b of the bordered Lambertian layer

$$T_b = p_u x_v \frac{b}{(a - r_u - r_v + a r_u r_v)\sinh(bSh) + b(1 - r_u r_v)\cosh(bSh)} \tag{3.106}$$

Remark: In the particular case where there is no bordering biface on the upper side, we have $s_u = 0$, $p_u = 1$, $r_u = 0$ and $x_u = 1$. By inserting these values into Eqs. (3.105) and (3.106), we obtain the global reflectance and transmittance of the layer bordered only at the lower side

$$R_{km} = \frac{(1 - a r_v)\sinh(bSh) + b r_v \cosh(bSh)}{(a - r_v)\sinh(bSh) + b\cosh(bSh)} \tag{3.107}$$

and

$$T_{km} = \frac{b}{(a - r_v)\sinh(bSh) + b\cosh(bSh)} \tag{3.108}$$

These expressions are those presented by Kubelka for the case of a scattering layer bounded at the lower side by a reflecting background of reflectance r_v [Kub 31, Kub48].

Let us now consider that, in addition to the background at the lower side, the Lambertian layer has an interface at the upper side. We can directly use Eqs. (3.105) and (3.106), where the upper biface represents the interface. However, Eqs. (3.105) and (3.106) are traditionally obtained indirectly via the so-called "Saunderson correction" [Sau42]. Saunderson's model considers the multiple reflections and transmissions of light between the interface and the Lambertian layer with the background, whose reflectance R_{km} and transmittance T_{km} are given by (3.107) and (3.108). We will have the opportunity to present this model as a particular case of our compositional model (Sect. 6.3.1).

Summary

We have presented the two types of bifaces by which light is scattered: the scattering bifaces, among which the rough interfaces and scattering layers, and the Lambertian bifaces. We have presented basic elements of the classical literature that may be used to compute their reflectance and their transmittance.

A homogenous layer where light is intensely scattering is considered as being a Lambertian biface. Its reflectance and transmittance, called "intrinsic", may be modeled using the Kubelka-Munk model. We have presented a solving method for the Kubelka-Munk differential equation system using the Laplace transform. First, general solutions are obtained giving the upward and the downward irradiances propagating within the layers as functions of the depth. Then, considering eventual reflections and transmissions taking place at the boundaries of the layer, we can write boundary equations and obtain the global reflectance and transmittance of the Lambertian layer.

More advanced models [Yan04a-c] may also be used when the scattering and absorption coefficients are functions of depth within the layer. Such models are outside the scope of the present study. However, according to our formalism, it is possible to consider non-symmetric layers, with different intrinsic reflectances and transmittances.

Chapter 5.

Multiple reflection-transmission of light in multifaces

This chapter is dedicated to the optical properties of multifaces. We first develop a step-by-step description of the transfer of light between the contained faces. The global reflectance and transmittance of the multiface are expressed by infinite sums (Sect. 5.1). Then, we present a special type of multiface, called "regular", in which light is transferred according to a single reflectance and a single transmittance per face (Sect. 5.2). The infinite sums can be reduced to closed-form expressions. The superposition of bifaces is algebraically represented by an operation on their transfer matrices, called "composition". The composition of two, resp. three bifaces are characterized by a "quadriface formula", resp. a "hexaface formula". These two compositional formulae are developed using Markov chains. They can be further composed iteratively (Sect. 5.3). Lastly, we complete our new formalism with the notion of "biface splitting", where a biface is represented by an equivalent quadriface (Sect. 5.4).

5.1 Light multiple reflection-transmission between bifaces

Previous chapters were dedicated to the characterization of bifaces. Here, we consider the superposition of various bifaces. We describe the transfers of light, i.e. the reflections and transmissions, between their faces. The transfer ratios are given by the reflectance and the transmittance of each face. These reflectances and transmittances may have been previously obtained experimentally or calculated using one of the optical models presented in Chapters 3 and 4. However, in order to develop a model applicable to any type of multiface, we keep the face reflectances and transmittances unspecified and consider them as variables.

5.1.1 Multiple reflection-transmission process

Every irradiance hitting a face in a multiface is split into a reflected irradiance component and a transmitted irradiance component. Each component is a certain fraction of the incident irradiance, having its own angular distribution. The components are themselves split into a reflected and a transmitted components, which will be again split etc. The splitting process, called *multiple reflection-transmission process*, is developed in various *steps*.

The split of the source light corresponds to the first step. In the second step, both the reflected and transmitted components are again split, yielding four irradiance components. These ones are at their turn split in the third step. The multiple reflection-transmission process continues indefinitely and creates an infinity of irradiance components. Each irradiance component is characterized by a different combination of successive reflections or/and transmissions and is considered as a *path*. The paths terminate when their respective irradiance component exits the multiface, thus contributing to the

total reflected irradiance or the total transmitted irradiance.

It will be handy to consider steps as time units. Thus, the numbers of reflections or/and transmissions undergone by the corresponding irradiance components, are considered as durations. We are in presence of a *discrete time process*.

We may represent the different paths in the form of a binary tree, whose branches represent the paths followed by the irradiances components. The branches end when the corresponding irradiance components exit the multiface. In the binary tree, arcs represent a face reflection or a face transmission and are weighted by the corresponding reflectance or transmittance. Every arc is terminated by a node whose two outgoing arcs represent the split into a reflected and a transmitted components. Since the angular distribution of light may vary in time, all arc weights should be considered different even for reflections and transmission taking place at a same face. Fig 5.1 shows the binary tree for a hexaface (three bifaces superposed), where the arcs representing reflections are curved in such a way that every arc of the three is contiguous to its associated face.

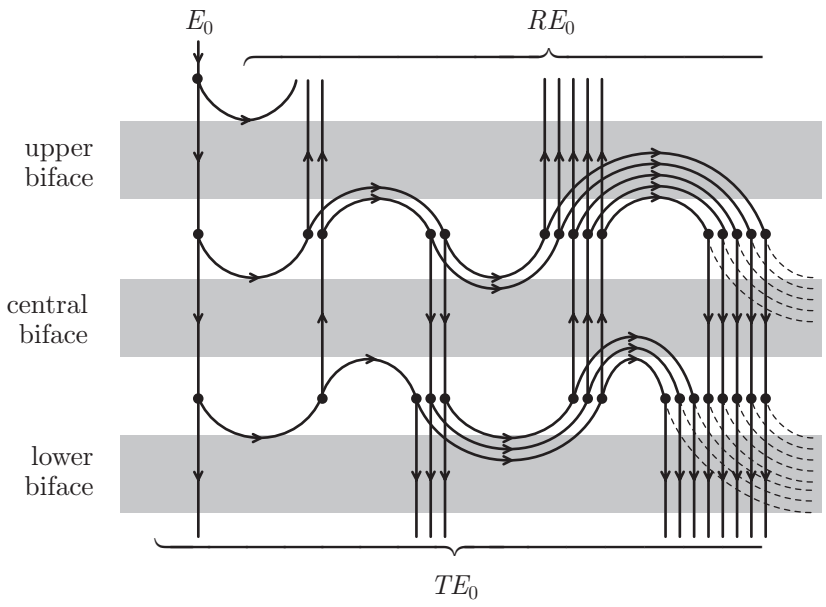

Fig. 5.1: Binary tree representing the multiple reflection-transmission process in a hexaface. Arcs represent face-to-face light transfers, i.e. reflections (curved arcs) or transmissions (vertical arcs), during which light is angularly redistributed. At nodes, light is split into a reflected and a transmitted component. The angular distribution of light is specific to each path. Arc weights, not specified here, are reflectances or transmittances, possibly all different.

Remark: Some bifaces are allowed to have a null reflectance or a null transmittance. This may yield degenerated cases of multiple reflection-transmission, i.e. possibly no multiple reflection-transmission at all.

5.1.2 Example of the quadriface

Let us consider the case of two superposed bifaces, forming a "quadriface". The nature of the bifaces is kept unspecified[1]. We just consider the BRDFs/BTDFs of their two faces, named in Fig. 5.2, from which are derived their directional reflectance/transmittance using Eq. (1.21). Directional reflectance $S_u(\theta)$ is derived from BRDF f_{s_u}, directional transmittance $P_u(\theta)$ is derived from BTDF f_{p_u}, etc. Thus, the upper and the lower bifaces have the respective fundamental transfer matrices

$$\begin{bmatrix} P_u(\theta) & S_u(\theta) \\ R_u(\theta) & X_u(\theta) \end{bmatrix} \quad \text{and} \quad \begin{bmatrix} X_v(\theta) & R_v(\theta) \\ S_v(\theta) & P_v(\theta) \end{bmatrix} \tag{5.1}$$

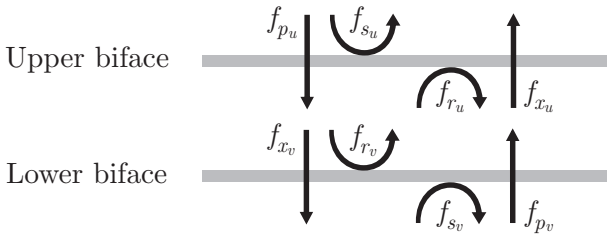

Fig. 5.2: BRDFs and BTDFs of the upper and lower bifaces in a quadriface.

Let us start describing the multiple reflection-transmission process. An incident irradiance E_0, angularly distributed according to a radiance function $L_0(d\omega_0)$, comes from the upper side and illuminates the upper face of the upper biface (Fig. 5.3). At time $k = 1$, E_0 is split into a reflected portion $s_u(1)E_0$ and a transmitted portion $p_u(1)E_0$. Fraction $s_u(1)$ is a diffuse reflectance deriving from the directional reflectance $S_u(\theta)$ according to Eq. (1.23). Likewise, $p_u(1)$ is a diffuse transmittance deriving from the directional transmittance $P_u(\theta)$

$$\begin{aligned} s_u(1) &= \frac{1}{E_0}\int_{d\omega_0\in\Omega} S_u(\theta_0)L_0(d\omega_0)\cos\theta_0 d\omega_0 \\ p_u(1) &= \frac{1}{E_0}\int_{d\omega_0\in\Omega} P_u(\theta_0)L_0(d\omega_0)\cos\theta_0 d\omega_0 \end{aligned} \tag{5.2}$$

The reflected irradiance $E_{r0} = s_u(1)E_0$ contributes to the total reflected irradiance E_r. The transmitted irradiance $E_1 = s_u(1)E_0$ has an angular distribution represented by a radiance function L_1, expressed as in Eq. (1.24)

$$L_1(d\omega_1) = \int_{d\omega_0\in\Omega} f_{p_u}(d\omega_0, d\omega_1)L_0(d\omega_0)\cos\theta_0 d\omega_0 \tag{5.3}$$

where f_{p_u} is the BTDF of the upper face of the upper biface.

[1] Readers who would like to have in mind examples of quadriface may think about, for instance, a nonabsorbing transparent glass slice having rough interfaces.

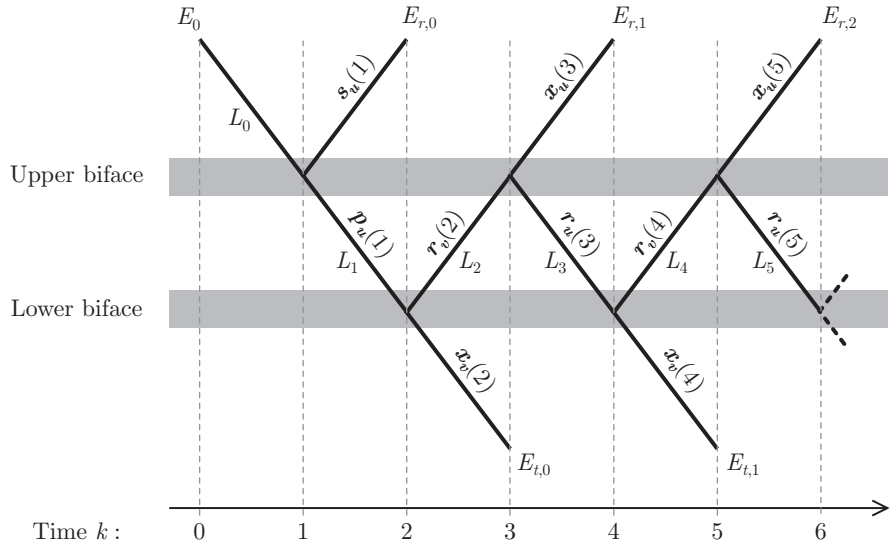

Fig. 5.3: Binary tree representing the multiple reflection-transmission process occurring within a quadriface.

At time $k = 2$, irradiance E_1 reaches the lower biface where it is split into a reflected portion $r_v(2)E_1$ and a transmitted portion $x_v(2)E_1$. Again, $r_v(2)$ is a diffuse reflectance and $x_v(2)$ a diffuse transmittance, expressed as in Eq. (1.23) with the radiance function L_1

$$\begin{aligned} r_v(2) &= \frac{1}{E_1}\int_{d\omega_1\in\Omega} R_v(\theta_1)\, L_1(d\omega_1)\cos\theta_1 d\omega_1 \\ x_v(2) &= \frac{1}{E_1}\int_{d\omega_1\in\Omega} X_v(\theta_1)\, L_1(d\omega_1)\cos\theta_1 d\omega_1 \end{aligned} \tag{5.4}$$

The transmitted irradiance $E_{t0} = x_v(2)E_1 = p_u(1)x_v(2)E_0$ exits the quadriface and contributes to the total transmitted irradiance E_t. The reflected irradiance $E_2 = p_u(1)r_v(2)E_0$ has an angular distribution represented by a radiance function L_2

$$L_2(d\omega_2) = \int_{d\omega_1\in\Omega} f_{r_v}(d\omega_1, d\omega_2) L_1(d\omega_1)\cos\theta_1 d\omega_1 \tag{5.5}$$

where f_{r_v} is the BRDF of the upper face of the lower biface.

At time $k = 3$, irradiance E_2 comes back to the upper biface, where it is again split into a reflected fraction $r_u(3)$ and a transmitted fraction $x_u(3)$, again expressed as in Eq. (1.23) with the radiance function L_2

$$\begin{aligned} r_u(3) &= \frac{1}{E_2}\int_{d\omega_2\in\Omega} R_u(\theta_2)\, L_2(d\omega_2)\cos\theta_2 d\omega_2 \\ x_u(3) &= \frac{1}{E_2}\int_{d\omega_2\in\Omega} X_u(\theta_2)\, L_2(d\omega_2)\cos\theta_2 d\omega_2 \end{aligned} \tag{5.6}$$

The transmitted irradiance $E_{r3} = x_u(3)\,E_2 = p_u(1)\,r_v(2)\,x_u(3)\,E_0$ contributes to the total transmitted irradiance E_t. The reflected irradiance $E_3 = p_u(1)\,r_v(2)\,r_u(3)\,E_0$ has an angular distribution represented by a radiance function L_3

$$L_3(d\omega_3) = \int_{d\omega_2 \in \Omega} f_{r_u}(d\omega_2, d\omega_3)\, L_2(d\omega_2) \cos\theta_2 d\omega_2 \tag{5.7}$$

We may pursue this description indefinitely. The first irradiance components exiting the quadriface are

$$E_{r,0} = s_u(1)E_0; \qquad E_{r,1} = p_u(1)r_v(2)x_u(3)E_0; \qquad E_{r,2} = p_u(1)r_v(2)r_u(3)r_v(4)x_u(5)E_0; \ ...$$
$$E_{t,0} = p_u(1)x_v(2)E_0; \quad E_{t,1} = p_u(1)r_v(2)r_u(3)x_v(4)\,E_0; \quad E_{t,2} = p_u(1)r_v(2)r_u(3)r_v(4)r_u(5)x_v(6)E_0; \ ...$$

We could express in the same manner all the irradiance components $E_{r,q}$ and $E_{t,q}$. Their sum would give respectively the total reflected irradiance E_r and the total transmitted irradiance E_t

$$E_r = \sum_{q=0}^{\infty} E_{r,q} \quad \text{and} \quad E_t = \sum_{q=0}^{\infty} E_{t,q} \tag{5.8}$$

By dividing Eqs. (5.8) by the incident irradiance E_0, one obtains the global reflectance R and the global transmittance T of the quadriface, which are also expressed as infinite sums

$$R = \sum_{q=0}^{\infty} r_q \quad \text{and} \quad T = \sum_{k=0}^{\infty} t_q \tag{5.9}$$

where the terms $r_q = E_{r,q}/E_0$ and $t_q = E_{t,q}/E_0$ are products of face reflectances and transmittances, themselves depending upon time parameter k.

5.1.3 Time-dependent and time-independent processes

Let us examine the time-dependence of the face reflectances and transmittances. These ones are expressed as functions of BRDFs and radiances functions. Since the optical properties of the faces are invariant, the BRDFs are also invariant. The only possible factor of the time-dependence is the angular distribution of light. It is evident, if we expand Eqs. (5.3), (5.5) and (5.7), that the radiance functions L_k are a priori different to each other

$$\begin{aligned}
L_1(d\omega) &= \int_{d\omega_0 \in \Omega} f_{p_u}(d\omega_0, d\omega) L_0(d\omega_0) \cos\theta_0 d\omega_0 \\
L_2(d\omega) &= \iint_{\substack{d\omega_0 \in \Omega \\ d\omega_1 \in \Omega}} f_{p_u}(d\omega_0, d\omega_1) f_{r_v}(d\omega_1, d\omega) L_0(d\omega_0) \cos\theta_0 d\omega_0 \cos\theta_1 d\omega_1 \\
L_3(d\omega) &= \iiint_{\substack{d\omega_0 \in \Omega \\ d\omega_1 \in \Omega \\ d\omega_2 \in \Omega}} f_{p_u}(d\omega_0, d\omega_1) f_{r_v}(d\omega_1, d\omega_2) f_{r_u}(d\omega_2, d\omega) L_0(d\omega_0) \cos\theta_0 d\omega_0 \cos\theta_1 d\omega_1 \cos\theta_2 d\omega_2
\end{aligned} \tag{5.10}$$

Hence, the reflectance and transmittance of the lower and upper bifaces are also functions of the time parameter k. We have a *time-dependent process*. The multiface is said to be *irregular*. The infinite sums of Eqs. (5.9) expressing the global reflectance R and the global transmittance T of the multiface are irreducible. We can assume that from a certain time, which should be determined thanks to a study specific to the considered materials, the terms become very small and can be neglected. Thus, the infinite sums would be reduced to the summation of a few relevant terms. Otherwise, we can use models of surface or/and volume scattering as those presented by Durant [Dur03] or Caron [Car03].

However, there exist some multifaces such that light has always the same angular distribution when it illuminates a same face. The radiance functions relative to a given face are proportional to each other. In the example of the quadriface above, radiance functions L_1, L_3, L_5,... illuminating the lower biface and radiance functions L_2, L_4, L_6,... illuminating the upper biface are such that, for all $d\omega$,

$$L_1(d\omega) = kL_3(d\omega) = k'L_5(d\omega) = \dots$$
$$L_2(d\omega) = k''L_4(d\omega) = k'''L_6(d\omega) = \dots$$

where k, k', k'' and k''' are constants. The reflectance and transmittance of the faces are constant over the multiple reflection-transmission process, i.e.,

$$r_v(2) = r_v(4) = r_v(6) = \dots$$
$$r_u(3) = r_u(5) = r_u(7) = \dots$$

The process is said to be *time-independent* and the multiface is said to be *regular*. In this case, the infinite sums of Eqs. (5.9) become geometrical series, with closed-form formulae for R and T [HH06]. We can obtain these expressions by factorizing the above infinite sums. Such a method is realizable for quadrifaces, but becomes impracticable as the number of bifaces increases. We will rather use a method relying on Markov chains whose complexity is almost identical for any dimension of multiface.

5.2 Regular multifaces

The present section aims at characterizing regular multifaces, and first at determining which type of multiface is amenable to be regular.

5.2.1 Conditions of regularity

Faces whose reflectance and transmittance are time-independent are called "regular faces". Thus, a multiface is regular when all its faces are regular. The following cases must be considered:

– **External faces:** They receive light only once, from a light source, at time origin. They are therefore independent of time and thus regular whatever the illumination geometry.

– **Lambertian faces:** They are regular without any restriction, since their reflectance and transmittance are independent of the incidence angular distribution (see Sect. 4.3). Furthermore, reflected and transmitted irradiances are uniformly distributed over the hemisphere, i.e. Lambertian.

– **Scattering faces:** They are *irregular* when their bordering face is scattering or transparent biface (of nonzero reflectance), because of a time-dependent multiple reflections process (light becomes more and more diffuse each time it hits the scattering face). However, when their bordering face is Lambertian, they are invariably illuminated by a Lambertian irradiance and are therefore regular.

– **Transparent faces:** For the same reasons as above, transparent faces are regular when they are bordered by Lambertian faces and irregular when they are bordered by scattering faces.

– **Successive transparent faces:** A directional incident light follows only the regular di-

rections. The angle of incidence on each face is constant. The multiface is therefore regular for directional incident light. For diffuse or Lambertian illuminations, the respective contribution of all the incident rays should computed separately and summed up afterwards (principle of directionality, see Sect. 3.3.3).

In summary, the multiface is regular when it does not contain any scattering biface, or when every contained scattering bifaces is directly bordered by a Lambertian biface.

5.2.2 Representations of regular multifaces

From now, only regular multifaces are considered. Each face is associated with its reflectance and its transmittance involved in the multiple reflection-transmission process. Likewise, to each biface is associated a single transfer matrix, containing the reflectance and transmittance of its two faces. Let us take the example of a hexaface (three bifaces) having respectively the transfer matrices

$$\begin{bmatrix} x_v & r_v \\ s_v & p_v \end{bmatrix}, \quad \begin{bmatrix} \tau & \rho \\ \rho' & \tau' \end{bmatrix} \quad \text{and} \quad \begin{bmatrix} p_u & s_u \\ r_u & x_u \end{bmatrix} \tag{5.11}$$

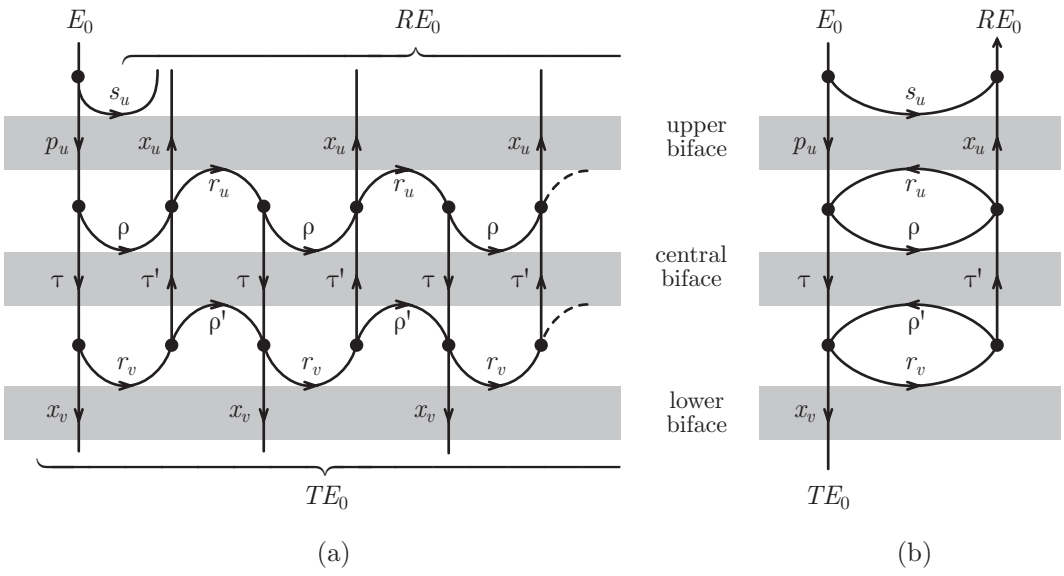

Fig. 5.4: Representation (a) by an infinite dimensional graph, (b) by a finite dimensional Markov graph, of the multiple reflection-transmission process occurring in a regular hexaface illuminated at the upper side.

Thanks to the time-independence of the process, the binary tree of Fig. 5.1 can be considerably simplified. Since every irradiance component incident on a face is reflected and transmitted in a same proportion, we may proceed to some groupments of arcs and nodes. For instance, each group of parallel arcs drawn in Fig. 5.1 may be represented by a single arc. Each clusters of nodes is consequently replaced by a single node. In the resulting graph, shown in Fig. 5.4a, nodes are both the converging point and the starting point of

arcs. They represent both the collecting and the splitting of irradiance components. In such a graphical representation, the development of the multiple reflection-transmission process in time is preserved, but the graph is infinite dimensional.

An even more compact representation is possible, although the visual representation of time is lost. All the arcs relative to a same reflection or transmission are grouped into a single arc. A finite graph is obtained, with only one reflection arc and one transmission arc per face (Fig. 5.4b). Since the values of arc weights are all percentages, such a graph is analogous to the graphical representation of a Markov chain.

The analogy between multiple reflection-transmission processes and Markov chains is highly profitable for our compositional model. We will take benefit of the well established mathematical methods embodied into the so-called Markov theory for establishing the formulae for multiface global reflectances and transmittances. The Markov matrix formalism has inspired us the idea of endowing also our compositional theory with a matrix-like formalism. Pursuing this idea, we now introduce a well-defined "product" of transfer matrices, called *composition* (notation $\bigcirc$), permitting to visualize under an algebraic form the superposition of bifaces in regular multifaces. Hence, the synthetic view of the light transfer process provided by the Markov graph is doubled by an algebraic equation that we call *composition equation*.

Consider a multiface with global transfer matrix $\mathbf{G}$, resulting from the superposition of a biface having the transfer matrix $\mathbf{F_1}$ on the upper side and a biface having the transfer matrix $\mathbf{F_2}$ on the lower side. The corresponding composition equation is written as

$$\mathbf{G} = \mathbf{F}_1 \bigcirc \mathbf{F}_2 \tag{5.12}$$

For example, the composition equation corresponding to the hexaface of Fig. 5.4 is

$$\begin{bmatrix} T_U & R_U \\ R_V & T_V \end{bmatrix} = \begin{bmatrix} p_u & s_u \\ r_u & x_u \end{bmatrix} \bigcirc \begin{bmatrix} \tau & \rho \\ \rho' & \tau' \end{bmatrix} \bigcirc \begin{bmatrix} x_v & r_v \\ s_v & p_v \end{bmatrix} \tag{5.13}$$

Note that the position of transfer matrices with respect to symbol $\bigcirc$ has an importance. The composition operation is not commutative. The definition of $\bigcirc$ will be given in Sect. 5.3.1 by the expressions for T_U, R_U, T_V and R_V as functions of the face reflectances and transmittances. Let us now present the Markov chains that will permit the efficient computation of these expressions.

5.2.3 Analogy between regular multifaces and Markov chains

A Markov chain is a convenient representation of the behavior of a physical system which describes the different states the system may occupy and indicates how the system moves from one state to another in time [Ste94]. Our conception of time has already been described in Sect. 5.1.1. In the context of multiple reflection-transmission processes, the system is the multiface. The different states occupied by the system are the incidence of light on the different faces. A path, i.e. a succession of reflections and transmissions, is represented by a succession of state-to-state transitions within the chain. Reflectances and transmittances become probabilities of transition. Table 5.1 completes the correspondence between multiple reflection-transmission processes and Markov chains.

Table 5.1: Correspondence between concepts underlying multiple reflection-transmission processes and Markov chains.

Multiface	Structured stochastic system
Light reaching a face or a detector	State
Reflection / transmission	Transition
Reflectance / transmittance	Transition probability
Time-dependent process	Time-dependent stochastic process
Time-independent process	Homogenous Markov chain
External faces	Ephemeral or absorbing states

A survey of basic definitions and results of Markov theory is proposed in Appendix B. Let us recall here that a stochastic process can be represented by a Markov chain only when every state-to-state transition has a time-independent probability to occur. Therefore, the Markov theory can be used only with regular multifaces.

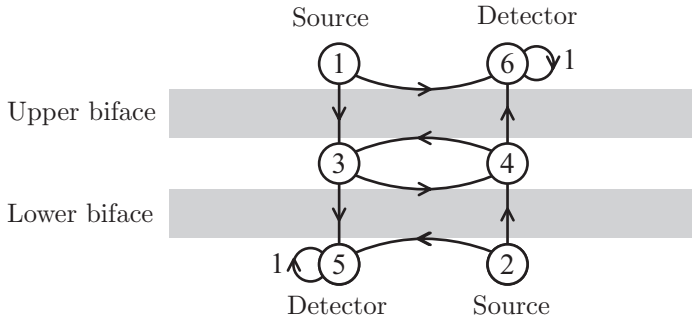

Fig. 5.5: Markov graph for a regular quadriface.

Consider a multiface having N faces, two light sources (one in each surrounding medium) and two detectors (idem). The N faces and the two detectors, each one able to receive light, are the $N+2$ states of our system. They are labeled with a number between 1 and $N+2$ according to the following convention[1] (see Fig. 5.5):

– Numbers 1 and 2 are associated to the states corresponding to the external faces, which receive light from the light sources (most external faces). Since they receive light only once at the time origin, they are ephemeral states;

– Numbers $N+1$ and $N+2$ are associated to the detectors. A *loop* connecting these states to themselves modelizes the fact that light captured by the detectors does no longer interfere with the bifaces. States 5 and 6 are *absorbing states*. We are therefore in presence of *absorbing Markov chains* (see Appendix B.4);

[1] All distributions of state labels are equivalent. We are therefore free to choose the more convenient one according to computational considerations.

– Odd numbers (resp. even numbers) are attributed to the states receiving the light propagating downwards (res. upwards). Odd numbers increase and even numbers decrease as the states are closer to the lower side.

Let be m_{ij} the probability of transition from state i to state j. Matrix $\mathbf{M} = \left(m_{ij}\right)$ is called the *single-step transition probability matrix* of the Markov chain. We note $m_{ij}^{(k)}$ the probability that a transition takes place from state i to state j in k steps. Probabilities $m_{ij}^{(k)}$ are placed in a *k-step transition probability matrix* $\mathbf{M}^{(k)}$. The k-step and single-step matrices are linked by the simple relation (see Eqs. (B.7) to (B.9) in Appendix B.2)

$$\mathbf{M}^{(k)} = \mathbf{M}^k \tag{5.14}$$

We are interested in the global reflectances and transmittances of the multiface. They correspond to the probability that the incident irradiance transits from a source to a detector, whatever the number of steps. Let $m_{1,N+1}^{\infty}$, $m_{1,N+2}^{\infty}$, $m_{2,N+1}^{\infty}$ and $m_{2,N+2}^{\infty}$ be the transition probabilities corresponding to the four possible source-detector combinations. They are elements of the "infinite-step" transition probability matrix $\mathbf{M}_{\infty} = \left(m_{ij}^{\infty}\right)$ defined as

$$\mathbf{M}_{\infty} = \lim_{k \to \infty} \mathbf{M}^k \tag{5.15}$$

The relationship between matrix $\mathbf{M}_{\infty}$ and the global transfer matrix of a multiface will be appear clearly with the simple example of a quadriface below.

5.3 Compositional model for regular multifaces

We just saw that the global transfer matrix of a regular multiface is a part of the infinite-step transition probability matrix associated with a Markov chain. Let us consider generic multifaces: a quadriface (two superposed bifaces), a hexaface (three superposed bifaces) and a N-dimensional multiface. For each case, by establishing the Markov chain and its associated single step probability matrix, and then by computing the infinite step transition probability matrix, we will obtain the global transfer matrix of the considered multiface. The obtained expressions, called "compositional formulae" will correspond to the definition of operation $\bigcirc$.

5.3.1 The quadriface formula

Let us consider the regular quadriface represented by the 6-states Markov chain in Fig. 5.6 and by the following composition equation

$$\begin{bmatrix} T_U & R_U \\ R_V & T_V \end{bmatrix} = \begin{bmatrix} p_u & s_u \\ r_u & x_u \end{bmatrix} \bigcirc \begin{bmatrix} x_v & r_v \\ s_v & p_v \end{bmatrix} \tag{5.16}$$

The single-step transition probability matrix $\mathbf{M}$ of the chain is obtained by placing the nonzero probabilities m_{ij} indicated in Fig. 5.6. For example, the probability p_u of transition from state 1 to state 3 is placed in row 1, column 3. Once all the elements featured in the graph are placed, $\mathbf{M}$ is filled with zeros

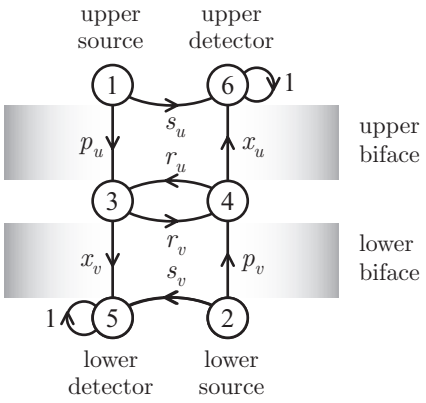

Fig. 5.6: Graph representing the multiple reflection-transmission process in a regular quadriface.

$$\mathbf{M} = \begin{bmatrix} 0 & 0 & p_u & 0 & 0 & s_u \\ 0 & 0 & 0 & p_v & s_v & 0 \\ 0 & 0 & 0 & r_v & x_v & 0 \\ 0 & 0 & r_u & 0 & 0 & x_u \\ 0 & 0 & 0 & 0 & 1 & 0 \\ 0 & 0 & 0 & 0 & 0 & 1 \end{bmatrix} \tag{5.17}$$

The location of light in time may be observed using a probability vector. We will use bold characters for the two last elements, which represent the amounts of light having reached the lower and the upper detectors respectively. Let us first consider that the incident light comes from the upper light source. At time origin, all light is in state 1, i.e. is incident on the upper face of the upper biface (see Fig. 5.6). The probability vector is

$$\mathbf{e}_0 = [1,\, 0,\, 0,\, 0,\, \mathbf{0},\, \mathbf{0}] \tag{5.18}$$

At time 1, the location of light within the quadriface is given by the product $\mathbf{e}_0 \cdot \mathbf{M}$

$$\mathbf{e}_1 = \mathbf{e}_0 \cdot \mathbf{M} = [0,\, 0,\, p_u,\, 0,\, \mathbf{0},\, \boldsymbol{s_u}]$$

A fraction s_u (external reflectance of the upper biface) of the incident light has already reached the upper detector. At time 2, the product $\mathbf{e}_1 \cdot \mathbf{M}$ shows that a fraction $p_u x_v$ has reached the lower detector

$$\mathbf{e}_2 = \mathbf{e}_1 \cdot \mathbf{M} = \mathbf{e}_0 \cdot \mathbf{M}^2 = [0,\, 0,\, 0,\, p_u r_v,\, \boldsymbol{p_u x_v},\, \boldsymbol{s_u}]$$

At time 3, the probability vector is

$$\mathbf{e}_3 = \mathbf{e}_2 \cdot \mathbf{M} = \mathbf{e}_0 \cdot \mathbf{M}^3 = [0,\, 0,\, p_u r_u r_v,\, 0,\, \boldsymbol{p_u x_v},\, \boldsymbol{s_u + p_u r_v x_u}]$$

Matrices $\mathbf{M}^2$ and $\mathbf{M}^3$ are respectively the two-step and the three-step transition probability matrices. One retrieves, with this short description, the general property (5.14) satisfied by transition probability matrices.

Pursuing the products of the probability vector by matrix $\mathbf{M}$, one would observe that

the proportion of light reaching the detectors increases and that the proportion of light remaining in other states decreases. At the "end" of the process, there is no remaining light within the multiface. The probability m_{15}^{∞} for the incident light to be captured by the lower detector corresponds to the upper global transmittance. Likewise, the proability m_{15}^{∞} to be captured by the upper detector corresponds to its upper global reflectance

$$\mathbf{e}_{\infty} = \mathbf{e}_0 \cdot \mathbf{M}_{\infty} = \left[0,\, 0,\, 0,\, 0,\, \boldsymbol{m}_{15}^{\infty},\, \boldsymbol{m}_{16}^{\infty}\right] \tag{5.19}$$

Let us now consider that light comes from the lower source. At time origin, the probability vector $\mathbf{e}_0$ is

$$\mathbf{e}_0 = [0,\, 1,\, 0,\, 0,\, \mathbf{0},\, \mathbf{0}] \tag{5.20}$$

By multiplying this vector by matrix $\mathbf{M}$ an infinite number of times, or by multiplying it by $\mathbf{M}_{\infty}$, which is equivalent, we would obtain a probability vector indicating once again that there is no remaining light within the multiface

$$\mathbf{e}_{\infty} = \mathbf{e}_0 \cdot \mathbf{M}_{\infty} = \left[0,\, 0,\, 0,\, 0,\, \boldsymbol{m}_{25}^{\infty},\, \boldsymbol{m}_{26}^{\infty}\right] \tag{5.21}$$

In (5.21), m_{25}^{∞} and m_{26}^{∞} correspond respectively to the lower global reflectance and transmittance of the quadriface. In Appendix B, we show that the chains representing multiple reflection-transmission processes are such that matrix $\mathbf{M}_{\infty}$ is of the form

$$\mathbf{M}_{\infty} = \left[\begin{array}{cccc|cc} 0 & 0 & 0 & 0 & \boxed{m_{15}^{\infty}} & \boxed{m_{16}^{\infty}} \\ 0 & 0 & 0 & 0 & \boxed{m_{25}^{\infty}} & \boxed{m_{26}^{\infty}} \\ 0 & 0 & 0 & 0 & \cdot & \cdot \\ 0 & 0 & 0 & 0 & \cdot & \cdot \\ \hline 0 & 0 & 0 & 0 & 1 & 0 \\ 0 & 0 & 0 & 0 & 0 & 1 \end{array}\right] \tag{5.22}$$

where the upper-right block corresponds to the global transfer matrix of the multiface

$$\begin{bmatrix} T_U & R_U \\ R_V & T_V \end{bmatrix} = \begin{bmatrix} m_{15}^{\infty} & m_{16}^{\infty} \\ m_{25}^{\infty} & m_{26}^{\infty} \end{bmatrix} \tag{5.23}$$

The computation of the upper-right block for the case of the quadriface is developed in Appendix C.1. The resulting expression for the global transfer matrix is

$$\begin{bmatrix} T_U & R_U \\ R_V & T_V \end{bmatrix} = \begin{bmatrix} p_u & s_u \\ r_u & x_u \end{bmatrix} \bigcirc \begin{bmatrix} x_v & r_v \\ s_v & p_v \end{bmatrix} = \begin{bmatrix} \dfrac{p_u x_v}{1 - r_u r_v} & s_u + \dfrac{p_u x_u r_v}{1 - r_u r_v} \\ s_v + \dfrac{p_v x_v r_u}{1 - r_u r_v} & \dfrac{p_v x_u}{1 - r_u r_v} \end{bmatrix} \tag{5.24}$$

Eq. (5.24) will be referred to as the *quadriface formula*. It corresponds to the definition of the composition symbol $\bigcirc$ as a (noncommutative) operation between transfer matrices. It is the most fundamental equation of the compositional model.

5.3.2 The hexaface formula

Let us now consider a regular hexaface, resulting from the superposition of three bifaces, called upper, central and lower. It is represented by the 8 states graph of Fig. 5.7 and by the composition equation

$$\begin{bmatrix} T_{UV} & R_{UU} \\ R_{VV} & T_{VU} \end{bmatrix} = \begin{bmatrix} p_u & s_u \\ r_u & x_u \end{bmatrix} \bigcirc \begin{bmatrix} \tau & \rho \\ \rho' & \tau' \end{bmatrix} \bigcirc \begin{bmatrix} x_v & r_v \\ s_v & p_v \end{bmatrix} \tag{5.25}$$

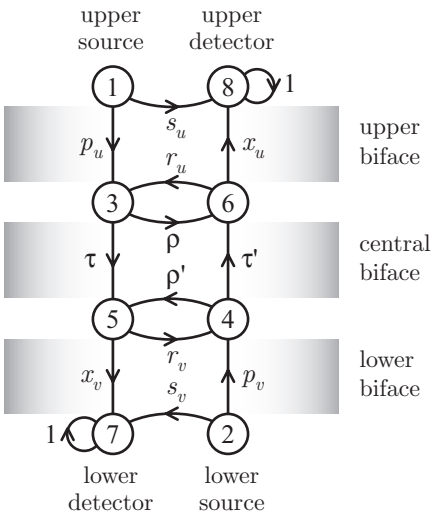

Fig. 5.7: Representation by a Markov graph of the multiple reflection-transmission occurring with three superposed bifaces.

Like for the quadriface, the global transfer matrix of the hexaface is the upper-right block of the infinite-step transition probability matrix $\mathbf{M}_\infty$ defined by Eq. (5.15) with the following single-step transition probability matrix $\mathbf{M}$

$$\mathbf{M} = \begin{vmatrix} 0 & 0 & p_u & 0 & 0 & 0 & 0 & s_u \\ 0 & 0 & 0 & p_v & 0 & 0 & s_v & 0 \\ 0 & 0 & 0 & 0 & \tau & \rho & 0 & 0 \\ 0 & 0 & 0 & 0 & \rho' & \tau' & 0 & 0 \\ 0 & 0 & 0 & r_v & 0 & 0 & x_v & 0 \\ 0 & 0 & r_u & 0 & 0 & 0 & 0 & x_u \\ 0 & 0 & 0 & 0 & 0 & 0 & 1 & 0 \\ 0 & 0 & 0 & 0 & 0 & 0 & 0 & 1 \end{vmatrix} \tag{5.26}$$

$\mathbf{M}$ presents a cross structure that was already noticeable in (5.17).

The computation of the upper-right block of $\mathbf{M}_\infty$ is developed in Appendix C.2. It yields the following equation, which will be referred to as the *hexaface formula*

$$\begin{bmatrix} T_U & R_U \\ R_V & T_V \end{bmatrix} = \begin{bmatrix} p_u & s_u \\ r_u & x_u \end{bmatrix} \bigcirc \begin{bmatrix} \tau & \rho \\ \rho' & \tau' \end{bmatrix} \bigcirc \begin{bmatrix} x_v & r_v \\ s_v & p_v \end{bmatrix}$$
$$= \begin{bmatrix} p_u x_v \dfrac{\tau}{D} & s_u + p_u x_u \dfrac{\rho - r_v\left(\rho\rho' - \tau\tau'\right)}{D} \\ s_v + p_v x_v \dfrac{\rho' - r_u\left(\rho\rho' - \tau\tau'\right)}{D} & p_v x_u \dfrac{\tau'}{D} \end{bmatrix} \tag{5.27}$$

with $D = \left(1 - r_u\rho\right)\left(1 - r_v\rho'\right) - r_u r_v \tau\tau'$.

5.3.3 Associativity of the composition of bifaces

The hexaface formula can also be obtained using twice the quadriface formula. First, two adjacent bifaces are selected within the hexaface and merged into a single biface, whose global transfer matrix is expressed using the quadriface formula. Then, the quadriface formula is applied again to this resulting biface and the third biface, leading to the global transfer matrix of the hexaface. We may compose first the left and the central transfer matrices

$$\left\{\begin{bmatrix} p_u & s_u \\ r_u & x_u \end{bmatrix} \bigcirc \begin{bmatrix} \tau & \rho \\ \rho' & \tau' \end{bmatrix}\right\} \bigcirc \begin{bmatrix} x_v & r_v \\ s_v & p_v \end{bmatrix} = \begin{bmatrix} \dfrac{p_u\tau}{1 - r_u\rho} & s_u + \dfrac{p_u x_u \rho}{1 - r_u\rho} \\ \rho' + \dfrac{r_u\tau\tau'}{1 - r_u\rho} & \dfrac{x_u\tau'}{1 - r_u\rho} \end{bmatrix} \bigcirc \begin{bmatrix} x_v & r_v \\ s_v & p_v \end{bmatrix} \tag{5.28}$$

or compose first the central and the right transfer matrices

$$\begin{bmatrix} p_u & s_u \\ r_u & x_u \end{bmatrix} \bigcirc \left\{\begin{bmatrix} \tau & \rho \\ \rho' & \tau' \end{bmatrix} \bigcirc \begin{bmatrix} x_v & r_v \\ s_v & p_v \end{bmatrix}\right\} = \begin{bmatrix} p_u & s_u \\ r_u & x_u \end{bmatrix} \bigcirc \begin{bmatrix} \dfrac{\tau x_v}{1 - \rho r_v} & \rho + \dfrac{\tau\tau' r_v}{1 - \rho r_v} \\ s_v + \dfrac{p_v x_v \rho'}{1 - \rho r_v} & \dfrac{\tau' p_v}{1 - \rho r_v} \end{bmatrix} \tag{5.29}$$

and check that in both cases the final transfer matrix is identical to Eq. (5.27). This shows the associativity of operation $\bigcirc$. For transfer matrices $\mathbf{F_1}$, $\mathbf{F_2}$ and $\mathbf{F_3}$, one has

$$\left(\mathbf{F}_1 \bigcirc \mathbf{F}_2\right) \bigcirc \mathbf{F}_3 = \mathbf{F}_1 \bigcirc \left(\mathbf{F}_2 \bigcirc \mathbf{F}_3\right) = \mathbf{F}_1 \bigcirc \mathbf{F}_2 \bigcirc \mathbf{F}_3 \tag{5.30}$$

5.3.4 Composition formula for more than two bifaces

We now consider a regular multiface composed of k bifaces. The corresponding Markov chain has $2k+2$ states (Fig. 5.8), numbered according to the labeling convention presented in Sect. 5.2.3. The single-step matrix $\mathbf{M}$ has the cross structure that has already been pointed out (the empty spaces should be considered as filled with zeros)

$$\mathbf{M} = \left[\begin{array}{c|ccc} \tau_1 & & & \rho_1 \\ & \tau'_2 & & \rho'_2 \\ & & \ddots \quad \iddots & \\ & & \tau_k \quad \rho_k & \\ & & \rho'_k \quad \tau'_k & \\ & & \iddots \quad \ddots & \\ & \rho_2 & & \tau_2 \\ \rho'_1 & & & \tau'_1 \\ \hline & & & 1 \\ & & & 1 \end{array}\right] \tag{5.31}$$

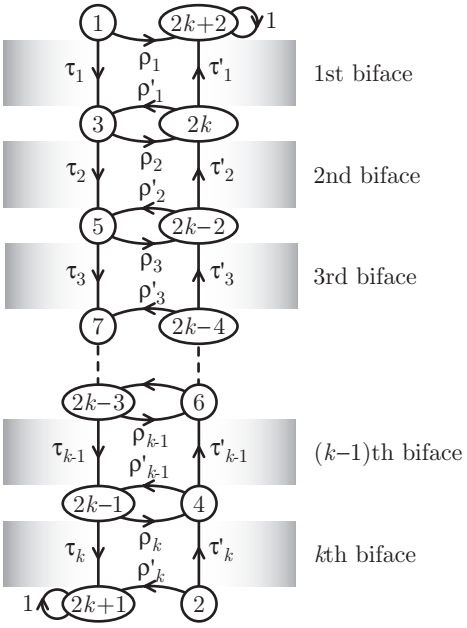

Fig. 5.8: Markov graph representing the multiple reflection-transmission process within k superposed bifaces.

Let $\mathbf{G}_j$ and $\mathbf{F}_{j+1}$ be respectively the transfer matrices of j successive bifaces and of a $(j+1)$th biface. At iteration j, the composition of $\mathbf{G}_j$ and $\mathbf{F}_{j+1}$ is

$$\mathbf{G}_{j+1} = \left|\begin{array}{ll} \mathbf{G}_j \circ \mathbf{F}_{j+1} & \\ or & (j = 1, 2, ..., k-1) \\ \mathbf{F}_{j+1} \circ \mathbf{G}_j & \end{array}\right. \tag{5.32}$$

according to whether the $(j+1)^{\text{th}}$ biface is at the upper or resp. at the lower side of the j first bifaces. Denoting by R_j, T_j, R'_j and T'_j the components of $\mathbf{G}_j$, the composition with

the $(j+1)^{\text{th}}$ biface at the lower side, given by the quadriface formula (5.32), gives the following iterative formula, called the *composition formula*

$$\begin{bmatrix} T_{j+1} & R_{j+1} \\ R'_{j+1} & T'_{j+1} \end{bmatrix} = \begin{bmatrix} T_j & R_j \\ R'_j & T'_j \end{bmatrix} \bigcirc \begin{bmatrix} \tau_{j+1} & \rho_{j+1} \\ \rho'_{j+1} & \tau'_{j+1} \end{bmatrix} = \begin{bmatrix} \dfrac{T_j \tau_{j+1}}{1 - R'_j \rho_{j+1}} & R_j + \dfrac{T_j T'_j \rho_{j+1}}{1 - R'_j \rho_{j+1}} \\ \rho'_{j+1} + \dfrac{R'_j \tau_{j+1} \tau'_{j+1}}{1 - R'_j \rho_{j+1}} & \dfrac{T'_j \tau'_{j+1}}{1 - R'_j \rho_{j+1}} \end{bmatrix} \tag{5.33}$$

5.4 Biface splitting

In compositional models, it is sometimes judicious to dissociate the different components of the transfer matrix characterizing a biface. Imagine two layers separated by an interface. We would like to compose the interface's upper face with the upper layer, and to compose its lower face with the lower layer. Since composition can be performed only with transfer matrices, we propose to characterize the interface with two transfer matrices. The interface becomes a quadriface having the same global transfer matrix as the original biface. We call this procedure "biface splitting".

Graphically, the split is performed like in Fig. 5.9. The upper (resp. lower) reflection arc is placed at the upper side of the upper biface (resp. the lower side of the upper biface). The other reflections arcs have a zero reflectance. The left (resp. right) transmission arc is placed at the left (resp. right) of the quadriface; we may choose to place it on the upper or the lower biface, the other left arc (resp. right arc) having the transmittance 1. Fig. 5.9 features two of the four split possibilities.

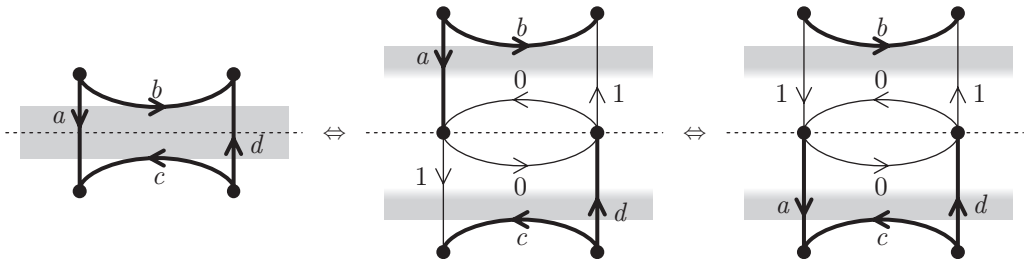

Fig. 5.9: Two possible splits of a biface.

We may write the following composition equations for the splits illustrated in Fig. 5.9, and check, thanks to the quadriface formula (5.24), the equality between the transfer matrix of the original biface and the global transfer matrices of the quadrifaces issued from the split operations

$$\begin{bmatrix} a & b \\ c & d \end{bmatrix} = \begin{bmatrix} a & b \\ 0 & 1 \end{bmatrix} \bigcirc \begin{bmatrix} 1 & 0 \\ c & d \end{bmatrix} = \begin{bmatrix} 1 & b \\ 0 & 1 \end{bmatrix} \bigcirc \begin{bmatrix} a & 0 \\ c & d \end{bmatrix} \tag{5.34}$$

Summary

In this chapter, we have described the multiple reflection-transmission process occurring in multifaces, first in the general case where the multiface global reflectance and transmittance are expressed as infinite sums, and then in the special case of regular multifaces whose global reflectance and transmittance have analytical expressions. The criteria of regularity have been clearly stated: the multiface is regular when it does not contain any scattering biface, or when every contained scattering biface is directly bordered by Lambertian bifaces. In regular multifaces, each face has a constant reflectance and a constant transmittance. This allows representing the multiple reflection-transmission process by a Markov chain. Bifaces also have a constant transfer matrix. Thus, the superposition of bifaces can now be characterized by a "composition" of their respective transfer matrix, i.e. by a well-defined associative and noncommutative product. We have presented, thanks to mathematical tools embodied in the Markov theory, a closed-form defining expression for the composition of two and three transfer matrices, characterizing the superposition of two and three bifaces respectively. These defining expressions are called the "quadriface formula" and the "hexaface formula". For more superposed bifaces, the quadriface or/and the hexaface formulae can be applied iteratively.

The compositional formulae rely only on the assumption that the multiface is regular, i.e. that each face has a single reflectance and a single transmittance involved in the multiple reflection-transmission process. In the next chapter, we show how these face reflectances and transmittances can be determined, given a particular combination of superposed bifaces, and a given measuring geometry. This will allow a revisitation of some classical models, as well as the development of new models in Chapters 7 and 8.

Note that the introduction of Markov chains was not strictly necessary. We could have derived the quadriface formula using a step-by-step description, and compose this formula with itself for obtaining the hexaface formula and the compositional formula. However, we have intentionally used the Markov theory for the elegance and the efficiency of its matrix formalism. Markov graphs are excellent representations of multiple reflection-transmission process within multilayers. Another reason for introducing Markov chains is the idea of a possible extension to multilayers having an unknown structure, i.e. an unknown number of layers and interfaces. By combining our compositional model with the theory of hidden Markov chains, we may obtain a new noninvasive method for studying multilayer specimens.

Chapter 6.

Reflectance and transmittance models

The present chapter concerns the application of the composition formulae established in Chapter 5 to specified multifaces. We first present how, for a given multiface, the reflectance and the transmittance of each of its face shall be determined. The nature of the faces (transparent, scattering, Lambertian), their neighborhood and the measuring geometry will be taken into account (Sect. 6.1). Then, classical compositional models and some of their extensions will be presented as examples where our formalism may be applied. Their expressions for reflectance, respectively transmittance, are derived by the simple application of the compositional formulae. We first treat multifaces composed uniquely of transparent bifaces and of Lambertian multifaces (Sect. 6.2). Then, we consider the superposition of transparent bifaces on a Lambertian background with three examples, including the well-known Williams-Clapper model (Sect. 6.3).

6.1 Elaboration of a reflectance and transmittance model

We have shown in Chapter 5 that the multiple reflection-transmission process of light occurring in a regular multiface can be described with a single reflectance and a single transmittance per face. Thus, a particular transfer matrix is associated to each biface, and the multiface is characterized by the composition of the particular transfer matrices of its composing bifaces. The quadriface and the hexaface formulae can be applied to convert the composition of biface transfer matrices into a global transfer matrix. However, we have not yet explained the reflectance and transmittance that should be associated with each face. This is the purpose of the following sections.

Two main factors should be taken into account in the specification of the face reflectances and transmittances: 1- the nature of the face (transparent, scattering, Lambertian), 2- their neighborhood, which determines the type of their respective illumination (transparent, scattering, Lambertian neighboring faces respectively provide a directional, diffuse, Lambertian illumination). A special treatment is necessary for external bifaces due to the influence of th

e selected measuring geometry.

Prior to the specification of the face reflectances and transmittances, let us draw up a brief inventory of the possible combinations of bifaces forming regular multifaces.

6.1.1 Types of regular bifaces

Regular bifaces may be split into three main categories:

– Transparent multifaces, made uniquely of transparent bifaces. All the face reflectances and transmittances are, directly or indirectly via Snell's laws, functions of the incidence

angle of the directional source light (principle of directionality, see Sect. 3.3.3).

– *Wholly-Lambertian multifaces*, composed uniquely of Lambertian bifaces[1]. The faces reflectances and transmittances are invariant, excepted for the external biface whose external reflectance and exit transmittance (i.e. the terms corresponding to the transfer of light towards the capturing device) depend on the geometry of observation;

– *Mixed multifaces*, in which Lambertian bifaces are superposed with scattering or/and transparent bifaces. Recall that scattering bifaces cannot be bordered by scattering nor reflecting transparent bifaces: the regularity would not be satisfied (Sect. 5.2.1).

6.1.2 Faces reflectances and transmittances in mixed multifaces

In mixed multifaces, the bifaces may be transparent, scattering or/and Lambertian. Lambertian bifaces are characterized by their invariant transfer matrix $\mathbf{F}_L$. Non-Lambertian bifaces, i.e. transparent and scattering bifaces, are characterized by their fundamental transfer matrix $\mathbf{F}_\theta$. In the present section, matrices $\mathbf{F}_L$ and $\mathbf{F}_\theta$ are noted respectively

$$\mathbf{F}_L = \begin{bmatrix} p_L & s_L \\ r_L & x_L \end{bmatrix} \quad \text{and} \quad \mathbf{F}_\theta = \begin{bmatrix} P(\theta) & S(\theta) \\ R(\theta) & X(\theta) \end{bmatrix} \tag{6.1}$$

The specification of the face reflectances and transmittances is performed in a different way for central bifaces and for external bifaces, the latter being affected by the measuring geometry (Fig 6.1).

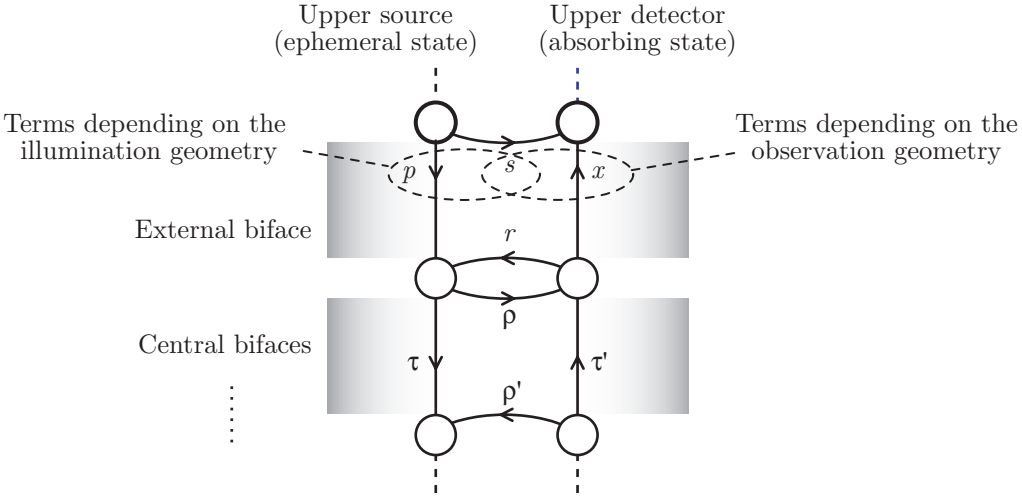

Fig. 6.1: Dependence of external biface reflectances and transmittances on the illumination and observation geometries.

[1] Wholly-Lambertian multifaces are special cases of Lambertian multifaces, according to the definition of Lambertian multiface given in Section 2.4.

When a Lambertian biface is at a central position within the multiface, its particular transfer matrix is the matrix $\mathbf{F}_L$ given by Eq. (6.1). A central biface that is non-Lambertian is bordered by Lambertian bifaces, and therefore receives Lambertian illuminations on its both sides. According to the notations introduced in Sect. 2.3, its fundamental transfer matrix $\mathbf{F}_\theta$, given in Eq. (6.1), becomes the particular transfer matrix

$$
{}^{L\rightarrow}\begin{bmatrix} T(\theta) & R(\theta) \\ R'(\theta) & T'(\theta) \end{bmatrix}_{\leftarrow L} = \begin{bmatrix} \int_{\theta=0}^{\pi/2} T(\theta)\sin 2\theta d\theta & \int_{\theta=0}^{\pi/2} R(\theta)\sin 2\theta d\theta \\ \int_{\theta=0}^{\pi/2} R'(\theta)\sin 2\theta d\theta & \int_{\theta=0}^{\pi/2} T'(\theta)\sin 2\theta d\theta \end{bmatrix} \tag{6.2}
$$

Let us now study the external bifaces[1]. We will consider here the upper external biface, the lower external biface being characterized equivalently with reversed notations. As stated in Sect. 2.4, every external biface is represented by a particular transfer matrix of the form

$$
\begin{bmatrix} p & s \\ r & x \end{bmatrix} \tag{6.3}
$$

where p is the penetration transmittance, s the external reflectance, r the internal reflectance and x the exit transmittance.

These four terms are determined according to the nature of the biface and the measuring geometry. Table 6.1 (see next page) draws up the inventory of particular transfer matrices considering the different types of biface (transparent, scattering, Lambertian), of light source (directional or Lambertian light source) and of capturing device (integrating sphere, radiance detector). The complete statement of these particular transfer matrices is presented in Appendix D.

6.1.3 Standard procedure for the development of a model

All the elements are now available for expressing the global reflectance and transmittance of any regular multiface:

1. Verify whether the superposed bifaces form a regular multiface, i.e. check that there is no succession of scattering bifaces or whether the contained scattering bifaces are directly bordered by Lambertian bifaces (Sect. 5.2.1).
2. Group consecutive transparent bifaces if any. Their fundamental transfer matrix can be obtained using the compositional formulae.
3. Determine the particular transfer matrix of each central biface according to its illumination, and of each external biface according to the measuring geometry, by referring to Table 6.1.
4. Write the composition equation with these particular transfer matrices. Apply the appropriate compositional formula(e) and derive the global transfer matrix of the multiface.

---

[1] An external biface may be a single interface (see Sect. 6.3.1), the superposition of flat interfaces and transparent layers (see Sect. 6.3.2 and 6.3.3), a rough interface as in matte opaque paints, a Lambertian layer, as in uncombed woolen or cotton fabrics, etc.

Table 6.1: Transfer matrix of the upper external biface specified according to the type of biface, the type of light source and the type of capturing device.

Integrating sphere	Radiance detector
Lambertian external biface	
(a) $\begin{matrix}{}^{any\rightarrow}\\ {}_{sph\leftarrow}\end{matrix}\begin{bmatrix} p_L & s_L \\ r_L & x_L \end{bmatrix}_{\leftarrow any} = \begin{bmatrix} p_L & s_L \\ r_L & x_L \end{bmatrix}$	(b) $\begin{matrix}{}^{any\rightarrow}\\ {}_{rad(\psi')\leftarrow}\end{matrix}\begin{bmatrix} p_L & s_L \\ r_L & x_L \end{bmatrix}_{\leftarrow any} = \begin{bmatrix} p_L & \xi s_L/\pi \\ r_L & \xi x_L/\pi \end{bmatrix}$
Scattering external biface	
Directional light source	
(c) $\begin{matrix}{}^{dir(\psi)\rightarrow}\\ {}_{sph\leftarrow}\end{matrix}\begin{bmatrix} P(\theta) & S(\theta) \\ R(\theta) & X(\theta) \end{bmatrix}_{\leftarrow L} = \begin{bmatrix} P(\psi) & S(\psi) \\ \int R & \int X \end{bmatrix}$	(d) $\begin{matrix}{}^{dir(\psi)\rightarrow}\\ {}_{rad(\psi')\leftarrow}\end{matrix}\begin{bmatrix} P(\theta) & S(\theta) \\ R(\theta) & X(\theta) \end{bmatrix}_{\leftarrow L} = \begin{bmatrix} P(\psi) & \xi f_R(\psi,\psi') \\ \int R & \xi \iint f_T(\psi') \end{bmatrix}$
Lambertian light source	
(e) $\begin{matrix}{}^{L\rightarrow}\\ {}_{sph\leftarrow}\end{matrix}\begin{bmatrix} P(\theta) & S(\theta) \\ R(\theta) & X(\theta) \end{bmatrix}_{\leftarrow L} = \begin{bmatrix} \int P & \int S \\ \int R & \int X \end{bmatrix}$	(f) $\begin{matrix}{}^{L\rightarrow}\\ {}_{rad(\psi')\leftarrow}\end{matrix}\begin{bmatrix} P(\theta) & S(\theta) \\ R(\theta) & X(\theta) \end{bmatrix}_{\leftarrow L} = \begin{bmatrix} \int P & \xi \iint f_R(\psi') \\ \int R & \xi \iint f_T(\psi') \end{bmatrix}$
Transparent external biface	
Directional light source	
(g) $\begin{matrix}{}^{dir(\psi)\rightarrow}\\ {}_{sph\leftarrow}\end{matrix}\begin{bmatrix} P(\theta) & S(\theta) \\ R(\theta) & X(\theta) \end{bmatrix}_{\leftarrow L} = \begin{bmatrix} P(\psi) & S(\psi) \\ \int R & \int X \end{bmatrix}$	(h) $\begin{matrix}{}^{dir(\psi)\rightarrow}\\ {}_{rad(\psi')\leftarrow}\end{matrix}\begin{bmatrix} P(\theta) & S(\theta) \\ R(\theta) & X(\theta) \end{bmatrix}_{\leftarrow L} = \begin{bmatrix} P(\psi) & 0 \\ \int R & \dfrac{\xi X(\psi_1')}{\pi(n_1/n_0)^2} \end{bmatrix}$
Lambertian light source	
(i) $\begin{matrix}{}^{L\rightarrow}\\ {}_{sph\leftarrow}\end{matrix}\begin{bmatrix} P(\theta) & S(\theta) \\ R(\theta) & X(\theta) \end{bmatrix}_{\leftarrow L} = \begin{bmatrix} \int P & \int S \\ \int R & \int X \end{bmatrix}$	(j) $\begin{matrix}{}^{L\rightarrow}\\ {}_{rad(\psi')\leftarrow}\end{matrix}\begin{bmatrix} P(\theta) & S(\theta) \\ R(\theta) & X(\theta) \end{bmatrix}_{\leftarrow L} = \begin{bmatrix} \int P & \xi S(\psi')/\pi \\ \int R & \dfrac{\xi X(\psi_1')}{\pi(n_1/n_0)^2} \end{bmatrix}$

Legend: The left matrices are invariant or fundamental transfer matrices [see Eq. (6.1)], with specification of the upper illumination (left superscript), the lower illumination (right subscript), and the capturing device (left subscript). Symbol L stands for "Lambertian", $dir(\psi)$ for "directional with incident angle ψ", $rad(\psi'')$ for "radiance detector with observation angle ψ''" and *sph* for "integrating sphere". Notation $\int g$ stands for $\int_{\theta=0}^{\pi/2} g(\theta)\sin 2\theta\, d\theta$, and notation $\iint g(\psi)$ for $\int_{\phi=0}^{2\pi}\int_{\theta=0}^{\pi/2} g(\theta,\phi;\psi)\sin\theta\cos\theta\, d\theta\, d\phi$. The term ξ is the apparatus constant characteristic to the radiance detectors (see Eq. A.12).

6.2 Classical models for transparent and wholly-Lambertian multifaces

6.2.1 Transparent multifaces

When transparent bifaces are consecutive, they form a transparent multiface. The transparent multiface is characterized by its fundamental transfer matrix, whose elements are directional reflectances and transmittances. In a first step, the compositional formulae are used to compute the fundamental transfer matrix of the multiface, first for each polarization component, then for natural light (Sect. 3.1.4). Afterwards, the measuring geometry can be considered in the same manner as for any other transparent biface.

For the purpose of illustration, let us consider again the example of a transparent layer bounded on its both sides by flat interfaces presented in Sect. 3.4. The upper interface, the transparent layer and the lower interfaces have respectively the fundamental transfer matrices [see Eqs. (3.25) and (3.39)]

$$\begin{bmatrix} T_{01}(\theta) & R_{01}(\theta) \\ R_{10}(\theta) & T_{10}(\theta) \end{bmatrix}, \quad \begin{bmatrix} t^{1/\cos\theta} & 0 \\ 0 & t^{1/\cos\theta} \end{bmatrix} \quad \text{and} \quad \begin{bmatrix} T_{12}(\theta) & R_{12}(\theta) \\ R_{21}(\theta) & T_{21}(\theta) \end{bmatrix} \tag{6.4}$$

where t is the normal transmittance of the transparent layer, and where $R_{xy}(\theta)$ and $T_{xy}(\theta)$ are Fresnel coefficients defined for an interface relative refractive index n_x/n_y (light comes from the medium of refractive index n_x with an incident angle θ).

Inside the multiface, directional incident light remains directional. According to Snell's third law, we have

$$n_0 \sin\theta_0 = n_1 \sin\theta_1 = n_2 \sin\theta_2 \tag{6.5}$$

where θ_0, θ_1 and θ_2 denote the orientation angle of light in the upper surrounding medium, the transparent layer and the lower surrounding medium respectively. Let us insert these particular directions in the fundamental transfer matrices above and deduce the particular transfer matrices

$$^{dir(\theta_0)\rightarrow}\begin{bmatrix} T_{01}(\theta) & R_{01}(\theta) \\ R_{10}(\theta) & T_{10}(\theta) \end{bmatrix}_{\leftarrow dir(\theta_1)} = \begin{bmatrix} T_{01}(\theta_0) & R_{01}(\theta_0) \\ R_{10}(\theta_1) & T_{10}(\theta_1) \end{bmatrix}, \tag{6.6}$$

$$^{dir(\theta_1)\rightarrow}\begin{bmatrix} t^{1/\cos\theta} & 0 \\ 0 & t^{1/\cos\theta} \end{bmatrix}_{\leftarrow dir(\theta_1)} = \begin{bmatrix} t^{1/\cos\theta_1} & 0 \\ 0 & t^{1/\cos\theta_1} \end{bmatrix} \tag{6.7}$$

and

$$^{dir(\theta_1)\rightarrow}\begin{bmatrix} T_{12}(\theta) & R_{12}(\theta) \\ R_{21}(\theta) & T_{21}(\theta) \end{bmatrix}_{\leftarrow dir(\theta_2)} = \begin{bmatrix} T_{12}(\theta_1) & R_{12}(\theta_1) \\ R_{21}(\theta_2) & T_{21}(\theta_2) \end{bmatrix} \tag{6.8}$$

Using Eqs. (3.23) and (3.24), we can write $R^*_{01}(\theta_0) = R^*_{10}(\theta_1)$, $T^*_{01}(\theta_0) = T^*_{10}(\theta_1)$, $R^*_{21}(\theta_2) = R^*_{12}(\theta_1)$ and $T^*_{21}(\theta_2) = T^*_{12}(\theta_1)$. This permits to express the three transfer matrices as functions of angle θ_1 only. Since, Fresnel's coefficients depend on the polarization of the

incident light, the composition equation is written for each polarization component

$$\begin{bmatrix} T^*_{012}(\theta_0) & R^*_{012}(\theta_0) \\ R^*_{210}(\theta_2) & T^*_{210}(\theta_2) \end{bmatrix} = \begin{bmatrix} T^*_{10}(\theta_1) & R^*_{10}(\theta_1) \\ R^*_{10}(\theta_1) & T^*_{10}(\theta_1) \end{bmatrix} \bigcirc \begin{bmatrix} t^{1/\cos\theta_1} & 0 \\ 0 & t^{1/\cos\theta_1} \end{bmatrix} \bigcirc \begin{bmatrix} T^*_{12}(\theta_1) & R^*_{12}(\theta_1) \\ R^*_{12}(\theta_1) & T^*_{12}(\theta_1) \end{bmatrix} \tag{6.9}$$

where symbol * represents symbol $\perp$ (perpendicular polarization) or symbol $||$ (parallel polarization). Thanks to the hexaface formula (5.27), Eq. (6.9) becomes

$$\begin{bmatrix} T^*_{012}(\theta_0) & R^*_{012}(\theta_0) \\ R^*_{210}(\theta_2) & T^*_{210}(\theta_2) \end{bmatrix} = \begin{bmatrix} \dfrac{T^*_{10}(\theta_1)T^*_{12}(\theta_1)t^{1/\cos\theta_1}}{1-R^*_{10}(\theta_1)R^*_{12}(\theta_1)t^{2/\cos\theta_1}} & R^*_{10}(\theta_1)+\dfrac{T^*_{10}(\theta_1)^2 R^*_{12}(\theta_1)t^{2/\cos\theta_1}}{1-R^*_{10}(\theta_1)R^*_{12}(\theta_1)t^{2/\cos\theta_1}} \\ R^*_{12}(\theta_1)+\dfrac{T^*_{10}(\theta_1)^2 R^*_{01}(\theta_1)t^{2/\cos\theta_1}}{1-R^*_{10}(\theta_1)R^*_{12}(\theta_1)t^{2/\cos\theta_1}} & \dfrac{T^*_{12}(\theta_1)T^*_{10}(\theta_1)t^{1/\cos\theta_1}}{1-R^*_{10}(\theta_1)R^*_{12}(\theta_1)t^{2/\cos\theta_1}} \end{bmatrix} \tag{6.10}$$

By averaging the contributions of the two polarization components, one obtains the fundamental matrix for natural light

$$\begin{bmatrix} T_{012}(\theta_0) & R_{012}(\theta_0) \\ R_{210}(\theta_2) & T_{210}(\theta_2) \end{bmatrix} = \frac{1}{2}\begin{bmatrix} T^{\perp}_{012}(\theta_0) & R^{\perp}_{012}(\theta_0) \\ R^{\perp}_{210}(\theta_2) & T^{\perp}_{210}(\theta_2) \end{bmatrix} + \frac{1}{2}\begin{bmatrix} T^{||}_{012}(\theta_0) & R^{||}_{012}(\theta_0) \\ R^{||}_{210}(\theta_2) & T^{||}_{210}(\theta_2) \end{bmatrix} \tag{6.11}$$

Eq. (6.10) contains the same expressions for $R^*_{012}(\theta_0)$, $T^*_{012}(\theta_0)$, $R^*_{210}(\theta_2)$ and $T^*_{210}(\theta_2)$ as those given by Eqs. (3.55) and (3.56). Hence, the expansive step-by-step computation developed in Sect. 3.4 has been replaced by the straightforward application of a compositional formula.

6.2.2 Wholly-Lambertian multifaces (Kubelka's model)

In 1954, Kubelka published a reflectance and transmittance model for nonhomogenous intensely scattering layers, whose scattering and absorption coefficients are functions of the depth within the layers [Kub54]. The model presented for two and more superposed layers relies on a description of light multiple reflection-transmission. All the layers are assumed to be intensely scattering and to have a same refractive index, also identical to those of the surrounding media. Therefore, there is no Fresnel reflections nor transmissions at the boundaries of the layers. We identify the layers as being Lambertian bifaces. The form a multiface without interfaces called a *wholly-Lambertian multiface*.

Let us first consider two superposed layers. Their upper reflectance, called resp. R_1 and R_2, are different from their lower reflectance, called resp. R_I and R_{II}. Their upper and lower transmittances are equal, i.e. $T_1 = T_I$ and $T_2 = T_{II}$. The resulting multiface, which is a Lambertian quadriface, is obviously regular (Sect. 5.2.1). Its global transfer matrix satisfies the following composition equation

$$\begin{bmatrix} T_{1,2} & R_{1,2} \\ R_{2,1} & T_{2,1} \end{bmatrix} = \begin{bmatrix} T_1 & R_1 \\ R_I & T_I \end{bmatrix} \bigcirc \begin{bmatrix} T_2 & R_2 \\ R_{II} & T_{II} \end{bmatrix} \tag{6.12}$$

Kubelka obtained the global reflectances and transmittances of superposed layers as geometrical series which he successfully simplified as simple expressions. The same expressions can be obtained directly by applying the quadriface formula (5.24)

$$\begin{bmatrix} T_{1,2} & R_{1,2} \\ R_{2,1} & T_{2,1} \end{bmatrix} = \begin{bmatrix} \dfrac{T_1 T_2}{1 - R_I R_2} & R_1 + \dfrac{T_1 T_I R_2}{1 - R_I R_2} \\ R_{II} + \dfrac{T_{II} T_2 R_I}{1 - R_I R_2} & \dfrac{T_I T_{II}}{1 - R_I R_2} \end{bmatrix} \tag{6.13}$$

By inserting equalities $T_1 = T_I$ and $T_2 = T_{II}$, Eq. (6.13) becomes

$$\begin{bmatrix} T_{1,2} & R_{1,2} \\ R_{2,1} & T_{2,1} \end{bmatrix} = \begin{bmatrix} \dfrac{T_1 T_2}{1 - R_I R_2} & R_1 + \dfrac{T_1^2 R_2}{1 - R_I R_2} \\ R_{II} + \dfrac{T_2^2 R_I}{1 - R_I R_2} & \dfrac{T_1 T_2}{1 - R_I R_2} \end{bmatrix}$$

The remarkable fact that $T_{1,2} = T_{2,1}$ is presented by Kubelka as the principle of "nonpolarity of transmittance" for intensely scattering layers.

For the superposition of three or more layers having the same refractive index, Kubelka proposes an iterative formulation that can be obtained in an equivalent way using our compositional formula (5.33).

6.3 Transparent bifaces superposed to a Lambertian background

As a first example of mixed multiface, we consider a Lambertian background bordered on its upper side by a transparent biface or a groupment of transparent bifaces. Such a multiface is regular since it does not contain any scattering biface. The background is considered only as reflector. We will therefore develop reflectance-only models. The light source and the capturing device are located in the upper surrounding medium (e.g. air).

Three types of transparent bifaces are studied: a flat interface (Sect. 6.3.1), a transparent layer with a flat interface at the air side (Sect. 6.3.2) and a transparent layer with a flat interface with air and flat interface with the background (Sect. 6.3.3).

6.3.1 Background with an interface with air (Saunderson's model)

The interface between the background (subscript 1, refractive index n) and air (subscript 0, refractive index assumed to be 1) is characterized by its fundamental transfer matrix composed of Fresnel coefficients [Eq. (3.25)]. It receives from the background a Lambertian illumination. On its upper side, directional light incomes at angle ψ; a radiance detector is placed at angle ψ'. According to formula (h) of Table 6.1, the flat interface has the particular transfer matrix

$$\begin{matrix} {\scriptstyle dir(\psi)\rightarrow} \\ {\scriptstyle rad(\psi')\leftarrow} \end{matrix} \begin{bmatrix} T_{01}(\theta) & R_{01}(\theta) \\ R_{10}(\theta) & T_{10}(\theta) \end{bmatrix}_{\leftarrow L} = \begin{bmatrix} T_{01}(\psi) & 0 \\ r_{10} & \dfrac{\xi}{\pi n^2} T_{10}\left(\psi_1'\right) \end{bmatrix} \tag{6.14}$$

where r_{10} is the Lambertian internal reflectance of the interface [Eq. (3.29)], and ψ_1' is related to the direction of the detector by Snell's third law

$$\psi_1' = \arcsin\left(\sin\psi'/n\right) \tag{6.15}$$

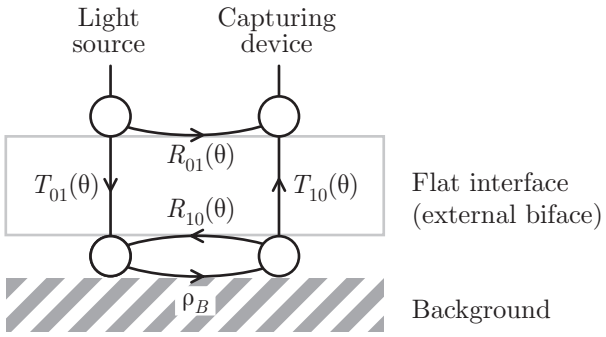

Fig. 6.2: Multiple reflection-transmission process occurring within a quadriface composed of a flat interface and a Lambertian background.

The background is completely characterized by its intrinsic reflectance ρ_B (Fig. 6.2), which occupies the upper right position in its transfer matrix. All other elements should be considered as "unspecified" (represented subsequently by a point). Likewise, the global transfer matrix of the multiface contains only the upper global reflectance $R_{rad(\psi')}$. The multiface is represented by the composition equation

$$\begin{bmatrix} \cdot & R_{rad(\psi')} \\ \cdot & \cdot \end{bmatrix} = \begin{bmatrix} T_{01}(\psi) & 0 \\ r_{10} & \dfrac{\xi}{\pi n^2} T_{10}\left(\psi_1'\right) \end{bmatrix} \bigcirc \begin{bmatrix} \cdot & \rho_B \\ \cdot & \cdot \end{bmatrix} \tag{6.16}$$

The quadriface formula (5.24) and the equality $T_{10}\left(\psi_1'\right) = T_{01}\left(\psi'\right)$ [Eq. (3.24)] yield

$$R_{rad(\psi')} = \frac{\xi}{\pi n^2} \cdot \frac{T_{01}(\psi) T_{01}\left(\psi'\right) \rho_B}{1 - r_{10}\rho_B} \tag{6.17}$$

By dividing this global reflectance $R_{rad(\psi')}$ by the reflectance $R_{ref} = \xi/\pi$ of a perfect white diffuser [see Appendix A, Eq. (A.14)], one obtains a reflectance factor $\hat{R}_{rad(\psi')}$ independent of the apparatus constant ξ

$$\hat{R}_{rad(\psi')} = \frac{1}{n^2} \cdot \frac{T_{01}(\psi) T_{01}\left(\psi'\right) \rho_B}{1 - r_{10}\rho_B} \tag{6.18}$$

The same expression as (6.18) has been derived in [HH04] from a step-by-step description of the multiple reflection-transmission process.

Let us now consider an integrating sphere as capturing device. According to formula (g) of Table 6.1, the interface has the particular transfer matrix

$$\begin{matrix} {\scriptstyle dir(\psi)\rightarrow} \\ {\scriptstyle sph\leftarrow} \end{matrix} \begin{bmatrix} T_{01}(\theta) & R_{01}(\theta) \\ R_{10}(\theta) & T_{10}(\theta) \end{bmatrix}_{\leftarrow L} = \begin{bmatrix} T_{01}(\psi) & R_{01}(\psi) \\ r_{10} & t_{10} \end{bmatrix} \tag{6.19}$$

where t_{10} is the lower Lambertian transmittance of the interface [Eq. (3.30)]. The composition equation becomes

$$\begin{bmatrix} \cdot & R_{sph} \\ \cdot & \cdot \end{bmatrix} = \begin{bmatrix} T_{01}(\psi) & R_{01}(\psi) \\ r_{10} & t_{10} \end{bmatrix} \bigcirc \begin{bmatrix} \cdot & \rho_B \\ \cdot & \cdot \end{bmatrix} \tag{6.20}$$

The quadriface formula (5.24) is again applied, yielding

$$R_{sph} = R_{01}(\psi) + T_{01}(\psi) t_{10} \frac{\rho_B}{1 - r_{10}\rho_B} \tag{6.21}$$

Expression (6.21) is known as the "Saunderson correction" for the Kubelka-Munk model. It is used when ρ_B is computed from the Kubelka-Munk differential equation system (Sect. 4.3.2) without taking into account the optical effects of the interface [HH04]. The original paper of Saunderson [Sau42] presents expression (6.21) in the following form

$$R' = \frac{k_1}{2} + (1 - k_1)(1 - k_2) \frac{R}{1 - k_2 R} \tag{6.22}$$

Saunderson's notations R', R, k_1 and k_2 respectively correspond to our notations R_{sph}, ρ_B, $R_{01}(\psi)$ and r_{10}. Transmittances $T_{01}(\psi)$ and t_{10} are represented by $1 - k_1$ and $1 - k_2$, which is justified by Eqs. (3.22) and (3.31) respectively. Furthermore, Saunderson specifies that his integrating sphere has a hole discarding about a half of the external reflection. This explains why the external reflectance is $k_1/2$ instead of k_1.

Remark: Let us consider a background having a rough interface. Although the external biface is scattering, it is bordered by a Lambertian biface (the background). The quadriface is therefore regular. A prior modelization of the interface's upper and lower BRDFs and BTDFs would permit to determine its fundamental transfer matrix. Equivalent expressions to (6.18) or (6.21) would be obtained for the reflectance factor of the multiface. However, with a non-Lambertian background, the quadriface would be irregular whatever the type of interface. Unless a specific study shows the contrary, the Saunderson cannot be applied with a non-Lambertian background.

6.3.2 Background coated by a transparent layer (Williams-Clapper model)

In 1953, Williams and Clapper proposed a prediction model for reflectance of photographs [WC53]. The considered specimens are composed of a Lambertian support coated with a transparent coloring layer having the same refractive index ($n = 1.53$) and forming a flat interface with air. The model is based on the 45°/0° measuring geometry (Sect. 1.3.1). Shore and Spoonhower have extended the Williams-Clapper model to any bidirectional geometry, as well as to geometries including an integrating sphere [SS01]. We propose to derive Shore and Spoonhower's general expressions using our formalism.

The Lambertian background has a reflectance ρ_B and transparent layer a normal transmittance t. The background and the transparent layer are assumed to have the same refractive index n (no interface between them). There is however a flat interface between the layer (medium 1) and the air (medium 0). The light source is directional (incident angle ψ) and the reflected light is captured by a radiance detector (observation angle $\psi' \neq \psi$). The specimen may be represented by a hexaface composed of the interface, the transparent layer and the Lambertian background (Fig. 6.3).

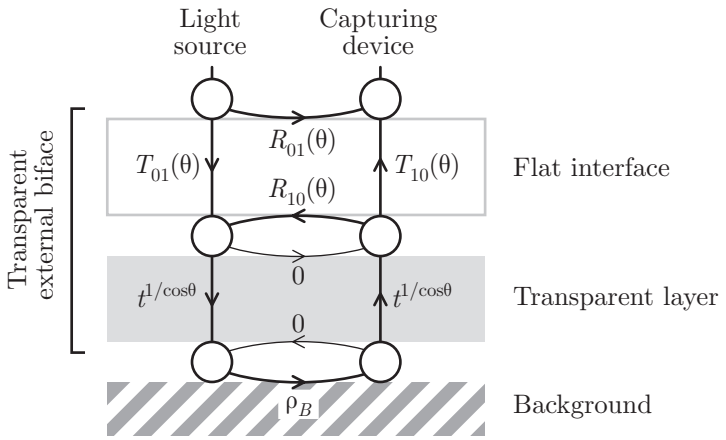

Fig. 6.3: Multiple reflection-transmission process occurring within a hexaface composed of a flat interface, a transparent layer and a Lambertian background.

The flat interface and the transparent layer have the fundamental transfer matrices (3.25) and (3.39) respectively. They are grouped into a single biface, which is subsequently external and transparent. The fundamental transfer matrix of this external transparent biface is determined using the quadriface formula

$$\begin{bmatrix} T_{01}(\theta) & R_{01}(\theta) \\ R_{10}(\theta_1) & T_{10}(\theta_1) \end{bmatrix} \bigcirc \begin{bmatrix} t^{1/\cos\theta_1} & 0 \\ 0 & t^{1/\cos\theta_1} \end{bmatrix} = \begin{bmatrix} T_{01}(\theta)t^{1/\cos\theta_1} & R_{01}(\theta) \\ R_{10}(\theta_1)t^{2/\cos\theta_1} & T_{10}(\theta_1)t^{1/\cos\theta_1} \end{bmatrix} \tag{6.23}$$

where θ and $\theta_1 = \arcsin(\sin\theta/n)$, related by Snell's law, represent the angles in the air and in the layer respectively.

Let us now determine the particular transfer matrix of the transparent external biface. It receives from the background a Lambertian illumination. At the upper side, the measuring geometry is bidirectional. Formula (h) of Table 6.1 gives

$$\begin{matrix} {\scriptstyle dir(\psi)\rightarrow} \\ {\scriptstyle rad(\psi')\leftarrow} \end{matrix} \begin{bmatrix} T_{01}(\theta)t^{1/\cos\theta_1} & R_{01}(\theta) \\ R_{10}(\theta_1)t^{2/\cos\theta_1} & T_{10}(\theta_1)t^{1/\cos\theta_1} \end{bmatrix}_{\leftarrow L} = \begin{bmatrix} T_{01}(\psi)t^{1/\cos\psi_1} & 0 \\ r_{10}(t) & \dfrac{\xi}{\pi n^2}T_{10}(\psi_1')t^{1/\cos\psi_1'} \end{bmatrix} \tag{6.24}$$

with $\psi_1 = \arcsin(\sin\psi/n)$, $\psi_1' = \arcsin(\sin\psi'/n)$, $T_{10}(\psi_1') = T_{01}(\psi')$, and

$$r_{10}(t) = \int_{\theta=0}^{\pi/2} R_{10}(\theta)t^{2/\cos\theta}\sin 2\theta d\theta \tag{6.25}$$

The background is then composed with the external transparent biface

$$\begin{bmatrix} \cdot & R_{rad(\psi')} \\ \cdot & \cdot \end{bmatrix} = \begin{bmatrix} T_{01}(\psi)t^{1/\cos\psi_1} & 0 \\ r_{10}(t) & \xi\dfrac{T_{01}(\psi')t^{1/\cos\psi_1'}}{\pi n^2} \end{bmatrix} \bigcirc \begin{bmatrix} \cdot & \rho_B \\ \cdot & \cdot \end{bmatrix} \tag{6.26}$$

Its global reflectance $R_{rad(\psi')}$ is obtained thanks to the quadriface formula (5.24)

$$R_{rad(\psi')} = \frac{\xi}{\pi n^2} \cdot \frac{T_{01}(\psi) T_{01}(\psi') t^{1/\cos\psi_1 + 1/\cos\psi_1'} \rho_B}{1 - \rho_B r_{10}(t)} \tag{6.27}$$

The corresponding reflectance factor $\hat{R}_{rad(\psi')} = R_{rad(\psi')}/R_{ref}$, defined in reference to a perfect white diffuser (reflectance $R_{ref} = \xi/\pi$, see Eq. A.14) is

$$\hat{R}_{rad(\psi')} = \frac{1}{n^2} \cdot \frac{T_{01}(\psi) T_{01}(\psi') t^{1/\cos\psi_1 + 1/\cos\psi_1'} \rho_B}{1 - \rho_B r_{10}(t)} \tag{6.28}$$

Expression (6.28) is identical to that presented by Shore and Spoonhower [SS01], also derived independently by Elias & al. [EM01, Eq. (8)]. A step-by-step description of the multiple reflection-transmission process [HH04] also leads to the same expression.

Williams and Clapper considered only the special values $n = 1.53$, $\psi = 45°$ and $\psi' = 0°$. By arranging the terms of Eq. (6.28), we retrieve their original expression

$$\hat{R}_{wc} = 0.183\ t^{2.13} \left[\frac{1}{2\rho_B} - \int_{\theta=0}^{\pi/2} R_{10}(\theta) t^{2/\cos\theta} \cos\theta \sin\theta d\theta \right]^{-1} \tag{6.29}$$

Shore and Spoonhower have also developed a model for a directional source and an integrating sphere. The corresponding global reflectance is expressed as

$$R_{sph} = R_{01}(\psi) + \frac{T_{01}(\psi) t^{1/\cos\psi_1} t_{10}(t) \rho_B}{1 - r_{10}(t) \rho_B} \tag{6.30}$$

A similar expression is presented in [HH04], but since the external reflection is assumed to be eliminated from the measurement, the term $R_{10}(\psi)$ corresponding to the specular reflection at the air-layer interface is omitted.

Let us retrieve expression (6.30) with our compositional formalism. The particular transfer matrix of the transparent external biface is derived from Formula (g) of Table 6.1

$$\begin{matrix} {\scriptstyle dir(\psi)\rightarrow} \\ {\scriptstyle sph\leftarrow} \end{matrix} \begin{bmatrix} T_{01}(\theta) t^{1/\cos\theta_1} & R_{01}(\theta) \\ R_{10}(\theta_1) t^{2/\cos\theta_1} & T_{10}(\theta_1) t^{1/\cos\theta_1} \end{bmatrix}_{\leftarrow L} = \begin{bmatrix} T_{01}(\psi) t^{1/\cos\psi_1} & R_{01}(\psi) \\ r_{10}(t) & t_{10}(t) \end{bmatrix} \tag{6.31}$$

where $r_{10}(t)$ is given by Eq. (6.25) and

$$t_{10}(t) = \int_{\theta=0}^{\pi/2} T_{10}(\theta) t^{1/\cos\theta} \sin 2\theta d\theta \,, \tag{6.32}$$

Expression (6.30) is then obtained by applying the quadriface formula to the composition equation

$$\begin{bmatrix} \cdot & R_{sph} \\ \cdot & \cdot \end{bmatrix} = \begin{bmatrix} T_{01}(\psi) t^{1/\cos\psi_1} & R_{01}(\psi) \\ r_{10}(t) & t_{10}(t) \end{bmatrix} \bigcirc \begin{bmatrix} \cdot & \rho_B \\ \cdot & \cdot \end{bmatrix} \tag{6.33}$$

Remark: Let us again consider that the interface is rough. Since the transparent layer has a zero reflectance, there is no multiple reflection between the rough interface and the transparent layer. The transparent layer grouped with the rough interface form a scattering biface, bordered at the bottom side by the Lambertian background. The resulting multiface is regular (Sect. 5.2.1). However, the multiface would be irregular if the transparent layer was replaced by a scattering layer having a nonzero reflectance, or if the background was scattering only instead of being Lambertian.

6.3.3 Background and transparent layer having different refractive indices

In order to cope with an eventual difference of refractive index between the layer and the background (resp. n_1 and n_2), it is necessary to introduce into the model an interface between them. The background-layer interface, assumed here to be flat, causes multiple reflections with the background at the lower side, and with the layer-air interface at the upper side (Fig. 6.5). This configuration has been presented very recently by Simonot & al as an extension of the Williams-Clapper model [SHH06]. The development of this model is based on a step-by-step description of the multiple reflection-transmission process of light.

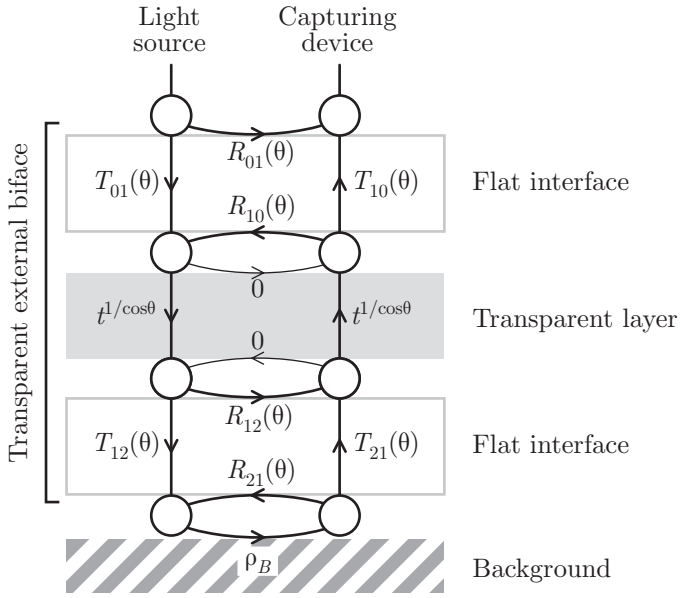

Fig. 6.5: Multiple reflection-transmission process occurring within a multiface composed of a transparent layer bounded by two interfaces and a Lambertian background.

Here, the external biface is composed of the air-layer interface, the transparent layer and the layer-background interface. The fundamental transfer matrix of such a transpar-

ent multiface has already been developed in Sect. 6.2.1 and is given by Eq. (6.11). Excepted this new fundamental transfer matrix, we have the same configuration as for the interface alone and for the transparent layer bounded by one interface.

For a bidirectional measuring geometry (incidence angle ψ and observation angle $\psi' \neq \psi$), the particular transfer matrix of the transparent external biface is (Table 6.1, formula h)

$$\begin{matrix} {\scriptstyle dir(\psi)\rightarrow} \\ {\scriptstyle rad(\psi')\leftarrow} \end{matrix} \begin{bmatrix} T_{012}(\theta) & R_{012}(\theta) \\ R_{210}(\theta_1) & T_{210}(\theta_1) \end{bmatrix}_{\leftarrow L} = \begin{bmatrix} T_{012}(\psi) & 0 \\ r_{210}(t) & \dfrac{\xi}{\pi n_2^2} T_{210}(\psi_2') \end{bmatrix} \tag{6.34}$$

with

$$r_{210}(t) = \int_{\theta=0}^{\pi/2} R_{210}(\theta) \sin 2\theta d\theta \,, \tag{6.35}$$

$T_{210}(\psi_2')$ may be replaced by $T_{012}(\psi')$ [Eq. (3.58)]. The composition equation is

$$\begin{bmatrix} \cdot & R_{rad(\psi')} \\ \cdot & \cdot \end{bmatrix} = \begin{bmatrix} T_{012}(\psi) & 0 \\ r_{210}(t) & \xi \dfrac{T_{012}(\psi')}{\pi n^2} \end{bmatrix} \bigcirc \begin{bmatrix} \cdot & \rho_B \\ \cdot & \cdot \end{bmatrix} \tag{6.36}$$

The quadriface formula then gives the following expression for the reflectance of the background coated with the transparent layer of different refractive index

$$R_{rad(\psi')} = \frac{\xi}{\pi n_2^2} \cdot \frac{T_{012}(\psi) T_{012}(\psi') \rho_B}{1 - \rho_B r_{210}(t)} \tag{6.37}$$

The corresponding reflectance factor $\hat{R}_{rad(\psi')} = R_{rad(\psi')} / R_{ref}$, defined in reference to a perfect white diffuser (reflectance $R_{ref} = \xi/\pi$), is

$$\hat{R}_{rad(\psi')} = \frac{1}{n_2^2} \cdot \frac{T_{012}(\psi) T_{012}(\psi') \rho_B}{1 - \rho_B r_{210}(t)} \tag{6.38}$$

For an integrating sphere geometry, the transfer matrix of the transparent external biface is given by formula (g) of Table 6.1

$$\begin{matrix} {\scriptstyle dir(\psi)\rightarrow} \\ {\scriptstyle sph\leftarrow} \end{matrix} \begin{bmatrix} T_{012}(\theta) & R_{012}(\theta) \\ R_{210}(\theta_1) & T_{210}(\theta_1) \end{bmatrix}_{\leftarrow L} = \begin{bmatrix} T_{012}(\psi) & R_{012}(\psi) \\ r_{210}(t) & t_{210}(t) \end{bmatrix} \tag{6.39}$$

where $r_{210}(t)$ is given by Eq. (6.35) and

$$t_{210}(t) = \int_{\theta=0}^{\pi/2} T_{210}(\theta) \sin 2\theta d\theta \,. \tag{6.40}$$

The reflectance of the coated background observed with an integrating sphere is

$$R_{sph} = R_{012}(\psi) + \frac{T_{012}(\psi) t_{012}(t) \rho_B}{1 - \rho_B r_{210}(t)} \tag{6.41}$$

Note that in [SHH06], the external reflection component $R_{012}(\psi)$ is omitted, being assumed to be discarded from the measurement.

The model of Simonot & al. is not restricted to a single transparent layer. The Lambertian background may be superposed with several transparent layers of different refractive indices, separated by flat interfaces. The grouping of the layers and interfaces is performed iteratively, with a formula equivalent to the compositional formula (5.33). Once the new fundamental transfer matrix is obtained, the same development as above may be followed.

Remark: The multiface becomes irregular if either one of the interfaces is rough, or the transparent layer is replaced by a scattering layer, or the background is weakly scattering instead of being Lambertian.

Summary

We have established how, given a multiface and a measuring geometry, the reflectance and the transmittance of each face can be determined. The elaboration of reflectance and transmittance models have been illustrated with classical models, i.e. the Kubelka's model and the Williams-Clapper model. The recent extensions of the Williams-Clapper model for the integrating sphere geometry (Shore and Spoonhower [SHO00]), and a non neglectible background-coating interface (Simonot, Hébert and Hersch [SHH06]) have also been retrieved.

We have not considered yet multifaces with alternations of transparent and Lambertian bifaces. We have neither found in the specialized literature any compositional model considering such multifaces. This is probably due to the fact that the description of a multiple reflection-transmission process in three or more superposed bifaces of different nature is hardly realizable with a step-by-step method. With the compositional model, we are now capable of considering mixed multifaces, such as superposed paper sheets (Chapter 7) and prints (Chapter 8). The superposition of glossy paper sheets, for example, yields a multiface comprising seven bifaces: two paper layers (Lambertian), four flat interfaces (transparent) and the air layer between the paper sheets (obviously also transparent).

Chapter 7.
Compositional models for paper

The present chapter aims at characterizing high quality paper sheets. The paper layer, assumed to be Lambertian, is characterized by its "intrinsic" reflectance and transmittance. It is bounded at both its sides by interfaces, assumed to be flat, characterized by Fresnel coefficients. A straightforward application of the compositional model gives global reflectances and transmittances of the paper sheet for a selected measuring geometry. Biface splittings enable dissociating the geometry-dependent terms from the other ones. We thus define a sheet "internal reflectance and transmittance" remaining invariant whatever the measuring geometry (Sect. 7.1). The relationship between our compositional model and the Kubelka-Munk model is analyzed. A method for deducing the intrinsic parameters of paper from measurements is also proposed. In Sect. 7.2, an advanced model considers the superposition of two sheets with full optical contact or without contact. We use this double sheet model for deducing from measurements the intrinsic parameters of paper independently of the measuring geometry (Sect. 7.3).

7.1 Single paper sheet model

Papers depend on the nature of the fibers (natural or synthetic) forming the paper bulk, the chemical treatment, the addition of optical brighteners for improving the paper whiteness and the surface coating. Paper sheets are generally characterized by reflectances, brightness, opacity, gloss, and Kubelka-Munk coefficients [BLMC01, Nis98].

Here, paper sheets are characterized by the intrinsic reflectance and transmittance of the paper substrate layer, considered without interfaces. This requires modeling the multiple reflections occurring at the internal side of the paper-air interfaces. Because of the angular dependence of the Fresnel coefficients, the measuring geometries must be taken into account. However, they may be not exactly known, e.g. when the illuminating light source is not collimated or not Lambertian as expected in our model. The observation geometry of measuring devices may also be uncertain. We therefore intent to develop a model independent of the measuring geometry.

The model presented here concerns high quality paper sheets, whose paper layer is made of a homogenous and nonfluorescent scattering layer assimilated to a Lambertian biface. White opaque plastic sheets are also concerned provided that the pigmented plastic scatters light sufficiently for being considered as a Lambertian layer. The surfaces of the sheet are assumed to be flat, hence forming two flat paper-air interfaces.

At the upper side of the sheet, a directional light incomes at angle ψ, and a radiance detector captures light at angle ψ' (we note ξ' its apparatus constant, defined in Appendix A.2). At the bottom side are placed a Lambertian light source and a radiance detector (apparatus constant ξ'', observation angle ψ''). For such a measuring geometry, the

global transfer matrix of the paper sheet is termed

$$\begin{bmatrix} T_{U1} & R_{U1} \\ R_{V1} & T_{V1} \end{bmatrix} \tag{7.1}$$

We propose to determine the elements of this global transfer matrix according to our compositional model.

7.1.1 Global reflectance and transmittance of a paper sheet

The paper sheet is represented by a hexaface, whose bifaces are respectively the upper air-paper interface, the paper layer, and the lower air-paper interface (Fig. 7.1). Such a hexaface is regular since it does not comprise any scattering biface (Sect. 5.2.1).

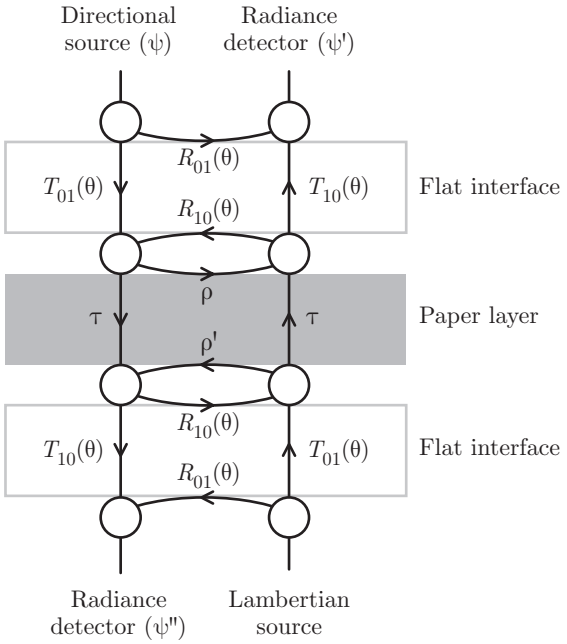

Fig. 7.1: Hexaface representing a paper sheet.

The Lambertian paper layer is characterized by its invariant transfer matrix (Sect. 6.1.2), containing its upper intrinsic reflectance ρ, its lower intrinsic reflectance ρ' (generally different from ρ) and its intrinsic transmittance τ (identical at the upper and the lower sides)

$$\begin{bmatrix} \tau & \rho \\ \rho' & \tau \end{bmatrix} \tag{7.2}$$

The interfaces are characterized by their fundamental transfer matrix [Eq. (3.25)] whose elements are Fresnel reflection and transmission coefficients parameterized by the refrac-

tive index n of the paper. Since they are external bifaces, their particular transfer matrix depends on the measuring geometry.

Let us first consider the upper interface. It is illuminated on its upper side by the directional light source (incident angle ψ) and on its lower side by the Lambertian light coming from the paper layer. It is observed at the upper side by a radiance detector (observation angle ψ'). With formula (h) of Table 6.1, and using relation $T_{10}(\psi'_1) = T_{01}(\psi')$, the upper interface has the particular transfer matrix

$$\begin{matrix} {\scriptstyle dir(\psi)\rightarrow} \\ \\ {\scriptstyle rad(\psi')\leftarrow} \end{matrix} \begin{bmatrix} T_{01}(\theta) & R_{01}(\theta) \\ R_{10}(\theta) & T_{10}(\theta) \end{bmatrix}_{\leftarrow L} = \begin{bmatrix} T_{01}(\psi) & 0 \\ r_{10} & \dfrac{\xi'}{\pi n^2} T_{01}(\psi') \end{bmatrix} \tag{7.3}$$

The lower interface is illuminated by Lambertian irradiances on both its faces. Its lower face is observed by a radiance detector at angle ψ''. Its particular transfer matrix is given by Formula (j) of Table 6.1, with reversed notations since we are in presence of a lower external biface

$$\begin{matrix} {\scriptstyle L\rightarrow} \\ \\ \\ \end{matrix} \begin{bmatrix} T_{10}(\theta) & R_{10}(\theta) \\ R_{01}(\theta) & T_{01}(\theta) \end{bmatrix}^{\rightarrow rad(\psi'')}_{\leftarrow L} = \begin{bmatrix} \dfrac{\xi''}{\pi n^2} T_{01}(\psi'') & r_{10} \\ \dfrac{\xi''}{\pi} R_{01}(\psi'') & t_{01} \end{bmatrix} \tag{7.4}$$

The composition equation representing the paper sheet is

$$\begin{bmatrix} T_{U1} & R_{U1} \\ R_{V1} & T_{V1} \end{bmatrix} = \begin{bmatrix} T_{01}(\psi) & 0 \\ r_{10} & \dfrac{\xi'}{\pi n^2} T_{01}(\psi') \end{bmatrix} \bigcirc \begin{bmatrix} \tau & \rho \\ \rho' & \tau \end{bmatrix} \bigcirc \begin{bmatrix} \dfrac{\xi''}{\pi n^2} T_{01}(\psi'') & r_{10} \\ \dfrac{\xi''}{\pi} R_{01}(\psi'') & t_{01} \end{bmatrix} \tag{7.5}$$

The hexaface formula (5.27) applied to the composition equation (7.5) gives the expression for the global transfer matrix of the paper sheet

$$\begin{bmatrix} T_{U1} & R_{U1} \\ R_{V1} & T_{V1} \end{bmatrix} = \begin{bmatrix} \dfrac{\xi'' T_{01}(\psi) T_{01}(\psi'')}{\pi n^2} \cdot \dfrac{\tau}{D'} & \dfrac{\xi' T_{01}(\psi) T_{01}(\psi')}{\pi n^2} \cdot \dfrac{\rho - r_{10}(\rho\rho' - \tau^2)}{D'} \\ \dfrac{\xi'' R_{01}(\psi'')}{\pi} + \dfrac{\xi'' t_{01} T_{01}(\psi'')}{\pi n^2} \cdot \dfrac{\rho' - r_{10}(\rho\rho' - \tau^2)}{D'} & \dfrac{\xi' t_{01} T_{01}(\psi')}{\pi n^2} \cdot \dfrac{\tau}{D'} \end{bmatrix} \tag{7.6}$$

with $D' = (1 - r_{10}\rho)(1 - r_{10}\rho') - r_{10}^2 \tau\tau'$.

In the case of a symmetric paper sheet, both faces of the paper layer have the same intrinsic reflectance ($\rho = \rho'$). The global transfer matrix of the sheet becomes

$$\begin{bmatrix} T_{U1} & R_{U1} \\ R_{V1} & T_{V1} \end{bmatrix} = \begin{bmatrix} \dfrac{\xi'' T_{01}(\psi) T_{01}(\psi'')}{\pi n^2} \cdot \dfrac{\tau}{D'} & \dfrac{\xi' T_{01}(\psi) T_{01}(\psi')}{\pi n^2} \cdot \dfrac{\rho - r_{10}(\rho^2 - \tau^2)}{D'} \\ \dfrac{\xi'' R_{01}(\psi'')}{\pi} + \dfrac{\xi'' t_{01} T_{01}(\psi'')}{\pi n^2} \cdot \dfrac{\rho - r_{10}(\rho^2 - \tau^2)}{D'} & \dfrac{\xi' t_{01} T_{01}(\psi')}{\pi n^2} \cdot \dfrac{\tau}{D'} \end{bmatrix} \tag{7.7}$$

with $D' = (1 - r_{10}\rho)^2 - (r_{10}\tau)^2$.

7.1.2 Internal reflectance and transmittance of a paper sheet

Eq. (7.6) shows clearly that the sheet global transfer matrix depend on the measuring geometry. However, this dependence is only due to the external reflectance, the penetration transmittance and the exit transmittance of the interfaces. In order to dissociate the geometry-dependent terms from the other terms, we propose to split the bifaces representing the interfaces (see Sect. 5.4). Their transfer matrix, given by Eqs. (7.3) and (7.4), are thus represented by a composition of two transfer matrices, a first one containing the external reflectance, the penetration transmittance and the exit transmittance (geometry-dependent terms), the second one containing the internal reflectance which is geometry-independent. The upper biface is split as

$$\begin{bmatrix} T_{01}(\psi) & 0 \\ r_{10} & \dfrac{\xi'}{\pi n^2}\,T_{01}(\psi') \end{bmatrix} = \begin{bmatrix} T_{01}(\psi) & 0 \\ 0 & \dfrac{\xi'}{\pi n^2}\,T_{01}(\psi') \end{bmatrix} \bigcirc \begin{bmatrix} 1 & 0 \\ r_{10} & 1 \end{bmatrix} \tag{7.8}$$

and the lower biface is split as

$$\begin{bmatrix} \dfrac{\xi''}{\pi n^2}\,T_{01}(\psi'') & r_{10} \\ \dfrac{\xi''}{\pi}\,R_{01}(\psi'') & t_{01} \end{bmatrix} = \begin{bmatrix} 1 & r_{10} \\ 0 & 1 \end{bmatrix} \bigcirc \begin{bmatrix} \dfrac{\xi''}{\pi n^2}\,T_{01}(\psi'') & 0 \\ \dfrac{\xi''}{\pi}\,R_{01}(\psi'') & t_{01} \end{bmatrix} \tag{7.9}$$

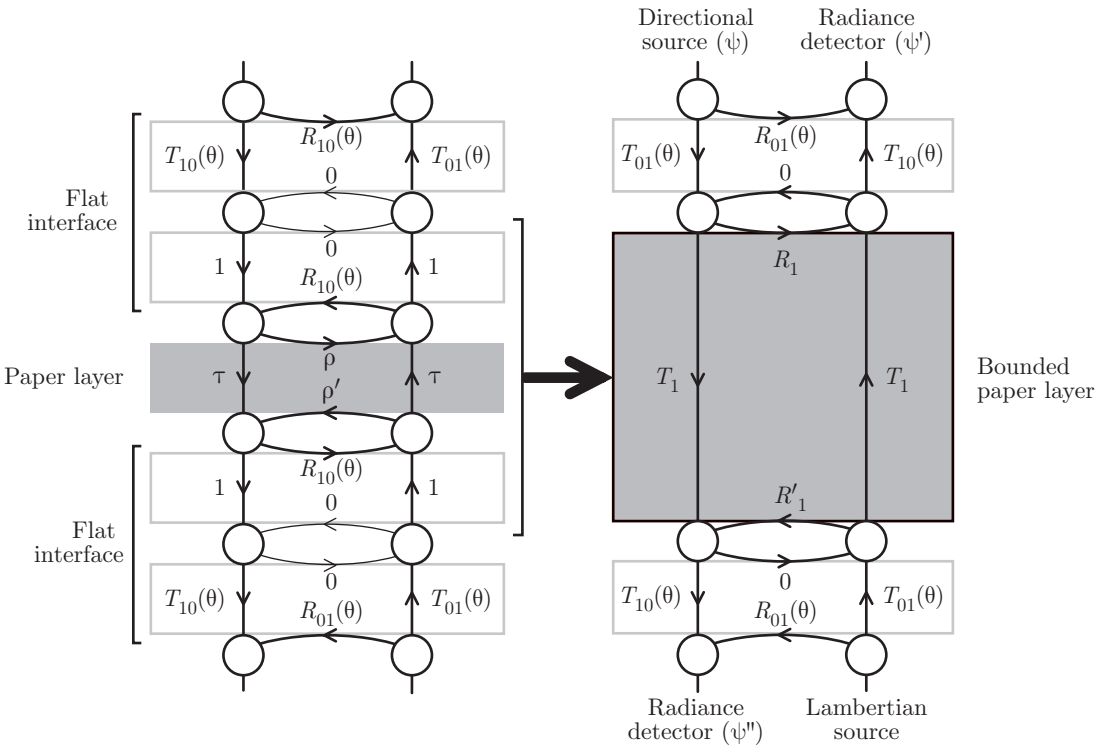

Fig. 7.2: Representation of a paper sheet with split interfaces. The paper layer and its bordering interfaces form a geometry-independent biface, called "bounded paper layer".

The composition equation of the paper sheet, originally given by Eq. (7.5), becomes

$$\begin{bmatrix} T_{U1} & R_{U1} \\ R_{V1} & T_{V1} \end{bmatrix} = \begin{bmatrix} T_{01}(\psi) & 0 \\ 0 & \dfrac{\xi'}{\pi n^2} T_{01}(\psi') \end{bmatrix} \bigcirc \begin{bmatrix} 1 & 0 \\ r_{10} & 1 \end{bmatrix} \bigcirc \begin{bmatrix} \tau & \rho \\ \rho & \tau \end{bmatrix} \bigcirc \begin{bmatrix} 1 & r_{10} \\ 0 & 1 \end{bmatrix} \bigcirc \begin{bmatrix} \dfrac{\xi''}{\pi n^2} T_{01}(\psi'') & 0 \\ \dfrac{\xi''}{\pi} R_{01}(\psi'') & t_{01} \end{bmatrix} \tag{7.10}$$

As indicated in Fig. 7.2, the three central bifaces are regrouped into a single biface, called the "bounded paper layer". The composition of the three central transfer matrices in Eq. (7.10), calculated according to the hexaface formula (5.27), gives the *internal transfer matrix* of the paper sheet

$$\begin{bmatrix} T_1 & R_1 \\ R_1' & T_1' \end{bmatrix} = \begin{bmatrix} 1 & 0 \\ r_{10} & 1 \end{bmatrix} \bigcirc \begin{bmatrix} \tau & \rho \\ \rho' & \tau \end{bmatrix} \bigcirc \begin{bmatrix} 1 & r_{10} \\ 0 & 1 \end{bmatrix} = \frac{1}{D'} \begin{bmatrix} \tau & \rho - r_{10}\left(\rho\rho' - \tau^2\right) \\ \rho' - r_{10}\left(\rho\rho' - \tau^2\right) & \tau \end{bmatrix} \tag{7.11}$$

where $D' = \left(1 - r_{10}\rho\right)\left(1 - r_{10}\rho'\right) - \left(r_{10}\tau\right)^2$.

Reflectances R_1 and R_1' are called the *internal reflectances* of the paper sheet and transmittances T_1 and T_1' are called the *internal transmittances*. They take into account the internal reflections at the paper-air interfaces, but not the surface reflection, the penetration nor the exit. Eq. (7.11) puts into evidence the fact that internal transmittances T_1 and T_1' are equal, even though the paper sheet is not symmetric. Light therefore crosses the bounded paper layer with the same attenuation independently on the sense of crossing. This property[1] may be given the name of "principle of nonpolarity of internal transmittance", in reference to the "principle of nonpolarity of transmittance" formulated by Kubelka for Lambertian multifaces having all the same refractive index (Sect. 6.2.2).

The relationship between the global and the internal transfer matrices follows directly Eq. (7.10)

$$\begin{bmatrix} T_{U1} & R_{U1} \\ R_{V1} & T_{V1} \end{bmatrix} = \begin{bmatrix} T_{01}(\psi) & 0 \\ 0 & \xi' \dfrac{T_{01}(\psi')}{\pi n^2} \end{bmatrix} \bigcirc \begin{bmatrix} T_1 & R_1 \\ R_1' & T_1 \end{bmatrix} \bigcirc \begin{bmatrix} \xi'' \dfrac{T_{01}(\psi'')}{\pi n^2} & 0 \\ \xi'' \dfrac{R_{01}(\psi'')}{\pi} & t_{01} \end{bmatrix} \tag{7.12}$$

Eq. (7.12) characterizes the dissociation in our single sheet model of the geometry-dependent and the geometry-independent terms. It tells us, in particular, that the global transmittances T_{U1} and T_{V1} are different only due to the light penetration and exit across the interfaces.

In the case of a symmetric paper sheet ($\rho = \rho'$), both internal reflectances are also equal, i.e. $R_1 = R_1'$. Eq. (7.11) becomes

$$\begin{bmatrix} T_1 & R_1 \\ R_1 & T_1 \end{bmatrix} = \frac{1}{\left(1 - r_{10}\rho\right)^2 - \left(r_{10}\tau\right)^2} \begin{bmatrix} \tau & \rho - r_{10}\left(\rho^2 - \tau^2\right) \\ \rho - r_{10}\left(\rho^2 - \tau^2\right) & \tau \end{bmatrix} \tag{7.13}$$

[1] The non-polarity of the bounded paper layer is also valid when the interfaces have different properties (relative refractive index, roughness, etc.)

7.1.3 Relation with the Kubelka-Munk model

We have characterized with expression (7.6) the optical properties of a paper sheet as functions of the intrinsic reflectances ρ and ρ' and transmittance τ of the paper layer. However, the characterization of paper is traditionally expressed with the parameters of the Kubelka-Munk model [KM31], i.e. with a scattering coefficient S, an absorption coefficient K, and the layer thickness h [BLMC01]. Let us establish the connection between the two models [HH06].

First note that the Kubelka-Munk model can be used only if the paper layer has the same coefficients at every point. We must therefore consider in our single sheet model that the paper layer has identical faces, i.e. $\rho = \rho'$.

We can choose among two methods for obtaining the global reflectance and transmittance of the sheet as functions of the Kubelka-Munk parameters. In the first method, which may be called the "direct method", the reflections and the transmissions by the interfaces are taken into account as boundary conditions while solving the Kubelka-Munk differential equation system. This corresponds exactly to the configuration of a Lambertian layer bounded by two bifaces, presented in Sect. 4.3.5. Here, the two bifaces are the flat interfaces. The global reflectance and transmittance of the sheet have the same expressions as R_b and T_b [Eqs. (3.105) and (3.106)], with the specific elements

$$\begin{bmatrix} p_u & s_u \\ r_u & x_u \end{bmatrix} = \begin{bmatrix} T_{01}(\psi) & 0 \\ r_{10} & \xi\dfrac{T_{01}(\psi')}{\pi n^2} \end{bmatrix} \quad \text{and} \quad \begin{bmatrix} x_v & r_v \\ s_v & p_v \end{bmatrix} = \begin{bmatrix} \xi\dfrac{T_{01}(\psi'')}{\pi n^2} & r_{10} \\ \xi\dfrac{R_{01}(\psi'')}{\pi} & t_{01} \end{bmatrix} \tag{7.14}$$

The second method, which may be called the "two steps method", consists in solving the Kubelka-Munk system for the Lambertian layer alone without considering the interfaces, which yields expressions (3.96) and (3.97) for its intrinsic reflectance ρ and transmittance τ, and then in using the compositional model (Eqs. (7.5) and (7.6)) for taking into account the reflections and the transmissions at the interfaces. One may verify that both methods are equivalent. The second method may be considered as an extended Saunderson correction for two bounding interfaces.

7.1.4 Deducing intrinsic parameters of paper from measurements

We would like to determine the intrinsic parameters ρ and ρ' and τ of a nonsymmetric paper sheet. We use a bidirectional spectrophotometer (typically build on the $45°/0°$ geometry) either in reflectance mode (light source on) or in transmittance mode (light source off). The spectrophotometer is placed upon the paper sheet, and a diffusing light table, placed below, is used as light source in transmittance mode. The measuring geometry is thus similar to the measuring geometry considered in Sect. 7.1.2, except that there is no detector at the lower side.

The spectrophotometer is first used in reflectance mode. We measure the reflectance R_{ref} of a perfect white diffuser, given by Eq. (A.14)

$$R_{ref} = \xi'/\pi \tag{7.15}$$

Then, we measure the upper global reflectance R_{U1} of the sheet as weel as the upper global reflectance $R_{U1}^{\rightleftarrows}$ of the same sheet positioned upside-down. According to Eq. (7.6), our model expresses reflectance R_{U1} as

$$R_{U1} = \frac{\xi'}{\pi n^2} T_{01}(\psi)\, T_{01}(\psi') \frac{\rho - r_{10}\left(\rho\rho' - \tau^2\right)}{\left(1 - r_{10}\rho\right)\left(1 - r_{10}\rho'\right) - \left(r_{10}\tau\right)^2}\,, \tag{7.16}$$

Reflectance $R_{U1}^{\rightleftarrows}$ is similarly expressed, the intrinsic reflectances ρ and ρ' being replaced by each other

$$R_{U1}^{\rightleftarrows} = \frac{\xi'}{\pi n^2} T_{01}(\psi)\, T_{01}(\psi') \frac{\rho' - r_{10}\left(\rho\rho' - \tau^2\right)}{\left(1 - r_{10}\rho\right)\left(1 - r_{10}\rho'\right) - \left(r_{10}\tau\right)^2} \tag{7.17}$$

The spectrophotometer is then used in transmittance mode. A first transmittance T_{ref} is measured without the sheet, considering air as the reference transmitter. In a similar manner as the perfect white diffuser, the light table emits a Lambertian irradiance, yielding a transmittance of air

$$T_{ref} = \xi'/\pi \tag{7.18}$$

The lower transmittance T_{V1} of the sheet is given by Eq. (7.6)

$$T_{V1} = \frac{\xi'}{\pi n^2} t_{01} T_{01}(\psi') \frac{\tau}{D'} \tag{7.19}$$

In order to have expressions independent of the apparatus constant ξ', we rather consider the reflectance factors $\hat{R}_{U1} = R_{U1}/R_{ref}$ and $\hat{R}_{U1}^{\rightleftarrows} = R_{U1}^{\rightleftarrows}/R_{ref}$ and the transmittance factor $\hat{T}_{V1} = T_{V1}/T_{ref}$. We obtain the three following equations

$$\hat{R}_{U1} = \frac{1}{n^2} T_{01}(\psi)\, T_{01}(\psi') \frac{\rho - r_{10}\left(\rho\rho' - \tau^2\right)}{\left(1 - r_{10}\rho\right)\left(1 - r_{10}\rho'\right) - \left(r_{10}\tau\right)^2} \tag{7.20}$$

$$\hat{R}_{U1}^{\rightleftarrows} = \frac{1}{n^2} T_{01}(\psi)\, T_{01}(\psi') \frac{\rho' - r_{10}\left(\rho\rho' - \tau^2\right)}{\left(1 - r_{10}\rho\right)\left(1 - r_{10}\rho'\right) - \left(r_{10}\tau\right)^2} \tag{7.21}$$

and

$$\hat{T}_{V1} = \frac{1}{n^2} t_{01} T_{01}(\psi') \frac{\tau}{\left(1 - r_{10}\rho\right)\left(1 - r_{10}\rho'\right) - \left(r_{10}\tau\right)^2} \tag{7.22}$$

Knowing the refractive index of the paper, the Fresnel coefficients and their integrations over the hemisphere (r_{10} and t_{01}, see Sect. 3.2.2) can be computed. The three equations (7.20), (7.21) and (7.22) thus allow to deduce wavelength by wavelength the intrinsic parameters ρ, ρ′ and τ.

The principal drawback of this method is the fact that it depends on the measuring geometry, due to the presence of the terms $T_{01}(\psi)$, $T_{01}(\psi')$ and t_{01}. Although these terms are easily computable thanks to Fresnel formulae [Eqs. (3.20), (3.22) and (3.28)], we are not always certain that the conditions of illumination respect our assumptions. We would

like to have three equations completely independent of the measuring geometry. The double sheet model that we present now makes it possible.

7.2 The double sheet model

As shown in Sect. 7.1.2, a single paper sheet may be characterized by an internal transfer matrix whose internal reflectances and transmittances R_1, R_1' and T_1 are independent of the measuring geometry. The geometry-dependent terms, i.e. the surface reflectances s, the penetration transmittances p and the exit transmittances x of the interfaces, are placed in separate transfer matrices. For the selected measuring geometry, the relation between the global and the internal transfer matrices is

$$\begin{bmatrix} T_{U1} & R_{U1} \\ R_{V1} & T_{V1} \end{bmatrix} = \begin{bmatrix} p_u & s_u \\ 0 & x_u \end{bmatrix} \bigcirc \begin{bmatrix} T_1 & R_1 \\ R_1' & T_1 \end{bmatrix} \bigcirc \begin{bmatrix} x_v & 0 \\ s_v & p_v \end{bmatrix} = \begin{bmatrix} p_u x_v T_1 & s_u + p_u x_u R_1 \\ s_v + p_v x_v R_1' & p_v x_u T_1 \end{bmatrix} \tag{7.23}$$

Let us now superpose two identical paper sheets, the lower sheet being positioned upside-down. Thus, the resulting double sheet is symmetric. Selecting the same measuring geometry as for a single sheet, we have an equivalent relation between the global transfer matrix of the double sheet and its internal transfer matrix

$$\begin{bmatrix} T_{U2} & R_{U2} \\ R_{V2} & T_{V2} \end{bmatrix} = \begin{bmatrix} p_u & s_u \\ 0 & x_u \end{bmatrix} \bigcirc \begin{bmatrix} T_2 & R_2 \\ R_2 & T_2 \end{bmatrix} \bigcirc \begin{bmatrix} x_v & 0 \\ s_v & p_v \end{bmatrix} = \begin{bmatrix} p_u x_v T_2 & s_u + p_u x_u R_2 \\ s_v + p_v x_v R_2 & p_v x_u T_2 \end{bmatrix} \tag{7.24}$$

In Eq. (7.24), the upper and lower internal reflectances (R_2) are identical due to the symmetry of the double sheet.

It may be observed from Eqs. (7.23) and (7.24) that the ratio of global transmittances T_{V2}/T_{V1} is equal to the ratio of internal transmittances T_2/T_1

$$\frac{T_{V2}}{T_{V1}} = \frac{p_v x_u T_2}{p_v x_u T_1} = \frac{T_2}{T_1} \tag{7.25}$$

Since both internal transmittances T_1 and T_2 are geometry-independent, the ratio T_{V2}/T_{V1} is also geometry-independent.

In the case of the reflectance, the ratio of measured reflectances R_{U2}/R_{U1} (likewise the ratio $R_{U2}/R_{U1}^{\rightleftarrows}$) is geometry-independent only when the surface reflection is discarded from the measure ($s_u = 0$), which is the case when a 45°/0° geometry is used

$$\frac{R_{U2}}{R_{U1}} = \frac{p_u x_u R_2}{p_u x_u R_1} = \frac{R_2}{R_1} \quad \text{and} \quad \frac{R_2}{R_{U1}^{\rightleftarrows}} = \frac{p_u x_u R_2}{p_u x_u R_1'} = \frac{R_2}{R_1'} \tag{7.26}$$

Let us develop expressions for R_2 and T_2 as functions of the paper intrinsic parameters ρ, ρ' and τ. This will then allow deducing these parameters from the geometry independent equations (7.25) and (7.26).

7.2.1 Model for a full contact between the sheets

When the two identical sheets are in full optical contact, there is not interface between the paper layers, which thus form a double layer of paper. The external interfaces are split in the same manner as for a single sheet (Sect. 7.1.2). We may therefore represent the double sheet by the composition equation

$$\begin{bmatrix} T_{U2} & R_{U2} \\ R_{V2} & T_{V2} \end{bmatrix} = \begin{bmatrix} p_u & s_u \\ 0 & x_u \end{bmatrix} \bigcirc \begin{bmatrix} 1 & 0 \\ r_{i0} & 1 \end{bmatrix} \bigcirc \begin{bmatrix} \tau & \rho \\ \rho' & \tau \end{bmatrix} \bigcirc \begin{bmatrix} \tau & \rho' \\ \rho & \tau \end{bmatrix} \bigcirc \begin{bmatrix} 1 & r_{i0} \\ 0 & 1 \end{bmatrix} \bigcirc \begin{bmatrix} x_v & 0 \\ s_v & p_v \end{bmatrix} \tag{7.27}$$

The internal transfer matrix of the double sheet results from the composition of the four central transfer matrices. The quadriface formula (5.24) is first applied to the two transfer matrices of the paper layers

$$\begin{bmatrix} T_2 & R_2 \\ R_2 & T_2 \end{bmatrix} = \begin{bmatrix} 1 & 0 \\ r_{i0} & 1 \end{bmatrix} \bigcirc \begin{bmatrix} \dfrac{\tau^2}{1-\rho'^2} & \rho + \dfrac{\tau^2\rho'}{1-\rho'^2} \\ \rho + \dfrac{\tau^2\rho'}{1-\rho'^2} & \dfrac{\tau^2}{1-\rho'^2} \end{bmatrix} \bigcirc \begin{bmatrix} 1 & r_{i0} \\ 0 & 1 \end{bmatrix} \tag{7.28}$$

Then, the hexaface formula (5.27) is applied to Eq. (7.28). As a result, the internal reflectance R_2 and transmittance T_2 of the double sheet are

$$R_2 = \frac{1}{D}\left[\rho + \frac{\rho'\tau^2}{1-\rho'^2} - r_{i0}\left(\rho + \frac{\tau^2}{1-\rho'}\right)\left(\rho + \frac{\tau^2}{1+\rho'}\right)\right] \quad \text{and} \quad T_2 = \frac{1}{D}\cdot\frac{\tau^2}{1-\rho'^2} \tag{7.29}$$

with

$$D = \left(1 - r_{i0}\rho - r_{i0}\frac{\rho'\tau^2}{1-\rho'^2}\right)^2 + \left(r_{i0}\frac{\tau^2}{1-\rho'^2}\right)^2 \tag{7.30}$$

The assumption of full optical contact between paper sheets is an ideal condition that is rarely realizable in practice, because bubbles or thin layers of air may have a nonneglectible effect. Instead, we separate the two sheets and thus create a planar air layer between them.

7.2.2 Model without contact between the sheets

The two paper sheets are now separated by a layer of air. The lower sheet is still identical to the upper sheet but positioned upside-down. The resulting multiface is composed of seven bifaces: four interfaces, two paper layers and the air layer. As previously, all the flat interfaces are split. The internal reflections at the paper side of the interfaces are considered together with the paper layers. We thus obtain two bounded paper layers (see Fig. 7.3) identical to those characterized in Sect. 7.1.2. Therefore, we reuse the internal reflectances R_1 and R_1' and the internal transmittance T_1 given by the single sheet internal transfer matrix (7.11). Because the two sheets are reversed, the upper and the lower bounded paper layers have slightly different transfer matrices, i.e. respectively

$$\begin{bmatrix} T_1 & R_1 \\ R_1' & T_1 \end{bmatrix} \quad \text{and} \quad \begin{bmatrix} T_1 & R_1' \\ R_1 & T_1 \end{bmatrix} \tag{7.31}$$

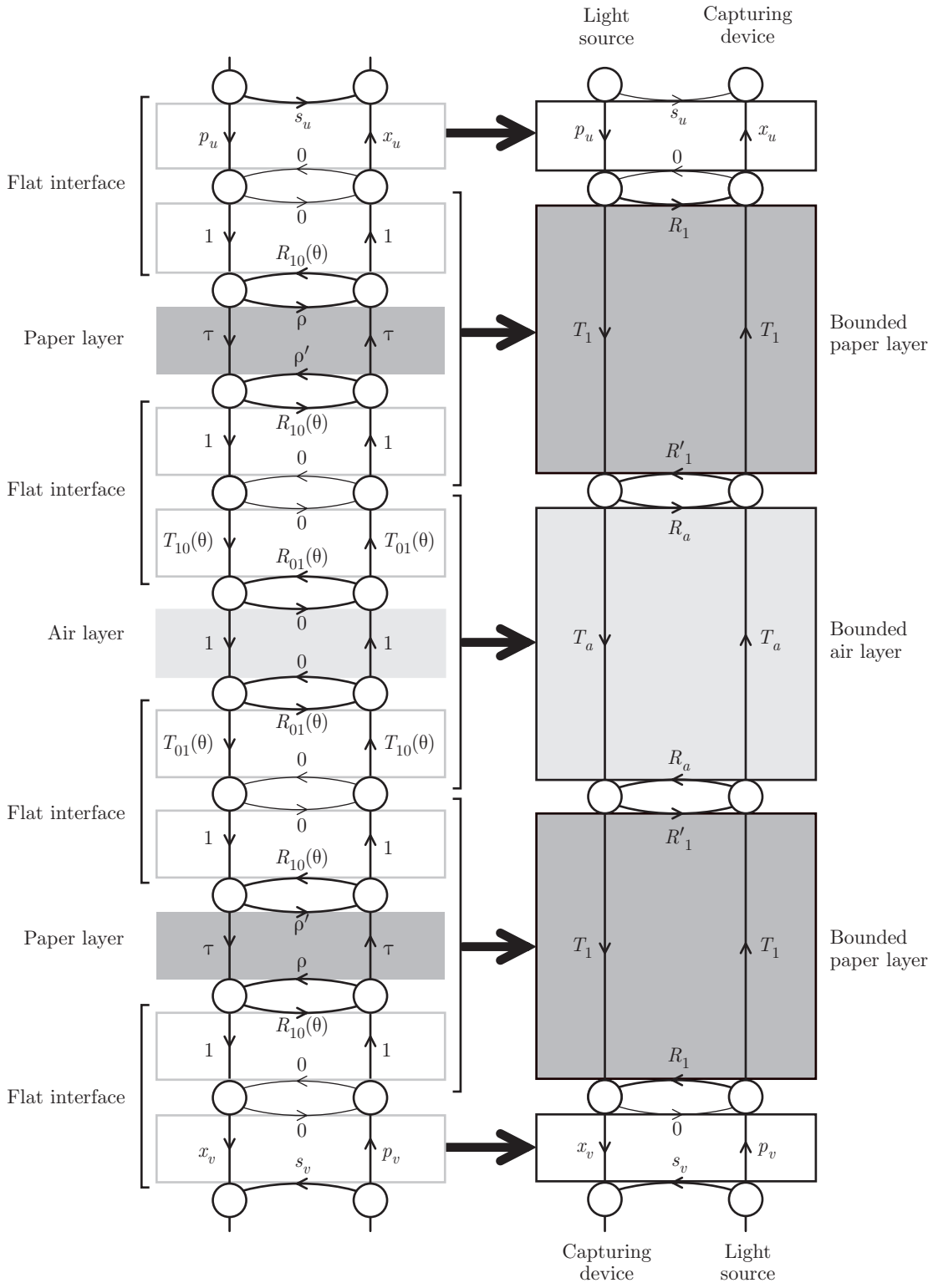

Fig. 7.3: Representation of two paper sheets superposed without contact. The air layer between the paper sheets and its bordering interfaces form a transparent multiface: the "bounded air layer".

The air layer has a zero reflectance and a unit transmittance. Its transfer matrix is

$$\begin{bmatrix} 1 & 0 \\ 0 & 1 \end{bmatrix} \tag{7.32}$$

We call "bounded air layer" the air layer considered with its bordering interfaces, excluded the paper-side reflections which are already embodied into the bounded paper layers. The fundamental transfer matrix of the bounded air layer results from the following composition

$$\begin{bmatrix} T_{10}(\theta_1) & 0 \\ R_{01}(\theta_0) & T_{01}(\theta_0) \end{bmatrix} \bigcirc \begin{bmatrix} 1 & 0 \\ 0 & 1 \end{bmatrix} \bigcirc \begin{bmatrix} T_{01}(\theta_0) & R_{01}(\theta_0) \\ 0 & T_{10}(\theta_1) \end{bmatrix} \tag{7.33}$$

Composition (7.33) should be computed first for the two polarization components and then, by averaging, for natural light. However, a numerical evaluation shows that for a standard refractive index of paper close to 1.5, the composition can be performed directly with the Fresnel coefficients for natural light. The hexaface formula (5.27) thus gives the following fundamental transfer matrix for the bounded air layer

$$\begin{bmatrix} \dfrac{T_{10}(\theta_1)\,T_{01}(\theta_0)}{1-R_{01}^2(\theta_0)} & \dfrac{T_{10}(\theta_1)\,T_{01}(\theta_0)\,R_{10}(\theta_1)}{1-R_{01}^2(\theta_0)} \\ \dfrac{T_{10}(\theta_1)\,T_{01}(\theta_0)\,R_{10}(\theta_1)}{1-R_{01}^2(\theta_0)} & \dfrac{T_{10}(\theta_1)\,T_{01}(\theta_0)}{1-R_{01}^2(\theta_0)} \end{bmatrix} \tag{7.34}$$

Eq. (7.34) may be simplified using relations $R_{01}(\theta_0) = R_{10}(\theta_1)$, $T_{01}(\theta_0) = T_{10}(\theta_1)$. With relation $T_{10}(\theta_1) = 1 - R_{10}(\theta_1)$ [Eq. (3.22)], one has

$$1 - R_{01}^2(\theta_0) = \big(1 + R_{10}(\theta_1)\big)\big(1 - R_{10}(\theta_1)\big) = \big(1 + R_{10}(\theta_1)\big)T_{10}(\theta_1)$$

The bounded air layer is symmetric. Both its faces receives a Lambertian illumination. They have therefore the same reflectance R_a and the same transmittance T_a

$$\begin{bmatrix} T_a & R_a \\ R_a & T_a \end{bmatrix} = \overset{L\rightarrow}{\left\{\begin{bmatrix} \dfrac{T_{10}(\theta_1)}{1+R_{10}(\theta_1)} & \dfrac{R_{10}(\theta_1)\,T_{10}(\theta_1)}{1+R_{10}(\theta_1)} \\ \dfrac{R_{10}(\theta_1)\,T_{10}(\theta_1)}{1+R_{10}(\theta_1)} & \dfrac{T_{10}(\theta_1)}{1+R_{10}(\theta_1)} \end{bmatrix}\right\}}_{\leftarrow L} \tag{7.35}$$

According to Eq. (6.2), one obtains

$$R_a = \int_{\theta=0}^{\pi/2} \frac{R_{10}(\theta_1)\,T_{10}(\theta_1)}{1+R_{10}(\theta_1)} \sin 2\theta_1 d\theta_1 \tag{7.36}$$

and

$$T_a = \int_{\theta=0}^{\pi/2} \frac{T_{10}(\theta_1)}{1+R_{10}(\theta_1)} \sin 2\theta_1 d\theta_1 \tag{7.37}$$

Remark: There is no absorption within the bounded air layer. The principle of conservation of energy should therefore be satisfied. The sum of reflectance R_a and transmittance T_a yields the fraction of Lambertian light coming from the paper layer that is not internally reflected by the paper-air interface, i.e. $R_a + T_a = 1 - r_{10}$.

Since their expression relies only on Fresnel coefficients, r_{10}, R_a and T_a depend only on the refractive index n of the paper. Numerical values of these terms are proposed for refractive indices comprised between 1.45 and 1.55 in Table 7.1.

Table 7.1: Numerical values of r_{10}, R_a and T_a as functions of the paper refractive index n

n	1.45	1.46	1.47	1.48	1.49	1.50	1.51	1.52	1.53	1.54	1.55
r_{10}	0.565	0.571	0.578	0.584	0.590	0.596	0.602	0.608	0.614	0.620	0.625
R_a	0.028	0.028	0.028	0.028	0.028	0.028	0.028	0.028	0.028	0.029	0.029
T_a	0.408	0.401	0.394	0.388	0.382	0.375	0.369	0.363	0.358	0.352	0.346

The multiface representing the double sheet is reduced to five bifaces (see Fig. 7.3): the upper bounded paper layer, the bounded air layer, the lower bounded paper layer, and the two geometry-dependent external bifaces. Composing the three "bounded layers" yields the internal transfer matrix of the double sheet

$$\begin{bmatrix} T_2 & R_2 \\ R_2 & T_2 \end{bmatrix} = \begin{bmatrix} T_1 & R_1 \\ R_1' & T_1 \end{bmatrix} \bigcirc \begin{bmatrix} T_a & R_a \\ R_a & T_a \end{bmatrix} \bigcirc \begin{bmatrix} T_1 & R_1' \\ R_1 & T_1 \end{bmatrix} \tag{7.38}$$

According to the hexaface formula (5.27), we obtain for the internal reflectance of the double sheet

$$R_2 = R_1 + T_1^2 \frac{R_a - \left(R_a^2 - T_a^2\right) R_1'}{\left(1 - R_a R_1'\right)^2 - \left(T_a R_1'\right)^2} \tag{7.39}$$

and for its internal reflectance

$$T_2 = \frac{T_a T_1^2}{\left(1 - R_a R_1'\right)^2 - \left(T_a R_1'\right)^2} \tag{7.40}$$

When the superposed sheets are symmetric, their internal reflectances R_1 and R_1' are equal [see Eq. (7.13)]. Thus, the internal reflectance and transmittance of the double sheet become

$$R_2 = R_1 + T_1^2 \frac{R_a - \left(R_a^2 - T_a^2\right) R_1}{\left(1 - R_a R_1\right)^2 - \left(T_a R_1\right)^2} \tag{7.41}$$

and

$$T_2 = \frac{T_a T_1^2}{\left(1 - R_a R_1\right)^2 - \left(T_a R_1\right)^2} \tag{7.42}$$

7.3 Experimental results

The single and double sheet models are used in the context of a reflectance and transmittance model for printed sheets (see Chapter 8). Two different printing supports are used: opaque white PVC pigmented with titanium dioxide, of refractive index 1.54, and high-quality paper, of refractive index assumed to be 1.5. Both types of sheets are symmetric ($\rho = \rho'$), nonfluorescent and have smooth surfaces. We want to deduce the intrinsic reflectance $\rho(\lambda)$ and transmittance $\tau(\lambda)$ from the spectral measurements in reflectance mode and transmittance mode. First, a geometry-dependent equations are used for deducing ρ and τ. Then, in order to ascertain the modelization of the measuring geometry in transmittance mode, a geometry-independent equation provided by the noncontact double sheet model is used.

The reflectance spectrum $R_{U1}(\lambda)$ of a single sheet is measured with the portative GrategMacbeth^{TM} Eye-One spectrophotometer, based on the 45°/0° geometry (see Sect. 1.3.1). First, the spectrum of a reference white tile is measured. Then, the spectrum of the selected specimen is measured. The spectrophotometer gives directly the ratio of the specimen's spectrum to the reference spectrum. It therefore gives a reflectance factor spectrum, noted $\hat{R}_{U1}(\lambda)$.

$\hat{R}_{U1}(\lambda)$, given by Eq. (7.21) with $\rho = \rho'$, $\psi = 45°$, and $\psi' = 0°$, is a function of the paper intrinsic reflectance $\rho(\lambda)$ and transmittance $\tau(\lambda)$

$$\hat{R}_{U1}(\lambda) = \frac{T_{01}(0°)\, T_{01}(45°)}{n^2} \cdot \frac{\rho - r_{10}\left(\rho^2 - \tau^2\right)}{\left(1 - r_{10}\rho\right)^2 - \left(r_{10}\tau\right)^2} \tag{7.43}$$

In transmittance mode, we measure the flux $\Phi_1(\lambda)$ transmitted through the printing support and the flux $\Phi_{ref}(\lambda)$ coming from the light table. The ratio $\Phi(\lambda)/\,\Phi_{ref}(\lambda)$ gives the transmittance factor $\hat{T}_{U1}(\lambda)$, expressed by Eq. (7.21) with $\rho(\lambda) = \rho'(\lambda)$ and $\psi' = 0°$

$$\hat{T}_{V1}(\lambda) = \frac{t_{01} T_{01}(0°)}{n^2} \cdot \frac{\tau}{\left(1 - r_{10}\rho\right)^2 - \left(r_{10}\tau\right)^2} \tag{7.44}$$

The intrinsic reflectance $\rho(\lambda)$ and transmittance $\tau(\lambda)$ are deduced numerically from Eqs. (7.43) and (7.44). Measured transmittance factors $\hat{R}_{U1}(\lambda)$ and $\hat{T}_{U1}(\lambda)$ are plotted in Fig. 7.4a for both the white PVC and the high quality paper. The deduced spectra of $\rho(\lambda)$ and $\tau(\lambda)$ correspond to the solid curves plotted in Fig. 7.4c.

In order to check whether the light table used for transmittance measurements is Lambertian as expected, we use the geometry-independent equations provided by the noncontact double sheet model. We measure the flux $\Phi_2(\lambda)$ of the two face-to-face superposed sheets. Measured fluxes $\Phi_1(\lambda)$ (single sheet) and $\Phi_2(\lambda)$ (double sheet) are plotted in Fig. 7.4b. The single sheet and the double sheet receives a same incident flux $\Phi_i(\lambda)$. The ratios $\Phi_1(\lambda)/\Phi_i(\lambda)$ and $\Phi_2(\lambda)/\Phi_i(\lambda)$ correspond respectively to the global transmittance of the single sheet, $T_{V1}(\lambda)$, and the global transmittance of the double sheet, $T_{V2}(\lambda)$. However, in the ratio $T_{V2}(\lambda)/\,T_{V1}(\lambda)$, the incident flux $\Phi_i(\lambda)$ cancels

$$\frac{\Phi_2(\lambda)}{\Phi_1(\lambda)} = \frac{T_{V2}(\lambda)}{T_{V1}(\lambda)} \tag{7.45}$$

According to Eq. (7.25), the ratio of global transmittances $T_{V2}(\lambda)/T_{V1}(\lambda)$ is equal to the ratio of internal transmittances $T_2(\lambda)/T_1(\lambda)$. From Eq. (7.42), we have

$$\frac{T_2(\lambda)}{T_1(\lambda)} = \frac{T_a T_1(\lambda)}{\left[1 - R_a R_1(\lambda)\right]^2 - \left[T_a R_1(\lambda)\right]^2} \tag{7.46}$$

where $R_1(\lambda)$ and $T_1(\lambda)$ are given by (7.13)

$$R_1(\lambda) = \frac{\rho(\lambda) - r_{10}\left[\rho^2(\lambda) - \tau^2(\lambda)\right]}{\left[1 - r_{10}\rho(\lambda)\right]^2 - \left[r_{10}\tau(\lambda)\right]^2} \quad \text{and} \quad T_1(\lambda) = \frac{\tau(\lambda)}{\left[1 - r_{10}\rho(\lambda)\right]^2 - \left[r_{10}\tau(\lambda)\right]^2} \tag{7.47}$$

$\rho(\lambda)$ and transmittance $\tau(\lambda)$ are again calculated, this time from the equation system formed by Eqs. (7.43) and (7.46). Eq. (7.43) is a geometry-dependent equation, where the $45°/0°$ geometry used in reflectance model is modeled, but we consider that this geometry is certain. However, Eq. (7.46) is geometry independent. This avoid to model the uncertain measuring geometry used in transmittance mode. The deduced spectra of $\rho(\lambda)$ and $\tau(\lambda)$ are plotted with dashed lines in Fig 8.4(c). They are compared with the spectra $\rho(\lambda)$ and $\tau(\lambda)$ previously deduced from Eqs. (7.43) and (7.44), plotted with solid lines. The small difference between the spectra obtained from the two methods for short and large wavelength is due to the low emission of the light table in these spectral ranges, which induces some noise in the measurements. The good matching of the curves in the reste of the spectrum confirms that the assumption of Lambertian illumination was satisfied. It is also a partial validation of our two superposed sheet model.

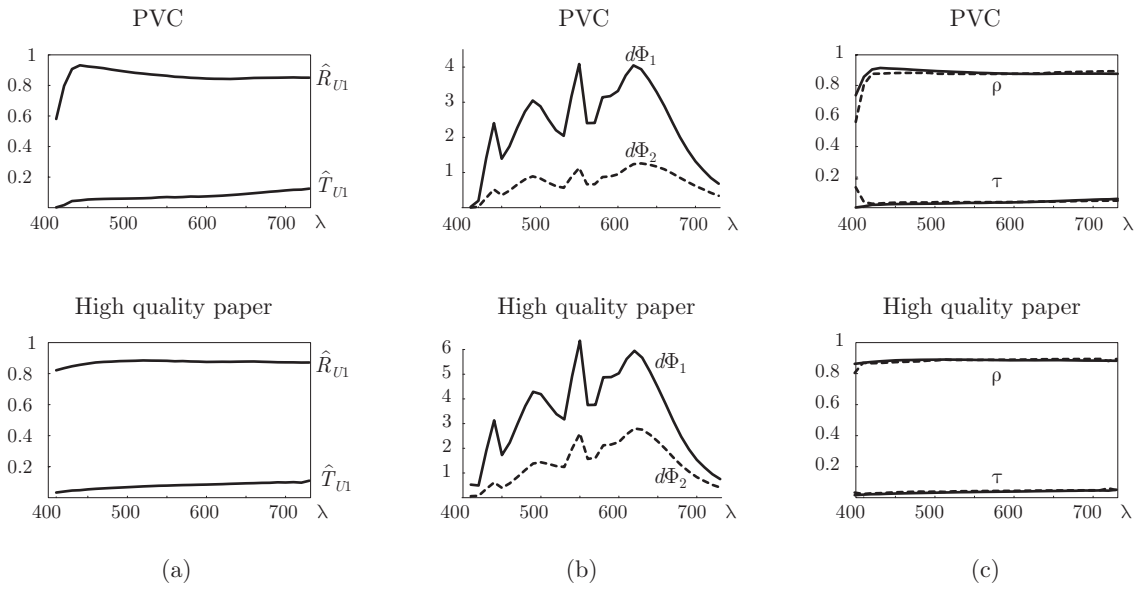

Fig. 7.4: (a) Reflectance factor and transmittance factor spectra measured on a single sheet; (b) measured flux spectra transmitted through (solid line:) the single and (dashed line:) the double sheets, expressed in arbitrary units; (c) intrinsic reflectance and transmittance spectra of the paper layer fitted from (solid line:) spectra plotted in a) and (dashed line:) spectra plotted in b).

Summary

We have applied the compositional model to the characterization of opaque and glossy paper sheets (Lambertian paper layer and flat interfaces with air). The representation of the paper sheet by a regular hexaface and the use of the hexaface formula enables expressing in a straightforward manner its global reflectance and transmittance for various measuring geometries. Furthermore, thanks to splits of the air-paper interfaces, we have dissociated the terms depending on the measuring geometry and the other terms. We thus have defined "internal" reflectances and transmittances, corresponding to the geometry-independent part of the global reflectances and transmittances. The compositional model appears to be adequate for the characterization of paper, in particular for the obtention of its intrinsic reflectances and transmittance. These intrinsic parameters may also be a step in the derivation of the Kubelka-Munk scattering and absorption coefficients from spectral measurements.

We have also presented two models for superposed sheets: a first model considers a full contact between two sheets, which is however difficult to realize in practice, and a second model without contact, which may be easily realized. Thanks to this second model, the terms depending on the measuring geometry can be completely discarded. This simplifies considerably the calibration of the measuring device, in particular for transmittance measurements which are often performed with custom setups. This model could not have been derived from the Kubelka-Munk model [Kub48] nor from the Kubelka model for superposed Lambertian layer [Kub54] because of the central air layer. It therefore represents a real progress in the modelization of multilayer specimens.

The single sheet model may be extended to matte paper sheets, provided the rough paper-air interfaces be appropriately characterized. The rough interfaces, which are scattering bifaces, are neighbored by a Lambertian biface. The hexaface therefore remains regular. However, two matte sheets superposed without contact form an irregular multiface, due to the adjacency of two scattering bifaces bounding the air layer. In the future, it would be interesting to study the influence of the surface roughness in the accuracy of the noncontact double sheet model.

Chapter 8.
Compositional models for prints

In this chapter, the compositional model is applied for the characterization of prints. A reflectance and transmittance model is developed for printing supports coated by a solid colorant layer, covering all the surface of the printing support. We show how the normal transmittance of the ink layers deduced from reflectance measurements can be ascertained by transmittance measurements (Sect. 8.1). Then, we present the specificities of halftone prints. We show that the compositional model can be applied only for high screen frequency halftone prints (Sect. 8.2). We extend the Williams-Clapper model for such halftone prints and present the classical Clapper-Yule model, which is a simplified version of our rigorous extension (Sect. 8.3). Finally a spectral prediction model is developed for recto-verso halftone prints with an experimental validation (Sect. 8.4)

8.1 Ink transmittance

As a first step in the characterization of prints, we propose to develop models permitting to deduce the normal transmittance of inks from reflectance and transmittance measurements. Consider a print composed of a symmetric paper sheet (i.e. having indistinguishable recto and verso) on which is deposited a solid ink layer. The following assumptions are made: the print has flat interfaces with air; there is no interface between ink and paper; the paper layer is Lambertian; and the ink layer is transparent. We desire to deduce the normal transmittance spectrum $t(\lambda)$ of the solid ink layer from the measure of the print's global reflectance or transmittance.

For the measure, we have at our disposal a directional light source and a radiance detector at the upper side, and a Lambertian light table at the bottom side. Three different measurements are possible: 1) a reflectance measurement with the bidirectional geometry, 2) a transmittance measurement with the ink positioned at the detector side (the light table illuminates the unprinted side), 3) a transmittance measurement with the ink positioned at the source side.

8.1.1 Reflectance and transmittance of solid ink patches

Let us first consider that the ink is positioned at the detector side. We aim at expressing the print upper global reflectance R_{up} and transmittance T_{up}, corresponding respectively to the measures 1) and 2) listed above. The measuring geometry is identical to that considered in Sect. 6.3.2 for the Williams-Clapper model. The difference here is that we also consider transmittance measurements and that the paper layer is characterized by its intrinsic reflectance ρ and its intrinsic transmittance τ, whereas it was only characterized by a reflectance ρ_B in Sect. 6.3.2. The corresponding graph is drawn in Fig. 8.1.

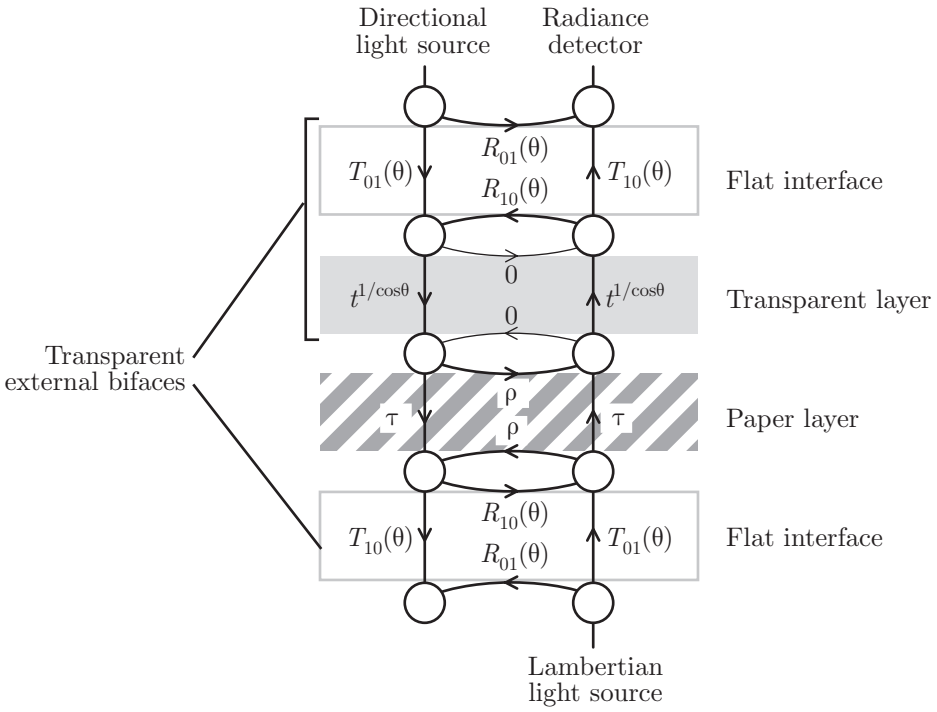

Fig. 8.1: Multiple reflection-transmission process occurring within a solid ink layer printed on the upper side of a symmetric paper sheet.

At the upper side, the ink layer and its interface with air are grouped. We obtain the same external biface as in Sect. 6.3.2, which is illuminated and observed in the same conditions (Lambertian illumination from the paper on the lower face, directional light source at angle ψ and radiance detector at angle ψ' on the upper face). Therefore, the ink layer and its interface have the same transfer matrix as in Eq. (6.24)

$$\begin{bmatrix} T_{01}(\psi)\, t^{1/\cos\psi_1} & 0 \\ r_{10}(t) & \xi \dfrac{T_{01}(\psi')\, t^{1/\cos\psi_1'}}{\pi n^2} \end{bmatrix} \tag{8.1}$$

with $r_{10}(t)$ given by Eq. (6.25). The transfer matrix of a symmetric paper layer has been presented in Sect. 7.1.4

$$\begin{bmatrix} \tau & \rho \\ \rho & \tau \end{bmatrix} \tag{8.2}$$

At the lower side, the paper is bounded by a flat interface, whose fundamental transfer matrix is similar to Eq. (3.25), with reversed indices 10 et 01 since here medium 1 representing the paper is at the upper side. The interface receives Lambertian illuminations on both its faces. It has therefore the particular transfer matrix [see Eq. (6.2)]

$$^{L\rightarrow}\begin{bmatrix} T_{10}(\theta) & R_{10}(\theta) \\ R_{01}(\theta) & T_{01}(\theta) \end{bmatrix}_{\leftarrow L} = \begin{bmatrix} t_{10} & r_{10} \\ r_{01} & t_{01} \end{bmatrix} \tag{8.3}$$

For the selected measuring geometry, the global transfer matrix of the print, with the ink layer on the detector side, is given by the composition equation

$$\begin{bmatrix} \cdot & R_{up} \\ \cdot & T_{up} \end{bmatrix} = \begin{bmatrix} T_{01}(\psi)\, t^{1/\cos\psi_1} & 0 \\ r_{10}(t) & \xi \dfrac{T_{01}(\psi')\, t^{1/\cos\psi_1'}}{\pi n^2} \end{bmatrix} \bigcirc \begin{bmatrix} \tau & \rho \\ \rho & \tau \end{bmatrix} \bigcirc \begin{bmatrix} t_{10} & r_{10} \\ r_{01} & t_{01} \end{bmatrix} \tag{8.4}$$

which gives, using the hexaface formula (5.27), the global reflectance

$$R_{up} = \frac{\xi}{\pi n^2}\, T_{01}(\psi)\, T_{01}(\psi')\, t^{1/\cos\psi_1} t^{1/\cos\psi_1'} \frac{\rho - r_{10}(\rho^2 - \tau^2)}{1 - \rho\,(r_{10} + r_{10}(t)) + r_{10} r_{10}(t)(\rho^2 - \tau^2)} \tag{8.5}$$

and the global transmittance

$$T_{up} = \frac{\xi}{\pi n^2}\, t_{01} T_{10}(\psi')\, t^{1/\cos\psi_1'} \frac{\tau}{1 - \rho\,(r_{10} + r_{10}(t)) + r_{10} r_{10}(t)(\rho^2 - \tau^2)} \tag{8.6}$$

Let us now consider that the ink layer is below, i.e. in front of the light source, which corresponds to the measure 3) listed in the introduction of Sect. 8.1. A transmittance T_{dn} is measured with the same geometry as T_{up}.

At the upper side, the external biface is the paper-air interface alone. Its transfer matrix is identical to Eq. (6.14) where the same geometry was considered. We directly replace $T_{10}(\psi_1')$ by $T_{01}(\psi')$ [Eq. (3.24)]

$$\begin{bmatrix} T_{01}(\psi) & 0 \\ r_{10} & \dfrac{\xi}{\pi n^2}\, T_{01}(\psi') \end{bmatrix} \tag{8.7}$$

At the lower side, the flat interface with the ink layer form a grouped transparent biface whose faces receive Lambertian illuminations. Its particular transfer matrix is obtained using the quadriface formula and then using Eq. (6.2)

$$\overset{L\rightarrow}{\left\{ \begin{bmatrix} t^{1/\cos\theta_1} & 0 \\ 0 & t^{1/\cos\theta_1} \end{bmatrix} \bigcirc \begin{bmatrix} T_{10}(\theta_1) & R_{10}(\theta_1) \\ R_{01}(\theta_0) & T_{01}(\theta_0) \end{bmatrix} \right\}_{\leftarrow L}} = \begin{bmatrix} t_{10}(t) & r_{10}(t) \\ r_{01} & t_{01}(t) \end{bmatrix} \tag{8.8}$$

where $r_{10}(t)$ is given by Eq. (6.25), $t_{10}(t)$ by Eq. (6.32) and $t_{01}(t)$ by

$$t_{01}(t) = \int_{\theta_0=0}^{\pi/2} T_{01}(\theta_0)\, t^{1/\cos\theta_1} \sin 2\theta_0 d\theta_0 \tag{8.9}$$

The paper layer still has the transfer matrix (8.2). Hence, the global transmittance T_{dn} of the print results from the composition

$$\begin{bmatrix} \cdot & \cdot \\ \cdot & T_{dn} \end{bmatrix} = \begin{bmatrix} T_{01}(\psi) & 0 \\ r_{10} & \dfrac{\xi}{\pi n^2}\, T_{01}(\psi') \end{bmatrix} \bigcirc \begin{bmatrix} \tau & \rho \\ \rho & \tau \end{bmatrix} \bigcirc \begin{bmatrix} t_{10}(t) & r_{10}(t) \\ r_{01} & t_{01}(t) \end{bmatrix} \tag{8.10}$$

which is computed with the hexaface formula (5.27). The global transmittance of the print with the ink at the source side is

$$T_{dn} = \frac{\xi}{\pi n^2} \cdot \frac{T_{01}\left(\psi'\right) t_{01}(t)\tau}{1-\rho\left(r_{10}+r_{10}(t)\right)+r_{10}r_{10}(t)\left(\rho^2-\tau^2\right)} \tag{8.11}$$

8.1.2 Deducing ink transmittances from measurements

Let us deduce numerically, wavelength by wavelength, the ink normal transmittance $t(\lambda)$ from one of the three formulae (8.5), (8.6) and (8.11), considering that $R_{up}(\lambda)$, $T_{up}(\lambda)$ and $T_{dn}(\lambda)$ have been measured.

Once again, in order to cancel the apparatus constant ξ (see Appendix A.2), we convert reflectances into reflectance factors by dividing them by a reference reflectance. We do the same for transmittances. We choose as reference the unprinted paper sheet, whose reflectance R_{U1} and transmittance T_{V1} are given by (7.7). One obtains the reflectance factor $\hat{R}_{up} = R_{up}/R_{U1}$, the transmittance factor $\hat{T}_{up} = T_{up}/T_{V1}$ and the transmittance factor $\hat{T}_{dn} = T_{dn}/T_{V1}$, expressed as

$$\begin{aligned}
\hat{R}_{up} &= t^{1/\cos\psi_1'+1/\cos\psi_1} \frac{\left(1-r_{10}\rho\right)^2-\left(r_{10}-\tau\right)^2}{1-\rho\left(r_{10}+r_{10}(t)\right)+r_{10}r_{10}(t)\left(\rho^2-\tau^2\right)} \\
\hat{T}_{up} &= t^{1/\cos\psi_1'} \frac{\left(1-r_{10}\rho\right)^2-\left(r_{10}-\tau\right)^2}{1-\rho\left(r_{10}+r_{10}(t)\right)+r_{10}r_{10}(t)\left(\rho^2-\tau^2\right)} \\
\hat{T}_{dn} &= \frac{t_{10}(t)}{t_{10}} \cdot \frac{\left(1-r_{10}\rho\right)^2-\left(r_{10}-\tau\right)^2}{1-\rho\left(r_{10}+r_{10}(t)\right)+r_{10}r_{10}(t)\left(\rho^2-\tau^2\right)}
\end{aligned} \tag{8.12}$$

If the assumptions underlying this model are satisfied (i.e. the paper is Lambertian, the ink layer is transparent, the interfaces are flat), the ink normal transmittance spectra deduced from each of the three formulae (8.12) should be equal. This has been tested with cyan, magenta and yellow inks printed on white PVC sheets with an offset press (Fig. 8.2).

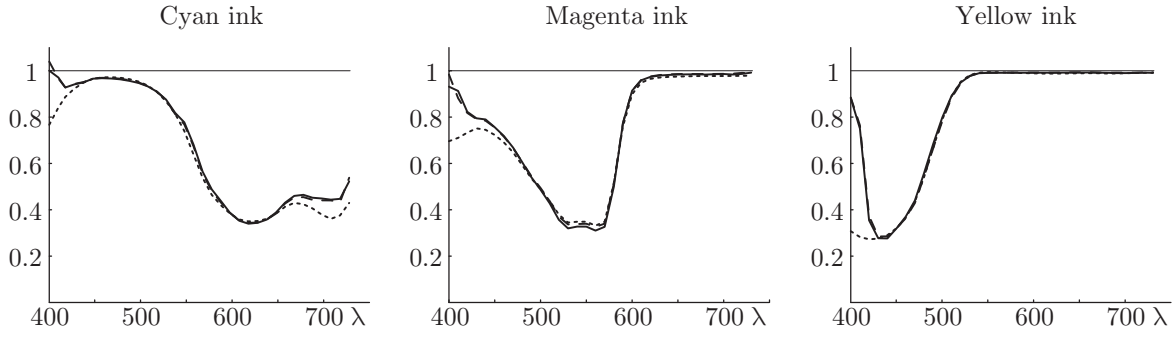

Fig. 8.2: Normal transmittance spectrum of solid cyan, magenta and yellow inks printed on white PVC, deduced from (dotted line:) the measure of global reflectance, (dashed line:) the measure of global transmittance with the ink at the detector side, and (solid line:) the measure of global transmittance with the ink at the source side.

For each ink, the ink transmittance spectra deduced from the three formula are identical, except for the short wavelengths where transmittance spectra are noisy, and for the large wavelengths for the cyan ink. A possible reason for this difference is the extremely low emission of the light table in these wavelength ranges which induces uncertainties in the measurements. The match for each ink in the remaining part of the spectrum is excellent. If we use the ink transmittance fitted from the transmittance measure with the ink layer on the source side or on the detector side, we obtain exactly the same prediction of print transmittance (CIELAB ΔE94 equal to 0). This shows the accuracy of the compositional model for the deduction of ink normal transmittance spectra.

8.2 Halftone prints

In contrast with paints where many different nuances may be obtained from a single dye or pigment by varying its concentration in a binding medium, the inks used in printing have a fixed concentration. Colors are formed by depositing on the paper surface ink dots (e.g. cyan, magenta, yellow, black) and color variations are obtained by varying the proportion of the paper surface covered by the dots of each primary ink. The resulting colors, perceived as homogenous by the eye due to its low-pass transfer function [OT86], are called "halftone colors" (Fig. 8.2).

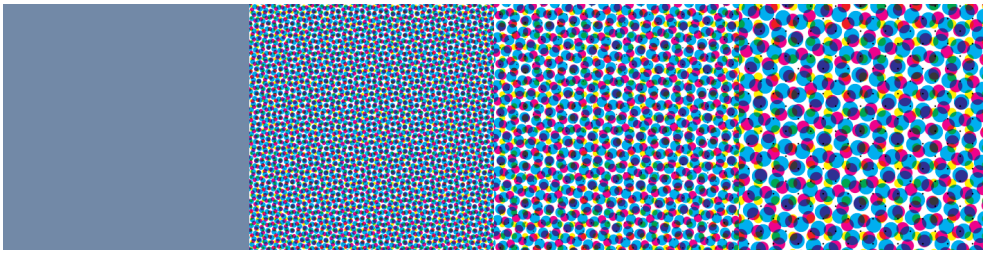

Fig. 8.2: Color generated by the superposition of dot screens of cyan, magenta, yellow and black primary inks with different screen periods.

8.2.1 Ideal halftone print

We consider as ideal halftone print the superposition of the following elements without interpenetration:

– a *printing support*, e.g. a paper sheet, composed of a Lambertian layer having flat surfaces (see Chapter 7);

– a *halftone inked layer*, representing the superposed ink dot screens as a single transparent layer, having the same refractive index as the printing support (no interface between the printing support and the inks);

– a flat interface between the halftone ink layer and air.

The halftone inked layer together with its interface with air forms a single optical element that is called the *halftone inked interface*. In the next sections, we consider such

ideal halftone prints. For experimental verifications, we have used printed patches whose characteristics were as close as possible to this ideal model.

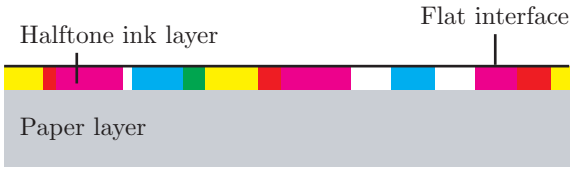

Fig. 8.3: Representation of an ideal halftone print.

8.2.2 Characterization of halftone inked layers

As shown in Fig 8.3, the primary ink dot screens overlap each other. The superposition of two solid inks yields a new colorant, e.g. the superposition of magenta and yellow inks yields the red colorant. Hence, the halftone inked layer is a juxtaposition of small colorant areas resulting from the superposition of the primary ink dot screens. When printing with cyan, magenta and yellow inks, we obtain the colorants white (no ink), cyan, magenta, yellow, red (magenta + yellow), green (cyan + yellow), blue (cyan + magenta), and black (cyan + magenta + yellow), which will be respectively denoted by the letters w, c, m, y, r, g, b and k. Each colorant i is characterized by its fractional surface coverage a_i, and its normal transmittance spectrum $t_i(\lambda)$. Normal transmittances may be deduced from reflectance or transmittance measurements according to the models presented in Sect. 8.1.

Considered individually, the primary inks cover respectively fractions c, m and y of the print surface. If the ink dots are placed so that there is no correlation between the patterns of the primary ink dot screens, the respective surface coverage of the resulting colorants can be calculated by the Demichel equations [Dem24]

$$\begin{aligned}
a_w &= (1-c)(1-m)(1-y) \\
a_c &= c(1-m)(1-y) \\
a_m &= (1-c)\,m(1-y) \\
a_y &= (1-c)(1-m)\,y \\
a_r &= (1-c)\,m\,y \\
a_g &= c(1-m)\,y \\
a_b &= c\,m(1-y) \\
a_k &= c\,m\,y
\end{aligned} \tag{8.13}$$

The *nominal surface coverage* of the primary inks is determined in advance by the color separation process [Yul67]. However, at print time, there are further interactions between the ink halftone and the paper and between the ink halftone and previously printed ink layers. A single ink halftone layer printed on paper generates an *effective dot surface coverage* which is generally larger than the corresponding nominal dot surface coverage value. The enlargement of the printed ink dot is called *dot gain*. The dot gain is the difference between effective and nominal dot surface coverages. When an ink halftone is

printed on top of another ink, e.g. a solid ink (100% surface coverage), the dot gain of the ink halftone is different than when it is printed alone on paper. Dot gain therefore strongly depends on the superposition condition, i.e. on which other inks a given ink halftone is superposed. Note that the dot gain of an already printed ink halftone may be modified by a second ink printed on top of that ink halftone [HECC05].

In analogy with the spectral Neugebauer reflectance model [Neu37, Vig90], the average normal transmittance $t(\lambda)$ of the halftone inked layer is given by the sum of the transmittances $t_i(\lambda)$ of the colorants weighted by their respective fractional surface coverage a_i

$$t(\lambda) = \sum_i a_i t_i(\lambda) \tag{8.14}$$

Likewise, the fundamental transfer matrix of the halftone inked interface is the sum of the fundamental transfer matrices of the colorants, each one given by Eq. (6.23), weighted by their respective fractional surface coverage a_i

$$\sum_i a_i \begin{bmatrix} T_{01}(\theta) t_i^{1/\cos\theta_1} & R_{01}(\theta) \\ R_{10}(\theta_1) t_i^{2/\cos\theta_1} & T_{10}(\theta_1) t_i^{1/\cos\theta_1} \end{bmatrix} \tag{8.15}$$

8.2.3 Validity of the compositional model with halftone prints

In the case where the halftone inked layer is considered as a homogenous transparent layer, the halftone print would be represented by the configuration studied in Sect. 6.3.2. Its global reflectance could be modeled by the Williams-Clapper [WC53] model or one of its extensions [SS01, HH04]. The fundamental question is therefore whether we are allowed using a compositional model with halftone inked layers, i.e. whether a halftone inked layer, or a halftone inked interface, can be considered as being a biface.

Bifaces have been defined in Chapter 2 as flat optical elements having homogenous optical properties. The notion of homogeneity must be considered at the scale of the multiple reflection-transmission phenomenon[1]. As an example, paper bulk is an extremely heterogeneous medium at the microscopic scale. Nevertheless, the paper layer behaves as a homogenous Lambertian reflector and transmitter when the light multiple reflection-transmission with its bordering interfaces is considered. The problem with halftone prints is to determine whether light traverses different colorants in the multiple reflection-transmission process. It is obvious that, because of the strong scattering within the paper layer, light undergoes a lateral shift between two internal reflections at the halftone inked interface. The typical distance of lateral propagation (which is a characteristic of the printing support), compared to the typical size of the colorant areas (which is directly linked to the halftone screen frequency, as shown by Fig. 8.4) is the key for determining whether the halftone ink interfaces is a biface or not.

[1] This question of "optical homogeneity" should be distinguished from the question of "visual homogeneity" which gives rise to a different domain of study principally centered around the characterization of the human visual system [OT86]. A halftone print can always be perceived as a homogenously colored surface provided that it is observed at sufficiently long distance (see Fig. 8.2).

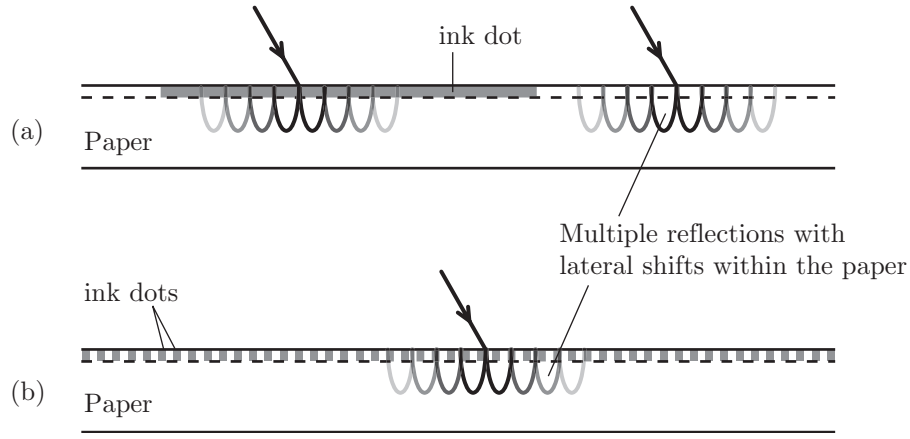

Fig. 8.4: Spatial response of light rays interacting with a halftone print of (a) low screen frequency and (b) high screen frequency.

The distance laterally traveled by the light is determined by the so-called *Point Spread Function* (PSF) of paper [ITM97, Rog98]. Three cases are generally considered

– **Low screen frequencies** (short PSF): the colorant areas are large compared to the lateral propagation of light within the printing support. Hence, an incident ray penetrating a given colorant stays in that colorant during all the process (Fig. 8.4a). The global reflectance of the halftone print is the sum of the contribution of each colorant

$$R = \sum_i a_i R_i \tag{8.16}$$

where a_i is the surface coverage of the colorant i and R_i corresponds to the global reflectance of a print where the colorant i covers all the surface of the printing support (Fig 2a).

– **High screen frequencies** (large PSF): the colorant areas are very small compared to the lateral propagation of light within the printing support. Hence, the halftone inked layer may be considered as a homogenous layer having the transmittance given by Eq. (8.14). There is no correlation between the successive colorants through which light is multiply reflected and transmitted (Fig. 8.4b). The halftone inked layer can be represented by a biface.

– **Middle screen frequencies**: The lateral light propagation distance inside the printing support is comparable to the screen period. The colorants in which light is successively reflected and transmitted are correlated. Light having penetrated an ink dot may exit from a close noninked region, giving thereby the illusion that the ink dot is larger than its real size. This effect is commonly called the "optical dot gain" phenomenon [Gus97].

Among the models proposed for modeling optical dot gain along the fifty past years, two models deserve to be mentioned. The first model, known as the Yule-Nielsen model [YN51, RH78, Vig90], relies on the following empirical equation

$$R = \left(\sum_i a_i R_i^{1/b} \right)^b \tag{8.17}$$

where parameter b ($1 \leqslant b \leqslant 2$) must be fitted from measured data, and where a_i and R_i have the same signification as in Eq. (8.16). Note that Eq. (8.16) corresponds to the particular case where $b = 1$.

The second model, recently published by Rogers [Rog00], proposes a rigorous mathematical description of the location of light at each step of the compositional model. It models the lateral propagation of light by probability distribution functions.

The above considerations lead us to the conclusion that our compositional model should be applied only to high screen frequency halftone prints.

8.3 Reflectance models for halftone prints

8.3.1 Extended Williams-Clapper model for halftone prints

A Lambertian background, having a reflectance ρ_B, is superposed with a high screen frequency halftone inked layer composed of only two colorants: ink (surface coverage a, normal transmittance t), and no-ink (surface coverage $1-a$, normal transmittance 1). According to Eq. (8.15), the halftone inked interface has the fundamental transfer matrix

$$(1-a)\begin{bmatrix} T_{01}(\theta) & R_{01}(\theta) \\ R_{10}(\theta_1) & T_{10}(\theta_1) \end{bmatrix} + a\begin{bmatrix} T_{01}(\theta)t^{1/\cos\theta_1} & R_{01}(\theta) \\ R_{10}(\theta_1)t^{2/\cos\theta_1} & T_{10}(\theta_1)t^{1/\cos\theta_1} \end{bmatrix} \tag{8.18}$$

with $\theta_1 = \arcsin\big(\sin\theta/n\big)$, n being the refractive index of the print.

Considering the halftone ink layer as any other transparent layer, we are exactly in the same configuration as in Sect. 6.3.2, except that the fundamental transfer matrix (6.23) shall be taken in place of (8.18). Let us consider the same bidirectional measuring geometry as in Sect. 6.3.2 (incidence angle ψ, observation angle ψ'). The halftone inked interface has the following particular transfer matrix, derived from Eq. (6.24)

$$(1-a)\begin{bmatrix} T_{01}(\psi) & 0 \\ r_{10} & \dfrac{\xi}{\pi n^2}\,T_{10}\big(\psi_1'\big) \end{bmatrix} + a\begin{bmatrix} T_{01}(\psi)t^{1/\cos\psi_1} & 0 \\ r_{10}(t) & \dfrac{\xi}{\pi n^2}\,T_{10}\big(\psi_1'\big)t^{1/\cos\psi_1'} \end{bmatrix} \tag{8.19}$$

where $T_{10}\big(\psi_1'\big) = T_{01}\big(\psi'\big)$. The transfer matrix (8.19) of the halftone inked interface is composed with the transfer matrix of the background

$$\begin{bmatrix} \cdot & R_{rad(\psi')} \\ \cdot & \cdot \end{bmatrix} = \left\{(1-a)\begin{bmatrix} T_{01}(\psi) & 0 \\ r_{10} & \dfrac{\xi}{\pi n^2}T_{01}\big(\psi'\big) \end{bmatrix} + a\begin{bmatrix} T_{01}(\psi)t^{1/\cos\psi_1} & 0 \\ r_{10}(t) & \dfrac{\xi}{\pi n^2}\,T_{01}\big(\psi'\big)t^{1/\cos\psi_1'} \end{bmatrix}\right\} \bigcirc \begin{bmatrix} \cdot & \rho_B \\ \cdot & \cdot \end{bmatrix}$$

The expression for the global reflectance $R_{rad(\psi')}$ obtained thanks to the quadriface formula, divided by the reflectance ξ/π of a perfect white diffuser, gives the reflectance factor $\hat{R}_{rad(\psi')}$ for the halftone print

$$\hat{R}_{rad(\psi')} = \frac{1}{n^2}\cdot\frac{T_{01}(\psi)T_{01}\big(\psi'\big)\big(1-a+at^{1/\cos\psi_1}\big)\big(1-a+at^{1/\cos\psi_1'}\big)\rho_B}{1-\rho_B\big[(1-a)r_{10}+ar_{10}(t)\big]} \tag{8.20}$$

where $r_{10}(t)$ is given by Eq. (6.25).

When light is captured by an integrating sphere, the halftone inked interface has the following particular transfer matrix, where the matrix corresponding to the ink areas is given by Eq. (6.24)

$$(1-a)\begin{bmatrix} T_{01}(\psi) & R_{01}(\psi) \\ r_{10} & t_{10} \end{bmatrix} + a\begin{bmatrix} T_{01}(\psi)\,t^{1/\cos\psi_1} & R_{01}(\psi) \\ r_{10}(t) & t_{10}(t) \end{bmatrix} \tag{8.21}$$

By composing this transfer matrix with the one of the background, one obtains a global reflectance R_{sph} which is also the reflectance factor $\hat{R}_{sph}$ defined in reference to the perfect white diffuser (its reflectance is 1)

$$\hat{R}_{sph} = \frac{T_{01}(\psi)\left(1-a+at^{1/\cos\psi_1}\right)\left[(1-a)t_{01}+at_{01}(t)\right]\rho_B}{1-\rho_B\left[(1-a)r_{10}+ar_{10}(t)\right]} \tag{8.22}$$

with t_{01} and $t_{01}(t)$ given respectively by Eqs. (3.28) and (8.9).

Eqs. (8.20) and (8.22) are the generalization of the Shore-Spoonhower model for the halftone print. We have not found yet any reference in the literature presenting such extension. Obviously, similar expressions may be developed for more than two colorants. The reflectance factor $\hat{R}_{rad(\psi')}$ corresponding to the bidirectional geometry may be expressed as

$$\hat{R}_{rad(\psi')} = \frac{T_{01}(\psi)\,T_{01}(\psi')}{n^2}\cdot\frac{\left(\sum a_i t_i^{1/\cos\psi_1}\right)\left(\sum a_i t_i^{1/\cos\psi_1'}\right)\rho_B}{1-\rho_B\left(\sum a_i r_{10}(t_i)\right)} \tag{8.23}$$

where t_i and a_i are respectively the normal transmittance and the fractional surface coverage of the colorant i, where ρ_B is the reflectance of the Lambertian background, and where $r_{10}(t_i)$ is given by Eq. (6.25).

8.3.2 Clapper-Yule model

The Clapper-Yule is a classical reflectance prediction model for high screen frequency halftone prints [CY53]. It expresses, for a directional incident light (incident angle ψ) and an integrating sphere, the reflectance of the halftone print as [HH04]

$$R_{cy} = T_{01}(\psi)(1-r_{10})\frac{\rho_B\,(1-a+at)^2}{1-\rho_B r_{10}\left(1-a+at^2\right)} \tag{8.24}$$

It corresponds to an approximation of the extended Shore-Spoonhower model presented above. The obliqueness of light is taken into account at the print-air interface, but not in the halftone inked layer. All the exponents on the ink normal transmittance are ignored, yielding to the following approximations [HH04]

$$\begin{aligned} \left(1-a+at^{1/\cos\psi_1}\right) &\simeq (1-a+at) \\ r_{10}(t) = \int_{\theta=0}^{\pi/2} R_{10}(\theta)t^{2/\cos\theta}\sin 2\theta d\theta &\simeq t^2\int_{\theta=0}^{\pi/2} R_{10}(\theta)\sin 2\theta d\theta = t^2 r_{10} \end{aligned}$$

$$
\begin{aligned}
t_{10}(t) = \int_{\theta=0}^{\pi/2} T_{10}(\theta) t^{1/\cos\theta} \sin 2\theta d\theta &\simeq t \int_{\theta=0}^{\pi/2} T_{10}(\theta) \sin 2\theta d\theta = t t_{10} = t(1 - r_{10}) \\
(1-a) r_{10} + a r_{10}(t) &\simeq \left(1 - a + a t^2\right) r_{10} \\
(1-a) t_{10} + a t_{10}(t) &\simeq (1 - a + at) t_{10}
\end{aligned}
$$

In their original paper, Clapper and Yule assume that these approximations have a very small effect on the accuracy of the reflectance predictions. This has been verified experimentally [HECC05]. The ink transmittance parameter, in the Clapper-Yule model, does not correspond precisely to a normal transmittance but rather to an average attenuation undergone by the diffuse light crossing the halftone ink layer.

8.3.3 Deducing dot surface coverages of paper from measurements

Once the intrinsic reflectance and transmittance of the printing support have been deduced from the reflectance and the transmittance of the unprinted printing support (see Sect. 7.1.4) and each colorant normal transmittance has been deduced from the reflectance and the transmittance of a print fully covered by the colorant, one can deduce the dot surface coverage from the measured reflectance and transmittance with single ink halftone patches.

For each ink, various patches are printed at different nominal coverages a_n. Their reflectance spectrum is measured with a spectrophotometer using, for example, a bidirectional measuring geometry (incidence angle ψ and observation angle ψ'). The effective dot surface coverage a can be deduced from the global reflectance model, given by Eq. (8.20). Using a linear interpolation, one obtains an approximated correspondence between the nominal and the effective dot surface coverage (Fig. 8.3a).

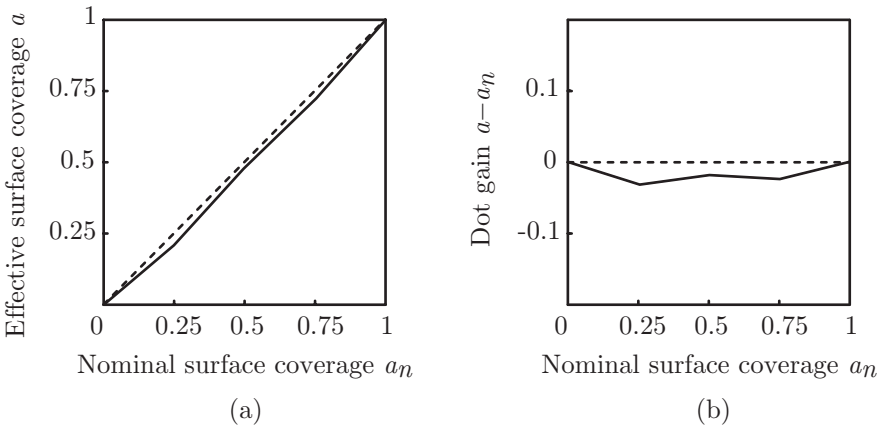

Fig. 8.3: (a) Nominal to effective dot surface coverage curve and (b) dot gain curve of cyan halftone patches printed at 180 lines per inch on white PVC sheets.

The dot gain, i.e. the difference $a - a_n$ of nominal and effective coverages, is a function of the nominal coverage, generally different for each primary ink. In Fig 8.3b, we observe a

negative dot gain, whereas dot gain is generally positive. Curves plotted in Fig. 8.3 have been obtained from patches printed with an offset press. The screen frequency, equal to 180 lines per inch, was higher than usual screen frequencies (150 lpi). Dot gain may have been overcompensated during the production of the offset films [Hir91], and the offset plate may have been overexposed during the insolation process, which is also calibrated for a frequency of 150 lpi.

8.3.4 Prediction of multi-ink halftone prints

When dot screens of various primary inks are superposed, the halftone inked layer comprises a certain number of colorants, having each one its normal transmittance t_i and its dot surface coverage a_i: no ink (also called "white" colorant), one primary ink (e.g. cyan, magenta, yellow), two superposed primary inks (e.g. red, green blue), three superposed primary inks (e.g. polychromatic black).

Consider a halftone patch printed with nominal dot surface coverages C, M and Y. What is the reflectance spectrum that would be measured from such a patch? The prediction model relies on Eq. (8.20), expressing the reflectance factor $\hat{R}_{rad(\psi')}$ of the print for a bidirectional measuring geometry and a perfect white diffuser as reference. The following parameters should be determined:

– The spectral intrinsic reflectance ρ_B of the printing support, which is deduced from the measured reflectance of the unprinted printing support;

– The spectral normal transmittances t_i of the different colorants, which are deduced from patches where each colorant is printed with a full surface coverage (see Sect. 8.1.2);

– The scalar (i.e. non-spectral) dot surface coverage a_i of the colorants. Effective dot surface coverages of the colorants can be computed according to the method proposed by Hersch & al. [HER95] since the surface coverage of primary inks depends whether they are printed alone or superposed with other ink(s), due to the *ink spreading* phenomenon [EH02].

8.4 Reflectance and transmittance model for recto-verso halftone prints

Thanks to our general compositional model, one may easily develop a prediction model for transmittance of halftone prints, with a straightforward extension to recto-verso prints.

We consider here a symmetric printing support printed on both sides by two different halftones. The recto-verso print may be represented by a hexaface, whose external bifaces are the recto and the verso halftone inked interfaces, and whose central layer is the substrate layer of the printing support, assumed to be Lambertian. Considering the print as ideal (Sect. 8.2.1), the hexaface is regular since it does not contains any scattering biface (Sect. 5.2.1).

Since the recto and the verso have been printed during different offset print passes, respective ink thicknesses and surface coverages are slightly different between the recto and the verso. We therefore calibrate separately the recto and the verso inked layers. The parameters of the halftone inked layer (normal transmittance and effective surface coverage of the colorants) are deduced from patches printed on the recto only (unprinted

verso), and those of the verso inked layer are deduced from patches printed on the verso only (unprinted recto).

We consider the same measuring geometry as for the characterization of paper (Sect. 7.1) and ink (Sect. 8.1), i.e. a directional incident light (incidence angle ψ) and a radiance detector (observation angle ψ') at the upper side, and a Lambertian illumination at the bottom side. This geometry enables measuring the upper reflectance $R_{rad(\psi')}$ and the lower transmittance $T_{rad(\psi')}$ of the print.

8.4.1 Reflectance and transmittance model

The halftone inked interfaces are characterized by their fundamental transfer matrix, given by Eq. (8.15). Let us deduce their particular transfer matrix for the measuring geometry specified above.

The upper halftone inked interface receives directional light on its upper face and Lambertian light on its lower face. Its upper face is also observed by the radiance detector. According to formula (h) of Table 6.1, the transfer matrix of the upper inked interface is

$$\begin{matrix} dir(\psi)\rightarrow \\ \\ rad(\psi')\leftarrow \end{matrix} \left\{ \sum_{\text{all } i} a_i \begin{bmatrix} T_{01}(\theta) t_i^{1/\cos\theta_1} & R_{01}(\theta) \\ R_{10}(\theta_1) t_i^{2/\cos\theta_1} & T_{10}(\theta_1) t_i^{1/\cos\theta_1} \end{bmatrix} \right\}_{\leftarrow L} = \begin{bmatrix} T_{01}(\psi) \sum a_i t_i^{1/\cos\psi_1} & 0 \\ \sum a_i r_{10}(t_i) & \dfrac{\xi' T_{01}(\psi')}{\pi n^2} \sum a_i t_i^{1/\cos\psi_1'} \end{bmatrix} \tag{8.25}$$

where t_i and a_i are respectively the normal transmittance and the surface coverage of colorants i printed on the recto.

The lower halftone inked interface is illuminated by Lambertian irradiances on its two sides. According to Eq. (6.2), it has the particular transfer matrix

$$\begin{matrix} L\rightarrow \\ \\ \\ \leftarrow L \end{matrix} \left\{ \sum_{\text{all } i} a_i' \begin{bmatrix} T_{10}(\theta) t_i'^{1/\cos\theta_1} & R_{10}(\theta_1) t_i'^{2/\cos\theta_1} \\ R_{01}(\theta) & T_{01}(\theta_1) t_i'^{1/\cos\theta_1} \end{bmatrix} \right\} = \begin{bmatrix} \sum a_i' \, t_{10}(t_i') & \sum a_i' \, r_{10}(t_i') \\ r_{01} & \sum a_i' \, t_{01}(t_i') \end{bmatrix} \tag{8.26}$$

where t_i' and a_i' are respectively the normal transmittance and the surface coverage of the colorant printed on the verso, and where $r_{10}(t)$, $t_{10}(t)$ and $t_{01}(t)$ are given respectively by Eqs. (6.25), (6.32) and (8.9). By composing the upper inked interface, the symmetric paper layer and the verso inked interface,

$$\begin{bmatrix} T_{01}(\psi) \sum a_i t_i^{1/\cos\psi_1} & 0 \\ \sum a_i r_{10}(t_i) & \dfrac{\xi' T_{01}(\psi')}{\pi n^2} \sum a_i t_i^{1/\cos\psi_1'} \end{bmatrix} \bigcirc \begin{bmatrix} \tau & \rho \\ \rho & \tau \end{bmatrix} \bigcirc \begin{bmatrix} \sum a_i' t_{10}(t_i') & \sum a_i' r_{10}(t_i') \\ r_{01} & \sum a_i' t_{01}(t_i') \end{bmatrix} \tag{8.27}$$

and then by using the hexaface formula (5.27), we obtain the global reflectance of the recto-verso halftone print

$$R_{rad(\psi')} = \frac{\xi'}{\pi n^2} \cdot \frac{T_{01}(\psi) T_{01}(\psi') \left[\sum a_i t_i^{1/\cos\psi_1}\right] \left[\sum a_i t_i^{1/\cos\psi_1'}\right] \left[\rho - \left[\sum a_i' r_{10}(t_i')\right] (\rho^2 - \tau^2)\right]}{\left[1 - \rho \sum a_i r_{10}(t_i)\right] \left[1 - \rho \sum a_i' \, r_{10}(t_i')\right] - \left[\sum a_i r_{10}(t_i)\right] \left[\sum a_i' r_{10}(t_i')\right] \tau^2} \tag{8.28}$$

and its global transmittance

$$T_{rad(\psi')} = \frac{\xi'}{\pi n^2} \cdot \frac{T_{01}(\psi')\left[\sum a_i t_i^{1/\cos\psi_1'}\right]\left[\sum a_i' t_{01}(t_i')\right]\tau}{\left[1-\rho\sum a_i r_{10}(t_i)\right]\left[1-\rho\sum a_i'\, r_{10}(t_i')\right]-\left[\sum a_i r_{10}(t_i)\right]\left[\sum a_i' r_{10}(t_i')\right]\tau^2} \tag{8.29}$$

The reflectance and transmittance model is calibrated by deducing from measurements the different parameters: the spectra of the intrinsic reflectance $\rho(\lambda)$ and transmittance $\tau(\lambda)$ of the printing support (see Sect. 7.1.4), the spectra of normal transmittances of each colorant on the recto, $t_i(\lambda)$, and each colorant on the verso, $t_i'(\lambda)$, (see Sect. 8.1.2), and the effective surface coverages of the colorants on the recto and the verso, respectively a_i and a_i' (see Sect. 8.3.3).

8.4.2 Experimental verification

We have tested the transmittance model [HH06] with recto-verso halftone patches printed at 180 lines per inch on white PVC, with cyan, magenta and yellow dot screens rotated by angles 75°, 15° and 0° respectively. The assumption of an ideal halftone print was almost satisfied thanks to the flatness of the PVC surfaces and the impossible penetration of the inks in the printing support. The bottom Lambertian illumination was realized with a diffusing light table. We used the same portative 45°/0° photospectrometer as described in Sect. 7.1.4.

During the time necessary to measure the transmittance of all the recto-verso patches, the irradiance emitted by the light table may vary. We therefore measured regularly the transmittance of the unprinted PVC sheet and divided all the patches transmittance spectra by the transmittance spectrum of the blank sheet. We obtained transmittance factor spectra. According to our model, the print transmittance factor $\hat{T}_{rad(\psi')}$ corresponds to the ratio of the print transmittance $T_{rad(\psi')}$, given by Eq. (8.29), to the support transmittance T_{V1} given by Eq. (8.29) with $a_0 = 1$ (white colorant) and $a_i = 0$ $(i \neq 0)$ (other colorants)

$$\hat{T}_{rad(\psi')} = \left[\sum a_i t_i^{1/\cos\psi_1'}\right]\frac{\left[\sum a_i' t_{01}(t_i')\right]}{t_{01}} \cdot \frac{\left(1-r_{10}\rho\right)^2-\left(r_{10}\tau\right)^2}{\left[1-\rho r_u\right]\left[1-\rho r_v\right]-r_u r_v \tau^2} \tag{8.30}$$

with

$$r_u = \sum a_i r_{10}(t_i) \quad \text{and} \quad r_v = \sum a_i'\, r_{10}(t_i')$$

and with $r_{10}(t)$ given by Eq. (6.25).

The calibration procedure is presented in Sect. 8.3.1. Recall that the parameters of the recto and the verso halftones, i.e. the normal transmittance and surface coverage of the recto and verso colorants, have been deduced from respectively recto-only patches and verso-only patches. Transmittance predictions are then performed for the recto-verso patches featured in Table 8.1. The difference between the predicted and the measured spectra is expressed according to the CIELAB ΔE94 color difference formulae [Sha03].

Table 8.1: Difference (in CIELAB ΔE94) between predicted and measured transmittance spectra for offset inks printed on white PVC.

		Ink on the verso								
		C	M	Y	R	G	B	K	C50	**average**
Ink on the recto	C	0.5	1.2	2.8	0.6	1.3	0.6	1.6	1.5	**1.3**
	M	2.2	1.2	0.9	0.9	1.3	0.9	1.6	0.9	**1.2**
	Y	1.0	0.7	0.5	0.8	0.9	0.3	1.6	1.3	**0.9**
	R	2.3	0.8	0.4	0.7	1.5	1.1	1.4	0.4	**1.1**
	G	0.5	0.5	2.6	0.7	0.8	0.4	3.3	2.3	**1.4**
	B	2.1	1.0	0.2	1.8	1.6	1.2	1.1	1.4	**1.3**
	K	2.0	1.6	0.4	1.5	0.7	1.5	1.4	1.7	**1.4**
	C25	0.6	2.3	0.7	2.0	2.3	0.7	1.7	0.7	**1.4**
	C50	0.5	2.0	1.6	1.9	2.0	1.1	2.5	0.8	**1.6**
	C75	0.2	2.0	1.7	1.6	1.5	0.7	1.5	0.5	**1.2**
	average	**1.2**	**1.3**	**1.2**	**1.3**	**1.4**	**0.9**	**1.8**	**1.2**	**1.3**

Legend: C stands for cyan solid inked layer, M for solid magenta, Y for solid yellow, R for superposed magenta and yellow solid inks yielding the red colorant, G for solid yellow and cyan (green colorant), B for solid cyan and magenta (blue colorant), K for the superposed cyan, magenta and yellow solid inks (black colorant); C25, C50 and C75 stand for cyan halftones of respective nominal surface coverages 0.25, 0.5 and 0.75.

The mean difference between the measured transmission spectra and the transmission spectra predicted according to the recto-verso model is $\Delta E94 = 1.3$. Almost 90% of the predicted transmittance spectra have a ΔE94 prediction error of less than 2, which corresponds to the normal offset printing accuracy. This experiment shows that the prediction accuracy that is achieved by the proposed model for transmittance spectra is excellent. It is similar to the prediction accuracy of reflection spectra that is achieved for recto only offset prints by the classical Clapper-Yule model [HECC05].

Summary

We have applied the compositional model to the characterization of prints. The ink transmittance can be deduced for each wavelength from the measurement of the global reflectance spectrum or the global transmittance spectrum of a patch printed with a solid ink layer. Both possibilities yields the same transmittance spectrum. The notion of biface and the Shore-Spoohower model have been extended to halftone inked layers with high screen frequency. We have shown that the classical Clapper-Yule model is an approximation of this model.

We have also developed a model for recto-verso multi-ink halftone print, experimentally validated with solid colorant patches and cyan halftones. The difference between measured and predicted spectra, expressed in CIELAB ΔE94, is 1.3, which is less than the threshold of the human eye perception. In the future, in order to predict accurately

the reflectance and the transmittance multi-ink recto-verso halftone patches, the ink spreading phenomenon shall be taken into account according to the model proposed by Hersch & al. [HECC05].

Conclusion

We presented a general model of multilayer reflectance and transmittance relying on geometrical optics and using a hierarchical description of the interaction of light with the different layers and interfaces forming the multilayer specimens. In the most general case, a step by step description of the multiple reflection-transmission of light in the multilayer yields a reflectance and a transmittance expressed as infinite sums. However, when the multilayer does not contain any rough interface or any weakly scattering layer (i.e. no scattering biface), or when each of these interfaces or layers is directly bordered by a strongly scattering layer, the step-by-step description can be avoided. Instead, we have advocated the use of closed-form formulae, called "compositional formulae", including the full multiple reflection-transmission process. We have introduced a special formalism allowing to derive in a straightforward manner the particular reflectance and transmittance that should be associated with each face. The geometries of the light sources and the capturing devices are included in this special formalism. Thanks to the notion of composition and the composition formulae, the establishment of multilayer reflectances and transmittances of multilayer specimens is considerably simplified.

The soundness of our approach has been proven by its ability to retrieve Kubelka's model, the Williams-Clapper model, the Saunderson correction, and the Clapper-Yule model. New models have also been developed that would have been very difficult to conceive without our compositional formalism. The new noncontact double sheet model permits to exclude the influence of the measuring geometry on the deduction of the paper intrinsic parameters. The prediction model for high screen frequency recto-verso halftone prints, verified experimentally, has an excellent accuracy.

In the future, we intent to check the relevance of the parameters deduced using the Clapper-Yule model, which is based on approximated equations (see Sect. 8.3.2). We also intent to verify to which extent, in low quality prints, interfaces can be considered as flat and inks can be considered as transparent without loss of the prediction accuracy. Thanks to the transmittance model, we now have enough equations for ascertaining parameters and exploring phenomena such as the light scattering inside the inks. In a further step, we may increase the number of measurement configurations, both in reflectance and transmittance mode, thanks to known filters. By composing the bifaces of the filters with the bifaces of the specimen, it will be possible to obtain new equations for parameter fittings without having to introduce additional unknown parameters.

Appendix A.
Complements of radiometry

A.1 Relationship between reflectance and BRDF

The reflectance of a material is defined for an incident flux angularly distributed according to a radiance function L_i, for a given solid angle of incidence Γ_i, and for a given solid angle of observation Γ_r (see Sect. 1.2.2). The following detailed calculation establishes the relationship between reflectance and BRDF.

Let us first take one direction within the incidence solid angle Γ_i, denoted by the differential solid angle $d\omega_i = \sin\theta_i d\theta_i d\phi_i$. We consider a radiance $L_i(d\omega_i)$ at the selected direction $d\omega_i$. The incident element of irradiance $dE_i(d\omega_i)$, given by Eq. (1.7), is

$$dE_i(d\omega_i) = L_i(d\omega_i)\cos\theta_i d\omega_i \tag{A.1}$$

Let us also consider one direction within the observation solid angle Γ_r, denoted by the differential solid angle $d\omega_r = \sin\theta_r d\theta_r d\phi_r$. The radiance reflected in this direction is the product of the incident element of irradiance dE_i by the bidirectional reflectance distribution function f_R [Eq. (1.14)]

$$L_r(d\omega_r) = f_R(d\omega_i,d\omega_r)dE_i(d\omega_i) \tag{A.2}$$

In order to obtain the reflectance $R_{\Gamma_i\to\Gamma_r}$, we must take into account all the directions of incidence within Γ_i and all the directions of observation within Γ_r. On the one hand, the reflected radiance $L_r(d\omega_r)$ corresponds to the reflected element of flux $d^2\Phi_r(d\omega_i,d\omega_r)$ considered with respect to the surface element ds and the infinitesimal solid angle $d\omega_r$

$$L_r(d\omega_r) = \frac{d^2\Phi_r(d\omega_i,d\omega_r)}{ds\cos\theta_r d\omega_r} \tag{A.3}$$

The combination of Eqs. (A.1), (A.2) and (A.3) yields

$$d^2\Phi_r(d\omega_i,d\omega_r) = ds f_R(d\omega_i,d\omega_r)L_i(d\omega_i)\cos\theta_i d\omega_i \cos\theta_r d\omega_r \tag{A.4}$$

The double sum of the reflected elements of flux $d^2\Phi_r(d\omega_i,d\omega_r)$ over the incidence solid angle Γ_i and over the observation solid angle Γ_i yields the total flux $d\Phi_r$ reflected within the cone Γ_r

$$d\Phi_r = ds\iint_{\substack{d\omega_i\in\Gamma_i\\ d\omega_r\in\Gamma_r}} f_R(d\omega_i,d\omega_r)L_i(d\omega_i)\cos\theta_i d\omega_i \cos\theta_r d\omega_r \tag{A.5}$$

On the other hand, the total incident flux $d\Phi_i$ is the sum over Γ_i of the directional elements of flux $d^2\Phi_i(d\omega_i) = dE_i(d\omega_i)ds$

$$d\Phi_i = ds \int_{d\omega_i \in \Gamma_i} L_i(d\omega_i) \cos\theta_i d\omega_i \tag{A.6}$$

The ratio $d\Phi_r / d\Phi_i$, issued from Eqs. (A.6) and (A.5), corresponds to reflectance $R_{\Gamma_i \to \Gamma_r}$

$$R_{\Gamma_i \to \Gamma_r} = \frac{\int_{d\omega_i \in \Gamma_i} \int_{d\omega_r \in \Gamma_r} f_R(d\omega_i, d\omega_r) L_i(d\omega_i) \cos\theta_i d\omega_i \cos\theta_r d\omega_r}{\int_{d\omega_i \in \Gamma_i} L_i(d\omega_i) \cos\theta_i d\omega_i} \tag{A.7}$$

A.2 Reflectance and transmittance measured with a radiance detector

A radiance detector receives an element of flux $d^2\Phi_d$ perpendicularly incident on its surface ds_d through its solid angle $d\Omega_d$, assumed to be small. In spectral prediction models, it is generally, convenient to consider the measured radiance L_d instead of the measured flux. The ratio of the measured radiance to the incident irradiance defines a pseudo-reflectance or a pseudo-transmittance. We propose here to establish the relationship existing between these quantities and the exact reflectance and transmittance, defined as ratio of fluxes.

The measured radiance is

$$L_d = \frac{d^2\Phi_d}{ds_d d\Omega_d} \tag{A.8}$$

According to the radiance invariance principle (see Sect. 1.1.3), radiance L_d is equal to the radiance L emitted by the specimen in the direction of the detector. This radiance is defined by the solid angle $d\omega = ds_d / x^2$ subtended by the detector's surface, where x is the distance between the detector and the specimen, and by the specimen's element of area $ds = d\Omega_d x^2 / \cos\theta$, where θ is the angle formed by radiance L with the specimen's normal (Fig. A.1)

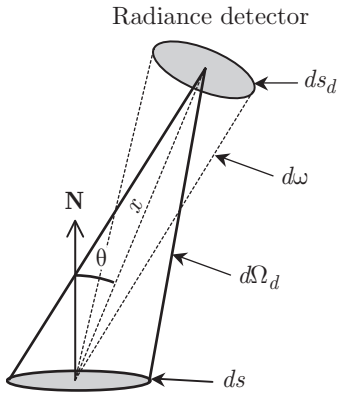

Fig. A.1: Radiance invariance between the radiance detector and an elemental area on the specimen.

According to the transfer volume conservation principle (see Sect. 1.1.3), one has

$$ds_d d\Omega_d = ds\, d\omega \cos\theta \tag{A.9}$$

Elemental area ds receives an incident element of flux $d^2\Phi_i$. The incident irradiance is

$$E_i = d^2\Phi_i / ds \tag{A.10}$$

The relationship between the ratio L_d/E_i and the ratio $d^2\Phi_d/d^2\Phi_i$ may be deduced from Eqs. (A.8), (A.9) and (A.10)

$$\frac{d^2\Phi_d}{d^2\Phi_i} = \frac{L_d ds_d d\Omega_d}{E_i ds} = \frac{L_d ds\, d\omega \cos\theta}{E_i ds} = \frac{ds_d \cos\theta}{x^2} \cdot \frac{L_d}{E_i} \tag{A.11}$$

Eq. (A.11) indicates that, for a fixed orientation θ of the detector, the ratio L_d/E_i is proportional to the ratio $d^2\Phi_d/d^2\Phi_i$, i.e. it is proportional to a reflectance, called R_{rad}. The coefficient of proportionality

$$\xi = ds_d \cos\theta / x^2 \tag{A.12}$$

is called the "apparatus constant" of the detector. It is a function of the angle of observation θ, the detector's area ds_d and the distance x between the detector and the specimen. The relationship between R_{rad} and the ratio L_d/E_i is therefore

$$R_{rad} = \xi \cdot \frac{L_d}{E_i} \tag{A.13}$$

Let us now consider a perfect white diffuser. It is a Lambertian reflector of reflectance equal to 1. The ratio $(L_d/E_i)_{ref}$ is equal to $1/\pi$, and the reflectance of this reference reflector is

$$R_{ref} = \xi/\pi \tag{A.14}$$

By dividing the specimen's reflectance by the reference reflectance, coefficient ξ cancels. The ratio R_{rad}/R_{ref} defines the reflectance factor $\hat{R}_{rad}$ of the specimen in reference to the perfect white diffuser

$$\hat{R}_{rad} = \frac{R_{rad}}{R_{ref}} = \frac{\pi L_d}{E_i} \tag{A.15}$$

A.3 Cosine correction in measures of BRDFs

A goniophotometer is composed of a directional light source and a radiance detector allowing measuring bidirectional reflectances for any direction of incidence and any direction of observation. We assume that the detector belongs to the incidence plane.

The directional light source emits a radiance L_i in the direction perpendicular to its surface ds_s, within a solid angle $d\Omega_s$ (Fig. A.2). Radiance L_i intercepts an area dA_s on the specimen. Elemental areas ds_s and dA_s are distant by a length x (length of the rotating arm of the goniophotometer). According to the radiance invariance principle, the radiance

received by dA_s, through the solid angle $d\omega_i$ subtended by ds_s, is equal to L_i

$$L_i = \frac{d^2\Phi_i}{ds_s d\Omega_s} = \frac{d^2\Phi_i}{dA_s \cos\theta_i d\omega_i} \tag{A.16}$$

with $$d\omega_i = \frac{ds_s}{x^2} \qquad \text{and} \qquad dA_s = \frac{d\Omega_s x^2}{\cos\theta_i} \tag{A.17}$$

The element of irradiance $dE_i(\theta_i)$ illuminating dA_s is

$$dE_i(\theta_i) = L_i \cos\theta_i d\omega_i = L_i \cos\theta_i \frac{ds_s}{x^2} \tag{A.18}$$

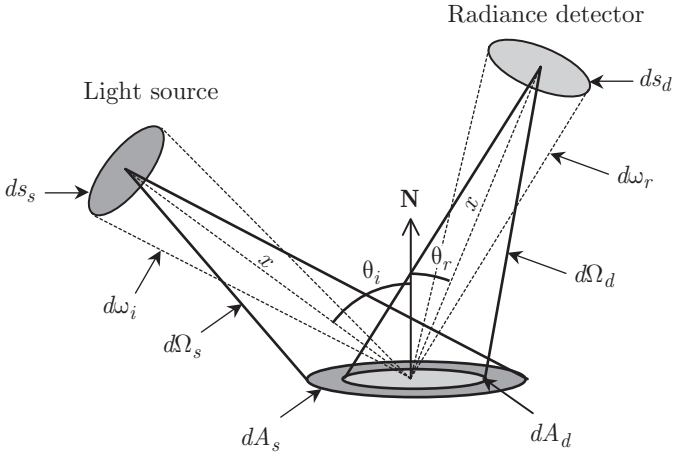

Fig. A.2: The radiance emitted by the light source through its solid angle $d\Omega_s$ illuminates a portion dA_s of the specimen. A portion $dA_d < dA_s$ is observed by the detector through its solid angle $d\Omega_d$.

The radiance detector receives the reflected flux $d^2\Phi_d(\theta_r)$ through its solid angle $d\Omega_d$ perpendicularly to its surface ds_d. It measures the radiance L_d expressed by Eq. (A.8). The solid angle $d\Omega_d$ of the detector intercepts an area dA_d on the specimen. The illuminated area dA_s and the observed area dA_d are different.

Let us first consider, as in Fig. C.1, that $dA_s > dA_d$. Since the incident light is directional, dA_s and dA_d both receive the same radiance L_i and thereby the same element of irradiance $dE_i(\theta_i)$, given by Eq. (A.18). According to the radiance invariance principle, the radiance L_d captured by the detector at angle θ_r is equal to the radiance $L_r(\theta_r)$ reflected by dA_d towards the detector

$$L_r(\theta_r) = \underbrace{\frac{d^2\Phi_d(\theta_r)}{dA_d \cos\theta_r d\omega_r}}_{L_d} = \underbrace{\frac{d^2\Phi_d(\theta_r)}{ds_d d\Omega_d}}_{L_r} \tag{A.19}$$

Hence, the BRDF f_R, defined as the ratio of the reflected radiance to the incident element

of irradiance $dE_i(\theta_i)$ is

$$f_R(\theta_i,\theta_r) = \frac{L_r(\theta_r)}{dE_i(\theta_i)} = \frac{d^2\Phi_d(\theta_r)}{ds_d d\Omega_d L_i \cos\theta_i \frac{ds_s}{x^2}} \tag{A.20}$$

Considering a fixed angle of incidence θ_i, the denominator $ds_d d\Omega_d L_i \cos\theta_i ds_s/x^2$ is a constant. The BRDF is proportional to the flux captured by the radiance detector

$$f_R(\theta_i,\theta_r) = k\, d^2\Phi_d(\theta_r) \tag{A.21}$$

Eq. (A.21) relies on the assumption that the observed area dA_d is completely illuminated, i.e. $dA_s > dA_d$. Let us now assume that, at a certain angle of observation, dA_d becomes larger than dA_s (Fig. A.3).

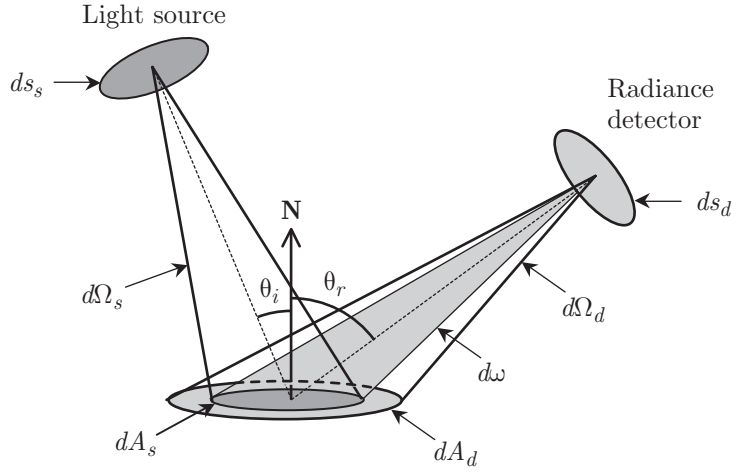

Fig. A.3: The area dA_d observed by the detector is larger than the area dA_i illuminated by the light source. The solid angle $d\omega$ through which the detector receives light is lower than its own solid angle $d\Omega_d$.

The solid angle $d\omega$ through which the detector receives light from the illuminated area on the specimen, i.e. from dA_s given by Eq. (A.17), is

$$d\omega = \frac{dA_s \cos\theta_r}{x^2} = d\Omega_s \frac{\cos\theta_r}{\cos\theta_i} \tag{A.22}$$

The radiance L_d captured by the detector thus becomes

$$L_d = \frac{d^2\Phi_d(\theta_r)}{ds_d d\omega} = \frac{d^2\Phi_d(\theta_r)\cos\theta_i}{ds_d d\Omega_s \cos\theta_r} \tag{A.23}$$

L_d is equal to the reflected radiance $L_r(\theta_r)$ according to the radiance invariance principle. The specimen's BRDF is therefore

$$f_R(\theta_i,\theta_r) = \frac{L_r(\theta_r)}{dE_i(\theta_i)} = \frac{d^2\Phi_d(\theta_r)}{ds_d d\Omega_s \cos\theta_r L_i(ds_s/x^2)} \tag{A.24}$$

Like previously, the term $ds_d d\Omega_s L_i ds_s/x^2$ is a constant. However, there remains a term $\cos\theta_r$. The flux captured by the detector is proportional to the BRDF multiplied by the cosine of the observation angle

$$d^2\Phi_d(\theta_r) = k' f_R(\theta_i,\theta_r)\cos\theta_r \tag{A.25}$$

In practice, the light source is positioned at a fixed angle θ_i and the detector rotates around the specimen from observation angles 0 to $\pi/2$. As the observation angle θ_r increases, the observed area also increases. If at $\theta_r = 0$ the observation area is fully illuminated by the incident light beam, there exists an angle θ_{lim} at which the illuminated and observed areas will be equal. At angles below θ_{lim}, the BRDF is given by Eq. (A.21), and at angles higher than θ_{lim}, the BRDF is given by Eq. (A.25). We may therefore introduce a correction function C permitting to convert the measured flux into the BRDF

$$f_R(\theta_i,\theta_r) = C(\theta_i,\theta_r) d^2\Phi_d(\theta_r) \tag{A.26}$$

with

$$C(\theta_i,\theta_r) = \begin{cases} 1 & \text{for } 0 \le \theta_r \le \theta_{\text{lim}} \\ \cos\theta_{\text{lim}}/\cos\theta_r & \text{for } \theta_{\text{lim}} \le \theta_r \le \pi/2 \end{cases} \tag{A.27}$$

Angle θ_{lim} can be determined experimentally. A Lambertian reflector, whose BRDF is constant, is selected. The arm of the goniophotometer carrying the directional light source is placed at a selected angle. The other arm, carrying the radiance detector, moves in the incidence plane from the normal of the specimen (0 degree) to the horizontal direction (90 degrees). The curve of the flux captured by the detector, expected to be a constant function, should rather have the shape featured in Fig. A.4. Angle θ_{lim} is the abscissa from which the curve decreases according to a cosine curve.

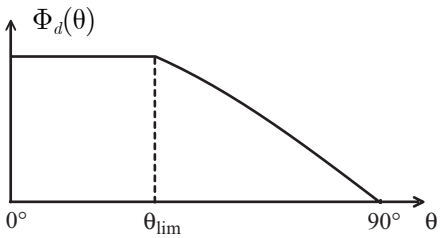

Fig. A.4: Curve of the flux $\Phi_d(\theta)$ measured by the gonio-photometer from a Lambertian reflector.

Remark: the minimal observed area, obtained for the observation $\theta_r = 0$, may yet be larger than the illuminated area. In this case, one has $\theta_{\text{lim}} = 0$. The curve of the flux measured from a Lambertian reflector will have a perfect cosine shape.

Appendix B.
Markov chains

Multiple reflection-transmission of light occurring in a regular multiface may be represented by Markov chains. We propose to recall here basic elements of the general theory of Markov chains, mainly borrowed from [Ste94] and [MT73] (Sect. B.1, B.2 and B.3). We then focus on absorbing Markov chains on which relies the compositional model (Sect. B.4).

B.1 Definition of a Markov chain

A Markov chain is a convenient representation of the behavior of a physical system which describes the different states that the system may occupy and indicates how the system moves from one state to another in time [Ste94].

Consider a system that may occupy a finite number of *states*. Random variables Y_0, Y_1, Y_2,..., Y_n give the respective state y_0, y_1, y_2,...,y_n in which the system is at discrete "times" 0, 1, 2,..., n. A sequence y_0, y_1, y_2,...,y_n of states corresponds to a certain realization of a random walk. The probability m that this realization occurs is the conditional probability that the irradiance is observed in state y_n at time n, given that it was previously observed in states y_0, y_1 ... y_{n-1} respectively at times 0, 1,...,n–1

$$m = \mathrm{Prob}\left\{Y_n = y_n \middle|\, Y_0 = y_0,\ldots,Y_{n-1} = y_{n-1}\right\} \tag{B.1}$$

This conditional probability m can also be interpreted as the probability of transition from state y_{n-1} to state y_n, given that it has previously moved from state y_0 to state y_1, from state y_1 to state y_2, etc. When the transition probability $y_{n-1} \to y_n$ is independent of the previous transitions $y_0 \to y_1$, $y_1 \to y_2$, ... $y_{n-2} \to y_{n-1}$, the stochastic process is said to be *memoryless*. This may be written as

$$\mathrm{Prob}\left\{Y_n = y_n | Y_0 = y_0,\ldots,Y_{n-1} = y_{n-1}\right\} = \mathrm{Prob}\left\{Y_n = y_n | Y_{n-1} = y_{n-1}\right\} \tag{B.2}$$

Equality (B.2) is the defining equation of a *discrete-time Markov chain*. When, furthermore, the transition probabilities $y_{n-1} \to y_n$ are independent of the time parameter n, the Markov chain is said to be a *homogenous discrete-time Markov chain* (HDMC). Hence, if the system is in a given state i, it evolves towards a given state j with a same probability whatever the time and whatever the previous states in which the system has been through.

B.2 Probability transition matrices

Let us consider a homogenous discrete-time Markov chain and two of its states i and j. The probability of transition from state i to state j is a constant (independent of the time

parameter n), called *single-step transition probability* and noted m_{ij}

$$m_{ij} = \text{Prob}\{Y_n = j | Y_{n-1} = i\} \tag{B.3}$$

Matrix $\mathbf{M} = \{m_{ij}\}$ is called the *single-step transition probability matrix* associated with the chain. $\mathbf{M}$ is a square matrix whose size corresponds to the number of states in the chain. Since elements m_{ij} are probabilities, they satisfy the inequality

$$0 \leqslant m_{ij} \leqslant 1 \tag{B.4}$$

The single-step transition probability matrix, which satisfies (B.4), is said to be a *non-negative matrix*. Furthermore, the sum of its row elements is less than 1, i.e. for all i,

$$\sum_j m_{ij} \leqslant 1 \tag{B.5}$$

We may generalize a single-step transition probability matrix to a k-step transition probability matrix $\mathbf{M}^{(k)}$ whose elements $m_{ij}^{(k)}$ are probabilities for transitions from a state i to a state j in k steps

$$m_{ij}^{(k)} = \text{Prob}\{X_{n+k} = j | X_n = i\} \tag{B.6}$$

These elements may be obtained from the single-step transition probabilities. It may be first seen that $m_{ij} = m_{ij}^{(1)}$. The Markov property, expressed by Eq. (B.2), gives the following recursive formula for the $m_{ij}^{(k)}$

$$m_{ij}^{(k)} = \sum_{\text{all } q} m_{iq}^{(p)} m_{qj}^{(k-p)}, \text{ for } 0 < l < n. \tag{B.7}$$

Relation (B.7) is called the *Chapman-Kolmogorov* equation for the Markov chain. In matrix notation, the Chapman-Kolmogorov equations are written as

$$\mathbf{M}^{(k)} = \mathbf{M}^{(p)} \mathbf{M}^{(k-p)}$$

Note in particular that

$$\mathbf{M}^{(k)} = \mathbf{M}^{(k-1)} \mathbf{M} = \mathbf{M} \mathbf{M}^{(k-1)} \tag{B.8}$$

Hence, the matrix on k-step transition probabilities is obtained by multiplying $(k-1)$ times the single-step transition probability matrix by itself, i.e.

$$\mathbf{M}^{(k)} = \mathbf{M}^k \tag{B.9}$$

An "infinite-step" transition probability matrix $\mathbf{M}_\infty$ can be as well defined by

$$\mathbf{M}_\infty = \lim_{k \to \infty} \mathbf{M}^k \tag{B.10}$$

Like the single-step, k-step and infinite-step transition probability matrices are nonnegative matrices and are independent of the time parameter n.

B.3 Properties of nonnegative, stochastic and substochastic matrices

Transition probability matrices are basically square matrices, which may be characterized by their *spectral radius*, i.e. their largest eigenvalue modulus. Given a square matrix $\mathbf{A}$ having a spectrum composed of the eigenvalues $\lambda_j(\mathbf{A})$, its spectral radius $\tilde{R}(\mathbf{A})$ is defined as

$$\tilde{R}(\mathbf{A}) = \max_j \left|\lambda_j(\mathbf{A})\right| \tag{B.11}$$

It can be shown that for any natural matrix norm $\left\| \cdot \right\|$

$$\tilde{R}(\mathbf{A}) \leqslant \|\mathbf{A}\| \tag{B.12}$$

It is true in particular for the matrix infinity-norm, defined as the maximum absolute row sum

$$\|\mathbf{A}\|_\infty = \max_i \left(\sum_{\text{all } j} |a_{ij}| \right) \tag{B.13}$$

In the case of transition probability matrices, it follows property (B.5) that

$$R(\mathbf{A}) \leqslant \|\mathbf{A}\|_\infty \leqslant 1 \tag{B.14}$$

Thus, all eigenvalues of a transition probability matrix have their modulus at most 1. This will be stated in the following paragraphs.

B.3.1 Non-Negative matrices

Nonnegative matrices are matrices whose elements are also positive or zero. Transition probability matrices are therefore nonnegative [Eq. (B.4)].

A nonnegative matrix $\mathbf{A}$ is said to be *decomposable* if it can be brought by a symmetric permutation of its rows and its columns to a triangular block matrix, i.e. if a permutation matrix $\mathbf{P}$ exists such that

$$\mathbf{P} \cdot \mathbf{A} \cdot \mathbf{P}^T = \begin{pmatrix} \mathbf{U} & \mathbf{W} \\ \mathbf{0} & \mathbf{V} \end{pmatrix} \tag{B.15}$$

where $\mathbf{U}$ and $\mathbf{V}$ are square nonzero matrices and $\mathbf{W}$ is, in general, rectangular.

B.3.2 Stochastic and substochastic matrices

A nonnegative matrix $\mathbf{A}$ is said to be a *stochastic* matrix if it satisfies the following two conditions

1. $\sum_{\text{all } j} a_{ij} = 1$ for all i.
2. At least one element in each column differs from zero.

Condition (1) implies that a transition is guaranteed to occur from state i to at least one state in the next time (that may be state i again). Condition (2) specifies that since each column has at least one nonzero element, there are no *ephemeral* states, i.e., states that

could not possibly exist after the first time transition. This second condition is generally omitted, being considered as trivial.

Nonnegative matrix **A** is *substochastic* if, instead of satisfying condition (1) above, it satisfies

$$\sum_j a_{ij} \leqslant 1 \tag{B.16}$$

Remark: In the context of multiple reflection-transmission processes, the physical interpretation of a stochastic process is the fact that each face redistributes completely the light it receives by reflection and transmission, without absorption. If light is absorbed by a certain face, one obtains

$$\sum_j a_{ij} < 1 \tag{B.17}$$

for the row i corresponding to that face, responsible of the substochasticity of **A**.

Property B.1: The spectral radius of stochastic matrices is one.

Proof: Let **A** be a nondecomposable stochastic matrix. Its spectral radius is

$$\tilde{R}(\mathbf{A}) \leqslant \|\mathbf{A}\|_\infty = \max_i \left(\sum_{\text{all } j} |a_{ij}| \right) \tag{B.18}$$

Owing to the defining condition (1) of stochastic matrices, one has $\|\mathbf{A}\|_\infty = 1$ and therefore $\tilde{R}(\mathbf{A}) \leqslant 1$. Since the sum of the elements of each of its rows is equal to 1, one has

$$\mathbf{Ae} = \mathbf{e} \tag{B.19}$$

with $\mathbf{e} = (1,1,...,1)^T$. It immediately follows that 1 is an eigenvalue of **A** and that $\tilde{R}(\mathbf{A}) = 1$. □

Property B.2: The spectral radius of substochastic matrices is strictly less than one.

Proof: Let $\mathbf{A} = \{a_{ij}\}$ be a nondecomposable substochastic matrix. Following the same reasoning line than for stochastic matrices, one may show that $\tilde{R}(\mathbf{A}) \leqslant 1$. Let us now show that 1 cannot be an eigenvalue of **A**.

A being substochastic, at least one of its rows has a sum strictly less than 1, i.e. a number i_0 exists such that

$$\sum_j a_{i_0 j} < 1 \tag{B.20}$$

Should 1 be an eigenvalue of **A**, then a vector $\mathbf{X} = [x_1, x_2, ..., x_n]$ would exist such that

$$\mathbf{X} = \mathbf{XA} \tag{B.21}$$

i.e., for all j

$$x_j = \sum_i a_{ij} x_i \tag{B.22}$$

Let us perform the sum of the x_j

$$\sum_j x_j = \sum_j \sum_i a_{ij} x_i = \sum_{i \neq i_0} \left(\sum_j a_{ij} \right) x_i + \left(\sum_j a_{i_0 j} \right) x_{i_0} \tag{B.23}$$

From inequality (B.20), one would obtain the following contradiction

$$\sum_j x_j < \sum_i x_i \quad \square \tag{B.24}$$

Lemma B.1: Let $\mathbf{A}$ be a substochastic matrix. It satisfies

$$\lim_{k \to \infty} \mathbf{A}^k = \mathbf{0} \tag{B.25}$$

and

$$\sum_{k=0}^{\infty} \mathbf{A}^k = (\mathbf{I} - \mathbf{A})^{-1} \tag{B.26}$$

where $\mathbf{0}$ and $\mathbf{I}$ are respectively the zero matrix and the identity matrix having the same size as $\mathbf{A}$. Eq. (B.25) generalizes the well-known scalar geometric series formulate

$$\sum_{k=0}^{\infty} x^k = \frac{1}{1-x} \tag{B.27}$$

In order to give a precise meaning to (B.26), one must first make sure that the series $\sum \mathbf{A}^k$ has a thorough meaning.

Let $1 > \lambda_1 \geqslant \lambda_2 \geqslant ... \geqslant \lambda_n$ be the eigenvalues of $\mathbf{A}$. If $\mathbf{A}$ is diagonalizable, there exists an invertible matrix $\mathbf{Q}$ such that

$$\mathbf{A} = \mathbf{Q} \cdot \begin{pmatrix} \lambda_1 & & \\ & \ddots & \\ & & \lambda_n \end{pmatrix} \cdot \mathbf{Q}^{-1} = \mathbf{Q} \cdot diag(\lambda_1,...,\lambda_n) \cdot \mathbf{Q}^{-1} \tag{B.28}$$

Therefore,

$$\mathbf{A}^k = \mathbf{Q} \cdot diag(\lambda_1^k,...,\lambda_n^k) \cdot \mathbf{Q}^{-1} \tag{B.29}$$

Since every $|\lambda_i|$ is strictly less than 1, entries λ_i^k of the diagonal matrix in Eq. (B.29) decreases towards zero as the exponent k increases, which gives Eq. (B.25). Furthermore, for all i, one can sum up

$$\sum_{k=0}^{\infty} \lambda_i^k = \frac{1}{1-\lambda_i} \tag{B.30}$$

From Eqs. (B.29) and (B.30), one has

$$\begin{aligned} (\mathbf{I} - \mathbf{A}) \sum_{k=0}^{N} \mathbf{A}^k &= \left(\mathbf{I} + \mathbf{A} + \mathbf{A}^2 + ... \right) - \mathbf{A} \cdot \left(\mathbf{I} + \mathbf{A} + \mathbf{A}^2 + ... \right) = \mathbf{I} - \mathbf{A}^{N+1} \\ &= \mathbf{I} - \mathbf{Q} \cdot diag(\lambda_1^{N+1},...,\lambda_n^{N+1}) \cdot \mathbf{Q}^{-1} \end{aligned}$$

Since all the eigenvalues of $\mathbf{A}$ are strictly less than 1, one has

$$\lim_{N\to\infty} diag\left(\lambda_1^{N+1},\ldots,\lambda_n^{N+1}\right) = \mathbf{0}$$

and therefore

$$\lim_{N\to\infty}(\mathbf{I}-\mathbf{A})\sum_{k=0}^{N}\mathbf{A}^k = \mathbf{I} \tag{B.31}$$

which finally yields Eq. (B.26). We conclude that the radius of convergence of matrix series is given by $\tilde{R}(\mathbf{A})<1$, where $\tilde{R}(\mathbf{A})$ is the matrix spectral radius.

B.4 Absorbing Markov chains

The ith state of a Markov chain is said to be *absorbing* if $m_{ii}=1$. It follows immediately relation (B.5) that $m_{ij}=0, (j\neq i)$. The set of conditions $m_{ii}=1$ and $m_{ij}=0, (j\neq i)$ is the mathematical statement expressing that once the system has reached state i, it never leaves anymore that state. A Markov chain is said to be *absorbing* if

1. There is at least one absorbing state,
2. There exists a transition (possibly in several steps but with a nonzero probability) from each nonabsorbing states to some absorbing state.

In studying absorbing chains, it is convenient to adopt certain conventions regarding the labeling of the states. Let us agree that the states are numbered in such a way that absorbing states are placed at the last positions. Then, if the chain contains N absorbing states, the single-step transition probability matrix $\mathbf{M}$ has the form [Mey00, p. 700]

$$\mathbf{M} = \begin{pmatrix} \mathbf{A} & \mathbf{B} \\ \mathbf{0} & \mathbf{I}_N \end{pmatrix} \tag{B.32}$$

where $\mathbf{A}$ is a square matrix whose elements are the probabilities of transition from a nonabsorbing state to a nonabsorbing state, $\mathbf{B}$ is a rectangular matrix having N columns whose elements are probabilities of transition from a nonabsorbing state to an absorbing state, $\mathbf{0}$ is a rectangular block of zeros having N rows, and $\mathbf{I}_N$ is the $N\times N$ identity matrix. Note that, according to the defining property 2 of absorbing chains, $\mathbf{B}$ is a nonzero matrix and $\mathbf{A}$ is consequently a substochastic matrix.

According to Eq. (B.9) and the block decomposition (B.32), one may write the 2-step transition probability matrix as

$$\mathbf{M}^2 = \begin{pmatrix} \mathbf{A} & \mathbf{B} \\ \mathbf{0} & \mathbf{I}_N \end{pmatrix}\cdot\begin{pmatrix} \mathbf{A} & \mathbf{B} \\ \mathbf{0} & \mathbf{I}_N \end{pmatrix} = \begin{pmatrix} \mathbf{A}^2 & \mathbf{AB}+\mathbf{B} \\ \mathbf{0} & \mathbf{I}_N \end{pmatrix} \tag{B.33}$$

The 3-step transition probability matrix may be written as

$$\mathbf{M}^3 = \begin{pmatrix} \mathbf{A}^2 & \mathbf{AB}+\mathbf{B} \\ \mathbf{0} & \mathbf{I}_N \end{pmatrix}\cdot\begin{pmatrix} \mathbf{A} & \mathbf{B} \\ \mathbf{0} & \mathbf{I}_N \end{pmatrix} = \begin{pmatrix} \mathbf{A}^3 & \mathbf{A}^2\mathbf{B}+\mathbf{AB}+\mathbf{B} \\ \mathbf{0} & \mathbf{I}_N \end{pmatrix} \tag{B.34}$$

Pursuing iteratively the products of $\mathbf{M}^k$ by $\mathbf{M}$, one would obtain the following k-step transition probability matrix

$$\mathbf{M}^k = \begin{pmatrix} \mathbf{A}^k & \sum_{j=0}^{k-1} \mathbf{A}^j \mathbf{B} \\ \mathbf{0} & \mathbf{I}_N \end{pmatrix} \tag{B.35}$$

and thereby, according to its defining equation (B.10), the following infinite-step transition probability matrix

$$\mathbf{M}_\infty = \begin{pmatrix} \lim_{k\to\infty} \mathbf{A}^k & \sum_{j=0}^{\infty} \mathbf{A}^j \mathbf{B} \\ \mathbf{0} & \mathbf{I}_N \end{pmatrix} \tag{B.36}$$

$\mathbf{A}$ being a substochastic matrix, it satisfies Eqs. (B.25) and (B.26). Thus, Eq. (B.36) becomes [Mey00, p. 701]

$$\mathbf{M}_\infty = \begin{pmatrix} \mathbf{0} & (\mathbf{I}-\mathbf{A})^{-1}\mathbf{B} \\ \mathbf{0} & \mathbf{I}_N \end{pmatrix} \tag{B.37}$$

where $\mathbf{I}$ is the identity matrix having the size of $\mathbf{A}$.

Appendix C.
Compositional formulae

In Chapter 5, we stated that the global transfer matrix of a regular multiface is the upper-right block of the infinite transfer matrix $\mathbf{M}_\infty$ associated to the Markov chain representing the multiface (see Eq. (5.22)). Since the Markov chain is absorbing (the states associated to the detectors are absorbing states, as seen in Sect. 5.2.3), we can directly use Eq. (B.37). Let us compute the transfer matrices of the quadriface and the hexaface presented in Sect. 5.3.1 and Sect. 5.3.2, yielding the quadriface and the hexaface formulae.

C.1 Quadriface formula

In Sect. 5.3.1, we presented a quadriface whose global transfer matrix $\mathbf{G}$ is defined by the composition equation

$$\mathbf{G} = \begin{bmatrix} T_U & R_U \\ R_V & T_V \end{bmatrix} = \begin{bmatrix} p_u & s_u \\ r_u & x_u \end{bmatrix} \bigcirc \begin{bmatrix} x_v & r_v \\ s_v & p_v \end{bmatrix} \tag{C.1}$$

The corresponding Markov chain, represented in Fig. 5.6, has the single-step transition probability matrix [see Eq. (5.17)]

$$\mathbf{M} = \begin{pmatrix} 0 & 0 & p_u & 0 & 0 & s_u \\ 0 & 0 & 0 & p_v & s_v & 0 \\ 0 & 0 & 0 & r_v & x_v & 0 \\ 0 & 0 & r_u & 0 & 0 & x_u \\ 0 & 0 & 0 & 0 & 1 & 0 \\ 0 & 0 & 0 & 0 & 0 & 1 \end{pmatrix} \tag{C.2}$$

Let us decompose $\mathbf{M}$ like in Eq. (B.32). Matrices $\mathbf{A}$ and $\mathbf{B}$ are subsequently decomposed into 2×2 blocks

$$\mathbf{M} = \left(\begin{array}{c|c} \mathbf{A} & \mathbf{B} \\ \hline \mathbf{0}_{24} & \mathbf{I} \end{array}\right) = \left(\begin{array}{c:c:c} \mathbf{0} & \mathbf{P} & \mathbf{S} \\ \hdashline \mathbf{0} & \mathbf{R} & \mathbf{X} \\ \hline \mathbf{0} & \mathbf{0} & \mathbf{I} \end{array}\right) = \left(\begin{array}{cc:cc:cc} 0 & 0 & p_u & 0 & 0 & s_u \\ 0 & 0 & 0 & p_v & s_v & 0 \\ \hdashline 0 & 0 & 0 & r_v & x_v & 0 \\ 0 & 0 & r_u & 0 & 0 & x_u \\ \hline 0 & 0 & 0 & 0 & 1 & 0 \\ 0 & 0 & 0 & 0 & 0 & 1 \end{array}\right) \tag{C.3}$$

with the following meaning for the different blocks: $\mathbf{P}$ contains the penetration transmittances of the upper and the lower bifaces, $\mathbf{S}$ their external reflectances, $\mathbf{R}$ their internal reflectances and $\mathbf{X}$ their exit transmittances. Let us note that either r_u or r_v is strictly less than 1. Otherwise, would $r_u = r_v = 1$, one would have $x_u = x_v = 0$ due to (B.16), which would mean that light cannot exit the multiface. Hence, block $\mathbf{A}$ is a substochastic matrix

(see Sect. B.3).

The global transfer matrix $\mathbf{G}$ is the upper-right 2×2 block of $\mathbf{M}_\infty$. According to Eq. (B.37), $\mathbf{G}$ is the upper 2×2 block of $(\mathbf{I}_4 - \mathbf{A})^{-1}\mathbf{B}$

$$\begin{pmatrix} \mathbf{G} \\ \cdot \end{pmatrix} = \left(\mathbf{I}_4 - \mathbf{A}\right)^{-1}\mathbf{B} \tag{C.4}$$

where the point represents an unspecified 2×2 block. One can write, using (C.3),

$$\left(\mathbf{I}_4 - \mathbf{A}\right) = \begin{pmatrix} \mathbf{I} & -\mathbf{P} \\ \mathbf{0} & \mathbf{I} - \mathbf{R} \end{pmatrix} \tag{C.5}$$

and, using a straightforward block computation,

$$\begin{pmatrix} \mathbf{I} & -\mathbf{P} \\ \mathbf{0} & \mathbf{I} - \mathbf{R} \end{pmatrix} \cdot \begin{pmatrix} \mathbf{I} & \mathbf{P}(\mathbf{I} - \mathbf{R})^{-1} \\ \mathbf{0} & (\mathbf{I} - \mathbf{R})^{-1} \end{pmatrix} = \begin{pmatrix} \mathbf{I} & \mathbf{0} \\ \mathbf{0} & \mathbf{I} \end{pmatrix} \tag{C.6}$$

Therefore,

$$\left(\mathbf{I}_4 - \mathbf{A}\right)^{-1} = \begin{pmatrix} \mathbf{I} & \mathbf{P}(\mathbf{I} - \mathbf{R})^{-1} \\ \mathbf{0} & (\mathbf{I} - \mathbf{R})^{-1} \end{pmatrix} \tag{C.7}$$

Then, using the decomposition of $\mathbf{B}$ as a function of blocks $\mathbf{S}$ and $\mathbf{X}$, one has

$$\left(\mathbf{I}_4 - \mathbf{A}\right)^{-1}\mathbf{B} = \begin{pmatrix} \mathbf{I} & \mathbf{P}(\mathbf{I} - \mathbf{R})^{-1} \\ \mathbf{0} & (\mathbf{I} - \mathbf{R})^{-1} \end{pmatrix} \cdot \begin{pmatrix} \mathbf{S} \\ \mathbf{X} \end{pmatrix} = \begin{pmatrix} \mathbf{S} + \mathbf{P}(\mathbf{I} - \mathbf{R})^{-1}\mathbf{X} \\ (\mathbf{I} - \mathbf{R})^{-1}\mathbf{X} \end{pmatrix} \tag{C.8}$$

$\left(\mathbf{I}_4 - \mathbf{A}\right)^{-1}\mathbf{B}$ is a 4×2 matrix whose upper 2×2 block corresponds to the global transfer matrix $\mathbf{G}$, i.e.

$$\mathbf{G} = \mathbf{S} + \mathbf{P}(\mathbf{I} - \mathbf{R})^{-1}\mathbf{X} \tag{C.9}$$

Matrix $\mathbf{I} - \mathbf{R}$ is expanded as

$$\mathbf{I} - \mathbf{R} = \begin{pmatrix} 1 & 0 \\ 0 & 1 \end{pmatrix} - \begin{pmatrix} 0 & r_v \\ r_u & 0 \end{pmatrix} = \begin{pmatrix} 1 & -r_v \\ -r_u & 1 \end{pmatrix} \tag{C.10}$$

Its determinant is $\Delta = 1 - r_u r_v > 0$, because $r_u r_v < 1$, and its inverse is

$$(\mathbf{I} - \mathbf{R})^{-1} = \frac{1}{\Delta}\begin{pmatrix} 1 & r_v \\ r_u & 1 \end{pmatrix} \tag{C.11}$$

By inserting (C.10) and (C.11) into (C.9), one finally obtains the quadriface formula

$$\mathbf{G} = \begin{pmatrix} 0 & s_u \\ s_v & 0 \end{pmatrix} + \frac{1}{\Delta} \begin{pmatrix} p_u & 0 \\ 0 & p_v \end{pmatrix} \cdot \begin{pmatrix} 1 & r_v \\ r_u & 1 \end{pmatrix} \cdot \begin{pmatrix} x_v & 0 \\ 0 & x_u \end{pmatrix} = \begin{pmatrix} \dfrac{p_u x_v}{1 - r_u r_v} & s_u + \dfrac{p_u x_u r_v}{1 - r_u r_v} \\ s_v + \dfrac{p_v x_v r_u}{1 - r_u r_v} & \dfrac{p_v x_u}{1 - r_u r_v} \end{pmatrix} \tag{C.12}$$

C.2 Hexaface formula

Let us now consider the hexaface defined in Sect. 5.3.2. The single-step transition probability matrix $\mathbf{M}$ of the corresponding chain is [see Eq. (5.26)]

$$\mathbf{M} = \begin{pmatrix} 0 & 0 & p_u & 0 & 0 & 0 & 0 & s_u \\ 0 & 0 & 0 & p_v & 0 & 0 & s_v & 0 \\ 0 & 0 & 0 & 0 & \tau & \rho & 0 & 0 \\ 0 & 0 & 0 & 0 & \rho' & \tau' & 0 & 0 \\ 0 & 0 & 0 & r_v & 0 & 0 & x_v & 0 \\ 0 & 0 & r_u & 0 & 0 & 0 & 0 & x_u \\ 0 & 0 & 0 & 0 & 0 & 0 & 1 & 0 \\ 0 & 0 & 0 & 0 & 0 & 0 & 0 & 1 \end{pmatrix} \tag{C.13}$$

$\mathbf{M}$ is decomposed as in Eq. (B.32), with blocks $\mathbf{A}$ and $\mathbf{B}$ subsequently subdivided in 2×2 blocks

$$\mathbf{A} = \left(\begin{array}{c|c|c} \mathbf{0} & \mathbf{P} & \mathbf{0} \\ \hline \mathbf{0} & \mathbf{0} & \mathbf{C} \\ \hline \mathbf{0} & \mathbf{R} & \mathbf{0} \end{array}\right) = \left(\begin{array}{cc:cc|cc} 0 & 0 & p_u & 0 & 0 & 0 \\ 0 & 0 & 0 & p_v & 0 & 0 \\ \hdashline 0 & 0 & 0 & 0 & \tau & \rho \\ 0 & 0 & 0 & 0 & \rho' & \tau' \\ \hline 0 & 0 & 0 & r_v & 0 & 0 \\ 0 & 0 & r_u & 0 & 0 & 0 \end{array}\right) \quad \text{and} \quad \mathbf{B} = \left(\begin{array}{c} \mathbf{S} \\ \hline \mathbf{0} \\ \hline \mathbf{X} \end{array}\right) = \left(\begin{array}{cc} 0 & s_u \\ \hdashline s_v & 0 \\ \hdashline 0 & 0 \\ 0 & 0 \\ \hdashline x_v & 0 \\ 0 & x_u \end{array}\right) \tag{C.14}$$

Again, either r_u or r_v is strictly less than 1 and block $\mathbf{A}$ is a substochastic matrix. The global transfer matrix $\mathbf{G}$ of the hexaface is the upper-right 2×2 block of matrix $\mathbf{M}_\infty$ given by Eq. (B.37). $\mathbf{G}$ is the upper 2×2 block of the 6×2 matrix $(\mathbf{I}_6 - \mathbf{A})^{-1}\mathbf{B}$.

$$\begin{pmatrix} \mathbf{G} \\ \cdot \\ \cdot \end{pmatrix} = \left(\mathbf{I}_6 - \mathbf{A}\right)^{-1} \mathbf{B} \tag{C.15}$$

Let us first calculate $(\mathbf{I}_6 - \mathbf{A})^{-1}$. It follows from decomposition (C.14) that

$$\mathbf{I}_6 - \mathbf{A} = \begin{pmatrix} \mathbf{I} & \mathbf{-P} & \mathbf{0} \\ \mathbf{0} & \mathbf{I} & \mathbf{-C} \\ \mathbf{0} & \mathbf{-R} & \mathbf{I} \end{pmatrix} \tag{C.16}$$

One can check by a straightforward direct multiplication that

$$\big(\mathbf{I}_6 - \mathbf{A}\big)^{-1} = \begin{pmatrix} \mathbf{I} & \mathbf{P}(\mathbf{I}-\mathbf{C}\mathbf{R})^{-1} & \mathbf{P}\mathbf{C}(\mathbf{I}-\mathbf{R}\mathbf{C})^{-1} \\ \mathbf{0} & (\mathbf{I}-\mathbf{C}\mathbf{R})^{-1} & \mathbf{C}(\mathbf{I}-\mathbf{R}\mathbf{C})^{-1} \\ \mathbf{0} & \mathbf{R}(\mathbf{I}-\mathbf{C}\mathbf{R})^{-1} & (\mathbf{I}-\mathbf{R}\mathbf{C})^{-1} \end{pmatrix} \tag{C.17}$$

Using the block decomposition of **B** [Eq. (C.14)], we obtain

$$\big(\mathbf{I}_6 - \mathbf{A}\big)^{-1}\mathbf{B} = \begin{pmatrix} \mathbf{S} + \mathbf{P}\mathbf{C}(\mathbf{I}-\mathbf{R}\mathbf{C})^{-1}\mathbf{X} \\ \mathbf{C}(\mathbf{I}-\mathbf{R}\mathbf{C})^{-1}\mathbf{X} \\ (\mathbf{I}-\mathbf{R}\mathbf{C})^{-1}\mathbf{X} \end{pmatrix} \tag{C.18}$$

$(\mathbf{I}_6 - \mathbf{A})^{-1}\mathbf{B}$ is a 6×2 matrix, whose upper 2×2 block is the global transfer matrix **G**

$$\mathbf{G} = \mathbf{S} + \mathbf{P}\mathbf{C}(\mathbf{I}-\mathbf{R}\mathbf{C})^{-1}\mathbf{X} \tag{C.19}$$

Remark: There is a striking analogy between matrix equation (C.19) and scalar equation (5.24) expressing the reflectance of a quadriface

$$R_U = s_u + p_u \frac{r_v}{1 - r_u r_v} x_u \tag{C.20}$$

Let us expand Eq. (C.19). First, one has

$$\mathbf{I}-\mathbf{R}\mathbf{C} = \begin{pmatrix} 1 & 0 \\ 0 & 1 \end{pmatrix} - \begin{pmatrix} 0 & r_v \\ r_u & 0 \end{pmatrix} \cdot \begin{pmatrix} \tau & \rho \\ \rho' & \tau' \end{pmatrix} = \begin{pmatrix} 1 - r_v\rho' & -r_v\tau' \\ -r_u\tau & 1 - r_u\rho \end{pmatrix} \tag{C.21}$$

whose determinant is

$$D = \big(1 - r_u\rho\big)\big(1 - r_v\rho'\big) - r_u r_v \tau\tau' \tag{C.22}$$

and whose inverse is

$$(\mathbf{I}-\mathbf{R}\mathbf{C})^{-1} = \frac{1}{D}\begin{pmatrix} 1 - r_u\rho & r_v\tau' \\ r_u\tau & 1 - r_v\rho' \end{pmatrix}. \tag{C.23}$$

Thus, Eq. (C.19) becomes

$$\mathbf{G} = \begin{pmatrix} 0 & s_u \\ s_v & 0 \end{pmatrix} + \frac{1}{D}\begin{pmatrix} p_u & 0 \\ 0 & p_v \end{pmatrix} \cdot \begin{pmatrix} \tau & \rho \\ \rho' & \tau' \end{pmatrix} \cdot \begin{pmatrix} 1 - r_u\rho & r_v\tau' \\ r_u\tau & 1 - r_v\rho' \end{pmatrix} \cdot \begin{pmatrix} x_v & 0 \\ 0 & x_u \end{pmatrix} \tag{C.24}$$

and we obtain the hexaface formula, with D given by Eq. (C.22)

$$\mathbf{G} = \begin{pmatrix} p_u x_v \dfrac{\tau}{D} & s_u + p_u x_u \dfrac{\rho - r_v\big(\rho\rho' - \tau\tau'\big)}{D} \\ s_v + p_v x_v \dfrac{\rho' - r_u\big(\rho\rho' - \tau\tau'\big)}{D} & p_v x_u \dfrac{\tau'}{D} \end{pmatrix}$$

Appendix D.
Characterization of the external bifaces

An external biface is characterized by a penetration transmittance p, an external reflectance s, an internal reflectance r and an exit transmittance x (see Sect. 2.4 and 6.1.2). The transfer matrices of the upper and the lower external bifaces are respectively

$$\begin{bmatrix} p & s \\ r & x \end{bmatrix} \quad \text{and} \quad \begin{bmatrix} x & r \\ s & p \end{bmatrix} \tag{D.1}$$

The present appendix aims a characterizing the upper external transfer matrix. We shall take into account the nature of the external biface (transparent, scattering, Lambertian) and the measuring geometry (directional or Lambertian light source / integrating sphere or radiance detector). We distinguish Lambertian bifaces, characterized by their invariant transfer matrix $\mathbf{F}_L$, and non-Lambertian bifaces, characterized by their fundamental transfer matrix $\mathbf{F}_\theta$. The elements of matrices $\mathbf{F}_L$ and $\mathbf{F}_\theta$ are respectively termed

$$\mathbf{F}_L = \begin{bmatrix} p_L & s_L \\ r_L & x_L \end{bmatrix} \quad \text{and} \quad \mathbf{F}_\theta = \begin{bmatrix} P(\theta) & S(\theta) \\ R(\theta) & X(\theta) \end{bmatrix} \tag{D.2}$$

Recall that, according to the criteria of regularity of the multifaces (Sect. 5.2.1), a non-Lambertian external biface is necessarily bordered by a Lambertian biface. It therefore receives a Lambertian illumination from the central biface.

Let us present successively the terms r, p, x and s for the upper external biface (light source and detector at the upper side). For each term, we will first consider that the external biface is Lambertian and then that it is non-Lambertian.

D.1 Internal reflectance r

The internal reflectance r is the fraction of light coming from the central biface that is reflected by the external biface. It depends neither on the geometry of illumination nor on the geometry of observation.

D.1.1 Lambertian external biface

The reflectance of the Lambertian biface, r_L, is invariant. Therefore, $r = r_L$.

D.1.2 Non-Lambertian external biface

When the external biface is non-Lambertian, it is characterized by its lower directional reflectance $R(\theta)$. It is illuminated by a Lambertian irradiance coming from the central biface. Therefore, the internal reflectance r of the external biface is a Lambertian reflectance, derived from $R(\theta)$ according to Eq. (1.29)

$$r = \int_{\theta=0}^{\pi/2} R(\theta) \sin 2\theta d\theta \tag{D.3}$$

D.2 Penetration transmittance p

The penetration transmittance p is the fraction of light coming from the light source that is transmitted to the central bifaces across the external biface.

D.2.1 Lambertian external biface

The Lambertian external biface has an invariant upper transmittance p_L, independently of the conditions of illumination. Therefore, the penetration transmittance is $p = p_L$.

D.2.2 Non-Lambertian external biface

The penetration transmittance of a non-Lambertian external biface depends on the geometry of illumination. The biface has a directional upper transmittance $P(\theta)$. When the source is directional, of angle ψ, then

$$p = P(\psi)\,, \tag{D.4}$$

When the source is Lambertian, the penetration transmittance is a Lambertian transmittance, related to $P(\theta)$ according to Eq. (1.29)

$$p = \int_{\theta=0}^{\pi/2} P(\theta) \sin 2\theta d\theta\,. \tag{D.5}$$

D.3 Exit transmittance x

The exit transmittance x is the fraction of light coming from the central biface that is captured by the optical device. It depends on the observation geometry: either the capturing device is an integrating sphere and all the exiting light is observed, or the capturing device is a radiance detector and only the light exiting in direction of the detector is captured.

D.3.1 Lambertian external biface

A Lambertian biface has a lower transmittance x_L. This transmittance accounts for the flux transmitted over the whole hemisphere.

Integrating sphere: The observation solid angle of the integrating sphere is the whole hemisphere, as in the definition of transmittance x_L. Therefore, the exit transmittance is $x = x_L$.

Radiance detector: The observation solid angle is differential, and not hemispherical as in the definition of x_L. Only a radiance L_t is captured. The transmitted irradiance E_t exiting the Lambertian biface is Lambertian. Therefore radiance L_t is equal to E_t/π independently of the observation direction (see Appendix A.2). The ratio L_t/E_i is proportional to the exit transmittance x, the proportionality factor being the apparatus constant ξ defined by

Eq. (A.12)

$$x = \xi \frac{L_t}{E_i} = \xi \frac{E_t/\pi}{E_i} = \xi x_L/\pi \tag{D.6}$$

D.3.2 Non-Lambertian external biface

The non-Lambertian external biface is characterized by its directional lower transmittance $X(\theta)$. It receives from the central biface a Lambertian illumination.

Integrating sphere: The observation solid angle of the integrating sphere is the whole hemisphere, as in the definition of transmittance $X(\theta)$. Since the incident light is Lambertian, the exit transmittance x is a Lambertian transmittance, related to $X(\theta)$ according to Eq. (1.29)

$$x = \int_{\theta=0}^{\pi/2} X(\theta) \sin 2\theta d\theta \tag{D.7}$$

Radiance detector: The exit transmittance x is the ratio of the radiance $L_t(\psi')$ transmitted in the direction of the detector (observation angle ψ'). We distinguish the case of a transparent and a scattering external biface.

Case of a transparent biface – Since the incident irradiance E_i is Lambertian, a radiance E_i/π incomes on the transparent external biface from every direction. According to Eq. (3.6), the radiance L_t captured by the radiance detector is

$$L_t(\psi') = \left(\frac{n_0}{n_1}\right)^2 X(\psi_1') \frac{E_i}{\pi} \tag{D.8}$$

where n_0 is the refractive index of the surrounding medium, n_1 is the refractive index of the neighboring Lambertian biface, and ψ_1' is related to ψ' by Snell's law: $n_1 \sin\psi_1' = n_0 \sin\psi'$. The ratio $L_t(\psi')/E_i$ is proportional (factor ξ, see Appendix A.2) to the exit transmittance of the transparent external biface

$$x = \xi \left(\frac{n_0}{n_1}\right)^2 \frac{X(\psi_1')}{\pi} \tag{D.9}$$

Case of a scattering biface – The radiance $L_t^{d\omega}(\psi')$ transmitted towards the radiance detector is related to the incident elements of irradiance $dE_i(d\omega)$ coming from the Lambertian central biface by the BTDF f_T [see Eq. (1.14)]

$$L_t^{d\omega}(\psi') = f_T(d\omega, \psi') dE_i(d\omega)$$

Since the incident irradiance E_i is Lambertian, a same radiance E_i/π illuminates the external biface from every direction. According to Eq. (1.7), the incident elements of irradiance are

$$dE_i(d\omega) = \frac{E_i}{\pi} \cos\theta d\omega \tag{D.10}$$

where θ is the incidence angle. By summing up the contributions of all the incident elements of irradiance, one obtains the total transmitted radiance $L_t(\psi')$,

$$\begin{aligned} L_t(\psi') &= \int_{d\omega\in\Omega} f_T(d\omega,\psi')\, dE_i(d\omega) \\ &= \frac{E_i}{\pi}\int_{d\omega\in\Omega} f_T(d\omega,\psi')\cos\theta\, d\omega \\ &= E_i\int_{\phi=0}^{2\pi}\int_{\theta=0}^{\pi/2} f_T(\theta,\psi')\sin\theta\cos\theta\, d\theta d\phi \end{aligned}$$

The ratio $L_t(\psi')/E_i$ is proportional (factor ξ) to the exit transmittance x

$$x = \xi\int_{\phi=0}^{2\pi}\int_{\theta=0}^{\pi/2} f_T(\theta,\psi')\sin\theta\cos\theta\, d\theta d\phi \tag{D.11}$$

D.4 External reflectance *s*

The external reflectance is the fraction of light coming from the light source that is reflected by the external biface and captured by the optical device. The external reflectance depends on the geometry of observation in the same manner as the exit transmittance. It also depends on the geometry of illumination.

D.4.1 Lambertian external biface

The reflectance of the Lambertian biface is independent of the geometry of illumination. With an integrating sphere, the observation solid angle is hemispherical, as in the definitions of the reflectance s_L. Therefore, the external reflectance is $s = s_L$. A radiance detector measured only a radiance in a particular direction. Since the light reflected by the external biface is Lambertian, a fraction $1/\pi$ propagates in every direction. Therefore, $s = \xi s_L/\pi$, where ξ is the apparatus constant of the radiance detector.

D.4.2 Non-Lambertian external biface

Four different measuring geometries must be considered, corresponding to the different combinations of illumination geometry (directional or Lambertian) and observation geometry (integrating sphere or radiance detector).

Directional illumination (incident angle ψ) / integrating sphere: the external reflectance s, i.e. the ratio of the flux reflected over the hemisphere to the incident directional flux, correspond precisely to the upper directional reflectance $S(\psi)$ of the biface.

Lambertian illumination / integrating sphere: s is given by the Lambertian reflectance of the biface, derived from its directional reflectance $S(\theta)$ according to Eq. (1.29)

$$s = \int_{\theta=0}^{\pi/2} S(\theta)\sin 2\theta\, d\theta \tag{D.12}$$

Directional illumination (incident angle ψ)/ radiance detector (observation angle ψ')

Case of a transparent biface – Light is reflected in the specular direction. Therefore, the radiance detector captures light only if it is in the specular direction, i.e. if $\psi' = \psi$. The ratio of the reflected to incident fluxes is given by the directional reflectance $S(\psi)$ of the biface

$$s = \begin{cases} S(\psi) & \text{if } \psi' = \psi \\ 0 & \text{otherwize} \end{cases} \tag{D.13}$$

Most of the time, angles ψ and ψ' are different. This permit to discard the externally reflected light from the measurement.

Case of a scattering biface – The radiance L_r captured by the detector and the incident element of irradiance dE_i are related by the BRDF f_R [see Eq. (1.14)]

$$L_r(\psi') = f_R(d\omega_i, \psi') dE_i(d\omega_i)$$

The reflectance s of the external biface is proportional to the ratio L_r/dE_i [see Eq. (A.13)]. Therefore,

$$s = \xi\, f_R(\psi, \psi')$$

Lambertian illumination / radiance detector (observation angle ψ'):

Case of transparent biface – The detector captures only the light that is incident in the corresponding regular direction. Only a fraction $1/\pi$ of the Lambertian incident irradiance E_i is oriented in that direction (incidence angle ψ'). According to Eq. (3.7), the reflected radiance L_r, which is also the radiance captured by the detector, is

$$L_r = S(\psi') \frac{E_i}{\pi} \tag{D.14}$$

The reflectance s of the external biface is proportional to the ratio L_r/E_i. Therefore,

$$s = \xi \frac{S(\psi')}{\pi} \tag{D.15}$$

Case of a scattering biface – Eq. (D.11) corresponds to the partial transmission of Lambertian incident light by a scattering biface towards a radiance detector. Here, we consider the partial reflection of Lambertian incident light by a scattering biface towards a radiance detector. We have the same equation as in Eq. (D.11), where the lower BTDF f_T is replaced by the upper BRDF f_R

$$s = \xi \int_{\phi=0}^{2\pi} \int_{\theta=0}^{\pi/2} f_R(\theta, \psi') \sin\theta \cos\theta\, d\theta\, d\phi \tag{D.16}$$

References

[BLMC01] Borch J., Lyne M. B., Mark R. E. and Charles C. (2001), *Handbook of Physical Testing of Paper: Volume 2,* Marcel Dekker, 2nd Ed., p. 95.

[Bru04] Bruce N. C. (2004), On the validity of the inclusion of geometrical shadowing functions in the multiple-scatter Kirchhoff approximation, *Wave Random Media*, **14**, 1–12.

[BS63] Beckmann P. and Spizzichino A. (1963), *The scattering of electromagnetic waves from rough surfaces,* MA Artech House INC, Norwood, pp. 70–98.

[BW99] Born M. and Wolf E. (1999), *Principle of Optics,* Pergamon, Oxford, 7th Edition.

[Car03] Caron J. (2003), *Diffusion de la lumière dans les milieux stratifiés: prise en compte des interfaces rugueuses et des effets de polarization*, PhD dissert., University of Paris VI.

[Cha60] Chandrasekhar S. (1960), *Radiative Transfert*, Dover, New-York.

[CLA02] Caron J., Lafait J. and Andraud C. (2002), Scalar Kirchhoff's model for light scattering from dielectric random rough surfaces, *Optics Communications*, **207**, 17–28.

[CT82] Cook R. L. and Torrance K. E. (1982), A Reflectance Model for Computer Graphics. *ACM Trans. On Graphics*, **1**, 7–24.

[CY53] Clapper F.R. and Yule J.A.C. (1953), The Effect of Multiple Internal Reflections on the Densities of Halftone Prints on Paper, *Journal of the Optical Society of America*, **43**, 600–603.

[Dem24] Demichel M.E. (1924), *Procédé*, **26**, 17–21.

[Des91] Desvignes F. (1991), *Rayonnements optiques*, *Radiométrie-Photométrie*, Masson, Paris.

[Dur03] Durant S. (2003), *Propagation de la lumière en milieu aléatoire, Rôle de l'absorption, de la diffusion dépendente et du couplage surface-volume*, PhD dissert., Ecole Centrale de Paris.

[EE02] Elias M. and Elias G. (2002), New and fast calculation for incoherent multiple scattering, *Journal of the Optical Society of America A*, **19**, 894–905.

[EH02] Emmel P. and Hersch R.D. (2002), Modeling Ink Spreading for Color Prediction, *Journal of Imaging Science and Technology*, **46**, 237-246.

[EM00] Elias M. and Menu M. (2000), Experimental characterization of a random metallic rough surface by spectrophotometric measurements in the visible range, *Optics communications*, **180**.

[EM01] Elias M. and Menu M. (2001), Characterization of surface states on patrimonial works of art, *Surface Engineering* **17**, 225, *Revue de Métallurgie,* **776** SMT14.

[Ger03] Germer T. (2003), Polarized light diffusely scattered under smooth and rough interfaces, *Polarization Science and Remote Sensing*, Proc. SPIE 5158, 193–204.

[Gla95] Glassner A. S. (1995), *Pinciples of Digital Image Synthesis*, Morgan Kaufmann Publishers, Inc, San Francisco, Vol. 2.

[Gus97] Gustavson S. (1997), *Dot gain in colour halftones*, PhD dissert. No 492, Linköping University.

[Hea91] Heavens O. S. (1991), *Optical Properties of Thin Films*, Dover Pub., New York.

[HECC05] Hersch R.D., Emmel P., Collaud F. and Crété F. (2005), Spectral reflection and dot surface prediction models for color halftone prints, *Journal of Electronic Imaging*, **14**, 33001–12.

[Hel02] Helgeson S. (2002), *Le nouveau design suédois*, Institut Suédois, Stockholm.

[Hir91] Hird K. F. (1991), *Offset Lithographic Technology*, Goodheart-Willcox Pub.

[HH04] Hébert M. and Hersch R.D. (2004), Classical print reflection models: a radiometric approach, *Journal of Imaging Science and Technology*, **48**, 363–374.

[HH05] Hébert M. and Hersch R.D. (2005), Extending the Clapper–Yule model to rough printing supports, *Journal of the Optical Society of America A*, **22**, 1952–1967.

[HH06] Hébert M. and Hersch R.D. (2006), A reflectance and transmittance model for recto-verso halftone prints, accepted for publication in *Journal of the Optical Society of America A* (April 9th 2006).

[HS98] Harris J.W. and Stocker H. (1998), *Handbook of mathematics and computational science*, Springer-Verlag, p. 736.

[HV04] Harrar M., Viénot F. (2004), What is controlling chromatic contrast in a complex scene ?, *CGIV 2004 Proceedings*, **2**, 51–54.

[ITM97] Inoue S., Tsumura N. and Miyake N. (1997), Measuring MTF of Paper by sinusoidal test pattern projection. *Journal of Imaging Science and Technology*, **41**, 657–661.

[Jud42] Judd D.B. (1942), Fresnel Reflection of Diffusely Incident Light, *Journal of the National Bureau of Standards*, **29**, 329–332.

[Kli71] Klier K. (1971), Absorption and scattering in plane parallel turbid media, *Journal of the Optical Society of America*, **62**, 882–885.

[KM31] Kubelka P. and Munk F. (1931), Ein Beitrag zur Optik der Farbanstriche, *Zeitschrift für technische Physik*, **12**, 593–601.

[Kor94] Korringa J. (1994), Early History of Multiple Scattering Theory for Ordered Systems, *Physics Reports*, **238**, 341.

[Kub48] Kubelka P. (1948), New contributions to the optics of intensely light-scattering material, part I, *Journal of the Optical Society of America A*, **38**, 448–457.

[Kub54] Kubelka P. (1954), New contributions to the optics of intensely light-scattering materials, part II: Non homogeneous layers, *Journal of the Optical Society of America A*, **44**, 330–335.

[LS99] Lambourne R. and Strivens T.A. (1999), *Paint and Surface Coatings – Theory and Practice*, 2nd Edition, Woodhead Publishing.

[McC94] McCluney W. R. (1994), *Introduction to Radiometry and Photometry*, Artech House.

[Mey00] Meyer C. D. (2000), *Matrix analysis and applied linear algebra*, SIAM, Philadelphia, (chapter 8).

[MG86] Maheu B. and Gouesbet G. (1986), Four-flux models to solve the scattering transfer equation: special cases, *Applied Optics*, **25**, 1122–1128.

[Mie08] Mie G. (1908), Beiträge zur Optik trübe Medien, speziell kolloidaler Metallösungen, *Annalen der Physik*, vierte Folge, Band **25**, 377–445.

[MLG84] Maheu B., Letouzan J.N. and Gouesbet G. (1984), Four-flux models to solve the scattering transfer equation in terms of Lorentz-Mie parameters, *Applied Optics*, **23**, 3353–3362.

[MR71] Mudgett P.S. and Richards L.W. (1971), Multiple scattering calculations for technology, *Applied Optics*, **10**, 1485–1502.

[MT73] Maki D. P. and Thompson M. (1973), *Mathematical models and applications*, Prentice-Hall, Englewood Cliffs.

[Neu37] Neugebauer H.E.J. (1937), Die theoretischen Grundlagen des Mehrfarbendrucks, *Z. Wissen. Photog.*, **36**, 36–73.

[Nic77] Nicomedus F.E. & al. (1977), *Geometrical considerations and nomenclature for reflectance*, NBS Monograph 160, NBS (now NIST), p. 52.

[NIK91] Nayar S.K., Ikeuchi K. and Kanade T. (1991), Surface reflection: physical and geometrical perspectives, *IEEE Transactions on Pattern Analysis and Machine Intelligence*, **13**, 611–634.

[Nis98] Niskanen, K.J. (1998) *Paper Physics*, Vol. 16. of nineteen books 'Papermaking Science and Technology' Fapet/Tappi, Atlanta.

[Ogi91] Ogilvy J.A. (1991), *Theory of wave scattering from random rough surfaces*, Institute of Physics Publishing, Bristol and Piladelphia.

[OKV04] Obein G., Knoblauch K. and Viénot F. (2004), Difference scaling of gloss: Nonlinearity, binocularity, and constancy, *Journal of Vision*, **4** (9), 711– 720.

[OT86] Olzak L. and Thomas J.P. (1986), *Handbook of perception and human performance*, Vol. 1: Seeing spatial patterns, Chapter 7.

[Per95] Perkampus H.-H. (1995), *Encyclopedia of Spectroscopy*, VCH.

[Pra88] Prahl S.A. (1988), *Light transport in tissues*, PhD dissertation, University of Texas.

[Ray71] Rayleigh L.J.S. (1871), On light from the sky, its Polarization and Colour. *Phylosophical Magazine*, **41**, 107–120, 174–279.

[Ray99] Rayleigh L.J.S. (1871), On Transmission of Light though an Atmosphere containing Small Particles in Suspension, and on the Origin of the Blue of the Sky, *Phylosophical Magazine*, **47**, 375–384.

[RH78] Ruckdeschel F. and Hauser O. (1978), Yule-Nielsen in printing: a physical analysis, *Applied Optics*, **17**, 3376–3383.

[Rog98] Rogers G. (1998), Effect of light scatter on halftone color, *Journal of the Optical Society of America A*, **15**, 1813–1821.

[Rog00] Rogers G. (2000), A Generalized Clapper-Yule Model of Halftone Reflectance, *Journal of Color Research and Application*, **25**, 402–407.

[Sau42] Saunderson J. L. (1942), Calculation of the color pigmented plastics, *Journal of the Optical Society of America*, **32**, 727–736.

[SCWJ88] Stamnes K., Chee Tsay S., Wiscombe W. and Jayaweera K. (1988), Numerically stable algorithm for discrete-ordinate-method radiative transfer in multiple scattering and emitting layer media, *Applied Optics*, **27**, 2502–2510.

[Sha03] Sharma A. (2003), Color fundamentals for digital imaging, in *Digital Color Imaging Handbook*, Ed. G. Sharma, RC Press, pp. 1–114.

[SHH06] Simonot L., Hébert M. and Hersch R. D. (2006), Extension of the Williams-Clapper model to stacked nondiffusing colored coatings with different refractive indices, *Journal of the Optical Society of America A*, **23**, 1432–1441.

[Sim02] Simonot L. (2002), *Etude expérimentale et modélisation de la diffusion de la lumière dans une couche de peinture colorée et translucide*, PhD dissert., University of Paris VI.

[Smi67] Smith B.G. (1967), Geometrical shadowing of a random rough surface, *IEEE Transaction on Antennas and Propagation*, **15**, 668–671.

[SS01] Shore J. D. and Spoonhower J. P. (2001), Reflection Density in Photographic Color Prints: Generalizations of the Williams-Clapper Transform, *Journal of Imaging Science and Technology*, **45**, 484–488.

[ST03] Simon K. and Trachsler B. (2003), A random walk approach for light scattering in material, *Discrete Mathematics and Theoretical Computer Science AC*, 289–300.

[Sta01] Stam J. (2001), An illumination model for a skin layer bounded by rough surfaces, *Rendering Techniques'01, Proc. of the 12th Eurographics workshop*, 39–52.

[Ste94] Stewart W.J. (1994), *Introduction to the numerical solution of Markov chains*, Princeton University Press, Princeton.

[Sto95] Stover J.C. (1995), *Optical scattering, measurement and analysis*, Second Edition, SPIE Optical Engineering Press, Bellingham.

[TS67] Torrance K.E. and Sparrow E.M. (1967), Theory for Off-Specular Reflection from Roughened Surfaces, *Journal of the Optical Society of America*, **57**, 1105–1114.

[Vig90] Viggiano J.A.S (1990), Modeling the Color of Multi-Colored Halftones, *Proceedings TAGA*, 44–62.

[VN97] Vargas W.E. and Niklasson G.A. (1997), Applicability conditions of the Kubelka-Munk theory, *Applied Optics*, **36**, 5580–5586.

[WC53] Williams F. C., Clapper F. R. (1953), Multiple Internal Reflections in Photographic Color Prints, *Journal of the Optical Society of America*, 29, 595–599.

[Wol98] Wolfe W. L. (1998), *Introduction to Radiometry*, SPIE Optical Engineering Press.

[YK04a] Yang L. and Kruse B. (2004), Revised Kubelka-Munk theory. I Theory and application, *Journal of the Optical Society of America A*, **21**, 1933-1941.

[YK04b] Yang L. and Kruse B. (2004), Revised Kubelka-Munk theory. II Unified framework for homogeneous and inhomogeneous optical media, *Journal of the Optical Society of America A*, **21**, 1942–1952.

[YK04c] Yang L. and Kruse B. (2004), Revised Kubelka-Munk theory. III A general theory of light propagation in scattering and absorptive media, *Journal of the Optical Society of America A*, **22**, 1866–1873.

[YN51] Yule J.A.C. and Nielsen W.J. (1951), The penetration of light into paper and its effect on halftone reproductions, *Proc. TAGA*, **3**, 65–76.

[Yul67] Yule J. A.C. (1967), *Principles of Color Reproduction*, John Wiley & Sons, New York.

[ZB03] Zuppiroli L. and Bussac M.-N. (2003), *Traité des couleurs*, Presses polytechniques universitaires romandes, Lausanne.

Biography

Mathieu Hébert was born on 1st of May 1977 in Nantes, France. He completed his education in Vendée (west of France) until the Baccalauréat in 1995. He pursued electronics and signal processing engineering studies at CPE-Lyon from 1995 to 2001, with one intermediate year (1999-2000) in the Hitachi Central Research Laboratories in Tokyo, Japan. Simultaneously to the degree of engineer, he obtained in 2001 a master diploma on image processing at the University Jean Monnet of Saint-Etienne. He then started working on his PhD research as an external doctoral student of the Peripheral System Laboratory (LSP) at the Ecole Polytechnique Fédérale de Lausanne (EPFL). He was also from 2001 to 2006 teaching assistant in mathematics at CPE-Lyon.

He his also interested in arts, principally music (composed piece for brass band, Robert Martin Ed., 1997) and theater (actor and director of the troupe "La Petite Chimère" in Lyon since 1997, writer of a play awarded in 1999).

He is a citizen of France and is married.

Scientific publications

Hébert M., Emmel P., Hersch R.D. (2002), A Prediction Model for Reflection on Varnished Metallic Plates, CGIV 2002 Proc. *IS&T Society for Imaging Science and Technology*, 453-458.

Hébert M. and Hersch R.D. (2004), Classical Print Reflection Models: A Radiometric Approach, *Journal of Imaging Science and Technology*, **48**, 363–374.

Hébert M., Hersch R.D. (2005), Extending the Clapper–Yule model to rough printing supports, *Journal of the Optical Society of America A*, **22**, 1952–1967.

Simonot L., Hébert M., and Hersch R. D. (2006), Extension of the Williams-Clapper model to stacked nondiffusing colored coatings with different refractive indices, *Journal of the Optical Society of America A*, **23**, 1432-1441.

Hébert M., Hersch R.D. (2006), A reflectance and transmittance model for recto-verso halftone prints, accepted for publication (April 9th 2006) in *Journal of the Optical Society of America A*.

Index

T

W

Frequently used formulae

– The quadriface formula

$$\begin{bmatrix} p_u & s_u \\ r_u & x_u \end{bmatrix} \bigcirc \begin{bmatrix} x_v & r_v \\ s_v & p_v \end{bmatrix} = \begin{bmatrix} \dfrac{p_u x_v}{1-r_u r_v} & s_u + \dfrac{p_u x_u r_v}{1-r_u r_v} \\ s_v + \dfrac{p_v x_v r_u}{1-r_u r_v} & \dfrac{p_v x_u}{1-r_u r_v} \end{bmatrix} \tag{5.23}$$

– The hexaface formula

$$\begin{bmatrix} p_u & s_u \\ r_u & x_u \end{bmatrix} \bigcirc \begin{bmatrix} \tau & \rho \\ \rho' & \tau' \end{bmatrix} \bigcirc \begin{bmatrix} x_v & r_v \\ s_v & p_v \end{bmatrix} = \begin{bmatrix} p_u x_v \dfrac{\tau}{D} & s_u + p_u x_u \dfrac{\rho - r_v\left(\rho\rho' - \tau\tau'\right)}{D} \\ s_v + p_v x_v \dfrac{\rho' - r_u\left(\rho\rho' - \tau\tau'\right)}{D} & p_v x_u \dfrac{\tau'}{D} \end{bmatrix} \tag{5.26}$$

with $D = \left(1 - r_u\rho\right)\left(1 - r_v\rho'\right) - r_u r_v \tau\tau'$.

– Properties satisfied by Fresnel reflection and transmission factors, when angles θ_0 and θ_1 are related by Snell's laws, i.e. $n_0 \sin\theta_0 = n_1 \sin\theta_1$

$$R_{10}(\theta_1) + T_{10}(\theta_1) = 1 \tag{3.21}$$

$$R_{10}(\theta_1) + T_{10}(\theta_1) = 1$$

$$R_{01}(\theta_0) = R_{10}(\theta_1) \tag{3.23}$$

$$T_{01}(\theta_0) = T_{10}(\theta_1) \tag{3.24}$$

– Lambertian reflectances and transmittances of a flat interface

$$r_{01} = \int_{\theta=0}^{\pi/2} R_{01}(\theta) \sin 2\theta \, d\theta \tag{3.27}$$

$$t_{01} = \int_{\theta=0}^{\pi/2} T_{01}(\theta) \sin 2\theta \, d\theta \tag{3.28}$$

$$r_{10} = \int_{\theta=0}^{\pi/2} R_{10}(\theta) \sin 2\theta \, d\theta \tag{3.29}$$

$$t_{10} = \int_{\theta=0}^{\pi/2} T_{10}(\theta) \sin 2\theta \, d\theta \tag{3.30}$$

– Lambertian reflectances and transmittances of a flat interface bordered by a transparent layer, having the refractive index n_1 and a normal transmittance t

$$r_{10}(t) = \int_{\theta=0}^{\pi/2} R_{10}(\theta) t^{2/\cos\theta} \sin 2\theta \, d\theta \tag{6.25}$$

$$t_{10}(t) = \int_{\theta=0}^{\pi/2} T_{10}(\theta) t^{1/\cos\theta} \sin 2\theta \, d\theta \tag{6.32}$$

$$t_{01}(t) = \int_{\theta_0=0}^{\pi/2} T_{01}(\theta_0)\, t^{1/\cos\theta_1} \sin 2\theta_0 \, d\theta_0 \tag{8.11}$$